CONTRIBUTION OF INTEGRINS AND ACTIN REGULATORS TO HUMAN DENDRITIC CELL PODOSOME BIOLOGY

João Pedro da Silva Metelo

Institute of Child Health

University College London

A thesis submitted for the degree of Doctor of Philosophy

2012

All the work presented in this thesis is entirely my own, with the following exceptions, indicated in the thesis: (1) one of the two batches of lentivectors pseudotyped with different envelopes was produced by Natalie Ward (Figure 3.3); (2) the production of lentivectors for CD29 shRNA expression, generation of CD29 knock-down THP1 cell lines for construct screening and CD29 mRNA analysis was performed by João Nunes (Figure 4.5 B); (3) Supplemental Data relative to human LAD DC was collected by Dr Siobhan Burns (Figure S.1 A); (4) canine DC used for Figure S.1 B and C (Supplemental Data) were cultured and plated by Dr Gerben Bouma; and (5) Supplemental Data referring to the CD18 hypomorphic mouse was collected by Luísa Saraiva.

Results described in Chapter 3 of this thesis are published in:

Metelo J, Ward N, Thrasher AJ, Burns SO. 2011. Lentivectors Are Efficient Tools to Manipulate the Dendritic Cell Cytoskeleton. Cytoskeleton 68(8):434-445.

This research was generously supported by a personal grant from Fundação para a Ciência e a Tecnologia, Portugal (Grant Reference No. SFRH/BD/36224/2007), funded by POPH-QREN, co-funded by the European Social Fund.

ABSTRACT

Dendritic cells (DC) are key cells of the innate immune system required to prime adaptive immunity. Migration is central to their function to enable immune surveillance of the whole body and for prompt activation of the adaptive immune system. Immature DC assemble specialised actin structures called podosomes which are thought to be critical for efficient adhesion-mediated migration. Podosomes are, therefore, considered to be essential for DC function.

Despite the great increase in literature regarding podosomes and related structures over recent years, still much is unknown about critical components, regulation and function of these structures in DC. Cytoskeletal studies of DC have been complicated by the fact that tools commonly employed for biological manipulation may constitute activation stimuli for DC and dramatically alter the DC cytoarchitecture. A panel of human THP1DC knock-down cell lines was generated using RNAi technology targeting factors suspected or known to be important for podosome formation and/or function such as the integrins CD18 and CD29 and the actin regulators HS1, WASp and WIP. Results obtained from functional analysis of the knock-down cell lines confirm CD18 to be specifically recruited to the DC podosomes and to be essential for their assembly. On the contrary, CD29 knock-down did not attenuate podosome assembly, even when reduced to levels that resulted in a defect in static adhesion. As previously reported, WASp and WIP expression was demonstrated to be necessary for podosome formation. Furthermore, a role for the cortactin homolog HS1 in CD18 activation in myeloid cells is suggested, as HS1 knock-down resulted in defective CD18-dependent adhesion and reduced podosome formation when cells were plated on ICAM but not on fibronectin.

The results presented here define a robust method for manipulating immature DC for cytoskeletal studies and advance our current understanding of the regulation of podosome assembly in human DC.

TABLE OF CONTENTS

LIST OF FIGURES AND TABLES

ACRONYMS AND ABBREVIATIONS

7-AAD	7-Aminoactinomycin D
A	Acidic domain
ADF/ cofilin	Actin depolymerising factor (family)
ADP	Adenosine diphosphate
AF	Alexa-fluor
amiRNA	Artificial miRNA
AMP	Adenosine monophosphate
ANCOVA	Analysis of covariance
APC	Antigen-presenting cell
Arp2/3	Actin related proteins 2 and 3 (complex)
ATP	Adenosinetriphosphate
B	Basic domain
BMDC	Bone marrow-derived (murine) DC
BSA	Bovine serum albumin
C	Central domain
C terminus	Carboxyl terminus
CBS	Cortactin binding site
CCL19	Chemokine (C-C motif) ligand 19
CCL21	Chemokine (C-C motif) ligand 21
CCR7	Chemokine (C-C motif) receptor 7
CD	Cluster of differentiation
cDC	Conventional DC
Cdc42	Cell division cycle protein 42
cDNA	Complementary DNA
cPPT	Central polypurine tract
CR16	Glucocortocoid-regulated protein
CT	Cycle time
CTS	Central termination sequence
DAPI	4,5-Diamino-2-phenylindole
DC	Dendritic cell
DC-SIGN	DC-specific intercellular adhesion molecule 3-grabbing non-integrin
DDC-IDC	Dermal DC or interstitial DC
DEC205	Dendritic and epithelial cell, 205KDa
DMSO	Dimethylsulphoxide
DNA	Deoxyribonucleic acid
dNTP	deoxyribonucleotide
dsDNA	Double-stranded DNA
dsRNA	Double-stranded RNA
dUTP	Deoxyuridinetriphosphate
EboZ	Ebola Zaire virus (glycoprotein)
ECL	Enhanced chemiluminescence
ECM	Extracellular matrix
EDTA	Ethylenediaminetetraacetic acid
eGFP	Enhanced green fluorescent protein
ELISA	Enzyme-linked immunosorbent assay
EMS1	Cortactin
EVH1	WASp homology domain 1 or Ena/VASp homology domain 1
FACS	Fluorescence activated cell sorting
F-actin	Filamentous actin
FC	Flow cytometry
FCS	Fetal calf serum
FS	Forward scatter
FT	Fourrier Transform
g-Actin	Globular actin
GAPDH	Glyceraldehyde-3-phosphate dehydrogenase
GBD	GTPase binding domain
GFP	Green fluorescent protein

GMCSF	Granulocyte-macrophage colony stimulating factor
gp64	*Autographica californica* virus glycoprotein
GTP	Guanosinetriphosphate
GTPase	Guanosinetriphosphatase
HIV	Human immunodeficiency virus
HRP	Horseradish peroxidase
HS1	Haematopoietic lineage cell-specific protein 1
ICAM	Intercellular adhesion molecule 1
iDC	Immature DC
IF	Immunofluorescence
IL4	Interleukin 4
IRM	Interference reflection microscopy
LAD	Leukocyte adhesion deficiency
LB	Luria-Bertani (broth)
LC	Langerhans cell
LPS	Lipopolysaccharide
LTR	Long terminal repeat
LUT	Look-up table
MACS	Magnetic activated cell sorting
MCP-1	Monocyte chemotactic protein 1
mDC	Mature DC
MFI	Median fluorescence intensity
MHC	Major histocompatibility complex
miRNA	Micro RNA
MLR	Mixed lymphocyte reaction
MLV-A	Amphotropic Murine Leukaemia Virus
M-MLV	Moloney Murine Leukaemia Virus
MMP	Matrix metalloproteinase
MMR	Macrophage mannose receptor
moDC	Monocyte-derived DC
MOI	Multiplicity of infection
mRNA	Messenger RNA
MT1MMP	Membrane-type 1 MMP
N terminus	Amino terminus
N-WASp	Neural WASp
OD	Optical Density
PBMC	Peripheral blood mononuclear cells
PBS	Phosphate buffered saline
PCR	Polymerase chain reaction
pDC	Plasmacytoid DC
PEI	Polyethylenimine
PFA	Paraformaldehyde
PHA	Phytohemagglutinin
PIP_2	Phosphatidylinositol-4,5-bisphosphate
PIP_3	Phosphatidylinositol-3,4,5-trisphosphate
PolyP	Proline-rich region
pre-miRNA	Precursor miRNA
pri-miRNA	Primary miRNA
PSTPIP1	Proline-serine-threonine phosphatase interacting protein 1
RISC	RNA-induced silencing complex
RNA	Ribonucleic acid
RNAi	RNA interference
ROI	Region of interest
RRE	Rev-responsive element
RRV	Ross River virus (glycoprotein)
RSV	Rous sarcoma virus
RT	Reverse transcriptase
RT	Room temperature
RT-qPCR	Reverse transcriptase quantitative PCR
SCAR	Suppressor of G-protein coupled cyclic AMP receptor
SDS-PAGE	Sodiumdodecylsulfate polyacrylamide gel electrophoresis
SFFV	Spleen focus forming virus (5'-LTR promoter)
SH2	Src homology 2 domain
SH3	Src homology 3 domain

SHD	SCAR homology domain
shRNA	Short hairpin RNA
SIN	Self-inactivating (virus)
siRNA	Small interference RNA
SS	Side scatter
ssRNA	Single-stranded RNA
TAE	Tris-Acetate EDTA (buffer)
TBS-T	TRIS buffered saline with 0.1% Tween
TCR	T-cell receptor
TCR	The RNA Consortium
TIRF	Total internal reflection fluorescence microscopy
TLR	Toll-like receptor
TOCA-1	Transducer of Cdc42-dependent actin assembly 1
UNT	Untransduced
V	Verpolin homology domain
VSVg	Vesicular stotamitis virus glycoprotein
WAS	Wiskott-Aldrich syndrome
WASH	WASp and SCAR homolog
WASp	Wiskott-Aldrich syndrome protein
WAVE	WASp family verpolin-homology protein
WB	Western blot
WBD	WASp/N-WASp binding domain
WHAMM	WASp homolog associated with actin, membranes and microtubules
WHD	WASp homology domain
WICH or WIRE	WIP and CR16 homologous protein or WIP related protein
WIP	WASp interacting protein
WPRE	Woodchuck hepatitis virus post-transcriptional regulatory element
XLN	X-linked neutropenia
XLT	X-linked thrombocytopenia

ACKNOWLEDGEMENTS

My first and deepest thanks go to Siobhán. Your guidance and scientific expertise were invaluable throughout the whole of this study, but most of all I would like to express my sincere gratitude for your patience, enthusiasm, support and encouragement without which I would not have been able to complete this endeavour. I am also especially grateful to Adrian, a source of precious discussion, advice and inspiration.

A more general word of thanks goes to all those at the Molecular Immunology Unit, ICH, not only for the technical and scientific support and assistance, in particular from the DC and WASp groups, but mostly for the warm welcome to London, the endless discussions in between science, the companionship, and the friendship. I feel very lucky to have shared these years with a few generations at MIU, all of whom have made it a fantastic place to work.

To the ones I love, not enough words can describe how grateful I am. A word of thanks goes to my parents and brother for their support in all its forms over these years. A special word to Maria João, who, even though from a distance, has helped to keep me sane with her uncompromised endless support and kindness. And finally, the greatest thank you has to be to my friends, for their love and generosity expressed in selfless words of enthusiasm in the worse times of this adventure but, and above all, with whom I have learned so much and with whom I have lived the most wonderful moments.

I wish to dedicate this thesis to my true London family: Pop, Aninhas, Alex, Nuno, Rita, Joana and Pedro. You have made this possible. Thank you for your friendship.

To my family

Chapter

1

INTRODUCTION

1.1 Podosomes and invadopodia

1.1.1. Podosomes

Podosomes are specialised adhesion structures found in monocyte-derived cells, such as macrophages, immature dendritic cells (DC) and osteoclasts. They are, in fact, the most prominent actin and adhesive structures found in these cells [Burns et al. 2001; Marchisio et al. 1984; Marchisio et al. 1987]. *In vitro*, when cells are plated in 2D systems, such as a glass slide coated with proteins from the extracellular matrix (ECM), the basal surface of the cells becomes in contact with the substrate. When monocyte-derived cells are cultured on such systems, they change their morphology from the round shape they present in suspension and spontaneously adhere to the substrate, extend large lamellipodia and spread. Usually they become polarised and initiate a migratory process. In the presence of specific chemoattractants, they may present directed migration towards the source of those signals, but even without such chemokines, they still present random migration on the 2D surface [Jones 2000]. When the actin cytoskeleton of these cells is visualised, the presence of dot-like structures at the ventral side of the cells is striking, particularly arranged in clusters behind the leading edge of migrating cells. These dense F-actin cores are surrounded by rings of integrins, which are transmembrane proteins

involved in the recognition of and attachment to extracellular matrix components and responsible for cell adhesion. These structures are called podosomes.

The term 'podosome' was coined in 1985 to designate feet-like protrusion of the ventral cell surface of fibroblasts transformed with Rous sarcoma virus (RSV). These structures were described as dot-shaped adhesive sites that represent close contact with the substratum. They were rich in F-actin, α-actinin and tyrosine-phosphorylated proteins as well as in vinculin, though vinculin presented a more peripheral staining evocative of a ring surrounding the actin core [Davidpfeuty and Singer 1980; Tarone et al. 1985]. Further investigations on these structures in RSV-transformed fibroblasts revealed that viral oncogenes encoding protein kinases from the Src family were what induced the rearrangement of normal fibroblast adhesion plaques into podosomes. By then, the only non-transformed cells that were known to form podosomes were monocyte-derived cells, particularly macrophages and osteoclasts [Marchisio et al. 1987]. However, podosomes have now been identified in a variety of other non-transformed cell types *in vitro*. For example, they can be found or induced in vascular smooth muscle cells [Hai et al. 2002], endothelial cells [Moreau et al. 2003] and epithelial cells [Spinardi et al. 2004].

In all cell types, podosomes present as short protrusions of the ventral cell surface that form close contact with the underlying substratum and constitute sites of cell adhesion. They present the distinctive morphology of a dense F-actin core, where actin-associated proteins, such as regulators of actin polymerisation, concentrate, surrounded by an adhesive ring where integrins are clustered together with integrin-associated proteins like vinculin and talin [Linder and Aepfelbacher 2003].

In 1989, the biological activity of local ECM degradation was attributed to podosome rosettes in RSV-transformed fibroblasts. These structures were therefore re-named 'invadopodia' [Chen 1989]. The term invadopodia was from then on used to designate actin protrusions of the basal cell membrane of transformed or cancer cells with an active focal ECM degradation activity. Since ECM degradation had not yet been attributed to podosomes in non-transformed cells, the term podosome became specific for those adhesion structures found in non-transformed cells.

1.1.2. Invadopodia vs. podosomes

Podosomes and invadopodia share several of their molecular components and both have the characteristic structure of a dense F-actin core surrounded by adhesion and scaffolding proteins [Gimona and Buccione 2006]. Nevertheless, they present fundamental structural differences. Invadopodia are typically long protrusions of the ventral cell membrane, found in cancer cells or transformed cells [Weaver 2006]. When compared to

podosomes, invadopodia are much larger (diameter of 8μm and several μm deep) than the minimal protrusions of podosomes (diameter of 1-2μm and depth of approximately 0.2-0.4μm) [Buccione et al. 2004]. Invadopodia are also more stable, with half-lives of hours, whereas podosomes have an average life-time of minutes [Baldassarre et al. 2003; Destaing et al. 2003; Kanehisa et al. 1990; van Helden et al. 2006; Yamaguchi et al. 2005]. One hallmark of invadopodia has been their localised ECM degradation activity. In fact, cancer progression and metastasis via local ECM degradation and protrusive migration have been strongly associated with invadopodia ever since their discovery [Linder and Aepfelbacher 2003; Weaver 2006]. Although podosomes have recently also been shown to co-localise with sites of focal ECM degradation, these are much shallower than those associated with invadopodia and it is not clear whether podosomes are involved in protrusive migration or merely in ECM sensing and remodelling [Linder 2007; Linder and Aepfelbacher 2003].

1.1.3. Invadosomes

Since 1985 there has been an expansion of research into podosomes and invadopodia with the uncovering of more associated proteins, stimuli for formation and regulation and the pursuit for *in vivo* relevance. This has led to obfuscation of the previously clear difference between podosomes and invadopodia. Initially, podosome formation was thought to be restricted to haematopoietic monocyte-derived cells. However, more and more cell types are currently acknowledged to form podosomes or podosome-like structures [Buccione et al. 2004; Linder and Aepfelbacher 2003]. Moreover, the ECM degradative function, which was initially thought to be restricted to invadopodia, has now also been associated with podosomes [Linder 2007; Linder and Aepfelbacher 2003]. As more information on both structures' molecular composition, biological functions and regulation arose and cell-type specific variations further complicated a precise assignment of the particular structure to one or another category, in 2008 the term 'invadosome' appeared to encompass all F-actin adhesive structures involved in ECM degradation. Underlying this new concept is the idea that podosomes and invadopodia may, in essence, be the same structure, with differences in manifestation due to the cell-type [Gimona et al. 2008].

The expression of either podosomes or invadopodia is closely related to the cellular context as the specific cell-type imposes differences in molecular composition and consequently in the structure, regulation and biological function of these structures [Gimona and Buccione 2006]. In this thesis I adopt the term podosomes for the structures formed in normal cells and invadopodia for structures found in cancer cells or transformed cells [Murphy and Courtneidge 2011]. Additionally, I further distinguish between two types of podosomes based on the cell type (and intrinsic molecular differences between cells): leukocyte podosomes and non-haematopoietic-cell podosomes. Finally, within

the former, it is useful to differentiate the podosomes formed by osteoclasts from those found in macrophages and DC due to marked differences in podosome morphology, organisation and function.

1.2 Podosome components

The molecular components of podosomes can be discussed on the basis of the morphology of these structures. They can, thus, be divided into: molecules localised to the core of the podosomes, related to the actin polymerisation machinery and its regulation; and components found in the adhesive ring of the podosomes, mainly integrins and integrin-associated proteins.

1.2.1. Actin core

Actin filament assembly

The podosome actin core is its most evident feature when the cytoskeleton of cells assembling podosomes is imaged by immunofluorescence. Actin is the most abundant protein in eukaryotic cells. It is a small 43KDa protein that can exist in the cell as monomeric actin (globular actin, g-actin) or as polymerised filaments (F-actin), constituting the actin cytoskeleton. This is what confers structure to a cell and the dynamic rearrangement of the actin cytoskeleton allows the cell to change its shape, for example for adhesion and migration.

Polymerisation of actin results in a double stranded right handed helix which is polarised due to the different affinity of ATP-bound g-actin for each end of the actin filament. The barbed or positive end elongates faster than the pointed or negative end. In biological systems, where there is limited concentration of available actin monomers, depolymerisation is favoured at the pointed end of existing actin filaments at similar rates to filament elongation occurring at the barbed end. This results in the generation of protrusive forces in the direction of the barbed end of the actin filaments. These forces generated by the actin cytoskeleton are what enables the cell to change its shape [Holmes et al. 1990; Kirschner 1980; Wegner 1982].

In order to control the expansion of F-actin networks, the cell has to control the number of barbed ends and their elongation rate. Capping proteins, such as gelsolin, bind the barbed ends of actin filaments with high affinity preventing further elongation. The blocking of the filament's barbed end results in an accumulation of ATP-bound actin monomers which promotes nucleation and filament branching. In contrast, capping of the pointed end by proteins such as spectrin or the Arp2/3 (Actin Related Proteins 2 and 3) complex blocks depolymerisation and results in longer filaments [Mullins et al. 1998; Rogers et al. 2003; Schafer et al. 1996]. The actin depolymerising factor (ADF/cofilin) family of proteins can bind actin subunits within the filaments and destabilise the helical structure leading to filament severing, resulting in shorter filaments and new barded and pointed ends. The availability of g-actin at the barbed ends can be controlled by proteins such as thymosin β_4, which sequesters monomeric actin, or profilin, which catalyses the exchange of ADP for ATP in actin monomers and shuttles actin subunits to the growing barbed end [Loisel et al. 1999; Pantaloni and Carlier 1993]. Finally, nucleation of actin monomers generates new actin filaments. In fact, actin polymerisation is not spontaneous and initiators or nucleators, such as the Arp2/3 complex, are necessary due to the inherent instability of actin dimers and trimers [Millard et al. 2004].

The Arp2/3 complex

The podosome actin core consists of a dense matrix of filamentous actin which is specifically organised by the Arp2/3 complex-dependent actin polymerisation machinery [Blundell et al. 2010; Monypenny et al. 2011]. The Arp2/3 complex is a multi-protein complex composed of 7 subunits that act as an actin nucleator. Arp2 and Arp3 are structurally similar to actin and it is hypothesised that these two subunits, together with an Arp2/3 activator such as a WASp/SCAR family protein (see below), can mimic the barbed end of an existing actin filament, thus enabling the generation of a new filament [Kelleher et al. 1995; Machesky et al. 1994; Robinson et al. 2001; Welch et al. 1997]. Arp2/3 initiates the polymerisation of a new actin filament anchored to an existing one with a 70° angle. Hence, activation of the Arp2/3 complex results in a meshwork of short branched actin filaments with a high density of barbed ends [Millard et al. 2004; Mullins et al. 1998] (Figure 1.1 B and C). Arp2/3 has been shown to be essential for several actin-dependent cellular processes including podosome formation. For example, competitive displacement of the Arp2/3 complex from macrophage podosomes by an Arp2/3-binding peptide resulted in the disappearance of podosomes [Linder et al. 2000].

WASp/N-WASp

In order for the Arp2/3 complex to act as an actin nucleator, a conformational change of the complex is required. A variety of proteins can activate the Arp2/3 complex, most notably proteins from the WASp/SCAR family [Kurisu and Takenawa 2009; Machesky et al. 1999]. The WASp/SCAR family of actin regulators consists of five members (Figure 1.1 A): the Wiskott-Aldrich Syndrome protein (WASp), which was the first to be identified and its expression is restricted to haematopoietic cells [Derry et al. 1994]; N-WASp (neural WASp), which is ubiquitously expressed, although with highest levels of expression in neurons [Miki et al. 1996]; 3 SCAR/WAVE proteins (suppressor of G-protein coupled cyclic AMP receptor or WASp family verpolin-homology protein) [Machesky and Insall 1998; Miki et al. 1998; Suetsugu et al. 1999]; and the 2 recently identified new members of this family WASH (WASp and SCAR homolog) [Linardopoulou et al. 2007] and WHAMM (WASp homolog associated with actin, membranes and microtubules) [Campellone et al. 2008]. All these proteins present a common homologous domain at their C-terminus called the VCA domain (verpolin homology domain, central domain and acidic domain). It is the binding of the VCA domain of a WASp/SCAR family protein to the Arp2/3 complex what activates Arp2/3. This interaction is required to initiate actin polymerisation [Higgs et al. 1999; Machesky and Insall 1998]. In addition to the VCA domain, proteins from the WASp/SCAR family also present a proline-rich region (polyP) adjacent to the VCA domain and a basic domain towards the N-terminus. WASp and N-WASp also have an EVH1 domain at the N-terminus (WASp homology domain 1 or Ena/VASp homology domain 1) and a central GTPase-binding domain (GBD). N-WASp shows approximately 50% homology with WASp and its domain structure is very similar to that of WASp, with the addition of a second V domain adjacent to the VCA.

Both WASp and N-WASp play non-redundant roles in podosome-related actin polymerisation. In non-haematopoietic cells, which lack WASp expression, N-WASp localises to and is critical for podosome formation [Mizutani et al. 2002; Moreau et al. 2003; Osiak et al. 2005; Spinardi et al. 2004] as well as for invadopodia formation [Yamaguchi et al. 2005]. In haematopoietic cells, which express both proteins, WASp localises with the Arp2/3 complex to the base of the actin core of podosomes, close to the basal membrane, where *de novo* actin polymerisation takes place [Burns et al. 2001; Calle et al. 2006a]. Moreover, podosome formation in leukocytes is dependent on functional WASp [Burns et al. 2001; Calle et al. 2004b; Linder et al. 1999]. RNAi-induced WASp depletion by just 40% prevented podosome formation in DC [Olivier et al. 2006] and reconstituting WASp expression in DC from WASp null mice or in macrophages and DC from patients with WAS (Wiskott-Aldrich Syndrome, a primary immunodeficiency caused by lack of functional WASp expression – see Section 1.5.1 Podosomes in human disease – the Wiskott-Aldrich Syndrome) could restore podosome formation [Charrier et al. 2005; Dewey et al. 2006]. N-WASp is expressed in myeloid cells at about one tenth of the level of WASp [Isaac et al. 2010]. N-WASp was found predominantly in vesicular compartments rather than in

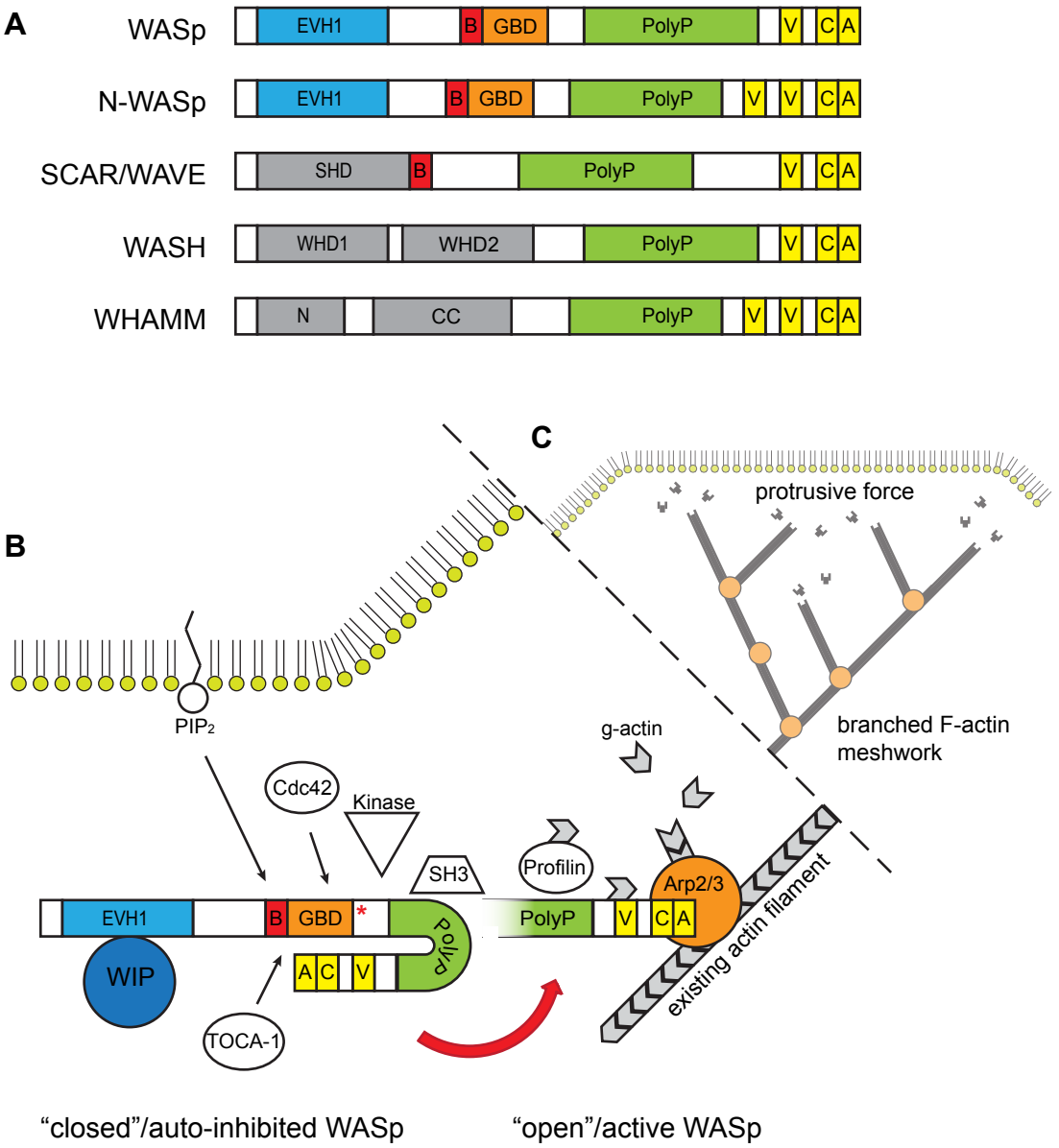

Figure 1.1. WASp/SCAR family of proteins and activation of Arp2/3-mediated actin polymerisation by WASp.

A The structure of the proteins comprising the WASp/SCAR family of actin regulators is presented. **B** Schematic representation of the mechanism of Arp2/3 activation by WASp. In resting conditions, WASp exists in a "closed"/auto-inhibited conformation bound to WIP via its EVH1 domain. Recruitment of WASp to sites of active actin polymerisation close to the plasma membrane may occur via PIP_2 (phosphatidylinositol-4,5-bisphosphate). Disruption of the auto-inhibited conformation of WASp and consequent exposure of its "effector" VCA domain is mediated by proteins such as the GTPase Cdc42 and TOCA-1. Several SH3-domain containing proteins can modulate WASp activity via interaction with the proline-rich domain. Phosphorylation of the WASp tyrosine Y291 (indicated with a red asterisk) is an important step in WASp activation. Once in the "open" conformation, WASp can bind the Arp2/3 complex, which docks to an existing actin filament and is able to initiate actin polymerization, resulting in a new actin filament at a 70° angle. Monomeric actin may be fed to the starting new actin filament by binding first to the V domain of WASp. Profilin can also interact with the proline-rich region of WASp and recycle actin monomers to the barbed end of the new actin filament. **C** This results in a branched F-actin meshwork with high density of barbed ends that exerts a protrusive force in the direction of the actin filaments' barbed ends. WASp: Wiskott-Aldrich syndrome protein; N-WASp: neural-WASp; SCAR/WAVE: suppressor

podosomes in murine DC and in both vesicular compartments as well as in podosomes in the murine macrophage cell line RAW/LR5 [Calle et al. 2006a; Nusblat et al. 2011]. RAW/LR5 macrophages with reduced expression of N-WASp using RNAi were able to assemble podosomes similarly to control cells. However, even though those cells presented normal podosomes, they were unable to degrade the ECM as efficiently [Nusblat et al. 2011]. N-WASp was suggested, when in physiological levels, to play a role in recruitment of the matrix metalloproteinase MT1MMP to podosomes to enable podosome-mediated ECM degradation Over-expression of N-WASp in RAW/LR5 cells depleted of WASp expression was able to compensate for the lack of WASp, specifically in regards to the morphological changes, chemotaxis deficiency and loss of podosomes following WASp depletion suggesting possible degree of redundancy between the two proteins [Isaac et al. 2010].

WASp/N-WASp regulators

WASp and N-WASp lack any catalytic domain. Instead, they act upon the Arp2/3 complex via their "effector" VCA domain to activate actin polymerisation (Figure 1.1 B). WASp and N-WASp naturally exist in an inactive auto-inhibited conformation where the VCA domain is hidden and inaccessible to the Arp2/3 complex. This is due to the intra-molecular interaction between the VCA domain and the basic and GBD regions of the protein. Upon WASp activation, the protein assumes an "open", or active, conformation where the VCA domain can interact with and activate the Arp2/3 complex and actin nucleation is promoted [Kim et al. 2000; Panchal et al. 2003; Prehoda et al. 2000]. Mutations in the GBD region where the VCA domain binds and which prevent that intramolecular interaction render WASp constitutively active. This is the basis of another WASp-related primary immunodeficiency called X-linked neutropenia (XLN), which is the result of uncontrolled actin polymerisation [Ancliff et al. 2006; Beel et al. 2009; Devriendt et al. 2001].

The modular domain structure of WASp and N-WASp allows binding and interaction with several different proteins and phospholipids. In this way, WASp/N-WASp acts as a hub for integrating inputs from several signalling cascades. The balance between activating and inhibitory factors is then translated to the actin cytoskeleton via regulation of the actin polymerisation activity of the Arp2/3 complex.

---

of G-protein coupled cyclic AMP receptor or WASp family verpolin-homology proteins 1-3; WASH: WASp and SCAR homolog; WHAMM: WASp homolog associated with actin, membranes and microtubules; EVH1: WASp homology domain 1 or Ena/VASp homology domain 1; B: basic domain; GBD: GTPase-binding domain; PolyP: proline-rich region; V: verpolin homology domain; C: central domain; A: acidic domain; SHD: SCAR homology domain; N: N-terminal domain with no significant homology to known proteins; CC: coiled-coil domain; WHD1 and 2: WASH homology domain 1 and 2; WIP: WASp interactin protein.

Several kinases, small GTPases and other regulatory proteins are recruited to the podosome core where they jointly regulate actin polymerisation via fine-tuning of WASp activity [Blundell et al. 2010; Monypenny et al. 2011]. WASp and N-WASp are directly activated by the Rho-type GTPase Cdc42 and podosome formation is dependent on this activator [Burns et al. 2001; Dovas et al. 2009]. Cdc42 binds WASp and acts by destabilising its auto-inhibitory conformation [Hemsath et al. 2005; Kim et al. 2000]. The phosphatidylinositides PIP_2 and PIP_3 are the predominant phosphatidylinositides throughout the cell and are important regulators of actin polymerisation. They are anchored to the cytosolic side of the plasma membrane and particularly concentrated at sites such as membrane ruffles. PIP_2 can modulate the activity of most groups of actin binding proteins, including Rho GTPases and WASp. PIP_2 has been proposed to act synergistically with Cdc42 in WASp/N-WASp activation, in a process mediated by TOCA-1 (transducer of Cdc42-dependent actin assembly 1) [Higgs and Pollard 2000; Ho et al. 2004]. Moreover, PIP_2 can bind the EVH1 domain of N-WASp and a similar interaction has been proposed to be responsible for WASp localisation to the cell membrane [Miki et al. 1996; Prehoda et al. 1999].

Phosphorylation of WASp/N-WASp in tyrosine and serine residues has also been shown to play a role in the regulation of activity. Constitutively phosphorylated serine residues in the VCA domain of WASp (S483 and S484) increase actin polymerisation by enhanced Arp2/3 binding [Cory et al. 2003]. Additionally, non-receptor tyrosine kinases, which have important roles in signalling downstream of activation of surface receptors, can both activate GTPases and directly phosphorylate WASp/N-WASp. WASp has been demonstrated to be tyrosine phosphorylated following a range of cell stimuli. A single conserved tyrosine phosphorylation site (Y291 in WASp and Y256 in N-WASp) is the target for a number of non-receptor tyrosine kinases such as Btk, Fyn and Hck. Phosphorylation of this tyrosine residue located in the GBD (region involved in the intramolecular interaction with the VCA domain when WASp is in the "closed" conformation) has been shown to activate WASp, presumably by destabilizing the auto-inhibited conformation [Cory et al. 2002; Suetsugu et al. 2002; Torres and Rosen 2003]. Moreover, Y291 phosphorylation may facilitate binding of SH2-domain containing proteins and sustain WASp activation [Cory et al. 2002; Torres and Rosen 2003]. Studies using phospho-mimicking (Y-tyrosine to E-glutamic acid) or phospho-dead (unphosphorylatable, Y-tyrosine to F-phenylalanine) WASp mutants have demonstrated that tyrosine phosphorylation of WASp is not only a key regulator of its activity but also of its stability. WASp activation and Y291 phosphorylation is associated with enhanced protein degradation, providing a pathway for down-regulation of WASp-induced actin polymerisation [Blundell et al. 2009; Cory et al. 2002]. In murine macrophages and DC, tyrosine phosphorylation of WASp (Y293 in murine WASp) was not an absolute requirement for podosome formation. Nevertheless, the phospho-dead WASp mutant resulted in fewer podosomes and with shorter half-lives [Blundell et al. 2009; Dovas et al. 2009]. Moreover, macrophage podosome-mediated ECM degradation required WASp phosphorylation [Dovas et al. 2009]. These results suggest WASp activity is regulated by a balance between phosphorylation and dephosphoryla-

tion of the protein.

A number of proteins are able to bind the WASp polyP domain, in particular SH3-domain containing proteins. The adapter protein PSTPIP1 (Proline-Serine-Threonine phosphatase interacting protein 1) can bind the polyP region of WASp via its SH3 domain and recruit the PTP-PEST phosphatase which dephosphorylates Y291 of WASp, thereby reducing its activity [Cote et al. 2002; Wu et al. 1998]. SH3-SH2 proteins are proteins with no intrinsic catalytic domain that act as scaffolding proteins, bringing together other effector proteins. They are able to bind proline-rich regions, usually associated with actin cytoskeleton regulators, via their SH3 domains, and phosphorylated tyrosine residues, normally found in targets of non-receptor tyrosine kinases, via their SH2 domain [Chen et al. 1998]. Examples of these are Nck and Grb, which have been shown to bind the polyP region of WASp/N-WASp and mediate its activation, together with Cdc42 or PIP_2 [Carlier et al. 2000]. Moreover, Nck has been shown to be able to bind WIP (see below) and to be involved in WASp recruitment to the immune synapse of T-cells [Anton et al. 1998]. Differential localization of Grb and Nck has been reported for invadopodia and podosomes: Nck specifically localised to invadopodia but not to podosomes in macrophages or endothelial cells nor to podosome-like structures found in Src-transformed fibroblasts; in contrast, Grb did not localise to invadopodia nor to macrophage podosomes, but to podosomes formed by non-haematopoietic cells and Src-transformed cells [Oser et al. 2011].

WIP

The verpolin family of proteins plays a major role in regulating the activity of WASp-family proteins and the dynamics of actin filaments. Verpolin is a yeast protein involved in cytoskeletal organisation [Donnelly et al. 1993]. There are three mammalian verpolin homologs, all known to interact with the WASp/N-WASp EVH1 domain: WIP (WASp interacting protein) [Ramesh et al. 1997], CR16 [Ho et al. 2001] and WICH or WIRE (WIP and CR16 homologous protein or WIP related protein) [Aspenstrom 2002; Kato et al. 2002]. Whereas CR16 and WICH are mostly expressed in neural tissues, suggesting a role in regulating N-WASp activity, WIP is ubiquitously expressed. However, WIP is found in much higher concentrations in haematopoietic cells than in other cell types, suggesting WIP to be the physiological verpolin protein to regulate the activity of WASp [Ramesh et al. 1997].

In its structure (Figure 1.2), WIP presents a double V domain at the N-terminus, via which it can directly interact with the Arp2/3 complex. It also presents profilin binding sites capable of binding actin. These domains enable WIP to stabilise actin filaments by binding F-actin and profilin [Martinez-Quiles et al. 2001]. WIP can also bind WASp directly, specifically to the EVH1 domain of WASp, via a WASp/N-WASp binding domain

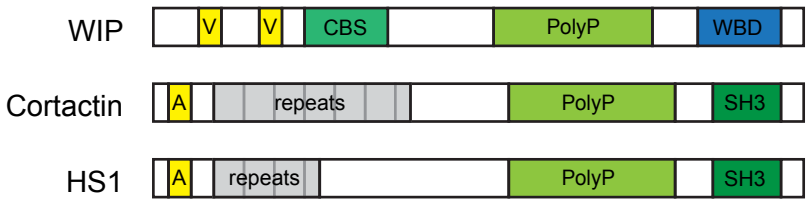

Figure 1.2. Structure of WIP, cortactin and HS1.
Schematic representation of the structure of WIP, cortactin and HS1. V: verpolin homology domain; CBS: cortactin binding site; PolyP: proline-rich region; WBD: WASp/N-WASp binding domain; A: acidic domain; repeats: 37 amino-acid repeats; SH3: Src homology 3 domain, via which cortactin can bind WIP.

(WBD) at the C-terminus, and this is considered to be a key feature of WIP. In resting lymphocytes most of WASp is constitutively found in a complex with WIP [de la Fuente et al. 2007; Sasahara et al. 2002]. WIP binding has been demonstrated to protect WASp from constitutive degradation by calpain and proteasome. As a consequence, the cytosolic level of WIP in haematopoietic cells determines that of WASp. For example, in a murine WIP knockout model WASp is also found to be deficient [Chou et al. 2006; de la Fuente et al. 2007; Konno et al. 2007]. Recent results analysing the function of WASp with clinically relevant mutations in the EVH1 domain, which confer low affinity for WIP, resulting in XLT (X-linked thrombocytopenia), a mild form of WAS with reduced expression levels of WASp, suggest a role for WIP not only in stabilising WASp but also in regulating WASp activity (Austen Worth, unpublished results). WIP has been shown to also bind cortactin, another actin polymerisation regulator also implicated in podosome actin dynamics, via a proline-rich region at the carboxyl end of the double V domain [Kinley et al. 2003].

WIP has been localised to endothelial cell podosomes [Moreau et al. 2003], murine osteoclast podosomes [Chabadel et al. 2007], murine splenic DC podosomes [Chou et al. 2006] and human primary and THP1-derived macrophage podosomes [Monypenny et al. 2011; Tsuboi 2007]. Moreover, it has been shown to be necessary for podosome formation and function. DC from a murine WIP null model show impaired podosome formation and this was not rescued by restoring WASp levels through pharmacological inhibition of WASp degradation using calpain inhibitors [Chou et al. 2006]. Moreover, blocking of WASp-WIP binding abrogated podosome formation in human macrophages and resulted in reduced cell polarization and inhibited chemotaxis [Tsuboi 2006]. WIP has been suggested not only to protect WASp from degradation but also to facilitate its localisation to podosome sites possibly by interacting with other adaptor proteins [Chou et al. 2006]. WIP has been implicated in podosome ECM degradation function. WIP null osteoclasts displayed reduced bone-resorbing activity even when podosome formation was rescued by activation of the CD44 receptor, found in the podosome cores of these cells [Chabadel et al. 2007]. Additionally, in splenic murine DC WIP was shown to be important for the recruitment of matrix metalloproteinases to podosome sites via interaction with cortactin [Banon-Rodriguez et al. 2011].

Cortactin and HS1

Cortactin (or EMS1) was first identified as an 85KDa substrate of Src-tyrosine kinase [Kanner et al. 1990; Schuuring et al. 1993; Wu et al. 1991]. In its structure (Figure 1.2) cortactin presents a central proline-rich region with 3 tyrosine phosphorylation sites. A variety of adaptor proteins can interact with cortactin via its phosphorylated tyrosines, which enable binding of SH2-domain containing proteins. Cortactin presents 6.5 37 amino-acid repeat motifs (cortactin repeats) which promote binding to and stabilisation of actin filaments, inhibiting filament debranching [Weaver et al. 2001; Weed et al. 2000]. The acidic N-terminal region of cortactin contains an acidic conserved sequence which enables binding to and activation of the Arp2/3 complex. Together with the F-actin binding region it is thought to stabilise the interaction of the Arp2/3 complex with actin filaments, inducing actin polymerisation [Uruno et al. 2001; Weaver et al. 2001]. An SH3 domain is present towards the C-terminal region. Cortactin binds WASp and N-WASp via this domain, colocalises with WASp/N-WASp at sites of active actin polymerisation, and acts synergistically with WASp/N-WASp resulting in enhanced Arp2/3 activation [Weaver et al. 2001]. The SH3 domain of cortactin is also responsible for WIP binding, which stimulates cortactin-mediated Arp2/3 activation. Moreover, interaction with cortactin has been suggested to be important for WIP localisation to actin polymerisation sites [Kinley et al. 2003].

Cortactin commonly co-localises with F-actin sites of dynamic peripheral membrane activity and it has been shown to contribute to cell polarity and lamellipodia formation [Kempiak et al. 2005; Weed et al. 2000]. Elevated gene levels of cortactin are associated with cancer progression in a variety of different human malignancies correlating with poor patient prognosis [Rodrigo et al. 2000; Schuuring 1995]. This has been proposed to be due to enhanced cell motility, invasion and metastasis [Huang et al. 1998; Li et al. 2001; Patel et al. 1998]. Cortactin has been shown to localise to and to be necessary for the formation of Src-transformed fibroblast podosome rosettes and invadopodia [Artym et al. 2006; Bowden et al. 1999; Wu et al. 1991] as well as podosomes in non-haematopoietic cells [Webb et al. 2006] and in osteoclasts [Chabadel et al. 2007; Tehrani et al. 2006]. Cortactin has also been shown to localise to murine splenic DC podosomes [Chou et al. 2006]. Colocalisation of cortactin and phosphotyrosine residues has been used to identify matrix-degrading invadopodia [Bowden et al. 2006]. Knock-down of cortactin inhibits invadopodia formation in carcinoma cells [Artym et al. 2006] and podosome formation in osteoclasts [Tehrani et al. 2006]. While most of the focus has been on the role of cortactin in actin assembly, recent data suggests that the primary role of cortactin may be in promoting protease secretion at invadopodia. Cortactin may link vesicular trafficking and dynamic actin polymerisation to regulate protease secretion for ECM degradation [Clark and Weaver 2008]. A similar role has been proposed for cortactin in splenic murine DC, where its interaction with WIP has proven to be necessary for cortactin localisation to podosomes as well as for efficient podosome-mediated ECM

degradation [Banon-Rodriguez et al. 2011].

Haematopoietic cells generally express the cortactin homolog HS1 (haematopoietic-lineage cell-specific protein 1). This 75KDa protein was originally isolated from a B-cell cDNA library and then independently isolated as a target for tyrosine phosphorylation in lymphocytes following antigen receptor engagement [Fukamachi et al. 1994; Kitamura et al. 1989; Kitamura et al. 1995; Takemoto et al. 1995; Yamanashi et al. 1993]. HS1 is closely related to cortactin (Figure 1.2). It presents 3.5 cortactin repeats and a coiled-coil domain in the central region which mediate binding to actin filaments as well as an acidic N-terminal domain necessary for Arp2/3 complex binding, all of which are required for HS1-induced Arp2/3 activation [Hao et al. 2005; Uruno et al. 2003] In the carboxyl terminus HS1 presents an SH3 domain with great homology to that of cortactin, enabling HS1 to act synergistically with N-WASp to induce Arp2/3 complex-mediated actin polymerisation [Uruno et al. 2003] and enabling HS1 to bind WIP as well [Dehring et al. 2011]. In the central proline-rich region HS1 has several tyrosine phosphorylation sites, similar to cortactin.

HS1 is rapidly phosphorylated downstream of platelet activation and translocated to the plasma membrane [Brunati et al. 2005; Kahner et al. 2008]. In lymphocytes, HS1 is phosphorylated by Syk and Src kinases as a result of antigen-receptor crosslinking and it is involved in the signal transduction pathway leading to clonal expansion and clonal deletion in thymic negative selection [Brunati et al. 1999; Taniuchi et al. 1995]. Phosphorylation of HS1 precedes translocation of the protein to lipid rafts, where it colocalises with WASp and the Arp2/3 complex [Hao et al. 2004]. HS1 has also been implicated in immune synapse and lytic synapse dynamics, being rapidly and transiently phosphorylated following cell activation [Brunati et al. 2005; Butler et al. 2008; Carrizosa et al. 2009; Gomez et al. 2006; Huang et al. 2008; Yamanashi et al. 1993]. Moreover, HS1 localises to the immune-synapse and it is required for the stabilisation of such actin structures, as T-cells are able to form actin-rich lamellipodia after TCR (T-cell receptor) engagement but these collapse rapidly in the absence of HS1 [Carrizosa et al. 2009; Gomez et al. 2006]. Moreover, HS1 has been linked to cellular adhesion and migration. The lack of HS1 in B-cells results in diminished cell adhesion and migration [Scielzo et al. 2010]. In NK cells HS1 phosphorylation controls NK cell adhesion to ICAM (intercellular adhesion molecule 1), via CD18 activation, lytic synapse formation and NK cell chemotaxis [Butler et al. 2008].

The function of HS1 has only very recently started to be investigated in myeloid cells. In bone marrow-derived murine DC (BMDC) HS1 localised to lamellipodial protrusions and podosomes and was demonstrated to be involved in lamellipodial dynamics, directional migration and podosome array organisation and localisation [Dehring et al. 2011]. HS1 localisation required its interaction with the WASp-WIP complex via WIP binding, in a similar way to what was reported for cortactin in murine splenic DC. However, in contrast with cortactin, HS1 was not necessary for efficient BMDC podosome-mediated ECM degradation [Banon-Rodriguez et al. 2011; Dehring et al. 2011].

1.2.2. Adhesive ring

Integrins

Adhesion molecules, in particular integrins, are specifically recruited to the podosome rings, surrounding the actin core. Integrins are a large family of transmembrane heterodimer proteins, each assembled by non-covalent association of one α and one β subunit. At present, 18 α and 8 β subunits have been identified in mammals, giving rise to 24 αβ pairs [Hynes 2002]. Integrins mediate cell-cell and cell-matrix adhesion, with different integrin heterodimers showing specificity for different ligands, and link the extracellular environment with the cell cytoskeleton [Hogg et al. 2011; Kinashi 2005].

Integrins at the surface of cells can present different avidities for their substrates. Conformational changes to the integrin structure, which regulate their affinity for the substrate, in combination with clustering of integrin molecules (increasing the number of receptor-ligand bonds) dictate the strength of adhesions [Carman and Springer 2003]. This enables for rapid, dynamic and localised integrin activation, independent of overall cell surface expression [Hogg et al. 2011; Kinashi 2005]. Integrins present short intracellular tails and long extracellular regions with multiple domains including a globular ligand-binding headpiece. The general model for integrin activation proposes a structural change from a "closed" or "bent" conformation, where the ligand-binding headpiece is hidden facing down towards the plasma membrane, to an "open" or "extended" conformation, with the headpiece away from the cell membrane and accessible to the ligand [Takagi and Springer 2002]. Changes in the avidity of integrins, by conformational integrin activation and clustering, can be triggered both from inside the cell, via signalling pathways downstream of other cellular receptors ("inside-out signalling"), or from outside of the cell via ligand binding, the integrins functioning as signal receptors and resulting in propagation of intracellular signals ("outside-in signalling").

By mediating cell-cell and cell-substrate adhesion, integrins are crucial both in embryonic development and tissue homeostasis [Hynes 1992]. Integrins are particularly important for several immunological functions. For example, integrin activation has been proposed to be necessary for leukocyte arrest on endothelial cells, extravasation from blood vessels, migration into lymphoid or inflamed tissues, and formation of the immune synapse between T-cells and antigen-presenting cells (APC) [Constantin et al. 2000; Monks et al. 1998; Springer 1995]. Failure to activate integrins, particularly the leukocyte restricted β_2 integrin, results in life threatening primary immunodeficiencies called Leukocyte Adhesion Deficiency (LAD) disorders (see Section 1.5.2 Podosomes in human disease – Leukocyte Adhesion Deficiency).

Integrins are differentially expressed in different tissues and cell types. Depending on the

cellular context, podosomes can cluster β_1, β_2 or β_3 integrins. For example, β_1 heterodimers are usually found in invadopodia and in podosomes in RSV-transformed fibroblasts [Mueller and Chen 1991] and in non-haematopoietic cells such as endothelial cells [Rottiers et al. 2009]. Eosinophils also cluster β_1 integrins in their podosomes [Johansson et al. 2004]. On the other hand, the leukocyte β_2 integrin is recruited to podosomes in monocytes, macrophages and DC [Burns et al. 2004b; Calle et al. 2004a; Duong and Rodan 2000; Gregoretti et al. 1994; Zamboninzallone et al. 1989], while osteoclasts present β_3 integrins as the major integrins in their podosomes [Pfaff and Jurdic 2001; Zamboninzallone et al. 1989].

Integrin-associated proteins

Integrin activation is associated with the binding of regulatory proteins to the cytoplasmic tails of the α and β integrin chains. These interactions are required to stabilise the extracellular "open" or active integrin conformation. In fact, during inside-out integrin activation, structural changes to the integrin extracellular regions are induced by cytoplasmic tail binding proteins, which are the final effector proteins for inside-out signalling pathways. These are also the first proteins of signalling cascades during outside-in signalling, triggered by ligand binding, where the integrin acts as a receptor [Hogg et al. 2011; Kim et al. 2003; Kinashi 2005]. Moreover, the mean by which integrins link the extracellular environment with the actin cytoskeleton are integrin-associated actin-binding proteins [Calderwood et al. 2000].

Talin is an important modulator of the affinity of β_1, β_2 and β_3 integrins. Binding of talin to the integrin's cytoplasmic tail promotes parting of the α and β integrin tails and consequent extention of the extracellular region and activation of the integrin [Carman and Springer 2003; Horwitz et al. 1986]. Additionally, talin contains binding sites for actin, vinculin, tyrosine kinases and phospholipids [Calderwood et al. 2000; Jockusch et al. 1995]. α-Actinin is another cytoskeletal protein capable of binding actin and vinculin which interacts with integrins to promote the active conformation in a similar fashion to talin [Jockusch et al. 1995; Sampath et al. 1998]. Both talin and α-actinin have been localised to podosomes [Duong and Rodan 2000; Marchisio et al. 1987]. Vinculin is a further podosome component involved in bridging integrins and the actin cytoskeleton [Duong and Rodan 2000; Marchisio et al. 1987; Tarone et al. 1985]. Although vinculin is not able to bind integrins directly, it can bind both talin and α-actinin. Moreover, it can bridge F-actin and paxillin, which in turn can bind integrins [Calderwood et al. 2000; Jockusch et al. 1995; Schaller 2001]. Binding of vinculin to talin and actin is regulated by the phospholipid PIP_2 [Gilmore and Burridge 1996]. As mentioned above, PIP_2 serves as a membrane anchoring point for several signalling and cytoskeletal molecules, and is involved in localised regulation of WASp-mediated actin polymerisation [Higgs and

Pollard 2000; Miki et al. 1996; Prehoda et al. 1999] The Arp2/3 complex has also been shown to be recruited to integrin-associated vinculin, in a process dependent on PIP_2 and Rac1 and this may constitute another link between actin polymerisation and integrin-mediated attachment [DeMali et al. 2002].

Other molecules implicated in integrin activation include several kinases. For example in T-cells, following TCR engagement, there is activation of Tec family kinases, such as Itk, upstream of LFA1 ($\alpha_L\beta_2$ integrin heterodimer) activation [Woods et al. 2001]. Itk is also involved in actin polymerisation after TCR engagement or cytokine activation of T-cells, for example through localised activation of Cdc42 and WASp at the immune synapse [Labno et al. 2003]. In the case of outside-in signalling, integrin-ligand binding, for example in leukocytes LFA1-ICAM binding, initiates an integrin-proximal tyrosine phosphorylation cascade of signalling events. Src kinases which are constitutively associated with the cytoplasmic β-chain auto-phosphorylate following integrin activation and then phosphorylate nearby signalling molecules, such as Syk tyrosine kinases, thus coupling integrin activation with actin polymerisation regulation [Giagulli et al. 2006; Hogg et al. 2011].

1.2.3. Matrix metalloproteinases

One functional characteristic of both invadopodia and podosomes is localised ECM degradation. The relevance of this feature is further developed in Section 1.4.2 DC podosomes in ECM degradation. Nevertheless, the existing evidence for the presence of matrix-degrading enzymes in these structures is presented here.

Matrix metalloproteinases (MMP) are the most important enzymes in ECM remodelling and invasive migration. The human MMP family comprises 24 members which can be grouped into soluble MMP and membrane-bound MMP (MTMMP). Soluble MMP are synthesised as inactive proenzymes and become active by proteolytical removal of the prodomain once they are secreted. Membrane-bound MMP are activated intracellularly and then expressed at the plasma membrane, where they are able to degrade ECM components as well as activate soluble MMP. Additionally, they can proteolytically liberate and modify growth factors and cytokines present in the extracellular environment [van Hinsbergh et al. 2006]. The gelatinases MMP2 and MMP9 have been shown to be secreted and to catalyse degradation of the substratum at invadopodia sites [Nakahara et al. 1997; Weaver 2006]. The membrane-bound MT1MMP has also been localised to assembled invadopodia and it is considered a marker for mature invadopodia development [Artym et al. 2006]. MMP2, MMP9 and MT1MMP have been demonstrated to be present in podosomes in non-haematopoietic endothelial cells [Osiak et al. 2005; Tatin et al. 2006; Varon et al. 2006]. Similarly, MT1MMP and MMP9 have been shown to be recruited to

osteoclast podosomes [Delaisse et al. 2000; Sato et al. 1997]. It is hypothesised that recruitment of MT1MMP to podosomes may allow for a focused and locally restricted area of MMP activation [Linder 2007]. In other haematopoietic cells, like macrophages and DC, however, no localization of soluble MMP to podosomes has been demonstrated. It has been shown that ECM degradation is catalysed by MT1MMP in murine BMDC using knock-out models and MMP inhibitors [Gawden-Bone et al. 2010; West et al. 2008]. In the murine macrophage cell line RAW/LR5 transgenic MT1MMP tagged with a fluorescent marker was showen to colocalise with macrophage podosomes and recruitment of MT1MMP to podosomes was shown to be dependent on N-WASp [Nusblat et al. 2011].

1.3 Dendritic cells

Dendritic cells are haematopoietic cells that constitute a very interesting model for the study of leukocyte podosomes. During their life-cycle, DC experience dramatic rearrangements of their actin cytoskeleton imposed by changes in their specific function as the sentinel of the immune system. Migration is central to their life-cycle and immunological function. In DC, podosomes and their regulation are believed to be closely linked to the immune function of these cells. Only immature DC present podosomes and their formation is transiently upregulated upon DC activation followed by complete abrogation of the ability to assemble such structures once full maturation is established [Burns et al. 2004b; West et al. 2008].

1.3.1. Types of dendritic cells

DC were observed for the first time in 1868 by Paul Langerhans. This German medical student observed skin DC, or Langerhans cells, but mistook them for cells from the nervous system due to their morphology, presenting long stellate dendrites [Langerhans 1868]. It was not until 1973 that dendritic cells (murine splenic DC) were again described, this time as a novel cell isolated from mouse spleen [Steinman and Cohn 1973]. Since then, several types of DC have been described and isolated from almost every tissue [Banchereau et al. 2000]. The development of *in vitro* techniques to generate DC using cytokine cocktails has greatly assisted in understanding their development and, as a consequence, a classification of DC into different subsets has emerged. Such methods, though, rely on the use of cytokines such as GMCSF (granulocyte-macrophage colony stimulating factor), which

normally exists only in very low levels in steady-state, and therefore the cells derived in this way might model inflammatory rather than homeostatic types of DC [Rossi and Young 2005]. Nevertheless, human DC are bone marrow-derived leukocytes and two main types of DC can be identified: conventional cDC and plasmacytoid pDC [Rossi and Young 2005]. Follicular DC are cells with long dendritic processes which were once thought to be another subset of dendritic cells. However, they are not from haematopoietic origin and are, instead, part of the stroma of lymph node follicles. These cells do not express major histocompatibility complex II (MHCII) molecules and have no role in T-, NK- or NKT-cell immunity. Instead, they assist in B-cell development in germinal centres [Clark et al. 1992; Rossi and Young 2005; van Nierop and de Groot 2002].

Conventional or myeloid (or non-plasmacytoid) DC are the typical "text-book" DC. They exist in an immature state in peripheral tissues where they present high antigen uptake activity. In a mature state, cDC localise to lymph nodes where they assume a role as professional antigen-presenting cells and control T-cell activation. Since there is no unique DC marker, myeloid DC can be identified by the absence of any lineage specific marker (CD2, CD3, CD4, CD8, CD14, CD15, CD19, CD56) together with strong expression of CD11c and MHCI and MHCII [Banchereau et al. 2000]. cDC include 3 subsets: monocyte-derived DC (moDC); dermal DC or interstitial DC (DDC-IDC); and Langerhans cells (LC) [Rossi and Young 2005]. The majority of moDC are distributed throughout almost all peripheral tissues as well as in lymphoid organs in an immature state, with very few circulating (0.1-0.5% of peripheral blood leukocytes [Timmerman and Levy 1999]); DDC-IDC are located in the sub-epithelial tissue of dermis and interstitia of solid organs; LC are found in the epithelial layers of skin and mucosa [Geissmann et al. 2010; Rossi and Young 2005]. In contrast with the other types of DC, LC are maintained locally under steady-state conditions and only replaced by blood-borne precursors after inflammatory changes to the skin [Merad et al. 2002]. Plasmacytoid DC morphologically resemble plasma cells. They have no myeloid markers and are therefore sometimes referred to as lymphoid DC. These are present in bone marrow, all peripheral organs and circulate in blood and their main physiological role is the response to viral infections by secretion of type I interferons and activation of viral-specific T-cells [Cella et al. 1999; Fonteneau et al. 2003; Siegal et al. 1999]. pDC are present in lymphoid tissues together with moDC, in particular in T-cell areas. In steady-state, the majority of DC found in lymph nodes is in an immature or semi-mature state and process self-antigens to induce and maintain tolerance; under inflammatory conditions the majority of DC found in lymph nodes are mature and become extremely potent immunogens [Lutz and Schuler 2002].

This thesis concentrates on myeloid DC, in particular moDC, and therefore, throughout the thesis, DC refers to the myeloid subset unless otherwise stated.

1.3.2. Dendritic cell life-cycle

Myeloid DC are bone-marrow derived cells. Circulating DC and precursors originating in the bone-marrow have to extravasate the blood vessels and transmigrate in order to populate peripheral tissues [Sallusto and Lanzavecchia 1999]. In peripheral tissues immature DC constitutively sample the microenvironment for antigens by macropinocytosis, endocytosis or phagocytosis. DC sample both self-antigens and harmless environmental antigens, thereby maintaining peripheral tolerance in steady-state, as well as potentially threatening antigens, resulting in induction of an immune response [Rossi and Young 2005]. The combination of the actively high motility of immature DC together with a highly dynamic dendritic morphology allows for efficient coverage of large areas of tissue as immune sentinels [Andersen et al. 2006]. Several receptors are involved in antigen recognition and uptake such as MMR, DEC205, DC-SIGN, complement receptors and Toll-like receptors (TLR) [Rossi and Young 2005]. Upon antigen encounter and in the presence of activation stimuli, such as inflammatory cytokines or bacterial or viral products, DC enter a maturation programme that will eventually transform the antigen-capturing cell into an antigen-presenting cell. First, the production and secretion of inflammatory cytokines is stimulated to recruit T-, NK- and NKT-cells to the site of infection and to activate other cells including other DC, thus controlling innate immunity [Rossi and Young 2005]. Concomitantly, antigen uptake ceases, antigen processing is enhanced and *de novo* synthesis of MHC molecules is triggered, resulting in the upregulation of MHC-peptide complexes at the cell surface. There is also upregulation of surface expression of activation markers, like CD25, and co-stimulatory molecules like CD40, CD83 and CD86, required for efficient T-cell priming [Banchereau et al. 2000; Cella et al. 1997; Rescigno et al. 1999]. Furthermore, during maturation DC upregulate expression of the CCR7 receptor, which recognises homeostatic chemokines of the lymph node T-cell area (CCL19 and CCL21), also produced by lymphatic endothelial cells [Randolph et al. 2005]. Maturation is thus accompanied by active translocation via afferent lymphatics to regional lymph nodes, where DC arrive fully mature [Flores-Romo 2001]. Once in the lymph node, mature DC home to the T-cell areas where they present the captured and processed antigen to T-cells [Banchereau et al. 2000]. A tight balance between co-stimulatory molecules and cytokine production by DC determines the outcome of the lymphocyte response. Depending on the antigen load, the duration of the DC-T-cell contact, the state of maturation and the specific maturation stimuli at the time of antigen uptake, different T-cell responses can be induced: antigen capture in the context of inflammation favours an imune response whereas antigen encounter with no inflammation signal favours a tolerogenic response [Langenkamp et al. 2000; Moser and Murphy 2000]. There is no evidence of DC leaving the lymph nodes where they eventually die after induction of an immune response [Banchereau et al. 2000; Flores-Romo 2001].

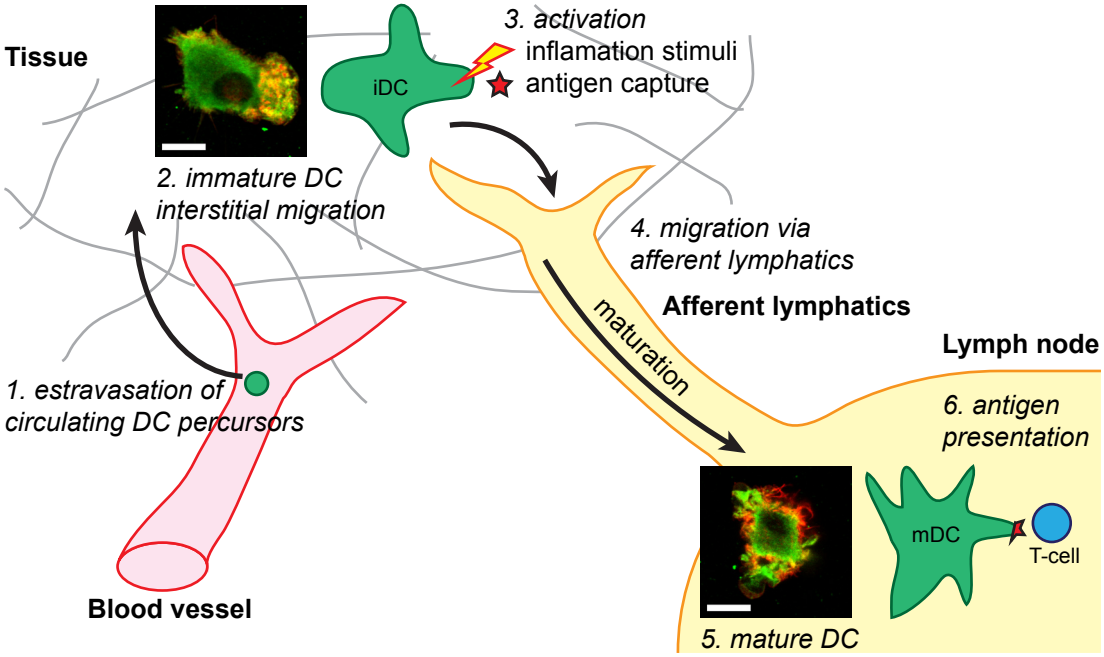

Figure 1.3. Migration and the DC life-cycle.
Migration is critical for DC immune function and is closely linked to the DC life cycle. Circulating DC and precursors originating in the bone marrow extravasate the blood vessels into peripheral tissues (1) where they reside as immature DC (iDC) scavenging for antigens. Immature DC (2) present high motility as well as highly dynamic dendritic morphology which enables them to cover large areas of tissue as immune sentinels. Upon antigen encounter and in the presence of inflammation signals (3) DC become activated and enter a maturation process. This is accompanied by migration to afferent lymphatics and translocation to the regional lymph nodes (4) where DC arrive fully mature (5). Once in the lymph node, mature DC (mDC) home to T-cell areas where they present the captured processed antigen to T-cells (6). DC eventually die in the lymph nodes after induction of an immune response. Confocal micrographs correspond to DC plated on fibronectin and stained for actin (red) and vinculin (green). Whereas iDC present themselves spread and with podosomes (F-actin cores surrounded by rings of vinculin), podosomes are absent from mDC and these present numerous ruffles. Scale bars: 10μm.

1.3.3. Dendritic cell migration

DC immune function is dependent on their migratory and tissue homing properties. Migration of DC is a fundamental aspect of their function as it allows them to cover practically all body tissues in their role in immune surveillance and for prompt activation of T-cells in lymph nodes to generate an immune response [Sallusto and Lanzavecchia 1999]. During their life-cycle, DC cross different tissues and tissue barriers (Figure 1.3). Circulating DC or DC precursors have to extravasate from blood vessels into tissues. Tissue resident DC migrate within the extravascular tissue during immune surveillance and upon initiation of maturation, DC migrate to afferent lymphatics. DC home for lymph nodes via afferent lymphatics in a way that is believed to be passive, assisted by flowing lymph [Randolph et al. 2005]. Finally, DC migrate to T-cell areas of lymph nodes where T-cell interaction takes place. Migration is, thus, a key component in the DC life-cycle.

Force generation: the actomyosin cytoskeleton

In order for a cell to actively move it needs (1) to generate force and (2) to transduce that intracellular force to the environment.

In leukocytes, the force to actively deform the cell is almost exclusively generated by the actomyosin cytoskeleton [Nourshargh et al. 2010]. This includes expansion of the actin network by active actin polymerization at the leading edge together with contraction by myosin II motors at the uropod, or trailing edge. Polarised actin polymerization at the front of the cell protrudes the mechanically resistant plasma membrane while pushing actin filaments backwards [Lammermann and Sixt 2009]. This is mediated by small Rho GTPases, which activate WASp family members to induce Arp2/3 actin polymerization. Deletion of Rac1 and Rac2 in DC or neutrophils results in spherical cells that are unable to migrate, both *in vitro* and *in vivo* [Benvenuti et al. 2004; Sun et al. 2004] and WASp deficiency causes reduced migration [Snapper et al. 2005]. The retrograde flow of actin filaments is supported by contraction of the actin cytoskeleton at the rear of the cell. Contractility is mediated by myosin II motors, which present actin cross-linking and contractile functions. Myosin II is concentrated towards the back of the cells where it generates hydrostatic pressure at the back that squeezes and propels the cytoplasm forward [Lammermann et al. 2008].

Force transduction: mesenchymal or amoeboid motility

In order to facilitate locomotion, the intracellular force generated by the actomyosin cytoskeleton needs to be transduced to the extracellular environment. There are two general models of migration defined by the way a cell transduces force: mesenchymal migration and amoeboid migration. In mesenchymal migration, forces generated by the retrograde flow of actin polymerization are coupled with the immobilized extracellular environment by transmembrane adhesion receptors. In leukocytes, integrins are the receptors that mediate traction, facilitating locomotion [Lauffenburger and Horwitz 1996; Renkawitz et al. 2009]. The typical example of mesenchymal migration is in 2D systems, where adhesion is a prerequisite for migration because cells cannot otherwise maintain contact with the surface [Lammermann and Sixt 2009]. In such systems, protrusive membrane structures called lamellipodia are generated by active actin polymerisation at the leading edge of the cells [Mullins et al. 1998]. Lamellipodial extension is complemented by the establishment of integrin adhesion sites, which constitute anchoring points that provide traction for the contractile forces generated by myosin motors, allowing the cells to progress [Jones 2000; Ridley et al. 2003]. In a tight 3D environment, however, there is forced contact between the cell and the substrate, reducing the need for transmembrane

adhesion receptors [Lammermann and Sixt 2009]. In an amoeboid mode of migration, the cell does not need to physically link its actin cytoskeleton with the extracellular environment. Instead, the deformation of the cell body driven by the actomyosin cytoskeleton is enough to push against the tight environment and result in locomotion [Lammermann and Sixt 2009]. Leukocytes have been shown to be able to migrate in both a mesenchymal and an amoeboid way according to the environemnt. For example, while neutrophils plated on a glass slide present integrin-dependent mesenchymal-type of migration, once they are squeezed between two glass slides they can adopt an amoeboid integrin-independent mode of migration [Malawista and Chevance 1997].

Leukocyte extravasation from blood vessels – an integrin-dependent process

Leukocyte extravasation from blood vessels (exit from the blood stream and penetration through the endothelial layer and basement membrane) is a clear situation of integrin-dependent migration as it clearly resembles migration in a 2D environment. Transmembrane adhesion receptors on endothelial cells on the lumen of blood vessels mediate physical anchoring of leukocytes. Chemokines immobilized on the endothelial cells regulate activation of leukocyte integrins. Following arrest, leukocytes drastically change their shape, from a mostly spherical to a flattened morphology and polarise with definition of a leading protrusive edge and a retracting tail to cross the endothelial layer and the basement membrane [Nourshargh et al. 2010]. Lymphocytes plated on endothelial cell monolayers have been shown to present small protrusions suggestive of podosomes on their ventral cell surface which preceded transcellular diapedesis [Carman et al. 2007].

Studies on leukocyte extravasation have mostly focused on lymphocytes or neutrophils, and very little data is available concerning DC. This is because (1) DC and their function were only very recently identified, (2) although extravasation of DC or precursors occurs to repopulate tissues, the majority of DC are tissue-resident and only very few are found circulating and (3) the migratory process considered most important in DC immune function is not extravasation for repopulation of tissues but the homing to lymph nodes via afferent lymphatics after activation for induction of T-cell immune responses. Nevertheless, it is accepted that DC extravasate the blood vessels in a similar way to other leukocytes [Robert et al. 1999; Sallusto and Lanzavecchia 1999].

Leukocyte extravascular migration – an integrin dependent or independent process?

After extravasation, leukocytes reach the interstitial space, a 3D environment which can

either be a fibrilar network of extracellular matrix components or a cell-packed cellular environment [Sixt 2011]. Great progress has been achieved in understanding extravasation, but little is known about leukocyte migration within the extravascular tissue, where controversy exists regarding the migration mode and the need and use of integrins [Nourshargh et al. 2010].

Before the identification of integrins, early reports suggested leukocyte adhesion-independent amoeboid migration in 3D matrices. Neutrophils were shown to invade collagen gels in a process largely independent of adhesion and proteolysis. The morphology of migratory neutrophils was consistent with squeezing through the collagen fibre gaps. Additionally, increased collagen density reduced invasion, consistent with fewer and smaller gaps within the matrix [Brown 1982]. Lymphocytes also observed in 3D collagen gels were described to move in a similar way, extending pseudopodia and squeezing through collagen fibre gaps [Haston et al. 1982]. With the identification of integrins it became widely assumed that extravasated leukocytes relied on the interaction of integrins with the ECM for interstitial migration. In trying to identify which integrins were involved in this process, evidence of migration modulated by integrin-mediated adhesion was accumulated. For example, using integrin functional-blocking antibodies resulted in reduced velocity of neutrophils migrating *in vitro* in 3D collagen gels as well as *in vivo* in the rat mesentery and reduced recruitment of neutrophils in a mouse air pouch model of acute inflammation [Werr et al. 2000; Werr et al. 1998]. Similar results were reported for T-cells, where integrin-blocking antibodies resulted in inhibition of both spontaneous and directional migration in 3D collagen gels [Franitza et al. 1999; Friedl et al. 1995]. Additionally, whereas adherent non-polarized neutrophils presented diffused integrin staining over the cell membrane, neutrophils migrating in collagen gels presented most intense integrin staining in the leading edge lamellipodium [Werr et al. 2000; Werr et al. 1998]. However, conflicting results have emerged. For example, migration of T-cells in 3D collagen gels was shown not to be affected by blocking β_1, β_2, β_3 and α_V integrins. The activation of β_1 integrins using an activating antibody resulted in cell arrest [Friedl et al. 1998]. Furthermore, T-cells migrating in 3D collagen gels were shown to concentrate β_1 integrins at the uropod rather than at the leading edge and those were not clustered in focal adhesion-type structures as there was no colocalization with F-actin, tyrosine kinases or phophotyrosine residues. [Friedl et al. 1998]. Another study has addressed the need for integrins in leukocyte extravascular migration by abrogating expression of all integrins in murine leukocytes using a genetic approach. It was shown that integrin expression was dispensable for efficient migration of mature DC, neutrophils and B-cells *in vitro* in 3D fibrin or collagen gels [Lammermann et al. 2008]. Moreover, mature DC expressing no integrins (integrin$^{-/-}$) injected subcutaneously into wild-type mouse footpads localised to T-cell areas of the draining lymph nodes in an indistinguishable manner to co-injected wild-type DC. No difference was observed in the migratory behaviour of wild-type and integrin$^{-/-}$ DC moving towards and entering lymphatic vessels in *ex vivo* explanted ear dermis nor in intranodal migration from the subcapsular lymph node sinus towards the T-cell areas using intravital two-photon microscopy of the popliteal lymph nodes

[Lammermann et al. 2008]. It was also shown that, although integrins are essential for DC adhesion to and migration on 2D substrates, mature DC can migrate in 3D matrices by the sole force of actin polymerization and actomyosin contractility was only essential to deform and propel the nucleous through narrow pores [Lammermann et al. 2008].

In a strictly haptokinetic migratory process, where migration is driven by adhesion molecules, cells are restricted to tissues where the extracellular environment has a composition compatible with their integrin repertoire. This creates a determinism that defines where cells are able to move. Leukocytes should not be subject to such constrains, as they are scattered throughout the body and have the potential to infiltrate all tissue types. Nevertheless, lymphocyte motility in lymph nodes has been shown to occur along a scaffold network. The fibroblastic reticular cell and the follicular dendritic cell networks function as substrates for T- and B-cell migration respectively [Bajenoff et al. 2006]. Also in the dermis, effector lymphocytes preferentially move along thick collagen bundles [Boissonnas et al. 2007]. It is currently not clear to what extent leukocytes use structures in the environment as pathways but the composition of the 3D environments may modulate rather than determine migration.

Mature DC upregulate CCR7 and chemotax to CCL19 and CCL21. It has been shown that soluble CCL19 and CCL21 promote directed migration of mature DC whereas immobilised CCL21 induces integrin-mediated adhesion and random migration restricted to the chemokine presenting surface [Schumann et al. 2010]. This suggests that when the chemokine is immobilized to surfaces, integrin activation is triggered, the cells become adhesive and migrate along the chemokine-decorated matrix structure. Integrins may therefore confine motility to specifically assigned surfaces or function as immobilizing anchors to slow down or stop movement [Sixt 2011].

It is not clear which type of migration, mesenchymal or amoeboid, is more energy efficient. During an integrin-dependent migratory process, there is the need to disengage integrins from the substrate to allow for cell progression. This is accomplished by locally deactivation of integrins but most importantly by contractile forces at the trailing edge, which induce integrin detachment [Nourshargh et al. 2010]. For example, it is observed that when myosin II is inhibited in neutrophils and T-cells migrating on adhesive substrates, the cells fail to properly retract the uropod and become more elongated due to inability to detach the trailing edge [Eddy et al. 2000; Morin et al. 2008; Smith et al. 2003]. Therefore, an integrin-independent migration which relies strongly on actin polymerization could be more energy efficient as it would overcome the need for contractility, as has been suggested for mature DC [Lammermann et al. 2008]. However, when mature DC migrate from an adhesive substrate onto one that does not support integrin-mediated adhesion, although they are able to move with similar velocity, they have to compensate for the lack of adhesion by increasing the rate of actin polymerization, therefore assuming a less energy efficient mode of migration [Renkawitz et al. 2009].

Lymphocytes have been demonstrated to be able to change the migratory mode from

mesenchymal to amoeboid depending on the environment. It has been proposed that the specific mode of migration results from a balance between adhesion, protrusion and contractility [Friedl 2004; Lammermann and Sixt 2009]. Even though it has been shown that mature DC are able to migrate without the use of integrins when embedded in 3D environments, in a physiological context DC probably use integrins to migrate along structures present in the substrate, as well as for retention, cell-cell communication and cell-cell adhesion [Sixt et al. 2006].

Immature dendritic cell extravascular migration

Studies concerning DC interstitial migration have resorted to mature DC because they chemotax to a defined set of chemokines, facilitating experimental design. It has been suggested that in the tightly confined environment of the interstitial space adhesion may be dispensable for force transduction and locomotion of mature DC [Lammermann et al. 2008; Lammermann and Sixt 2009]. Immature DC and DC precursors, however, have to first extravasate from blood vessels, in a process which requires engagement of integrins, and once in peripheral tissues they present mostly random migration [Robert et al. 1999; Sallusto and Lanzavecchia 1999]. Studies of DC distribution in an LAD mouse model, where no CD18 expression is detectable (see Section 1.5.2 Podosomes in human disease – Leukocyte Adhesion Deficiency), have demonstrated CD18 is in part required for immature DC and DC precursors emigration from the blood stream to populate the mouse lungs [Schneeberger et al. 2000]. Additionally, analysis of lymph nodes from human LAD patients revealed a significant reduction in the numbers of DC in these organs, further suggesting the importance of CD18 for efficient regulation of DC migration *in vivo* [Fiorini et al. 2002]. Another indication of an adhesion-dependent mode of migration of immature DC comes from WAS, the other human condition known to result in a defect in podosome formation (see Section 1.5.1 Podosomes in human disease – the Wiskott-Aldrich Syndrome). WAS manifestations can be considered, at least in part, as the result of a cell trafficking disorder [Thrasher et al. 1998]. The lack of leukocyte podosomes is due to actin polymerisation deregulation and, at least in part, the observed DC phenotype could be due to the inability of those cells to cluster β_2 integrins in podosomes and the consequent defects in adhesion-dependent migration.

DC maturation results in dramatic changes to the morphology of the cells and their actin cytoskeleton. Immature DC plated on 2D substrates spontaneously adhere and spread and present random mesenchymal-type of migration. Notably, only immature DC assemble podosomes. With the onset of maturation, DC transiently upregulate podosome formation but within 8-12 hours they completely lose their ability to assemble podosomes, lose adhesive properties, become rounded and detach from the substrate and become covered with membrane ruffles and filopodia, presumably for efficient

interaction with T-cells [Burns et al. 2004b; West et al. 2008]. Whereas β_2 integrins are clustered at podosomes in immature DC and presumably mediate tight adhesion to ICAM substrates, mature DC present diffuse integrin staining rather than discrete clustering in adhesion structures. Additionally, immature DC present slower speed of migration than mature DC in 2D systems *in vitro* [Burns et al. 2004b; van Helden et al. 2006]. All these results suggest a stronger role of integrins and adhesion in immature DC motility than in mature cells. A physiological role for podosomes in DC motility would thus be confined to DC in peripheral tissues as immune sentinels. Moreover, due to the observed up-regulation of podosomes in the onset of maturation and the specific clustering of β_2 integrins in these structures, a possible role in transendothelial migration is envisaged in crossing the lymphatic endothelium when entering the afferent lymphatics.

1.3.4. Dendritic cell podosomes

The most prominent actin structure of immature DC are podosomes. Podosomes in DC were first identified in 2001 in human immature monocyte-derived DC plated on 2D substrates [Burns et al. 2001]. DC podosomes are formed at the ventral side of the cell, commonly found in patches behind the leading edge of polarised cells [Burns et al. 2004b]. They are highly dynamic with half-lives between 30sec and 5min [Chou et al. 2006]. DC podosomes are roughly 1μm in diameter and 1μm thick [Calle et al. 2006a]. Similarly to podosomes in other leukocytes, the Arp2/3-dependent actin polymerization machinery, controlled by WASp, is localised at the base of the DC podosome core [Burns et al. 2001; Calle et al. 2006a]. WASp is a crutial component of podosomes and in the absence of WASp DC are unable to assemble podosomes [Burns et al. 2001; Calle et al. 2004a]. The actin core of the podosome also includes tyrosine-phosphorylated proteins [Burns et al. 2001]. WIP is also required for DC podosome formation by stabilising WASp as well as possibly recruiting WASp to initiate DC podosome core formation [Chou et al. 2006]. Although WIP has not been formally demonstrated to localise to human DC podosomes, it has been shown to localise to leukocyte podosomes including splenic murine DC [Chabadel et al. 2007; Chou et al. 2006; Monypenny et al. 2011; Tsuboi 2007]. Other actin regulators such as cortactin and HS1 have also been implicated in DC podosomes [Banon-Rodriguez et al. 2011; Chou et al. 2006; Dehring et al. 2011]. Gelsolin, an actin capping protein that localises to podosome cores, has been shown to be necessary for murine osteoclast podosome formation and function [Chellaiah et al. 2000; Marchisio et al. 1987]. However, DC podosome formation is gelsolin-independent [Hammarfjord et al. 2011]. Vinculin, paxillin and talin link the actin core and the adhesive ring of the DC podosome [Burns et al. 2001; Calle et al. 2006a; Calle et al. 2004a; Gawden-Bone et al. 2010]. β_2 integrins (CD18) have been reported to be specifically clustered in the DC podosome rings [Burns et al. 2004b] although one subsequent report has shown β_1

integrin (CD29) localising to DC podosomes as well [van Helden et al. 2006]. β_2 integrins are essential for the formation of DC podosomes. In the absence of CD18, DC are not able to form defined actin cores (Siobhan Burns, unpublished data), suggesting cooperation between actin regulators and integrins during podosome assembly to form fully mature podosome. MT1MMP has been shown to be responsible for ECM degradation by murine DC [Gawden-Bone et al. 2010; West et al. 2008]. However, MT1MMP localization to DC podosomes has not been reported.

1.4 Podosome function in DC

Podosomes were initially thought to be natural structures of leukocytes alone. Although it is now acknowledged that podosomes are formed in a variety of other cell types, leukocyte podosomes retain high relative importance due to the fact that leukocytes, including DC, are highly motile cells with migration being critical for their function. The following sections detail what is currently known about the function of podosomes with special incidence on haematopoietic and dendritic cell podosomes.

1.4.1. Podosomes in DC adhesion and migration

Podosomes are sites of integrin clustering and localise several signalling and scaffolding proteins also found in other adhesive structures such as focal adhesions [Gimona and Buccione 2006]. Additionally, they are only formed at the ventral side of cells and constitute sites of close contact with the underlying substratum, as has been demonstrated using interference reflection microscopy (IRM) and total internal reflection fluorescence microscopy (TIRF) [Calle et al. 2006a; Calle et al. 2006b; Calle et al. 2004b; Linder and Kopp 2005]. Moreover, DC lacking WASp, and thus podosomes, are not able to cluster β_2 integrins at podosomes and show impaired adhesion under flow to ICAM (β_2 ligand) but not to fibronectin (β_1 ligand) [Burns et al. 2004b]. In the case of osteoclasts, in their bone resorbing phase, podosomes are critical for achieving tight adhesion in the formation of the sealing zones (the function of podosomes in osteoclasts is discussed in more detail in Section 1.4.2 DC podosomes in ECM degradation).

In DC, as well as in macrophages, podosomes are thought to be important for competent integrin-mediated adhesion-dependent migration. The specific recruitment of CD18 to DC podosomes and the requirement for podosomes for adhesion to ICAM suggests

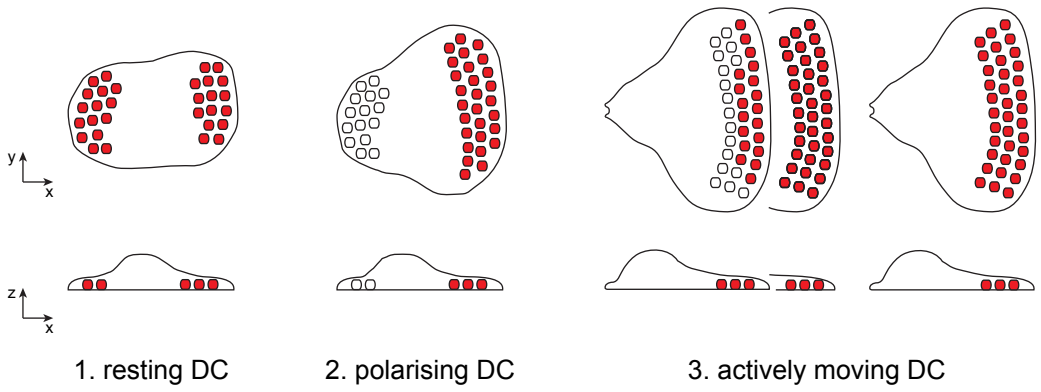

Figure 1.4. Podosomes in DC migration.
Schematic representation of one DC plated on a 2D substrate in the xy and xz planes. Podosomes are indicated as red dots. Resting DC naturally adhere to the substrate, extend lamellipodia and spread and assemble podosomes (1). Upon a stimulus for migration the cell polarizes (2) with the definition of a leading edge and consequent relocation of podosomes to the leading edge. As new lamellipodia is extended at the leading edge of the cell (3), rapid assembly of new podosomes at the front of the cell behind the newly formed lamellipodia is observed so as to stabilise the protrusion. This happens together with the retraction of the uropod, resulting in cell translocation. Also, older podosomes located at the rear of the podosome patch disassemble, permitting the podosome patch to accompany the progression of the leading edge lamellipodia.

podosomes to be important adhesion structures in transmigration across endothelial barriers [Burns et al. 2004b]. Additionally, podosomes are most often assembled in patches behind the leading edge of migrating cells so as to stabilise the newly formed lamellipodia and podosome turnover has been demonstrated to be necessary for efficient leukocyte migration [Burns et al. 2001; Calle et al. 2006a; Calle et al. 2004a; Goto et al. 2002] . As the cell moves forward, rapid assembly of new podosomes at the front of the cell behind the leading edge is observed together with disassembly of podosomes at the rear of the podosome patch, permitting the podosome patch to accompany the progression of the leading edge lamellipodia (Figure 1.4), [Calle et al. 2006b; Monypenny et al. 2011].

Cellular models deficient in podosome formation result in altered lamellipodial dynamics and defective migration. Human DC lacking functional expression of β_2 integrins are unable to assemble podosomes, which correlates with the inability to stabilise newly formed lamellipodia and impaired chemotaxis (Siobhan Burns, unpublished data; [Fiorini et al. 2002]). A similar phenotype is observed when DC are devoid of podosomes due to defects in actin polymerisation, for example due to the lack of functional WASp. Such cells are still able to form lamellipodia but these collapse, presumably due to the absence of adhesion structures that would otherwise stabilise them, resulting in slower speeds of migration [Binks et al. 1998; Burns et al. 2001]. Additionally, DC from a murine WASp knock-out model show reduced lymph node homing *in vivo* [de Noronha et al. 2005]. In a similar way, monocytes and macrophages deficient in functional WASp also show defects in polarization and chemotaxis [Badolato et al. 1998; Jones et al. 2002; Linder et al. 1999;

Zicha et al. 1998] It should be noted, though, that the defects observed in cells lacking functional WASp may be due to altered cytoskeletal organization and dynamics and not directly due to the absence of podosomes.

1.4.2. DC podosomes in ECM degradation

Invadopodia are characterised by the capacity of focal degradation of the underlying matrix. This feature is thought to enable tumour metastasis by facilitating invasion of the underlying tumour stroma and intravasation into blood or lymphatic vessels [Buccione et al. 2004; Weaver 2006]. Recently, focal degradation of the underlying ECM has also been attributed to podosomes. ECM degradation localised under podosome patches has been observed first in non-haematopoietic cells [Burgstaller and Gimona 2005; Linder and Aepfelbacher 2003; Mizutani et al. 2002; Osiak et al. 2005; Quintavalle et al. 2010; Rottiers et al. 2009; Tatin et al. 2006; Varon et al. 2006] but later also in macrophages and DC [Banon-Rodriguez et al. 2011; Dovas et al. 2009; Gawden-Bone et al. 2010; Linder 2007; West et al. 2008; Yamaguchi et al. 2006]. In particular, immature murine DC have been shown to degrade the ECM via MT1MMP as DC from MT1MMP null mice, although able to assemble podosomes, present defective matrix degradation [West et al. 2008]. Additionally, splenic DC podosomes have been described as active sites of ECM degradation in a transwell system [Gawden-Bone et al. 2010] and DC lacking WIP were deficient in ECM degradation possibly due to defective MT1MMP targeting to podosomes [Banon-Rodriguez et al. 2011]. However, MMP have not been shown to localise to DC podosomes. In leukocyte podosomes, excluding osteoclasts, the only MMP localised to podosomes has been MT1MMP to murine macrophage podosomes [Nusblat et al. 2011].

Whereas invadopodia intensely degrade the ECM and their presence and the upregulation of their components correlates with the metastatic ability of malignant cells, only shallow podosome associated ECM degradation is observed and this is limited to the immediate vicinity of the podosomes. This suggests that podosome-mediated ECM degradation may have mainly an alternative function that is not associated with invasive migration. For example, limited proteolysis could allow for the cell to sense the environment and release and/or activate signalling molecules such as immobilised chemokines [Chang and Werb 2001; Clark and Weaver 2008; Linder 2007].

Osteoclasts are cells derived from the monocytic lineage specialised in bone remodelling which also present podosomes. ECM degradation is critical for the function of these cells. Osteoclasts cycle between a highly migratory and a stationary, actively bone-resorbing, phenotype. Migratory osteoclasts assemble podosomes typically concentrated behind their leading edge, correlating with the migratory phenotype [Destaing et al. 2003; Lakkakorpi and Vaananen 1996; Sato et al. 1997]. However, upon transition to a stationary

phase, osteoclast podosomes reorganise by clustering and fusion into a podosome belt around the periphery of the cell. This band of condensed podosomes outlines and isolates a sealed compartment called the resorption lacuna. It is the organization of this podosome belt that allows tight seal of the resorption lacuna, which is essential for the maintenance of acidic conditions in this extracellular compartment for bone matrix degradation and resorption [Calle et al. 2004b; Destaing et al. 2003; Kanehisa et al. 1990; Lakkakorpi and Vaananen 1996; Pfaff and Jurdic 2001]. MT1MMP and MMP9 have been shown to be recruited to osteoclast podosomes [Delaisse et al. 2000; Sato et al. 1997]. Despite that, the exact role of osteoclast podosomes in ECM degradation is not clear. In stationary osteoclasts the podosome belt actually constitutes a zone of tight adhesion, sealing the resorption lacuna, where ECM degradation occurs, rather than sites of active ECM proteolysis [Calle et al. 2004b; Kanehisa et al. 1990].

1.5 Podosome relevance *in vivo*

It is not clear whether podosomes are physiological structures or mere artefacts of 2D cell culture systems. There is currently very scarce evidence of the existence of podosomes *in vivo* and their physiological relevance is still not established.

Most studies of podosomes have resorted to *in vitro* 2D systems. In the few studies involving *in vitro* 3D culture systems macrophages and DC have been shown to form long actin protrusions enriched in podosome components and associated with robust matrix degradation, rather than the typical podosome structures found in 2D systems [Gawden-Bone et al. 2010; Van Goethem et al. 2011; Van Goethem et al. 2010]. The only studies where structures suggestive of podosomes have been identified either in *ex vivo* tissue samples or *in vivo* relate to 2D geometries. Podosome rosettes were identified in vascular endothelial cells in mouse arterial vessel segments incubated *ex vivo* with TGFβ [Rottiers et al. 2009]. These were formed in the ventral side of the endothelial cells in close contact with the vascular smooth muscle cell layer and resembled podosomes formed by vascular endothelial cells cultured *in vitro* with TGFβ [Rottiers et al. 2009]. Podosome belts in rabbit osteoclasts outlining the resorption lacuna were also apparent in *ex vivo* thin bone slices stained for actin [Kanehisa et al. 1990]. Finally, a very recent work has shown structures in vascular smooth muscle cells *in vivo* that concentrate podosome components and whose morphology resembles podosome rosettes [Quintavalle et al. 2010].

The first physiological process linked to podosomes was bone resorption by osteoclasts. Substrate recognition by migratory osteoclasts induces a switch in morphology into a

resting, actively bone-resorpting phenotype, which is associated with podosome condensation into the sealing zone and formation of the resorption lacuna [Chellaiah et al. 1998; Lakkakorpi and Vaananen 1996]. A direct correlation between reduced podosome expression and decreased bone resorption has been demonstrated [Miyauchi et al. 1990]. However, more recent studies advise reservation regarding this physiological role of osteoclast podosomes (further discussed in the next section). It has been suggested that podosomes may be involved in leukocyte extravasation and tissue transmigration as well as in extravascular migration, as discussed above, although evidence for this is still circumstantial [Buccione et al. 2004; Burns et al. 2004b; Linder and Aepfelbacher 2003].

1.5.1. Podosomes in human disease – the Wiskott Aldrich Syndrome

Two human conditions have been identified where leukocytes are unable to assemble podosomes. However, it is not obvious that any part of the clinical phenotype is specifically due to a lack of podosome formation rather than due to other associated complications.

The Wiskott-Aldrich Syndrome (WAS) is a rare X-linked primary immunodeficiency where patients present with eczema, thrombocytopenia and severe immune deficiency. WAS patients also have an increased incidence of autoimmune disease and malignancy. WAS is caused by mutations in the WASp gene which result in complete absence or reduced expression and function of WASp, leading to a broad range of leukocyte defects [Derry et al. 1994; Kirchhausen 1998; Sullivan et al. 1994; Thrasher and Burns 2010]. A WAS murine model has been generated by gene targeted mutation. It has many similarities to the human clinical condition particularly in regard to immune cell function [Snapper et al. 1998; Zhang et al. 1999]. The cytoskeletal architecture defects caused by lack of functional WASp are seen in multiple haematopoietic lineages and compromise functions such as proliferation, phagocytosis, cytotoxicity and immunological synapse formation [Bouma et al. 2011; Dupre et al. 2002; Gismondi et al. 2004; Leverrier et al. 2001; Molina et al. 1993]. In addition, adhesion and directed migration of leukocytes are also defective both *in vitro* as well as *in vivo* in the murine WAS model [Binks et al. 1998; Burns et al. 2001; de Noronha et al. 2005; Linder et al. 1999; Snapper et al. 2005]. In fact, WAS has been considered to be, at least in part, a cell trafficking disorder [Thrasher et al. 1998].

WASp is recruited to the podosome core and it is essential for podosome formation in DC and macrophages [Burns et al. 2001; Calle et al. 2004a; Linder et al. 1999]. The lack of functional WASp results in the failure of DC to cluster β_2 integrins at the podosomes and this has the consequence of impaired adhesion to ICAM (specific β_2 ligand) but not to fibronectin (β_1 ligand) [Burns et al. 2004b]. The defects in adhesion and migration of macrophages and DC from WAS patients or from WAS mice have been associated with

the absence of podosomes [Burns et al. 2001; Calle et al. 2004a]. However, the lack of WASp has several other detrimental effects in immune cell development and function and therefore the observed defects in myeloid cell trafficking cannot be solely attributed to the absence of podosomes [Burns et al. 2004a; Thrasher and Burns 2010; Thrasher et al. 1998].

WASp is also required for the formation of osteoclast podosomes. Due to the link between podosomes, sealing zone formation and bone remodelling, one would expect WAS patients to present bone abnormalities. However, there is only scant indication that there may be an association between bone disorders and WAS. There have only been 4 WAS patients reported with features of infantile hyperostosis, and those may have been caused by infection or trauma and autoimmunity rather than due to an inherent osteoclast defect [Abinun et al. 1988; Chandrakasan et al. 2011; McEnery and Nash 1973]. Additionally, in the murine WAS model, even though the lack of WASp was shown to disrupt the formation of osteoclast podosomes and to result in reduced bone resorption activity *in vitro* [Calle et al. 2004b], bone-resorption defects *in vivo* were only apparent when mutant mice were subjected to a resorptive challenge by performing an ovariectomy and not in a homeostatic context [Calle et al. 2004b; Chellaiah et al. 2000].

1.5.2. Podosomes in human disease – Leukocyte Adhesion Deficiency

Leukocyte Adhesion Deficiency type-I (LAD-I) is an autosomal recessive primary immunodeficiency characterised by recurrent necrotic soft tissue infections and impaired wound healing with lack of pus formation. LAD-I is due to complete or partial absence of expression or abrogated function of the β_2 family of integrins [Anderson and Springer 1987; Hogg and Bates 2000]. This leukocyte exclusive family of integrins is characterised by the common β_2 chain and comprises 4 heterodimers: LFA1 (lymphocyte function-associated antigen 1, $\alpha_L\beta_2$, CD11a/CD18); Mac-1 (macrophage-1 antigen, complement receptor 3, CR3, $\alpha_M\beta_2$, CD11b/CD18); p150,95 (complement receptor 4, CR4, $\alpha_X\beta_2$, CD11c/CD18); and $\alpha_D\beta_2$ (CD11d/CD18). β_2 integrins are widely expressed in leukocyte subsets implying a wide range of cellular effects. Despite this, LAD-I is commonly characterised as a neutrophil disorder. Neutrophils rely on β_2 integrins for adhesion to the vascular endothelium and extravasation from the blood stream and failure to achieve this results in neutrophilia, a defining feature of the disorder. Additionally, LAD-I leukocytes fail to accumulate at sites of infection or tissue injury, hence the lack of pus [Bouma et al. 2010; Hogg and Bates 2000]. Nevertheless, β_2 integrins are important for several other immunological functions, affecting all leukocytes, such as the formation of the immune synapse, cytotoxic T-cell binding to their targets, phagocytosis and chemotaxis [Hogg et al. 2011; Monks et al. 1998]. LAD-I manifestations correlate with the levels of β_2 integrin expression. The disorder can be classified as severe, for virtually no CD18 expression

(<0.3% of normal), or moderate or mild , where 2.5-31% CD18 expression is detected (as measured by flow cytometry immunoassay) [Anderson et al. 1985; Anderson and Springer 1987]

DC from LAD patients show severe impairment of chemotaxis and transendothelial migration [Fiorini et al. 2002]. Immature moDC recruit β_2 integrins to their podosomes [Burns et al. 2004b] and DC from severe LAD patients are unable to assemble podosomes (Supplemental Data – Models of integrin deficiency; Siobhan Burns, unpublished data). In addition, these cells show diffused actin polymerisation at the leading edge and defects in lamellipodial dynamics and stabilization similar to those observed in DC from WAS patients (Siobhan Burns, unpublished data).

There are two other types of leukocyte adhesion deficiency, with much lower incidence than LAD-I: LAD-II where granulocytes are unable to bind selectins on the endothelium due to mutations in the guanosine diphosphate–fucose transporter gene [Etzioni et al. 1992; Hidalgo et al. 2003]; and LAD-III where β_2 integrin expression is normal but mutations in the haematopoietic restricted Kindlin-3 gene hinder integrin activation through "inside-out" signalling pathways [Kuijpers et al. 2009; McDowall et al. 2003; Mory et al. 2008; Svensson et al. 2009]. The cytoskeleton of DC from patients with these conditions has not been examined so it is unknown whether podosome formation is also affected. Nevertheless, it is hypothesised that DC from LAD-III patients should also not be able to form podosomes.

There are three animal models of LAD-I, all of which present similar manifestations to the human form of the disease: murine, bovine and canine. Bovine and canine LAD are naturally occurring diseases [Giger et al. 1987; Shuster et al. 1992] whereas a hypomorphic (resulting in low-level CD18 expression, resembling mild LAD) and a CD18 null mutant mouse have been generated [Scharffetter-Kochanek et al. 1998; Wilson et al. 1993]. Dendritic cells from the canine LAD model and from the hypomorphic mouse were investigated for their ability to assemble podosomes. In contrast with DC from the human LAD counterpart, canine LAD DC and BMDC from the hypomorphic mouse model were as efficient at assembling podosomes as cells from wild-type animals, which may reflect species specific variations and residual CD18 function respectively (Supplemental Data – Models of integrin deficiency). The ability of DC from the CD18 null murine model to assemble podosomes has not been reported. If podosome assembly by those cells would be defective, then that could be an interesting source of cells lacking the ability to assemble podosomes due to integrin deficiency.

1.6 Manipulating the DC cytoskeleton

1.6.1. Genetic manipulation of DC

Circulating DC represent only 0.1-0.5% of peripheral blood leukocytes [Timmerman and Levy 1999]. The development of techniques for *ex vivo* generation of DC, from $CD34^+$ progenitors [Caux et al. 1992] or most commonly from $CD14^+$ circulating monocytes [Sallusto and Lanzavecchia 1994] has permitted the use of DC for experimental purposes both for basic biology studies as well as for clinical applications.

The genetic manipulation of monocyte-derived DC, to alter gene and protein expression, has been achieved using both viral and non-viral methods. The maturation state of the modified DC may be critical for biological studies as well as for therapeutic applications as DC function changes dramatically with maturation. In particular, the maturation state of DC has to be tightly controlled for in cytoskeletal studies, and there is evidence that methods, currently widely used, may affect activation and induce maturation, thus resulting in undesirable cytoskeletal changes. In this thesis genetic manipulation is utilised for expression of shRNA sequences (discussed in Section 1.6.2 RNA interference).

Manipulating antigen presentation

A great number of studies involving manipulation of DC refer to the exploitation of this cell type as a potent inducer of an immune response in the development of immune-therapeutic applications. DC antigen loading can be achieved by pulsing DC with cell lysates, purified proteins or peptides [Timmerman and Levy 1999]. Viral and non-viral vectors have also been used to alter antigen presentation by genetic manipulation of DC, with the former being considered most effective, particularly using adenovirus and HIV-1 (human immunodeficiency virus type 1) based vectors [Breckpot et al. 2004]. Whereas in the development of DC vaccines mature DC will ultimately be used, in cytoskeletal studies of podosomes it is a prime consideration that modified DC retain their immature phenotype.

Viral vectors for DC manipulation

Gammaretroviral vectors based on the murine leukaemia virus have successfully been

used to generate genetically modified DC from transduced $CD34^+$ precursors [Reeves et al. 1996]. These vectors, however, rely on mitosis for nuclear entry and therefore are unable to transduce non-dividing cells, such as moDC [Lewis and Emerman 1994]. Adenoviral vectors and lentivectors, on the other hand, are able to transduce non-dividing cells. Adenoviral vectors have been demonstrated to be efficient at transducing moDC but express viral components that promote DC activation and maturation [Morelli et al. 2000; Tan et al. 2005], rendering them unsuitable for the use in studies where immature DC are required. Lentiviral vectors can also efficiently transduce moDC but concerns remain about whether they induce cellular activation. Wild-type HIV-1 has been suggested to naturally activate moDC [Harman et al. 2006]. In murine studies, lentivectors have been shown to induce maturation *in vitro* and *in vivo* [Breckpot et al. 2010; Tan et al. 2005] but more variable effects on maturation of human DC, in terms of expression of surface markers, cytokine release and immunological function, have been reported [Breckpot et al. 2007; Chinnasamy et al. 2000; Esslinger et al. 2002; Gruber et al. 2000; Rouas et al. 2002; Tan et al. 2005], possibly as a result of differences in experimental protocols. Although lentiviral vectors have been used in some studies of the human and murine DC cytoskeleton [Banon-Rodriguez et al. 2011; Blundell et al. 2008; Chou et al. 2006; Olivier et al. 2006], there have been no formal studies to determine whether and to what extent cytoskeletal structure and function of immature DC is intrinsically altered by lentivector transduction.

Lentiviral vectors

Lentiviruses, such as HIV, are a type of retrovirus. During their life-cycle, retrovirus alternate between the provirus form and the virion form. The provirus consists of dsDNA integrated into the host cell genome, from which viral genomic ssRNA and viral proteins are expressed using the host's machinery. The viral components are then packaged into virion particles enveloped by a host-derived plasma membrane containing receptor glycoproteins from the virus. Nascent retroviral virions are able to incorporate envelope proteins from other enveloped virus with no homology to their own, in a phenomenon known as pseudotyping [Sanders 2002]. Soon after release, virions undergo a maturation process, dependent on processing of viral proteins by the viral protease, rendering them infectious [Briggs et al. 2003]. The mature virions can then bind and enter a new host cell, which occurs via recognition of a host cell surface receptor by the virus envelope glycoprotein. After cell entry, the virion undergoes the processes of uncoating, reverse transcription of the viral genomic RNA and transport to the nucleous. Lentivirus, such as HIV-1, are able integrate into non-dividing cells while gammaretroviruses are not. Whereas the latter can only access host chromosomes for integration when the nuclear envelope breaks down during cell division, the former are able to cross the nuclear membrane [Lewis and Emerman 1994]. Integration into a host cell chromosome results

in a new provirus, thus completing the cycle.

Lentiviral vectors were developed based on HIV-1 [Naldini et al. 1996]. The basic principle was to replace the coding region of the viral genome with a transgene cDNA. Viral elements required in *cis* for RNA packaging, reverse transcription and integration were retained in the transfer vector. All additional proteins necessary for viral production are supplied to the virion producing cells in *trans* in an independent packaging construct. The resulting virion becomes only capable of one round of infection, since no viral proteins will be expressed by the target cell. In order to reduce the risk of recombination between the transfer plasmid and the packaging plasmid, which could result in replication-competent virions, a second generation lentivector was developed, comprised of a 3 plasmid system: the transfer vector with essential *cis* elements (packaging signal (Ψ), viral LTRs, primer binding site (PBS), polypurine tract and Rev-responsive element (RRE)); a packaging plasmid with gag, gag-pol, Tat and Rev but devoid of all accessory proteins; and the envelope plasmid [Zufferey et al. 1997]. To further improve safety, the U3 region of the 3' viral LTR was deleted from the transfer plasmid, thus eliminating the LTR promoter activity in the integrated provirus, resulting in self-inactivating (SIN) lentivectors. Constitutive promoters have then to be incorporated in the transgene expression cassette [Zufferey et al. 1998]. The transfer vector can also include the HIV-1 central polypurine tract (cPPT) and central termination sequence (CTS) elements which lead to higher titres and facilitate reverse transcription and nuclear entry of non-dividing cells [Follenzi et al. 2000; Zennou et al. 2000] and the woodchuck hepatitis virus post-transcriptional regulatory element (WPRE) which enhances transgene expression [Demaison et al. 2002; Donello et al. 1998].

After integration, transgene expression in the target cell is subject to positional effects as adjacent chromosomal elements may modulate gene expression [Ellis 2005]. Additionally, subsequent epigenetic effects, including DNA methylation and histone deacetylation, as part of the host defences against transposable element expansion, may result in decreased expression or even complete transgene silencing [Bonasio et al. 2010].

The possibility of pseudotyping lentivectors allows targeting of specific cell types and changes the physical properties of the virions. The vesicular stomatitis virus glycoprotein (VSVg) is the most commonly used envelope to pseudotype lentivectors. It confers broad tropism, high stability allowing ultracentrifugation for concentration of viral supernatants and it has effectively become the standard to which all alternative pseudotypes are compared [Burns et al. 1993; Naldini et al. 1996].

1.6.2. RNA interference

RNA interference (RNAi) is a post-transcriptional gene silencing mechanism induced by sequence-specific double-stranded RNA (dsRNA) targeting of mRNA transcripts. Since the concept of antisense regulation of gene expression was first put forward, in the 1980s [Izant and Weintraub 1984], RNAi has evolved into a powerful technique for gene silencing [Caplen 2004; Leung and Whittaker 2005]. This antisense regulatory mechanism relies on hybridisation between the guide strand of 21-27 nucleotide dsRNA molecules, called small interference RNA (siRNA) or micro RNA (miRNA), and a target mRNA transcript. Gene expression is thus negatively regulated either by inhibition of translation or by induction of degradation of the target mRNA [Inui et al. 2010; Tomari and Zamore 2005]. This mechanism is phylogenetically conserved and is proposed to have evolved as an RNA-mediated antiviral defence response [Ratcliff et al. 1999]. Expression of endogenous miRNA occurs in a time- and tissue-specific manner and is involved in regulation of such different functions as cell cycle, development, cancer and viral replication [Bartel 2004; Inui et al. 2010].

Cellular miRNA are transcribed by RNA Polymerase III as a ~70nt long primary micro RNA (pri-miRNA). This encompasses a stem-loop structure that is liberated from the primary transcript by the nuclear ribonuclease Drosha and is called a precursor micro RNA (pre-miRNA). The hairpin is exported to the cytoplasm where it is further processed by the enzyme Dicer into the mature length miRNA. This dsRNA molecule presents 2nt 3' overhangs on either end and thermodynamic asymmetry determining that the strand with less stable 5' end is the guide strand and is preferentially loaded onto the multicomponent RNA-induced silencing complex (RISC). RISC promotes complementary hybridisation with the target mRNA resulting in translational repression, mRNA dead-enylation or RISC-mediated mRNA degradation [Meister and Tuschl 2004; Sontheimer 2005; Tomari and Zamore 2005].

Exploiting RNAi

The use of the RNAi mechanism to artificially achieve suppression of gene expression first happened in 1998 [Fire et al. 1998] and the exploitation of the RNAi machinery in mammalian cells was demonstrated soon after [Elbashir et al. 2001]. Transient gene silencing was achieved by transfecting synthetic small interference RNA (siRNA) molecules into the cell cytoplasm where they can be loaded onto RISC. RNAi became a revolutionary approach to gene expression studies, particularly in drug development, and it is now a powerful established tool widely used in loss-of-function genetic screens. siRNA results in only transient knock-down effects. In order to overcome this difficulty,

viral vector systems have been developed in order to induce stable endogenous expression of short hairpin RNA (shRNA) molecules, which mimic the natural occurring pri-miRNA structure [Tuschl 2002].

An artificial shRNA construct may target the coding region or the untranslated regions of the target mRNA transcript but must form the stem-loop secondary structure of pri-miRNA and factors such as the G+C content, preferential nucleotide positions in the stem-loop and the thermodynamic asymmetry required for RISC loading of the guide strand must be guaranteed [Khvorova et al. 2003; Mittal 2004; Reynolds et al. 2004]. There are several algorithms publicly available for the design of artificial shRNA constructs. Nevertheless, the efficiency of processing and translational down-regulation of a specific construct is difficult to predict and therefore the experimental testing and validation of shRNA sequences is required [Grimm et al. 2006; Luo and Chang 2004].

Controlling for off-target effects

The possibility of sequence-dependent off-target effects should be taken into consideration when using RNAi technology. The expression of genes with incomplete complementarity to the antisense siRNA sequence may be inadvertently down-regulated due to high-tolerance of mismatches between the siRNA and target mRNA [Du et al. 2005; Holen et al. 2005]. An immune response may also be induced by activation of an interferon response mediated by the dsRNA-dependent protein kinase PKR [Bridge et al. 2003; Sledz et al. 2003] as well by dsRNA recognition by TLR7 [Hornung et al. 2005]. These concerns can usually be addressed during shRNA sequence design by decreasing the homology with other known genes and avoiding specific motifs in the shRNA constructs [Cullen 2006; Judge et al. 2005]. Non sequence-specific off-target effects include the saturation of the cellular RNAi machinery and inhibition of endogenous miRNA expression with consequent deregulation of important cellular processes. The need for controlled expression of the artificial shRNA, either by reducing the copy number (viral load) or by using specially chosen RNA Polymerase II promoters, has been advocated, even though this could compromise knock-down efficiency [Beer et al. 2010; Grimm et al. 2006]. It has recently been suggested that the saturation of the RNAi pathway may be overcome by new design techniques which use endogenous miRNA backbones to harbour the shRNA sequences (artificial micro RNA – amiRNA) [McBride et al. 2008]. Nevertheless, non sequence-specific off-target effects should still be controlled for by using a non-targetting shRNA construct. The use of redundant shRNA sequences (different sequences targeting the same transcript) and rescue experiments where the original phenotype is reconstituted by an shRNA-resistant cDNA construct have also been suggested as improvements of standard shRNA protocols to address the problem of non-specific effects [Cullen 2006; Echeverri et al. 2006]. In this thesis shRNA is used as a method to knock-down

expression of specific integrins and actin-associated proteins to study their importance in DC biology.

1.7 Summary and aims of the project

1.7.1. Summary

Podosomes are specialised actin adhesion structures which are increasingly thought to be ubiquitous to several cell types [Gimona et al. 2008]. They are assembled by haematopoietic cells from the myeloid lineage, such as DC and macrophages [Burns et al. 2001; Marchisio et al. 1987], but also by non-haematopoietic cells like endothelial cells and vascular smooth muscle cells [Hai et al. 2002; Moreau et al. 2003]. Src-transformed cells and cancer cells also assemble similar structures, called invadopodia [Chen 1989; Weaver 2006]. Podosomes are structures formed on the ventral side of cells plated on 2D substrates composed of a dense F-actin core, where actin polymerisation-related proteins concentrate, surrounded by a ring of integrins and integrin-associated proteins. Podosomes are typically found in patches just behind the leading edge of migrating cells. Podosomes are adhesion structures considered particularly important in migration since they stabilise newly formed lamellipodia by functioning as anchors that prevent lamellipodial collapse and enable transduction to the environment of force generated by the actomyosin cytoskeleton, resulting in cell translocation. Especially owing to results obtained in cancer research, invadopodia and podosomes are increasingly considered important degradative structures for invasive migration [Linder 2007]

DC are a very interesting cell type for the study of podosomes and their function. DC link the innate and adaptive immune systems. Migration is critical for their function and it is central to their life-cycle [Banchereau et al. 2000; Rossi and Young 2005]. Circulating DC or DC precursors extravasate the blood vessels to populate peripheral tissues. As immune sentinels they migrate through the extravascular tissue continuously scavenging the environment for antigens. Once in the presence of inflammation stimuli, DC initiate a maturation process, downregulating antigen uptake and upregulating expression of MCH and costimulatory molecules. They home for lymph nodes by migrating to afferent lymphatics and then translocate via lymphatics aided by lymph flow to lymph nodes, where they arrive fully mature. Mature DC in the lymph nodes migrate then to T-cell areas where they present antigens to T-cells, thus inducing an immune response.

Migration on 2D surfaces is acknowledged to be integrin dependent. Particularly in the case of extravasation, integrins are essential for establishment of tight adhesion of leukocytes to the blood vessel endothelial lumen, arrest and transendothelial migration. There is controversy, however, over the need for and use of integrins by leukocytes when migrating in packed 3D environments [Nourshargh et al. 2010]. Results from both *in vivo* and *in vitro* experiments give contradicting evidence of integrin-dependent and integrin-independent migration. Specifically regarding DC, mature DC have been shown to be able to migrate effectively without using integrins although the energetic efficiency of this mode of migration is not clear [Lammermann et al. 2008; Renkawitz et al. 2009]. A possible role for integrins in leukocyte extravascular migration is suggested in the recognition of substrate and constriction of migration to specific substrates [Sixt 2011]. Additionally, the role of integrins in transmigration across lymphatic endothelial surfaces has been poorly studied [Randolph et al. 2005].

DC podosomes are only assembled by immature DC. Maturation of DC correlates with dramatic alterations of their cytoskeleton, in line with changes in immune function. Podosomes are transiently upregulated during the first stages of the maturation process following TLR activation before being completely lost [Burns et al. 2004b; West et al. 2008]. This suggests a role for podosomes in DC migration in extravascular tissues as immune sentinels and for migration to afferent lymphatics and lymphatic endothelial transmigration during the initial phase of maturation. The fact that DC podosomes concentrate β_2 integrins in their podosomes stresses the possible importance of these structures in endothelial cell adhesion and transmigration [Burns et al. 2004b].

1.7.2. Aims and overview

The current knowledge regarding podosomes originated from research done in several different cell types, from different species, and using different culture systems. The majority of research into DC podosomes has been done in the mouse system, mainly due to the availability of transgenic mice. However, even then, different subsets of DC have different functions, different expression patterns, and their podosomes behave differently. It is important to take this into account when interpreting published data and extrapolating to the human context, as important differences occur between the immune system of mice and humans. **The present project aims to advance our knowledge of the formation and function of human DC podosomes, regarding which few studies have been published.** There are only two human conditions where DC are known to be deficient in podosome formation: WAS and LAD. However, even in a national centre for paediatric primary immunodeficiencies like ours, DC from such patients are a scarce biological resource. Studies of the immature DC cytoskeleton are further complicated by difficulties in manipulating DC while retaining their immature phenotype.

First, the potential of lentivectors as a tool for the manipulation of the DC cytoskeleton while retaining an immature phenotype was addressed. The aim was to optimise a transduction protocol, compare different viral envelopes, paying close attention to the upregulation of maturation surface markers. The immune function of transduced cells was assessed, in particular their antigen uptake and T-cell stimulatory capacities. Also, the cytoskeleton of transduced DC was analysed, including podosome formation and migration.

In a second phase of the project, the goal was to generate a panel of cell lines with reduced expression of proteins that have been suggested to be important in human DC podosomes. Lentivectors were used to induce stable expression of shRNA sequences against such targets to achieve efficient knock-down.

Finally, to investigate the effect of these candidate proteins in podosome biology, the effects of their knock-down were tested. The cell lines generated by RNAi were characterised in functional assays using differential substrates: ICAM, specific for β_2 integrins; and fibronectin, β_1 integrin ligand. Features analysed were: adhesion; basic cell morphology of adherent cells (size and shape); podosome formation; podosome array characterization (distribution and compactness); podosome morphology (size and shape); and adhesions dynamics.

Chapter

2

MATERIALS AND METHODS

2.1 General reagents and equipment

Unless otherwise stated, all chemicals were supplied by Sigma.

General buffers and solutions used are listed in Table 2.1. Water used was always deionised MilliQ grade water (Millipore), except for reconstitution of reagents used in cell culture where cell culture grade water was used.

A bench-top microcentrifuge Heraeus Biocentrifuge Fresco was used for all molecular biology and biochemistry techniques except when larger volumes were processed or higher centrifugation g-force required, in which case a Sorvall Evolution RC superspeed centrifuge was used. All cell culture centrifugation steps were performed in a Sorvall Legent RT table-top centrifuge. Viral supernatants were concentrated at low g-force in the same table-top centrifuge and at high g-force in a Sorvall Discovery SE ultracentrifuge.

Table 2.1. General buffers and solutions.

Name	Composition	Storage
Phosphate buffered saline (PBS)	11.9mM phosphates, 137mM $NaCl_2$, 2.7mM KCl	10X stock from Fisher Bioreagents; for cell culture 1X PBS from Gibco was used; stored at RT
Tris buffered saline – Tween (TBS-T)	150mM NaCl, 25mM Tris-HCl pH 7.6 + 0.1% Tween	10X stock solution stored at RT; Tween added to 1X TBS prior to use
BSA blocking buffer	5% BSA in TBS-T	Prepared prior to use
Tris-Acetate EDTA (TAE)	40mM Tris-acetate and 5mM EDTA	10X stock solution stored at RT
6x DNA loading buffer	10mM Tris pH 7.5, 50mM EDTA, 15% Ficol 400 and 0.05% bromophenol blue	Stored at RT
Luria-Bertani (LB) broth	10g/L tryptone, 5g/L yeast extract, 5g/L NaCl	Invitrogen ready-made mix; autoclaved and stored at 4°C
LB-agar	LB + 15g/L agar	Invitrogen ready-made mix; autoclaved, poured into Petri dishes (with antibiotic) and stored at 4°C
Cell fixing buffer (adherent cells)	4% PFA, 3% sucrose in PBS, pH 7.4	NaOH pellet added to dissolve PFA and pH corrected. Stored at -20°C
Cell fixing buffer (suspension cells)	1% PFA, 0.75% sucrose in PBS, pH 7.4	Diluted from 4% stock prior to use
Cell permeabilisation solution (adherent cells)	0.5% Triton X-100 in PBS	Diluted from 1% Triton X-100 stock prior to use; stored at RT
Cell permeabilisation solution (suspension cells)	0.1% Triton X-100 in PBS	Diluted from 1% Triton X-100 stock prior to use; stored at RT
MACS buffer	2mM EDTA, 0.5% BSA in PBS	Cell culture grade reagents; prepared prior to use
Cell lysis buffer	1% IGPAL or NP-40, 130mM NaCl, 20mM Tris-HCl pH 8, 1mM EDTA, 10mM NaF, 2mM NaOrthovanadate, 1% aprotinin, 10μM pepstatin, 1mM PMSF, 10μg/mL leupeptin and 50μM calpastatin	Prepared prior to use

2.2 Molecular cloning

Plasmid DNA isolation kits (QIAprep Spin Miniprep and Maxiprep kits) were from Quiagen as well as QIAquick PCR Purification and Gel Extraction kits.

Recombinant endonucleases were purchased from Promega, New England Biolabs or Fermentas. All DNA modifying recombinant enzymes were from Promega except T4 DNA Ligase which was from New England Biolabs. Agarose was from Invitrogen and 1Kb+ DNA Ladder was from Promega.

All oligonucleotides were produced by Invitrogen except RT-qPCR (reverse-transcriptase quantitative polymerase chain reaction) primers and probes which were from Applied Biosystems. dNTPs were from Promega. DNA sequencing was performed by Eurofins-MWG.

2.2.1. Plasmids

The lentiviral plasmids used in this project are represented in Figure 2.1. They are all self-inactivating second generation lentiviral transfer plasmids. pLN-SEW was used for expression of GFP in human monocyte-derived DC (pHR'SIN-cPPT-SEW [Demaison et al. 2002]). This contains the SFFV promoter (spleen focus forming virus 5'-LTR) driving eGFP expression. pDual-Cre-Cherry is a lentivector based on the pLN-SEW but with two independent expression cassettes, one with SFFV driving Cre recombinase expression and another with the ubiquitin promoter driving mCherry expression [Escors et al. 2008]. pLVTHM is an shRNA expression lentivector plasmid with shRNA expression driven by the H1 RNA Poymerase III promoter. It has an eGFP transduction marker driven by the human EF1α promoter and the shRNA expression cassette located within the 3'-LTR of the viral genome. The whole 3'-LTR, including the shRNA expression cassette, is replicated into the 5'-LTR of the integrated provirus during reverse transcription. The shRNA expression cassette is designed so as to allow for direct cloning of shRNA sequences into the lentiviral vector using unique MluI-ClaI sites [Wiznerowicz and Trono 2003]. pKLO.1-puro is another shRNA expression plasmid with shRNA expression driven by the U6 RNA Polymerase III promoter and the human PGK promoter driving expression of a puromycin resistance gene [Root et al. 2006]. This plasmid harbours the shRNA sequences against β_1 (CD29) and β_2 (CD18) integrins from the TRC shRNA library (Sigma).

The plasmid pBluscript (Stratagene) was used as a cloning plasmid. This vector contains an extensive sequence with multiple unique restriction endonuclease recognition sites

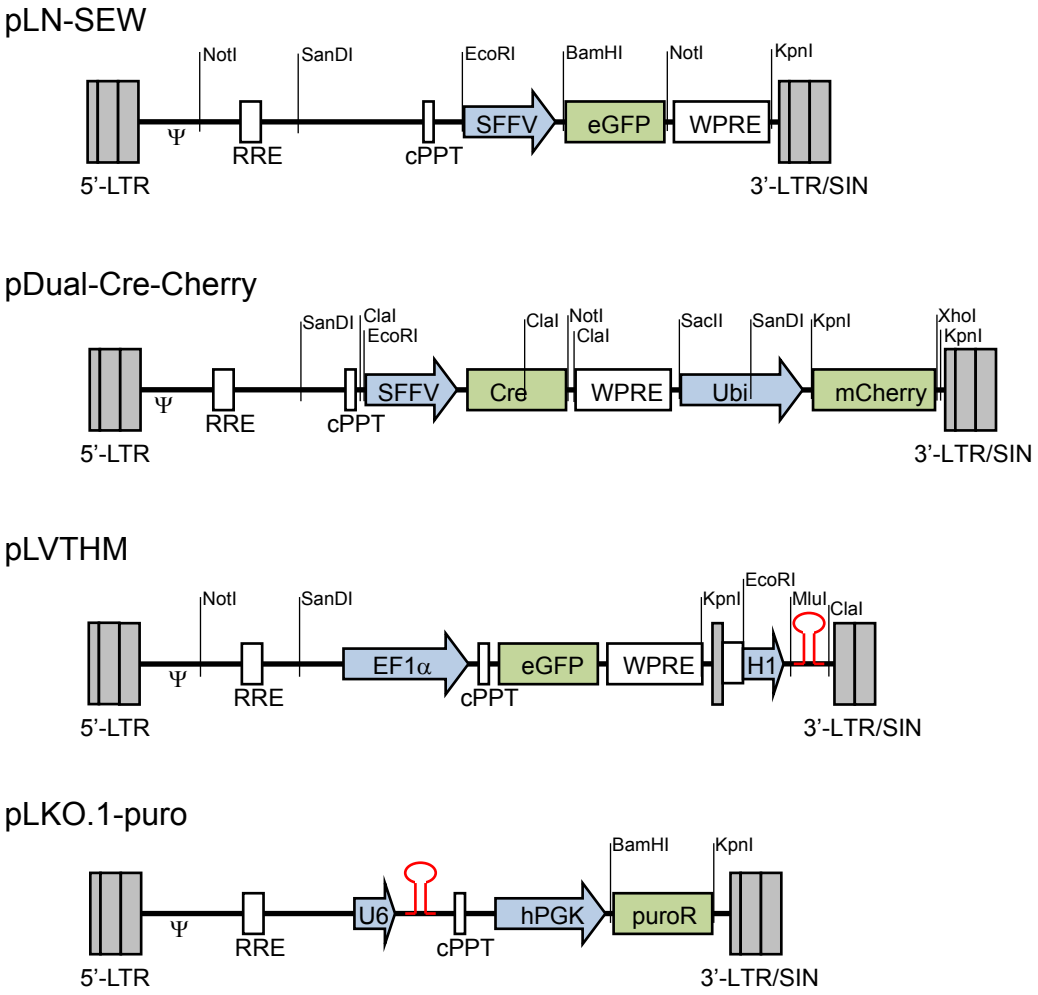

Figure 2.1. Plasmids.
Schematic representation of the lentiviral genome from the plasmids used in this project. 5'-LTR: HIV-1 long terminal repeat. 3'-LTR/SIN: HIV-1 long terminal repeat with deleted U3 region. Ψ: packaging signal. RRE: rev responsive element. cPPT: HIV-1 central polypurine tract and central termination sequence. SFFV: 3' long terminal repeat of the spleen focus forming virus (internal promoter). U6 and H1: RNA Polymerase III promoters. hPGK: human phosphoglycerate kinase promoter. Ubi: ubiquitin promoter. EF1α: elongation factor 1α promoter. eGFP: enhanced green fluorescent protein. puroR: puromycin resistance gene (puromycin N-acetyl-transferase). Cre: Cre recombinase. mCherry: mCherry protein. WPRE: woodchuck hepatitis virus post-transcriptional regulatory element. Recognition sites of selected restriction endonucleases are shown.

within the LacZ gene (β-galactosidase).

2.2.2. Cloning Strategies

pLKO.1-GFPW plasmid was generated by replacing the puromycin resistance gene in pKLO.1-puro by the eGFP and WPRE sequences from pLN-SEW using BamHI and KpnI.

There were 11 variants of this plasmid, containing different shRNA sequences (see Chapter 4, Figure 4.4).

An shRNA expression plasmid based on pDual-Cre-Cherry was generated. The SFFV-eGFP cassette was taken from pLN-SEW to replace SFFV-Cre in pDual-Cre-Cherry using EcoRI and NotI. The shRNA expression cassette containing the H1 promoter was taken from pLVTHM with EcoRI and ClaI and cloned into the cloning vector pBluescript. The H1 cassette was then excised using SacII and XhoI and cloned into the modified pDual by replacing the Ubi-Cherry sequence, flanked by SacII and XhoI. The resulting plasmid pDual-SEW-H1 contained the reporter gene GFP driven by SFFV and the WPRE element and, in an independent expression cassette, the H1 promoter followed by the unique sites MluI and XhoI.

The shRNA expression cassette was further taken from pDual-SEW-H1 with EcoRI and KpnI and placed into pLVTHM, replacing the sequence flanked by EcoRI and ClaI. Furthermore, the sequence between SanDI and KpnI of pLVTHM was replaced by the sequence flaked by the same enzymes from pLN-SEW plasmid (containing cPPT, SFFV, GFP and WPRE). The resulting plasmid pLN-SEWTH thus presents SFFV driving the transduction marker eGFP and the WPRE element and an independent shRNA expression cassette harboured within the 3' LTR (which is replicated into the 5'-LTR of the provirus) with the H1 promoter followed by the unique restriction sites MluI and XhoI. Oligonucleotides were designed for the expression of shRNA against WASp, WIP and HS1, together with a non-targeting control sequence (CTRW) (see Chapter 4, Figure 4.11). The shRNA sequences were flanked by the MluI and XhoI endonuclease recognition sites to allow cloning into pLN-SEWTH.

All constructs were confirmed by sequencing.

2.2.3. Growth and transformation of *E. coli* for plasmid DNA producion

Escherichia coli strain Stbl3 (Invitrogen) were grown at 37°C on solid LB-agar Petri dishes for clone isolation or in liquid LB media in an orbital shaker at 225rpm for DNA production. Selection of plasmid-transformed bacteria was performed by culturing in media supplemented with the relevant antibiotic: 100µg/mL ampicillin or 50µg/mL kanamycin. Long term storage of bacterial cultures was done at -80°C in 20% glycerol in LB media.

Chemical-competent *E. coli* were prepared by culturing the bacteria in 100mL liquid LB media until the exponential growth phase was reached (optical density at 600nm OD_{600}=0.6, measured with a NanoDrop ND-1000 spectrophotometer). Bacteria were pelleted by centrifugation at 4°C at 4000rpm for 10min and resuspended in 20mL

ice-cold 100mM $CaCl_2$ and incubated for 20min on ice. Following another centrifugation step, bacteria were resuspended in 4mL ice-cold 100mM $CaCl_2$ plus 1mL glycerol (20% glycerol in 100mM $CaCl_2$ solution) and 100µL aliquots were prepared and stored at -80°C. To transform chemical-competent bacteria, these were thawed on ice and incubated with 10-20µL of plasmid DNA solution or ligation product on ice for 30min. The cells were heat-shocked for 45sec at 42°C and immediately put back on ice for 2min. 300µL LB media (no antibiotic) was added and bacteria were incubated at 37°C with agitation for 1h before being plated on LB agar plates with the relevant antibiotic and incubated at 37°C overnight for clone isolation.

Small-scale isolation of plasmid DNA was done using the Miniprep kit from a 1.5mL harvest from a 5mL overnight bacterial culture and the Maxiprep kit was used for large-scale plasmid DNA extraction from 250mL overnight cultures, both according to the manufacturer's instructions.

The DNA concentration of samples was assessed by measuring the absorvance at 260nm on a NanoDrop ND-1000 spectrophotometer. DNA samples were stored at -20°C.

2.2.4. Restriction digests

1-2µg plasmid DNA was digested by one or several restriction endonucleases in 1X supplied compatible buffer in a final volume of 10-20µL for 30min-1h at the enzyme's appropriate temperature. The amount of enzyme was typically 5% and never exceeding 10% of the total reaction volume. When no compatible buffer was available, multiple digests were performed sequentially, in which case the buffer salts were removed using a PCR Purification kit according to the manufacturer's instructions or the digested DNA was isolated by agarose gel electrophoresis (see below) prior to subsequent digests.

When blunt ends were required after a digest resulting in 5' single-stranded DNA overhangs, these were filled taking advantage of the 5'-3' polymerase activity of the DNA Polymerase I Large (Klenow) Fragment. The reaction was carried out with 40µM each dNTP and with correction of the buffer conditions using 10X DNA Polymerase I buffer (supplied by the enzyme manufacturer). After 30min incubation at 37°C the enzyme was inactivated by heating to 75°C for 10min. The DNA was then purified with a PCR Purification kit or by agarose gel electrophoresis (see below).

The 5' DNA termini of the backbone for a ligation reaction was dephosphorylated after digestion and before gel electrophoresis isolation with Shrimp Alkaline Phosphatase with the buffer conditions adjusted with the provided buffer in a total volume of 50µL. The reaction was carried out alternating the incubation temperature between 37°C and 56°C every 15min for 1h with fresh enzyme added after 30min.

2.2.5. Annealing DNA oligonucleotides for subcloning

2μL of each oligonucleotide (forward and reverse) from a 100μM stock were diluted in 50μL of 1X T4 DNA Ligase buffer (from Promega) and incubated at 95°C for 5min followed by 20min at 75°C, 10min at 70°C and allowed to cool down to room temperature. 5μL of this annealed oligonucleotide solution was phosphorylated in the 5' termini by incubation with 0.5μL T4 Polynucleotide Kinase in 1X T4 DNA Ligase buffer in a total volume of 20μL for 1h at 37°C. 5μL of the phosphorylated annealed oligonucleotides were used for the subsequent ligation reaction.

2.2.6. Agarose gel electrophoresis and isolation of DNA fragments

DNA fragments were resolved in 0.7-1.5% agarose gel electrophoresis in TAE buffer at 70-150V. Samples were loaded into the gel with DNA Loading buffer and 1Kb+ DNA Ladder was run alongside the samples. Ethidium bromide was added to the gel at a concentration of 0.5μg/mL for DNA visualization on a UV transiluminator or a UVIdoc gel documentation system (UVItec). The DNA fragments of interest were excised from the agarose gel and purified using a Gel Extraction kit following the manufacturer's instructions.

2.2.7. Ligation and checking of ligated plasmids

100ng of backbone was used for ligation with insert DNA in a 1:3 molar ratio of backbone to insert using 0.5μL T4 DNA Ligase in 1X T4 DNA Ligase buffer (New England Bioloabs) in final volume 10-20μL. When ligating compatible protruding ends the reaction mix was incubated at room temperature for 1h and when ligating blunt ends the reaction was carried out at room temperature for 2-4h or at 4°C overnight. Ligation products were then transformed into competent bacteria. These were plated out onto LB-agar plates for selection of bacterial colonies.

Colonies were screened for the presence of the correct plasmid DNA construct. Liquid bacterial cultures were started from individual colonies and after small-scale DNA extraction plasmid DNA was digested with restriction endonucleases selected so that the pattern of the restriction fragments upon electrophoresis resolution would allow identification of the correct ligated plasmid.

2.3 Cell culture

Unless otherwise stated, all reagents used in cell culture were supplied by Gibco (Invitrogen). Fetal calf serum (FCS) (Sigma) was heat inactivated at 60°C for 1h prior to use. Tissue culture plastics were from Nunc.

All cells were maintained in humidified incubators at 37°C and 5% CO_2.

The cell concentration and viability was determined by diluting 10µL of the cell suspension in 0.4% Trypan Blue solution (Sigma) and counting at least 50 cells using a haemocytometer. Alternatively, the cell concentration was determined by flow cytometry as described below.

For long term storage of cells, 1-5x10^6 cells were pelleted by centrifugation at 1500rpm for 5min at 4°C and resuspended in 0.5mL ice-cold FCS and transferred to a 1.5mL cryovial. 0.5mL ice-cold 2X freezing media (20% DMSO in FCS) was added and cells were frozen to -80°C in an isopropanol bath before being transferred to liquid nitrogen. To revive frozen cells, vials were rapidly thawed in a 37°C water bath and added to 10mL fresh warmed culture media and centrifuged to wash off the DMSO. The cells were then resuspended in culture media and seeded in culture plates.

All cell lines in culture were regularly screened for mycoplasma infection. Contaminated cultures were either disposed of or treated with 10µg/mL ciprofloxacin for 2 weeks and re-tested for the presence of mycoplasma.

2.3.1. Cell lines

All cell lines were donated by members of the Molecular Immunology Unit (UCL-Institute of Child Health).

293T cell line

293T cell line is a highly transfectable cell line derived from the HEK293 human embryonic kidney cell line that expresses the SV40 large T-antigen which allows for episomal replication of transfected plasmids containing the SV40 origin of replication. This cell line was cultured in DMEM GlutaMAX supplemented with 10% FCS and P/S (100units/mL penicillin and 100ug/mL streptomycin) in 15cm culture plates. For splitting, the

adherent cells were rinsed once with PBS to remove the FCS and then detached by incubation for 2-5min at 37°C with trypsin-EDTA. Fresh media with FCS was added to inactivate the trypsin, the cell suspension was collected and pelleted by centrifugation at 1500rpm for 5min at 4°C and the pellet was resuspended in fresh warm media and replated. 293T cells were routinely passaged upon reaching 90-95% confluence and split 1:3 to 1:10.

THP1 and THP1-derived cell lines

The human acute monocytic leukaemia cell line THP1 was cultured in RPMI 1640 GlutaMAX supplemented with 10% FCS and P/S. These cells were kept at 0.2-1x10^6 cells/mL in culture flasks. For splitting, these non-adherent cells were collected and centrifuged at 1500rpm for 5min at 4°C, the pellet was resuspended in fresh warm media and the cells were replated accordingly.

THP1 cells were differentiated into THP1-derived immature DC (THP1DC) by culturing over a period of 6 days in the presence of 10ng/mL rhIL4 (recombinant human interleukin-4) and 10ng/mL rhGMCSF (recombinant human granulocyte-macrophage colony stimulating factor) [Berges et al. 2005]. 2x10^5 cells were plated in 400µL complete media with cytokines in 24 well plates on day 0 and split 1:4 on day 2 and 1:2 on day 5 and fresh cytokines were added both times. On days 6 or 7, the cultures were scraped and both adherent and non-adherent cells were harvested for use.

PLB

The human acute myeloid leukaemia PLB cell line was cultured and maintained as the THP1 cell line.

Jurkat

The Jurkat leukaemia T-cell line was cultured in the same way as THP1 and PLB cell lines except that they were maintained in upright T75 culture flasks.

2.3.2. Primary cells

Human monocyte-derived DC

Human primary DC were derived from circulating monocytes by culture in the presence of rhIL4 and rhGMCSF [Sallusto and Lanzavecchia 1994]. Up to 50mL peripheral blood was donated by healthy volunteers with ethical approval and informed consent and collected with 5mM EDTA (Sigma). Blood was diluted 1:1 with PBS and peripheral blood mononuclear cells (PBMC) were isolated by density gradient centrifugation with Ficoll-Paque Plus (GE Healthcare) at 2000rpm for 20min at 20°C with no break. PBMC were washed twice with PBS and monocytes were further selected either using the adhesion method or magnetic assisted cell sorting (MACS) beads for CD14 (Miltenyi Biotec). The former consisted on plating PBMC on a culture dish for 4 hours in RPMI 1640 GlutaMAX with 10% FCS and P/S, during which monocytes adhered, and then washing off the non-adherent lymphocytes. For the MACS method 1µL MACS beads were added per $2x10^6$ PBMC and incubated in MACS buffer for 15min at 4°C. Cells were washed and added to a MACS MS column previously primed with 500µL MACS buffer. The column was washed 3 times with MACS buffer and monocytes were then eluted with 1mL MACS buffer. Monocytes were washed in RPMI once, resuspended and seeded at $2x10^5$ cells per well in a 24 well plate in 300µL RPMI with 10% FCS and P/S and cultured over a period of 6-9 days with 2.5ng/mL rhIL-4 and 10ng/mL rhGMCSF. On days 2 and 5 the cytokines were replenished and 100µL fresh media was added. Maturation was induced by overnight culture with 100ng/mL *E. coli* lipopolysaccharides (LPS – Sigma). Cells were harvested by scraping, therefore collecting both adherent and non-adherent cells.

2.4 Lentiviral vector preparation and transduction of target cells

2.4.1. Lentiviral vector production

Second generation lentiviral vectors were produced by transient transfection of 293T cells. The packaging plasmid pCMV-ΔR8.74 (containing the gag-pol, tat and rev genes), the VSVg (vesicular stomatitis virus glycoprotein) envelope plasmid pMDG-2 and the MLV-A (amphotropic murine leukaemia virus) envelope plasmid were from the Molecular

Immunology Unit (UCL-Institute of Child Health). The gp64 envelope plasmid (glycoprotein from the insect fusion virus *Autographica californica*) was a kind gift from Dr Paul McCray Jr, University of Iowa [Sinn et al. 2005], EboZ envelope plasmid (glycoprotein from the Ebola Zaire virus) was a kind gift from Dr François Loic Cossett, Université de Lyon [Sandrin et al. 2002] and RRV envelope plasmid (Ross River virus glycoprotein) was a kind gift from Dr David Sanders, Purdue University [Sharkey et al. 2001].

VSVg, gp64, EboZ and RRV pseudotyped vectors

Lentiviral vectors pseudotyped with VSVg, gp64, EboZ and RRV were produced by transient transfection of 293T cells using polyethyleneimine (PEI). 293T cells were seeded in 15cm culture dishes the day before transfection to achieve 90% confluence. The transfection media per plate was prepared by mixing 5mL OptiMEM with 2nM PEI (0.1µL PEI 10mM stock) (0.22µm filtered) with 5mL OptiMEM with 50µg of vector plasmid, 32.5µg packaging plasmid and 17.5µg VSVg envelope plasmid or 32.5µg gp64, EboZ or RRV envelope plasmids (also 0.22µm filtered). The transfection media was incubated for 20min at room temperature to allow PEI-DNA complexes to form. The cells were rinsed with PBS and incubated at 37°C and 5% CO_2 for 4 hours with transfection media. The transfection media was then replaced with fresh culture media and this was renewed one day later. Viral supernatants were harvested 48h post-transfection and replaced by fresh culture media which was harvested 72h post-transfection. After filtration through a 0.22µm filter to remove cellular debris the viral supernatants were concentrated by ultracentrifugation at 23000 rpm for 2h at 4°C for VSVg, gp64 and EboZ vectors or at 10000rpm for 15h at 4°C for RRV vectors. The viral pellets were incubated for 20min on ice with 100µL RPMI and then resuspended, aliquoted and stored at -80°C.

MLV-A pseudotyped vectors

For the production of MLV-A pseudotyped vectors 293T cells were transfected with 19.2µg vector plasmid, 28.8µg packaging plasmid and 28.8µg envelope plasmid using the calcium phosphate method (Calcium Phosphate Transfection Kit, Invitrogen, according to the manufacturer's instructions). Briefly, the plasmid DNA was mixed with a concentrated $CaCl_2$ solution and then added dropwise to a phosphate buffer solution with constant mixing by aeration and incubated at room temperature for 30min in order to form a fine precipitate. 293T cells seeded in 15cm culture dishes to 90% confluence were rinsed with PBS and incubated with 10mL transfection media for 4h. The transfection media was removed and replaced by fresh culture media, and this was renewed 24h later. Viral supernatants were harvested 48h and 72h post transfection, filtered through

a 0.22μm filter and concentrated by 20h centrifugation at 4000rpm at 4°C. Concentrated virions were aliquoted and stored at -80°C.

Titration of lentiviral vector preparations

The infectious titres of the viral preparations were determined in 293T cells by measuring transgene expression. 293T cells were seeded in 24 well plates at 10^5 per well in 500μL culture media. The next day viral aliquots were thawed and a serial dilution was prepared in 200μL compete media (dilutions 1:50, 1:250, 1:1250, 1:6250, 1:31250). The 293T media was replaced by the viral dilutions' culture media. 3 days later, the culture media was removed, the cells rinsed with PBS and incubated with 50μL trypsin-EDTA for 2-5min and collected with 150μL complete media. Cells were fixed and transgene expression determined by flow cytometry (see below). The titre was calculated as the number of transduced cells per viral preparation volume taking into consideration only the samples with transduction between 5% and 40% (where there is a linear relation between virus transduction and viral preparation volume). Viral titres in the order of 10^8-10^9 TU/mL (transduction units/mL) were consistently obtained.

The physical titres were determined by measuring the reverse transcriptase (RT) activity in the viral preparation using an enzyme linked immunosorbent assay (ELISA) (Reverse Transcriptase Assay, colorimetric, from Roche Applied Science) as per manufacturer's instructions. Briefly, concentrated vector aliquots were thawed, diluted 1:200, 1:250 and 1:300, the virions were lysed, mixed with a template/primer hybrid, dNTPs and digoxigenin- and biotin-labelled dUTP and incubated for 3h at 37°C to allow synthesis of a new DNA strand (with labelled dUTP) by the RT enzyme in the samples. The amount of DNA synthesised, as a measure of RT activity, was quantified by ELISA: the reaction mix was transferred to a microplate coated with streptavidin, to which biotin-labelled DNA binds, the plates were incubated with a peroxidase-labelled anti-dioxigenin antibody, the peroxidase substrate ABTS was added and the coloured reaction product was detected by measuring the absorbance at 405nm in a microplate reader, which correlates linearly to the amount of DNA in the sample. A calibration curve was performed using the standard RT solutions provided with the assay kit and the titres were calculated as the amount of RT per viral preparation volume.

2.4.2. Transduction of cell lines and primary DC

The amount of virus used for transduction of target cells was determined by arbitrarily

fixing a value for the multiplicity of infection (MOI). This corresponds to the number of transduction units used per target cell.

Transduction of THP1, PLB and Jurkat cells

$5x10^5$ cells were seeded in 12 well plates in 500µL complete media and 5µL viral aliquot was added (MOI of 5-10). The cells were expanded and 3 days later the transgene expression was measured by flow cytometry (see below). The cultures were then enriched in transduced cells by fluorescence-activated cell sorting (FACS) and clonal cell lines were generated by FACS as well (see below).

Transduction of human primary DC

Human primary DC were cultured as described above. Unless otherwise stated, transduction was carried out on day 0 of culture on freshly isolated monocytes by adding the appropriate volume of viral preparation (MOI or amount of RT as stated in the text) in the total culture media volume of 300µL. When viral transduction was carried out on days 2 or 5 of culture, the viral preparation volume was added to the cultures together with fresh cytokines in 100µL fresh culture media. Viral supernatants were not washed off and the cells were cultured for a total of 8 days, after which they were harvested. Transgene expression was assessed by flow cytometry (see below) at least 3 days after transfection.

2.4.3. DC transduction efficiency of differently pseudotyped vectors

Primary human DC were transduced with viral vectors over a range of RT amounts from 0 (untransduced DC) to 2.5pgRT/cell (corresponding to VSVg equivalent MOI higher than 150) in order to calculate a transduction curve. The efficiency of the vectors in transducing DC was determined by calculating the slope of the linear region of the transduction curve (transduction between 5% and 40%) and expressed as transduction units per ngRT (TU/ngRT).

2.5 Reverse transcriptase quantitative PCR (RT-qPCR)

2.5.1. mRNA extraction

1-10x10^6 cells were washed in PBS, pelleted and stored at -80°C. Cell pellets were resuspended in 1mL TRIzol Reagent (Invitrogen) and incubated at room temperature for 5min. 200µL chloroform was added and the samples were mixed by shaking vigorously for 15sec and left to stand at room temperature from 10min. The samples were then centrifuged for 5min at 13000rpm, resulting in the separation of 3 phases: a protein-rich red organic bottom layer, a cloudy DNA interphase and a top clear aqueous phase containing the RNA. The aqueous phase was transferred to a fresh tube and the RNA was precipitated by adding 0.5mL isopropanol and incubating for 10min at room temperature. The RNA was pelleted by centrifugation at 13000rpm for 10min, the supernatant was discarded and the pellet was washed with 1mL 70% ethanol, air dried and then dissolved in 50µL water. The RNA concentration of samples was assessed by measuring the absorvance at 260nm on a NanoDrop ND-1000 spectrophotometer. RNA samples were stored at -80°C.

2.5.2. Synthesis of cDNA from mRNA

RNA was reverse transcribed using M-MLV reverse transcriptase (Applied Biosystems) according to manufacturer's instructions. 2µg total RNA was mixed with 1µL RNAse inhibitor, 2µL random hexamers (at 50µM) or 1µL 16-mers oligo-dT (at 100µM) and 4µL of 10mM each dNTP (Applied Biosystems). The samples were incubated at 70°C for 10min to denature dsRNA and prevent nonspecific binding of the primers, and were then placed on ice. 2µL 10x PCR buffer, 2µL $MgCl_2$, 1µL RT and water to make up a total reaction volume of 20µL was added to each sample and incubated for 1h at 48°C. The resulting cDNA/RNA hybrid samples were store at -20°C and used as template for quantitative PCR analysis. The same procedure was performed in parallel but without RT enzyme so as to control for genomic DNA contamination.

2.5.3. PCR reaction and RNA quantification

PCR reactions were done in triplicate in a final volume of 25µL with 3µL cDNA/RNA sample prepared as described above, 1µL forward and reverse primers and probe mix (0.9µM each primer and 0.2µM probe, from TaqMan Gene Expression Assays, Applied Biosystems, using intra-intron primers) and 1X mastermix Platinum qPCR SuperMix-UDG with ROX (Invitrogen). β-Actin was used as housekeeping gene. PCR reactions were performed in the ABI Prism 7000 Sequence Detection System with default cycling parameters: initial steps of 2min at 50°C and 10min at 95°C followed by 40 cycles of 95°C for 15sec and 60°C for 1min.

Relative quantification

The cycle threshold was arbitrarily set to a value where the fluorescence of all PCR reactions was increasing exponentially. The cycle time (CT) needed for each reaction to reach the cycle threshold was so determined. The cycle time for the mRNA of interest relative to the housekeeping gene (ΔCT) was calculated as the difference between the CT of the reaction for the mRNA of interest and the CT of the reaction for the housekeeping gene. These ΔCT were then compared to a reference (untransduced) sample by calculating the ΔΔCT ($\Delta CT_{sample} - \Delta CT_{reference}$) and the fold increase/decrease in mRNA in one sample relative to the reference sample was calculated as $2^{-\Delta\Delta CT}$.

2.6 Protein analysis by Western blotting

The following reagents and equipment for Western blotting were from Invitrogen NuPAGE system: NuPAGE LDS Sample Buffer, NuPAGE Reducing Agent, NuPAGE Novex Bis-Tris pre-cast 4-12% gels, NuPAGE MOPS/MES SDS Running Buffer, NuPAGE Antioxidant, NuPAGE transfer buffer and XCell SureLock Mini-Cell or XCell4 SureLock Midi-Cell gel tanks. Pre-stained protein standard was from Fermentas (PageRuler Prestained Protein Ladder). Membrane blotting was done using a Biorad Semidry Blotter and membranes were developed with the SuperSignal West Pico (Pierce) enhanced chemiluminescence (ECL) substrate and a supercooled camera and UVIchemi chemiluminescence gel documentation system (UVItec).

All membrane washes were done with TBS-T and blocking was done using BSA blocking buffer.

2.6.1. Cell lysis

Cells for Western blotting were harvested, washed once in PBS, pelleted and stored at -80°C until lysis. Cell pellets were resuspended in Cell Lysis Buffer at $10x10^6$cells/mL (usually 10^6 cells in 100µL lysis buffer) and incubated for 10min on ice. The samples were centrifuged at 13000rpm for 10min at 4°C and the supernatants (lysates) were transferred to fresh tubes and stored at -80°C. Protein lysates were denatured and reduced at 70°C for 10min with 1X Sample Buffer and 1X Reducing Agent (5.5µL of a mix of 80µL 4X Sample Buffer and 30µL 10X Reducing Agent were added to each 10µL lysate). Reduced samples were stored at -20°C.

2.6.2. SDS-PAGE and Western blotting

Pre-cast gel wells were rinsed 3 times with Running Buffer and then assembled in the gel tank. Prior to loading, samples were heated again to 70°C for 10min and centrifuged at 13000rpm for 5min at 4°C. Outer wells were filled with Loading Buffer and 5uL of pre-stained protein standard was run alongside samples. All wells were toped up with Loading Buffer to the same volume. 500µL Antioxidant was added to the inner (cathode) chamber and electrophoresis was run for 1-2h at 150-200V with the gel tank on ice to prevent overheating.

Gels were removed from the cassettes and proteins transferred to Milipore Immobilon PVDF membranes (previously labelled with a ball-point pen and activated in methanol for 5min) using a semidry blotter with 2X NuPage Transfer Buffer at 18V for 45min.

2.6.3. Immunoblotting

Membranes were blocked in BSA blocking buffer for 2h (all incubations were made on an orbital shaker or rotor). When appropriate, membranes were wrapped in cling film and cut into strips for different antibody staining. Membranes were incubated with

Table 2.2. Antibodies and fluorescent dyes.

Name	Description	Raised in	Label	Manufacturer	Reference	Use	Dilution
vinculin	Human vinculin	mouse	none	Sigma	V-9131	IF	1:250
cCD18	Canine CD18	mouse	none	Serotec	MCA1780	IF	1:50/1:20
CD18	Human CD18	mouse	none	BD Biosciences	555922	IF	1:100
CD18-PECy5	Human CD18	mouse	PE-Cy5	BD Pharmingen	557528	FC	5uL/sample
CD29 (4B7R)	Human CD29	mouse	none	Serotec	MCA1949	IF	1:100
CD29 (P5D2)	Human CD29	mouse	none	ICRF London	clone P5D2	IF	1:100
CD29 (HUTS-4)	Human CD29	mouse	none	Millipore	MAB2079Z	IF	1:100
CD29-PE	Human CD29	mouse	PE	BD Pharmingen	555443	FC	5uL/sample
CD86-PE	Human CD86	mouse	PE	BD Pharmingen	555658	FC	5uL/sample
HLADR-PE	Human HLADR	mouse	PE	BD Biosciences	347401	FC	5uL/sample
CD11c-APC	Human CD11c	mouse	APC	BD Pharmingen	555392	FC	5uL/sample
HS1	Human HS1	mouse	none	BD Biosciences	610540	WB/IF	1:1000 / 1:50
Cortactin (4F11)	Human cortactin	mouse	none	Millipore	05-180	WB	1:1000
WASp (B9)	Human WASp	mouse	none	Santa Cruz	sc-13139	WB	1:1000
WIP (H-224)	Human WIP	mouse	none	Santa Cruz	sc-25533	WB	1:1000
GAPDH	Rabbit GAPDH	mouse	none	Santa Cruz	sc-32233	WB	1:1000
anti mouse Cy5	Mouse immunoglobulins	goat	Cy5	Jackson ImmunoResearch	115-175-003	IF	1:200
anti mouse HRP	Mouse	sheep	HRP	GE Healthcare	NXA931	WB	1:2000
DAPI	n.a.	n.a.	n.a.	Sigma	D9542	IF	1:250
Rho-phalloidin	n.a.	n.a.	Rhodamine	Molecular Probes	R415	IF	1:100
AF488-phalloidin	n.a.	n.a.	AF488	Molecular Probes	A12379	IF	1:100
AF647-phalloidin	n.a.	n.a.	AF647	Molecular Probes	A22287	IF	1:100
7-AAD	n.a.	n.a.	n.a.	Sigma	A9700-aMG	FC	1uL/sample

PE Phycoerythrine; AF Alexa-fluor; IF immunofluorescence; FC Flow cytometry; WB Western blotting; n.a. not applicable.

primary (unconjugated) antibody diluted in 2% BSA in TBS-T for 2h to overnight, washed 5 times in TBS-T, incubated with secondary (HRP-conjugated) antibody in 1% BSA in TBS-T for 1h, washed 5 times in TBS-T and incubated with ECL substrate for 5 min before protein bands were visualised. Antibodies and concentrations used for immunoblotting are listed in Table 2.2. For re-blotting, membranes were washed 5 times in TBS-T and then incubated with the appropriate antibodies as described above – stripping of the membranes was not necessary because protein bands were sufficiently resolved not to overlap.

2.6.4. Quantification by densitometry

Quantification of protein bands was done using the UVIband software (UVItec) to measure their densitometry. Images were taken in such fashion that the full range of the camera's sensitivity was used but ensuring that saturation was not reached. Background subtraction was done manually per band and direct comparisons were only made between bands run in the same gel and developed at the same time.

For relative expression levels, the densitometry of each protein band was divided by the densitometry of the GAPDH band (used as loading control) and this was then divided by the result for the reference (untransduced) sample.

2.7 Flow cytometry

All flow cytometry analysis was performed in the CyAn ADP flow cytometer analyser and with Summit version 4.1 software (DakoCymotation/Beckman Coulter) using a live cell gate on a forward-scatter vs. side-scatter plot. Control unstained and single-stained samples were always prepared, as well as samples with secondary antibody only or isotype control antibodies when absolute levels of expression were to be determined. Fluorescently-activated cell sorting (FACS) was either performed in a Beckman Coulter EPICS Altra Cell Sorter by myself or in a MoFlo XDP Cell Sorter by a member of the ICH/GOSH Flow Cytometry Core Facility (UCL-Institute of Child Health/Great Ormond Street Hospital for Children). Antibodies and dies used are listed in Table 2.2.

2.7.1. Flow cytometry analysis

Phenotyping and transgene expression was done by flow cytometry on samples of 0.1-1x10^6 cells resuspended in a final volume of 300µL PBS in 5mL polypropylene tubes. When analysing live cells, the analysis was done immediately after manipulation. For fixed samples, these were kept at 4°C and analysed within 2 days. Cells were resuspended by vortexing, all incubations were performed in the dark and all washes were done with PBS and centrifugation was at 1500rpm for 5min at 4°C.

For surface staining, cells were harvested, washed and resuspended in 100µL PBS. The relevant antibody was added and the samples incubated for 30min at 4°C, after which the excess antibody was washed off. If a secondary antibody was required, the procedure described above was repeated. Cells were resuspended in 300µL PBS and analysed immediately or fixed in 100µL fixing buffer for 30min at room temperature, washed and resuspended in 300µL PBS and stored at 4°C. For intracellular staining, cells were fixed in 100µL for 30min at room temperature, permeabilised in 100µL permeabilisation buffer for 5min at room temperature and then incubated with the relevant antibodies in permeabilisation buffer. After washing, the samples were resuspended in 300µL PBS.

For the detection of fluorescent transgene expression, the cells were simply harvested and resuspended in either 300µL fixing buffer or in PBS and immediately analysed.

Analysis of cell viability was performed on live unfixed cells, kept on ice throughout, using 7-AAD (7-aminoactinomycin D, 5µL of 1mg/mL stock solution per sample).

The concentration of cell cultures was determined by flow cytometry using AccuCheck Counting Beads (Invitrogen). 100µL cell culture was harvested, diluted with 200µL PBS, 10µL bead suspension added and run in the flow cytometer. The absolute number of cells was calculated relative to the number of beads detected by the cytometer.

2.7.2. Cell sorting

Cells were harvested, washed and resuspended in culture media with 2% FCS at 1-2x10^6cells/mL. Cells were sorted on the basis of fluorescent marker expression and collected in media with 20% FCS. When sorting bulk populations, sorted cells were centrifuged, resuspended in complete media and plated in culture plates and expanded. When generating clonal cell lines, single cells were sorted into U-bottom 96 well plates containing 200µL media with 20% FCS. These were then allowed to grow for 1-2 weeks and clones that successfully grew were further expanded.

2.8 Immunofluorescence

2.8.1. Coverslip and glass slide preparation

Glass coverslips (22x22mm) were treated with 1M HCl overnight, washed with deionised water, stored in ethanol and flamed before use. When using glass slides, 8-well Lab-Tek chamber slides were used or otherwise wells of approximately 10x10mm were drawn onto regular glass slides with an ImmEdge hydrophobic barrier pen (Vector Laboratories). Coverslips or glass slides were coated with either 10µg/mL fibronectin (from human plasma, purchased from Sigma) in PBS or 5µg/mL recombinant human intercellular adhesion molecule 1 (ICAM, from R&D Systems) in PBS for 1h at 37°C or overnight at 4°C. The excess substrate was washed off and the coverslips or slides washed with PBS and culture media prior to plating cells. 200µL cell suspension was plated per glass coverslips and 100µL per well on glass slides at a concentration of 10^5 cells/mL.

2.8.2. Immunostaining

All washes were done by dipping the glass coverslip/slide in 3 consecutive PBS baths. All incubations were done at room temperature and in the dark. Antibodies and dyes used are listed in Table 2.2.

Non-adherent cells were washed off with PBS and adherent cells were fixed in cell fixing buffer for 30min. Cells were permeabilised for 5min, washed and incubated with the relevant primary antibodies for 30min. The excess antibodies were washed off, cover slips/slides were washed and further incubated for 30min with secondary antibodies. Phalloidin and DAPI were added together with the secondary antibodies. After washing, the samples were rinsed with deionised water and glass slides and coverslips were mounted with ProLong Gold Antifade Reagent (Molecular Probes) and sealed with nail polish. Slides were stored at 4°C until imaging.

2.8.3. Localisation of podosome components

For localisation experiments, samples were imaged by confocal microscopy using the

Leica Confocal Scanning microscope TCS SP2 or the Zeiss Confocal Scanning microscope LSM 710 with a 63X oil immersion objective.

2.8.4. Analysis of cell morphology and polarization

THP1DC plated onto fibronectin or ICAM coated coverslips were allowed to adhere and spread for 48h, after which they were labelled with rhodamine-phalloidin and random fields were imaged using the Zeiss Axiovert 135 fluorescence microscope and a Hamamatsu digital camera (C4742-95) and Volocity 4.2 software (Improvision). Cells were counted and morphological parameters calculated automatically using ImageJ (National Institutes of Health, MD) and automated subroutines written in-house. All images were first randomised to blind for the experimental condition. Areas with mainly single cells were cropped and clusters of cells and cells touching the edges of the images were discarded. Cells were identified by manual thresholding and their edges smoothed by consecutively applying the dilate and erode functions. The number of cells was recorded as well as the circularity and aspect ratio of individual cells. This process was automated using MeasureParticles_.txt ImageJ macro (Supplemental Materials and Methods). Circularity was defined as $4.\pi.\text{area} / \text{perimeter}^2$; a value of 1 corresponds to a perfect circle and values approaching 0 mean increasingly elongated shapes (increasing perimeter for the same area). Aspect ratio was the ratio of the major axis over the minor axis of the best fitting ellipse for the cell shape. In order to determine de percentage of polarised cells, 100 cells were first scored manually as polarised or not and the best indicator for polarization between circularity and aspect ratio was defined to be an aspect ratio larger than 1.6. 4 independent experiments were done and a minimum of 50 cells per conditions and per experiment were analysed, except for one of the experiments where only 24 and 39 cells were analysed for conditions UNT and HS1-16 respectively.

2.8.5. Identification and characterization of podosomes

Plated cells were labelled with anti-vinculin antibody (and Cy5-conjugated secondary antibody) and phalloidin and imaged using the Zeiss Confocal Scanning microscope LSM 710. To determine the percentage of cells that assembled podosomes, a minimum of 100 cells per condition were scored for the presence or absence of podosomes.

In order to characterize podosomes in single cells, z-stacks with 5 images were taken incorporating the whole podosome core. These were randomly coded to blind for the experimental condition and processed using ImageJ to enhance contrast and sharpness

of podosomes by applying a 10 pixel bandpass filter, auto-adjusting levels, applying a 1 pixel radius median filter, and taking the maximum intensity z-projection of the actin signal using StackProcess_1.txt macro (Supplemental Materials and Methods). Podosome arrays were characterised by eye as: in the middle of the cell; behind the leading edge; touching the leading edge; or on the side of the cells. Images were duplicated and a region of interest (ROI) was drawn by hand defining the podosome array borders and podosomes were identified automatically inside the defined ROI by thresholding to 50% of the dynamic range and applying the functions erode, watershed and dilate. This was automated by running the ImageJ macro PodosomeArray_and_Podosomes_Masks.txt (Supplemental Materials and Methods) for each individual image, enabling measurement of the area and saving the podosome array mask, identifying individual podosomes and analysing them. Individual podosome masks were also saved using this macro. These were then used to manually confirm all automatically identified podosomes.

2.9 Functional assays

2.9.1. Adhesions dynamics by IRM

Interference reflexion microscopy (IRM) analysis of adhesions dynamics was performed using the Zeiss Confocal Scanning microscope LSM 710 with a 63X oil immersion lens and an incubation chamber to assure constant 37°C. THP1DC were plated onto glass coverslips coated with fibronectin or ICAM and allowed to adhere. Coverslips were assembled with culture media equilibrated in a 37°C and 5% CO_2 incubator onto glass slides that had a cavity and sealed with a mix of paraffin and bees wax. IRM images were taken every 0.5sec using the 488nm laser line with a 80/20 dichroic beam splitter to allow detection of reflected light with the same wavelength. The focus plane was set to the coverslip-culture medium interface and maintained by constant manual adjustment. Videos were processed using automated subroutines written for ImageJ.

32 frame sequences with 2 frames per second where focusing was maintained were identified and scanning line background noise was removed by Fourier Transform (FT) analysis using macro FFTFilter6512tifBatch.txt and the purposely designed filter Filter6_512.tif (Supplemental Materials and Methods). Adhesion areas were cropped and processed to enhance contrast and sharpness as follows: auto-levels were applied followed by a highpass filter with radius 10, auto-levels reapplied followed by a 2 pixel median filter [Holt et al. 2008]. This was automated using ImageJ macro IRMProcess_

NEW.txt. (Supplemental Materials and Methods).

In order to calculate an Adhesion Index [Holt et al. 2008] the ImageJ macro HistogramIRM_macro.txt (Supplemental Materials and Methods) was run. Individual frames were thresholded at 50% of the 8 bit dynamic range so contact points appeared black, sets of 4 consecutive frames 1sec apart were then overlaid as average intensity z-projections and the histogram values of the new images were copied to a Microsoft Excel spread sheet for further calculations. The resulting images contained 5 grey levels corresponding to areas where there were no adhesion sites in any of the frames (255 – white), adhesions present in 1 or 2 frames (grey levels 191 or 127 – lighter greys) or more stable adhesion areas (64 or 0 – dark grey or black). The Adhesion Index was calculated as the ratio between the darker pixels (levels 0 and 63) and the total number of pixels (levels 0, 63, 191, 127 and 255).

To calculate a Turnover Index, another ImageJ macro was used on the cropped videos: IRMProcess_NEW_NEW_2ndAnalysis.txt (Supplemental Materials and Methods). The LUT (look-up table) of the processed individual frames was converted into an equally spaced 4 grey level LUT. The difference between two consecutive images 1sec apart was calculated and the histogram levels used to calculate the Turnover Index as the ratio between the adhesion areas that changed by one level between the two frames (darker pixels, grey level 64) and the total number of pixels (levels 0, 64, 128 and 192). Variations on this Turnover Index were calculated: an 8 grey level LUT was used (IRMProcess_NEW_NEW_3rdAnalysis_NEW.txt); frames 0.5sec apart were analysed with 4 grey level LUT (IRMProcess_NEW_NEW_4thAnalysis.txt); or frames 0.5sec apart were analysed with 8 grey level LUT (IRMProcess_NEW_NEW_5thAnalysis.txt) (Supplemental Materials and Methods).

2.9.2. Mixed lymphocyte reaction

PBMC were plated in triplicate at $2x10^5$ cells/well in 96-well plates in AIM V medium (Gibco) and stimulated with allogeneic DC (DC to effector cell ratio as indicated) in a total volume of 200µL. After 5 days of culture, PBMC were pulsed with 1 µCi/well [^{3}H]thymidine (GE Healthcare) for 20 hours, after which plates were frozen at -20°C until further analysis. To determine the amount of [^{3}H]thymidine incorporation, which correlates with lymphocyte proliferation, cells were harvested onto a filter mat using a plate harvester and the amount of [^{3}H] per well was measured with a MicroBeta TriLux (PerkinElmer Life and Analytical Sciences). Wells with no stimulating cells and with stimulating cells alone were also prepared and used to set the background for test cultures. 10µg/mL phytohemagglutinin (PHA) was used as positive control for stimulation and lymphocyte proliferation. The data are presented with the response from unstimulated responding

cells and stimulating cells alone subtracted from the response of test cultures.

2.9.3. Dextran uptake

DC were harvested, resuspended at $2x10^5$ cells/mL in RPMI, and 100µL of the cell suspension was added into 5mL polypropylene tubes. Tubes were placed on ice for 5min after which 1mg/mL rhodamine-conjugated dextran (Molecular Probes) was added. Tubes were transferred to a 37°C water bath and incubated for 0, 15, 30, 45 and 60min. The samples were immediately washed twice with ice-cold PBS and twice with culture media and plated onto poly-L-lysine coated glass slides. After 2h the cells were fixed, permeabilised and stained with AF647-phalloidin and DAPI as described above. Slides were imaged with the Leica laser scanning confocal microscope TCS SP2 to detect GFP, Rhodamine, AF647 and DAPI. A minimum of 100 cells for each condition (GFP positive and GFP negative) were scored as positive or negative for dextran signal using ImageJ.

An analysis of the covariance (ANCOVA) of Log10 dextran uptake with time, using the experimental condition as a fixed factor, was performed in the SPSS statistics software. A full factorial model was used to estimate the marginal mean values of dextran uptake for each condition, and differences between these means were assessed using a Bonferroni correction.

2.9.4. Migration assay

DC were plated on fibronectin-coated glass coverslips and allowed to adhere for 3h to overnight. Glass coverslips were assembled onto Dunn chambers with culture media equilibrated in a 37°C and 5% CO_2 incubator and sealed with a mix of paraffin and bees wax. Cell motility was recorded using a Zeiss Axiovert 135 microscope with a 10X phase contrast lens (Zeiss). Images of bright field and GFP fluorescence were acquired every 5 minutes using a Hamamatsu digital camera and Volocity 4.2 software. Images were analysed using Volocity 4.2 software. Migration was determined by manually tracing the leading edge of individual cells for each frame.

2.9.5. Adhesion assay

Transduced (GFP^+) and untransduced (GFP^-) THP1 cells were harvested, resuspended in complete media at a concentration of $5x10^5$ cells/mL and mixed in a 1:1 ratio. 500µL of the resulting cell suspension was analysed by flow cytometry to determine the exact ratio of transduced to untransduced cells in each sample and 100µL of the cell suspension was plated in duplicates onto wells drawn on glass slides and previously coated with either fibronectin or ICAM. 30min and 1h after plating, the non-adherent cells were washed off and the samples fixed, stained with rhodamine-phalloidin and DAPI and imaged with the Zeiss Confocal Scanning Microscope LSM 710 or the Zeiss Axiovert 135 fluorescence microscope. GFP, DAPI and rhodamine signals were recorded with a minimum of 300 cells per well imaged. GFP^+ and GFP^- cells were counted using ImageJ and the percentage of transduced adherent cells was determined. The adhesion capacity of transduced cell lines relative to untransduced cells was calculated as the ratio of the percentage of adherent transduced cells to the percentage of transduced cells in the initial cell suspension (as determined by flow cytometry).

Chapter

3

LENTIVECTORS AS POTENTIAL TOOLS FOR MANIPULATING THE IMMATURE DC CYTOSKELETON

3.1 Introduction

The use of DC for experimental purposes has been made possible by the advance over the past decades in techniques to allow *ex vivo* generation of DC from circulating precursors. In DC cytoskeletal studies, in particular for the study of DC podosomes, which are assembled in immature DC only, great care has to be taken regarding the activation the cells since manipulation strategies may constitute activation stimuli and, thus, result in DC maturation and loss of the immature phenotype. Lentiviral vectors, in particular, have arisen as potential tools for the genetic manipulation of DC for both experimental and therapeutic studies. However, there is contradictory evidence in the literature regarding their effect on the activation of these cells.

The potential of SIN lentivectors to transduce human monocyte-derived DC while retaining their immaturity was analysed. Lentivectors harbouring an eGFP expressing cassette and pseudotyped with different envelopes were used and transduction experiments were performed so as to establish a transduction protocol, paying particular attention to the immature phenotype of the transduced DC. Further characterization of transduced cells was made both in terms of their function as immature immune cells as well as their cy-

toskeleton, namely, the ability to assemble podosomes and migratory behaviour.

3.2 Comparison of monocyte isolation method for generating moDC

Ex vivo generation of monocyte-derived human DC is achieved by culturing peripheral blood monocytes over 5 days in the presence of interleukin-4 (IL-4) and granulocyte-monocyte colony stimulating factor (GMCSF) [Sallusto and Lanzavecchia 1994]. First, peripheral blood mononuclear cells (PBMC) have to be isolated from peripheral blood by density gradient centrifugation over ficoll, and then monocytes can be further selected by two methods: adhesion method or magnetic activated cell sorting (MACS) using anti-CD14 magnetic beads. We compared the two monocyte isolation methods in regards to the purity and the viability of the final DC culture, as assessed by CD11c and 7-AAD staining by flow cytometry (Figure 3.1 A). The MACS method resulted in purer DC cultures (87% $CD11c^+$ cells compared to only 55% obtained for the adhesion method) as well as a slightly lower percentage of dead cells (10% vs. 13% $7\text{-}AAD^+$ cells within the $CD11c^+$ cells) (Figure 3.1 A). Two cell populations are clearly identified in the flow cytometry forward scatter vs. side scatter plots from this experiment (Figure 3.1 A), one with larger and more granular cells, corresponding to the $CD11c^+$ cells, and another of smaller and rounder cells, the major contaminant present in the adhesion method DC culture, which the scatter signals suggest to be lymphocytes.

DC maturation is characterized by significant up-regulation of surface MHCII and T-cell co-stimulatory molecules, such as CD80 and CD86 [Banchereau et al. 2000]. Hence we analysed the expression levels of these molecules in the DC resulting from the two isolation methods. DC generated by MACS were mostly negative for CD86 whereas those prepared with the adhesion method presented higher levels of CD86 expression (Figure 3.1 B). As for MHCII, both monocyte isolation methods resulted in HLADR positive DC but cells prepared with magnetic beads were low expressers whereas HLADR expression was up-regulated in DC prepared by the adhesion method (Figure 3.1 B).

Due to a higher purity and reduced DC activation, the MACS method was used in all subsequent experiments, where a CD11c purity of above 95% was consistently obtained in the resulting DC cultures (data not shown).

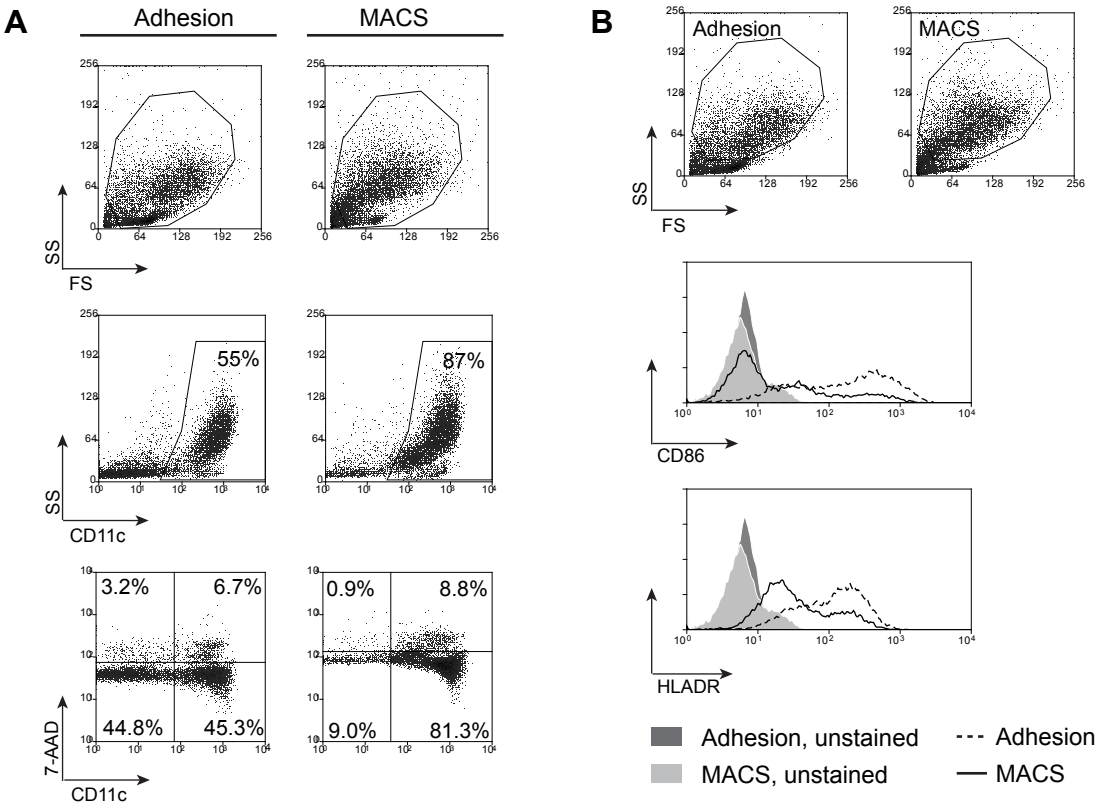

Figure 3.1. MACS monocyte isolation method yields purer monocyte derived DC cultures and results in lower cell activation.
A Monocyte derived DC cultures generated using either the adhesion method or anti-CD14 magnetic beads (MACS) for monocyte isolation were analysed by flow cytometry. Cells were stained with anti-CD11c antibody and the viability dye 7-AAD. **B** Surface expression of the activation markers CD86 and HLADR was also compared by flow cytometry. Results presented as overlay histograms correspond to $CD11c^+$ events which fall within the "live-gate" shown in the forward scatter vs. side scatter plots in the top row.

3.3 Comparison of transduction of moDC at different times during differentiation

The second generation SIN lentiviral vector pLN-SEW was used in this study. The viral construct contained an expression cassette comprised of the spleen focus forming virus internal promoter (SFFV) driving the expression of enhanced green fluorescent protein (eGFP), the HIV-1 central polypurine tract (cPPT) and central termination sequence (CTS) elements as well as the woodchuck hepatitis virus post-transcriptional regulatory element (WPRE) [Demaison et al. 2002] (Figure 3.2 A). The presence of the cPPT and CTS elements results in higher titres and facilitates reverse transcription and nuclear entry, thus improving transduction [Follenzi et al. 2000; Zennou et al. 2000]. The incorporation of WPRE in the 3' untranslated region of the transgene results in increased amounts of transgene mRNA in the cytoplasm, leading to higher transgene expression [Donello et al.

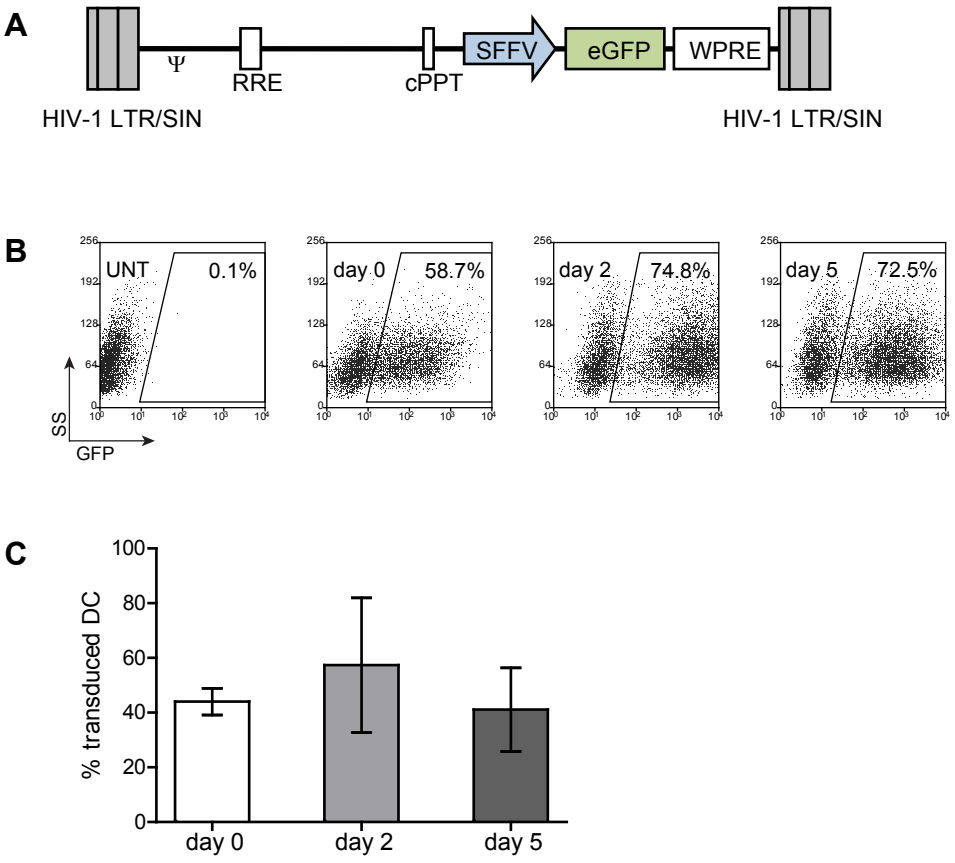

Figure 3.2. DC are efficiently transduced on day 0, 2 or 5 of differentiation culture. **A** Schematic representation of the proviral form of the lentivector pLN-SEW, used to transduce DC. HIV-1 LTR/SIN: HIV-1 long terminal repeat with U3 region deleted. Ψ: packaging signal. RRE: rev responsive element. cPPT: HIV-1 central polypurine tract and central termination sequence. SFFV: 3' long terminal repeat of the spleen focus forming virus (promoter). eGFP: enhanced green fluorescent protein. WPRE: woodchuck hepatitis virus post-transcriptional regulatory element. **B** DC were transduced with VSVg-pseudotyped lentivectors on days 0, 2 and 5 of culture (MOI 20, 0.3pgRT/cell) and transduction was assessed by eGFP expression. Flow cytometry plots for one experiment are presented as well as **C** the aggregated results from 3 independent transduction experiments using 2 viral batches and 3 different donors (mean percentage of transduced cells ± SD). Flow cytometry analysis was done using a "live-gate" and also gating on CD11c positive cells.

1998]. These elements have also been shown to enhance gene transfer efficiency as well as transgene expression in primary haematopoietic cells *in vivo* [Demaison et al. 2002] as well as in DC *in vitro* [Breckpot et al. 2003].

The first thing addressed regarding DC transduction was whether lentivectors could equally transduce immature DC and their precursors during the differentiation process from peripheral blood monocytes. Monocytes (day 0 of culture), cells in an intermediate stage of differentiation (day 2 of culture) and completely differentiated immature DC (day 5 of culture) were transduced with VSVg-pseudotyped lentivectors and the percentage of transduced DC (GFP^+ cells) was determined on day 8 of culture by flow cytometry (Figure 3.2 B). It has been suggested that fully differentiated DC are less permissive to infection

by HIV-1 and HIV-1-derived vectors [Breckpot et al. 2004b; Cameron et al. 1996; Granelli-Piperno et al. 1998; Schroers et al. 2000] and reverse transcription has been shown to be blocked in mature DC [GranelliPiperno et al. 1997] and therefore previous studies using lentivectors have transduced moDC 1-3 days into differentiation [Breckpot et al. 2004a; Breckpot et al. 2003; Breckpot et al. 2007; Rouas et al. 2002; Schroers et al. 2000]. In our study, however, the average percentage of transduced cells was not significantly different between transduction in the earlier or later days of differentiation (MOI of 20 resulted in 44% ± 5% transduced cells at day 0; 57% ± 25% at day 2; and 41% ± 26% at day 5 – Figure 3.2 C). Nevertheless, results were more variable for cells transduced in later stages of differentiation, suggesting an advantage of transduction on day 0. Lentiviral transduction did not affect cell viability, as assessed by 7-AAD staining (1-3% 7-AAD positive cells for all cultures regardless of transduction; data not shown).

3.4 Comparison of the efficiency of different pseudotypes in transducing moDC

Pseudotyping lentivectors with different envelopes can improve their physical properties such as stability, as well as confer specific tropism, leading to more specific and enhanced gene transfer. Lentivectors were pseudotyped with VSVg or the envelope proteins from the Ross River virus (RRV), the amphotropic murine leukaemia virus (MLV-A), the Ebola Zaire virus (EboZ) or the insect fusion virus *Autographica californica* (gp64) in order to compare their efficiency in transducing DC. Physical titres (in pg reverse transcriptase activity per cell – pgRT/cell) rather than infectious titres were determined to allow direct comparison between the different vectors. One of the two batches of lentivectors with different pseudotypes was produced by Natalie Ward (PhD student, Molecular Immunology Unit, UCL-Institute of Child Health). All vectors were functional as they were competent at transducing 293T cells (Figure 3.3 A). However, only VSVg- and RRV-pseudotyped vectors resulted in detectable transgene expression in DC with VSVg-pseudotyped vectors being 23 times more efficient (Figure 3.3 B).

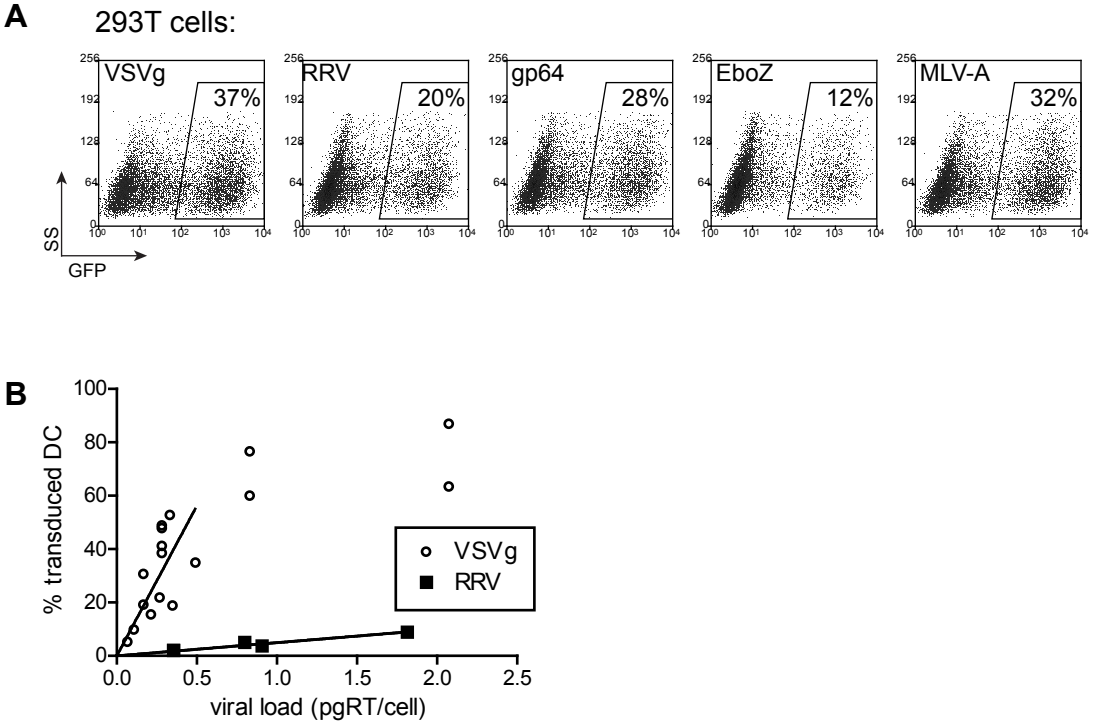

Figure 3.3. VSVg-pseudotyped lentivectors are most efficient at transducing DC.
A Lentiviral vectors pseudotyped with different viral envelopes (VSVg, RRV, gp64, EboZ and MLV-A) was produced and tested in 293T cells. Flow cytometry plots of 293T cells transduced with those vectors are shown. **B** DC were transduced on day 0 of culture with lentivectors pseudotyped with VSVg, RRV, gp64, EboZ and MLV-A with viral loads up to 2.5 pgRT/cell and transduction was assessed by flow cytometry. Only transduction with VSVg- and RRV-pseudotyped vectors resulted in detectable transgene expression in DC. The transduction efficiency of these vectors, calculated as the slope of the linear region of the transduction curve, was 112±13 transduction units/pgRT for VGVg-pseudotyped vectors and 5.9±0.3 transduction units/pgRT for RRV-pseudotyped vectors.

3.5 Characterisation of transduced DC maturation phenotype and immunological function

In order to investigate if transduction induced DC activation and maturation, the expression levels of CD86 and MHCII molecules were measured in GFP^+ DC after transduction by VSVg-pseudotyped vectors. Prior to LPS stimulation, DC cultures exposed to viral vectors demonstrated a small increase in surface expression levels of both CD86 and HLADR in both GFP^+ and GFP^- populations compared to untreated cultures (Figure 3.4 A and B). This increase was not statistically significant for cells transduced on days 0 or 2 and the expression levels of these two maturation markers were significantly lower than in LPS-matured DC (Figure 3.4 B). Cells transduced on day 5 presented an intermediate phenotype: CD86 was significantly up-regulated compared to untransduced cultures but not to levels comparable to LPS-matured cells and HLADR was up-regulated to levels comparable to LPS-matured cultures. Preservation of an immature phenotype

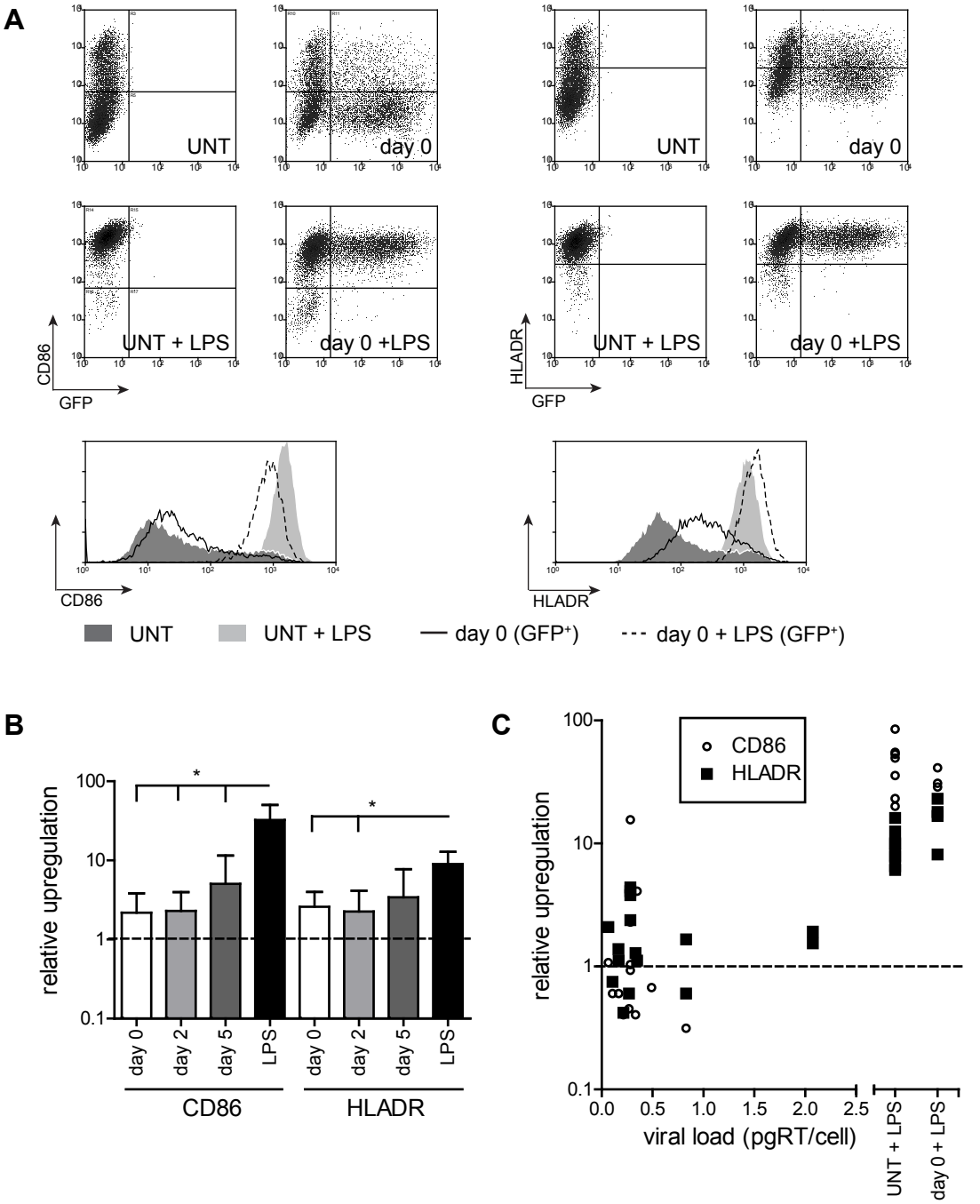

Figure 3.4. DC transduced in the first two days of culture are phenotypically immature.

The surface expression of CD86 and HLADR in DC transduced with VSVg-pseudotyped vectors was measured by flow cytometry. The same transduced and untransduced cultures were further matured by incubation with LPS and the resulting surface levels of both maturation markers were assessed. **A** Dot-plot flow cytometry results for one representative experiment where transduction was performed on day 0 of culture are presented together with the corresponding overlaid histograms. All analysis was done using a "live-gate" and gating on $CD11c^+$ cells. **B** The up-regulation of CD86 and HLADR in GFP^+ DC transduced on days 0, 2 and 5 of culture (MOI 20, 0.3pgRT/cell) was calculated relative to untransduced immature cells (MFI ± SD) for 3 independent experiments using 2 viral batches and 3 different donors. A small up-regulation of both surface receptors was observed but this was significantly lower than after stimulation with LPS (* $p<0.05$, *t*-test). **C** The up-regulation of surface expression of CD86 and HLADR in DC transduced on day 0 with increasing viral loads is shown. Up-regulation of these markers was only

was independent of the viral load used and even when using viral loads up to 2.5pgRT/cell for transduction on day 0 with VSVg-pseudotyped vectors, corresponding to an MOI higher than 150 and resulting in up to more than 80% transduction, only a small and non-significant up-regulation of those markers was detected (Figure 3.4 C). Similar results were obtained for DC transduced with RRV-pseudotyped vectors (data not shown).

DC immunological function changes with maturation. While immature DC are efficient at antigen uptake, through endocytosis and pinocytosis, this function is down-regulated as DC mature and become proficient antigen-presenting cells and potent T-cell activators [Banchereau et al. 2000]. We tested whether transduction by lentivectors would affect antigen uptake or presentation. Using soluble dextran as a model antigen, we observed that antigen pinocytosis was unaltered by transduction and undistinguishable from that of untransduced DC (Figure 3.5 A and B). As expected, dextran pinocytosis was abrogated in LPS-matured DC (Figure 3.5 A and B). In order to test the ability of transduced DC to induce T-cell proliferation an allogeneic mixed lymphocyte reaction (MLR) was set up. Transduced and untransduced DC were similarly poor at inducing T-cell proliferation whereas LPS-induced maturation of transduced DC increased T-cell stimulatory capacity to the same extent as LPS-matured untransduced cells (Figure 3.5 C). Taken together, these results show that lentiviral transduction did not alter immature DC immunological function or their potential for subsequent maturation.

3.6 Characterisation of transduced moDC cytoskeletal function

Having established that lentiviral transduction does not induce DC maturation, as assessed by surface marker expression and immune function assays, we wanted to confirm that transduction also did not alter DC cytoskeletal properties, in particular podosome formation and migration. Podosomes are only assembled by immature DC and they are rapidly lost during DC maturation [Burns et al. 2004; West et al. 2008]. Transduced and untransduced DC were scored for the presence of podosomes after plating on fibronectin. Podosomes were identified at the ventral surface of adherent DC by their characteristic structure comprising an f-actin core surrounded by a ring of vinculin (Figure 3.6 A). In some transduced DC cultures a reduction of the number of cells assembling podosomes was observed. This led to a small but significant reduction in the average percentage of transduced DC assembling podosomes (Figure 3.6 B). Nevertheless, this reduction

---

significant when induced by LPS-maturation in both transduced (GFP^+) and untransduced (UNT) cells ($p<0.0001$, *t*-test).

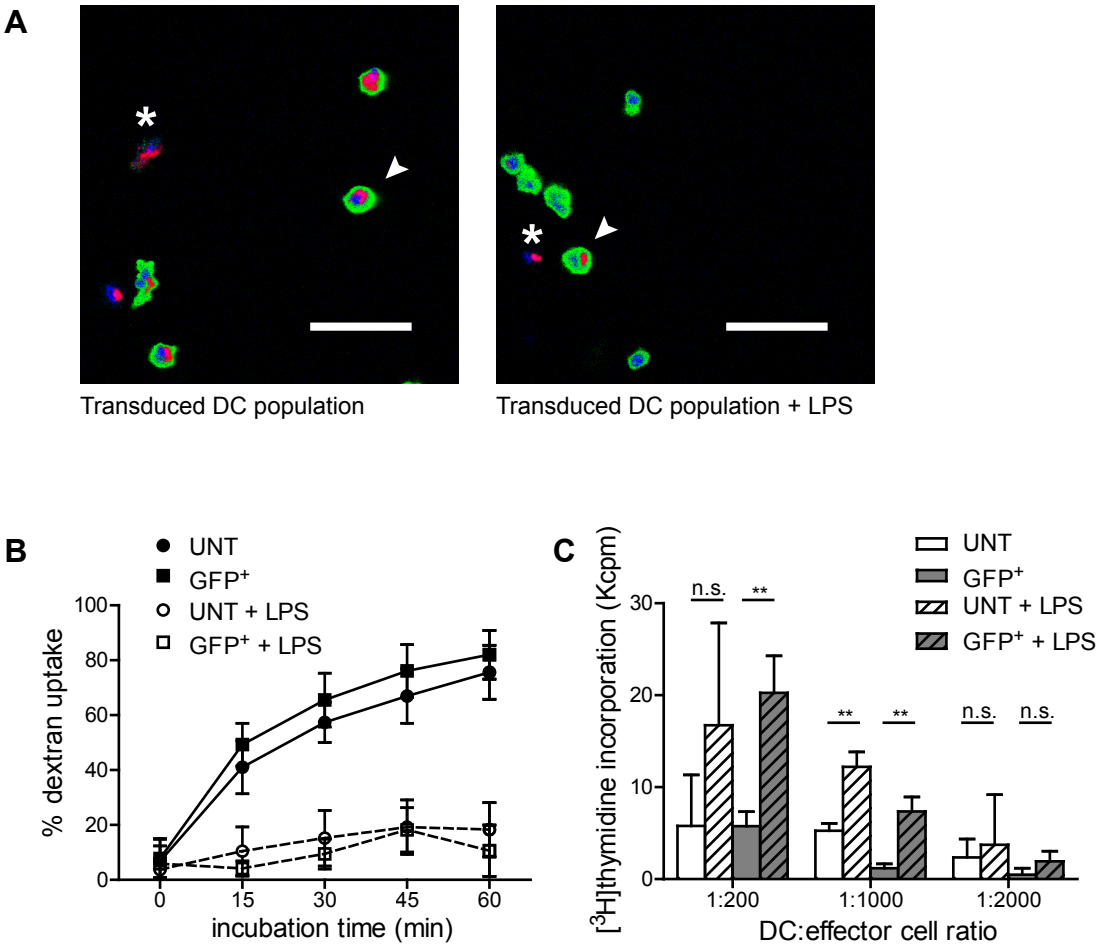

Figure 3.5. Transduced DC are functionally immature.
A Untransduced (UNT) and transduced DC cultures were incubated with fluorescently labelled dextran as a model antigen. These were analysed by fluorescence microscopy and representative micrographs of LPS-untreated and -treated transduced cultures are presented (scale bars: 50μm). GFP⁺ cells are readily identified (green) and rhodamine-dextran (red) can be detected around the nucleus (blue) in both transduced and untransduced cells: arrow heads indicate GFP⁺ transduced cells with dextran signal; asterisks indicate GFP⁻ untransduced cells with dextran signal. **B** A minimum of 100 cells per condition per experiment was scored for dextran signal and the percentage of DC that uptook antigen after different incubation times is shown for 3 independent experiments using 3 different donors (mean ± SD). The antigen uptake capacity of LPS-stimulated DC over time was significantly reduced compared with unstimulated immature cells regardless of transduction ($p<0.001$, ANCOVA). **C** An allogeneic MLR was performed. T-cell proliferation, as indicated by [^{3}H]thymidine incorporation, is presented for one of 3 independent experiments with 3 different mismatched donor pairs (mean ± SD of triplicate wells). The T-cell stimulatory capacity of LPS-matured DC was significantly higher than for immature cells, regardless of transduction (** $p<0.005$, n.s. not significant, *t*-test).

was not comparable to the almost complete inhibition of podosome assembly observed after LPS-induced maturation (Figure 3.6B). Also, no defect was detected in adhesion to fibronectin as the percentage of GFP⁺ cells adherent to fibronectin-coated coverslips and analysed by confocal microscopy was the same as determined by flow cytometry (data not shown).

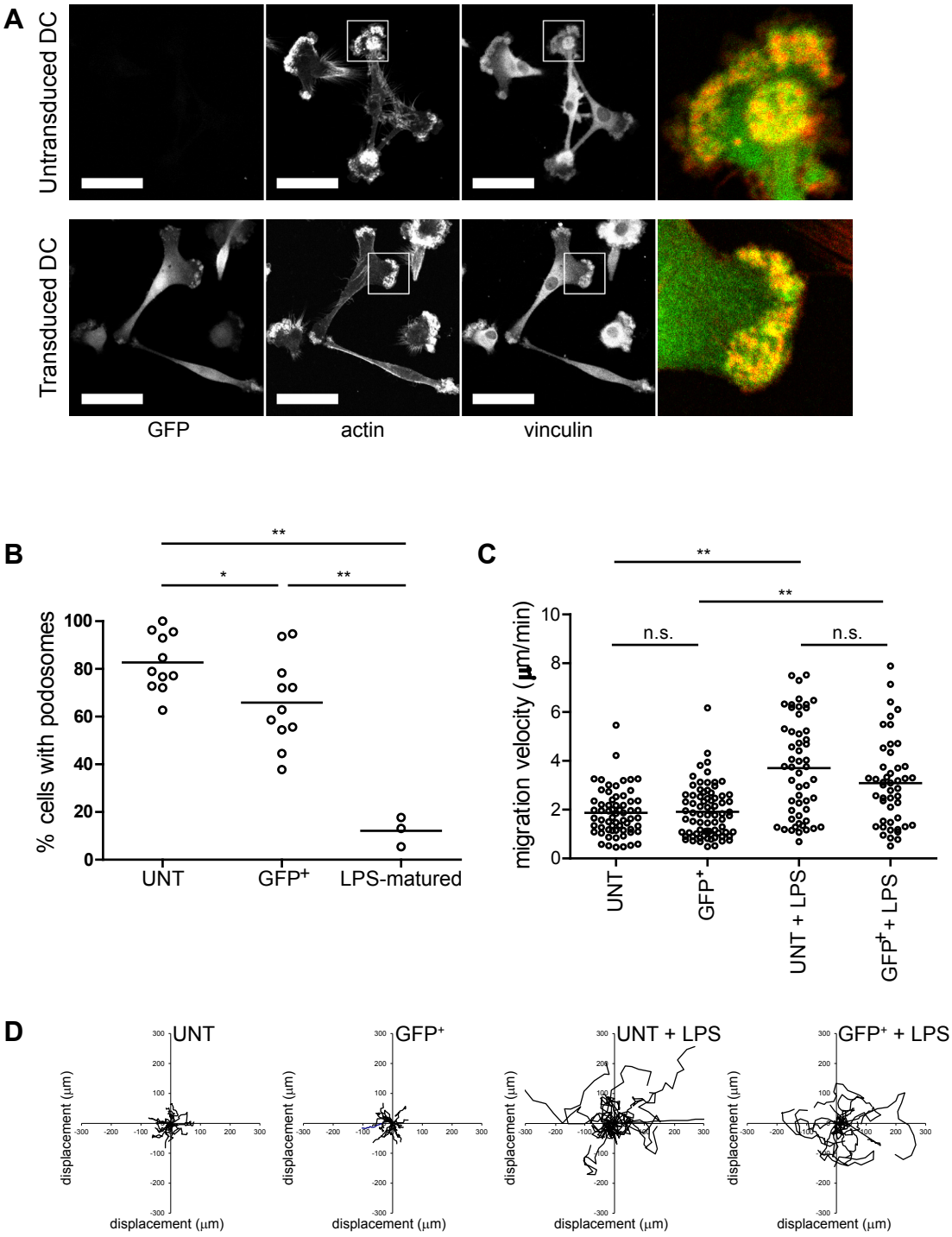

Figure 3.6. Transduced immature DC assemble podosomes and present normal migration.

A Representative confocal micrographs of untransduced (UNT) and transduced DC (GFP⁺) plated on fibronectin-coated slides are shown (scale bars: 50μm). GFP signal indicates transduced cells. Podosomes are readily identified after staining for actin (rhodamine-phalloidin, red) and vinculin (Cy5 secondary antibody, green in merged image). **B** The percentage of DC with podosomes was determined, with a minimum of 100 cells scored per experiment for the presence of podosomes (*p<0.05, ** p<0.005; *t*-test). **C** Untransduced and transduced DC untreated or treated with LPS to induce maturation were plated on fibronectin and imaged by time-lapse microscopy. Subsequently individual cells were tracked by marking their leading edge for each frame of film. The velocity of migration of individual cells was calculated for 3 independent experiments. Combined

Migration is another important actin-regulated process in DC that is altered by maturation [Burns et al. 2001]. It has previously been shown that immature DC plated on 2D substrates are more strongly adherent and have slower random migration than mature DC [Burns et al. 2004]. Using time lapse microscopy, DC plated on fibronectin were imaged in Dunn chambers [Zicha et al. 1991], individual DC were tracked for over 60min and the speed of migration was determined. Transduced and untransduced cells both migrated with a slow speed typical of immature cells (1.9μm/min, Figure 3.6 C). This was evidenced by short distances of migration or displacement (Figure 3.6 D). When maturation was induced by LPS the average migration velocity increased to a similar degree for untransduced and transduced DC (3.7μm/min and 3.1μm/min respectively, Figure 3.6 C), resulting in increased cell displacement (Figure 3.6 D). Together, these results suggest that lentiviral gene transfer caused no alteration to the cells' migratory machinery regulation.

3.7 Discussion

Studies aimed at examining immature DC biology, including understanding cytoskeletal regulation in DC, have been hampered by paucity of suitable reagents to alter gene and protein expression. The two major reasons are (1) that DC are non-dividing and therefore not suitable for vectors that rely on mitosis for nuclear entry and (2) that DC are extremely sensitive to activation by a wide range of biological reagents, resulting in cell maturation and thus inducing dramatic re-organisation of the cytoskeleton. Lentivectors based on HIV-1 have been shown to be efficient vectors for the genetic modification of human DC [Breckpot et al. 2004b] but concerns remain about their effect on DC maturation. Here, the potential for lentivectors to generate genetically modified human DC with an immature phenotype was determined. Using a VSVg-pseudotyped second generation SIN lentivector, we were able to achieve high levels of transduction (up to 87%). Similar levels of transduction were achieved in monocytes (day 0 of culture, immediately after monocyte isolation), differentiating cells (day 2 of culture) and fully differentiated immature DC (day 5 of culture) even though it had previously been suggested that moDC are less permissive to transduction after day 3 of the differentiation protocol [Breckpot et al. 2003]. Transduction on day 0 of culture is nevertheless advantageous as

---

results are shown where each dot represents one individual cell (** $p<0.005$, *t*-test). **D** Examples of 60 min tracks are presented.

less variation in transduction efficiency was detected when vectors were added at the beginning of moDC differentiation compared with later stages of culture and, additionally, maximal transgene expression then coincides with the end of the 5 day differentiation program [Schroers et al. 2000], minimizing time in culture and cell manipulation. The moDC differentiation medium contained FCS as it has been shown that HIV-1 based vectors can undergo cell entry and reverse transcription in monocytes but that nuclear entry is impaired unless the cells are cultured in FCS [Neil et al. 2001]. The use of MACS method to isolate monocytes from PBMC resulted in purer and less activated DC cultures. Moreover, monocyte activation through the CD14 receptor improves lentiviral transduction of monocytes [Breckpot et al. 2004a] and therefore the use of CD14 bead selection in this study is likely to play an important role in achieving efficient transduction on day 0 of culture and removing the need to use potentially activating polycationic adjuvants, co-centrifugation or multiple exposures to the virus to obtain high levels of transduced cells [Rouas et al. 2002].

Initially, the lentivectors used were pseudotyped with the widely used VSVg envelope, which presents broad tropism and confers high stability to the viral particles, allowing for concentration of viral supernatants by ultracentrifugation [Burns et al. 1993; Yee et al. 1994]. In order to determine whether we could improve upon our results with VSVg, we compared the transduction efficiency with lentivectors pesudotyped with other naturally existing envelopes: RRV, gp64, EboZ and MLV-A. Virions pseudotyped with RRV envelope proteins preferentially transduce different neuronal cell types compared with VSVg-pseudotyped vectors [Kang et al. 2002] and RRV has been described to tranduce liver cells with 20-fold higher efficacy than VSVg. EboZ tropism for muscle cells has been described [MacKenzie et al. 2002] and gp64 has been previously shown to be a poor envelope protein for transduction of haematopoietic cell lines [Schauber et al. 2004] but neither had previously been tested in DC. Although MLV-A has been shown to have particular tropism for haematopoietic cell types [Hanawa et al. 2002], again, it has not been previously tested in DC. Viral loads up to 2.5pgRT/cell (corresponding to an equivalent VSVg MOI higher than 150) resulted in undetectable transduction by gp64-, EboZ- and MLV-A-pseudotyped vectors. MLV-A has been reported to be more effective than VSVg in transducing human haematopoietic progenitor cells [Hanawa et al. 2002] but no transduction of moDC was observed. Only virus pseudotyped with VSVg and the RRV envelope were capable of transducing moDC and VSVg-pseudotyped vectors were 23-fold more efficient. VSVg is, thus, the most suitable pseudotype of those tested here for *in vitro* DC transduction.

The main purpose of this study was to determine whether transduced DC could retain an immature phenotype after lentiviral transduction, which is of particular importance for the study of immature DC biology including podosome assembly and migration. There is controversy in the literature about whether SIN lentiviral transduction inherently induces activation and maturation of human DC [Breckpot et al. 2007; Chinnasamy et al. 2000; Esslinger et al. 2002; Gruber et al. 2000; Rouas et al. 2002; Tan et al. 2005]. Studies

that have specifically examined the effect of lentiviral vectors on human DC phenotype and function suggest correlation between maturation and increasing MOI [Breckpot et al. 2007; Rouas et al. 2002; Tan et al. 2005] so that MOI less than 15 resulted in immature DC while higher MOI induced maturation, evidenced by an increase in surface expression of MHCII and costimulatory molecules, secretion of pro-inflammatory cytokines and enhanced T-cell stimulatory capacity. The effect of lentiviral transduction on the DC cytoskeleton has not been specifically examined in published studies. In this study, no significant up-regulation of surface expression of maturation markers was observed when transduction was performed at early stages of moDC differentiation (day 0 or 2 of culture from $CD14^+$ precursors). Even at high viral loads (MOI above 150, resulting in more than 80% transduction) DC transduced on day 0 retained an immature phenotype. Additionally, viral transduction was not associated with alteration of antigen uptake or presentation indicating preservation of functional immaturity. Finally, lentiviral transduction caused only a minor reduction in podosome assembly which had no significant effect on migratory capacity. Therefore, no significant alteration of the immature DC phenotype, immunological function or cytoskeletal structure was observed following lentiviral transduction of $CD14^+$ precursors.

There are several possible explanations for the different effects of lentiviral vectors on DC maturity between studies. Cell source and isolation method may be important. CD14 selection (MACS method) compared to plastic adherence methods improves monocyte purity, reducing final DC activation by contaminating lymphocytes [Breckpot et al. 2004a; Chinnasamy et al. 2005]. Contaminating endotoxin, adjuvants such as polybrene or protamine sulphate (which were not used in this study but are common in most others) or impurities including vesicotubular structures in the viral preparation [Pichlmair et al. 2007] may also provide a maturation stimulus. In other studies, maturation of human and murine myeloid DC has been attributed to lentiviral transduction itself, via dose-dependent activation of the Toll-like receptors (TLR) 3, 7 and 8 [Breckpot et al. 2007; Breckpot et al. 2010]. Human $CD14^+$ monocytes express no or very low basal levels of TLR 3 and 7 [Bekeredjian-Ding et al. 2006; Iwasaki and Medzhitov 2004; Kadowaki et al. 2001; Matsumoto et al. 2003; Muzio et al. 2000; Schreibelt et al.] and it is therefore conceivable that preservation of immaturity seen with our protocol could result in part from reduced sensitivity of $CD14^+$ bead-selected monocytes to lentiviral induced TLR activation. Although phenotypic immaturity was preserved in cells transduced on day 2 of culture, significant upregulation of maturation markers were seen if transduction occurred on day 5 of DC differentiation. As all of the functional assays reported here were performed in $CD14^+$ cells transduced on day 0 of culture, the possibility that lentivector-induced maturation effects may be seen if cells are transduced at later time points cannot be ruled out. Other effects of DC activation, such as alterations in cytokine release, were not examined but may be important for some functional applications of transduced DC and therefore warrant future investigation.

The data presented shows that human moDC can be most efficiently transduced by VSVg-

pseudotyped lentivectors with preservation of phenotypic and functional immaturity. MACS method for monocyte isolation from PBMC is advantageous, as well as transduction at the monocyte precursor stage, both for practical reasons and because it may also promote the generation of immature DC. Transduction with 0.5 pgRT/cell (MOI ~30) resulted in ~50% transduction efficiency, leading to a mixed culture of transduced and untransduced cells, the latter of which can act as internal controls in functional assays. Of particular importance for this thesis, the immature DC cytoskeleton was not significantly altered by lentiviral transduction. Furthermore, lentivector transduction did not impair the ability of DC to become phenotypically and functionally mature in response to activation stimuli such as LPS. Together these results confirm the suitability of lentivectors for generation of genetically modified immature DC for cytoskeletal and other biological studies.

Chapter

4

GENERATION OF KNOCK-DOWN HUMAN MYELOID CELL LINES FOR INTEGRINS AND ACTIN REGULATORS

4.1 Introduction

The use of cellular models lacking or with reduced expression of certain proteins has generated useful data regarding the formation, regulation and function of DC podosomes. The majority of studies refer to the murine system, where several models are available that knock-out individual podosome components. However, there is variability between species both in protein expression patterns and in protein function and in this study the aim was to work primarily in the human context. There are only two described human disorders where DC podosome formation is impaired by loss of expression of podosome components: WAS and LAD ([Burns et al. 2001] and Siobhan Burns, unpublished data). Cells from such patients, in particular from LAD patients, are very scarce resources. Hence, it was decided to generate a panel of human cell lines deficient in known and potential podosome components. This was done using RNAi technology. Lentiviral vectors were used to deliver shRNA cassettes to the human monocytic leukaemia THP1 cell line, which can be differentiated into cells resembling immature DC (THP1DC) [Berges et al. 2005].

Integrins are an essential component of podosomes in their role as adhesion structures. There are conflicting reports regarding which family of integrins is recruited to human

DC podosomes. On one hand, the leukocyte β_2 integrin has been demonstrated to be specifically recruited to podosome rings in monocyte-derived DC and to be essential for podosome formation, while β_1 integrins were reported to be excluded from podosome areas ([Burns et al. 2004] and Siobhan Burns, unpublished data). On the other hand, β_1 integrins have subsequently been shown to be concentrated at podosome rings and to mediate adhesion to fibronectin [van Helden et al. 2006]. The question remains about the relative importance of these integrins in DC podosome formation and function. In order to attempt to answer this question, THP1 cell lines were generated with reduced expression of either integrin.

WASp is acknowledged to be critical for podosome formation, as the actin polymerisation machinery engaged in podosome formation in human DC is WASp dependent [Burns et al. 2001]. The WASp chaperone WIP has also been demonstrated to be essential for podosome formation in murine DC. On one hand, WIP is required for WASp expression by preventing its premature degradation. On the other hand, recruitment of podosome components such as WASp, cortactin and MT1MMP has been shown to be WIP-dependent in splenic murine DC [Banon-Rodriguez et al. 2011; Chou et al. 2006]. However, WIP recruitment to human DC podosomes has not been formally demonstrated and its function in DC podosomes has also not been investigated in the human context. Expression of WASp and WIP was knocked-down in THP1 cells.

Cortactin is another actin nucleator that has been implicated in invadopodia as well as in podosome formation and function. HS1, a cortactin homolog, has only very recently been explored in myeloid cells and has been implicated in podosome array organisation. The expression of cortactin in murine DC appears to be subset specific, with splenic DC expressing cortactin but bone marrow-derived DC only expressing HS1 [Banon-Rodriguez et al. 2011; Dehring et al. 2011]. Here, the specific expression pattern of cortactin and HS1 in human DC was investigated and HS1 was taken as target for the shRNA knock-down strategy.

4.2 THP1DC are proficient at assembling podosomes

DC can be easily differentiated from leukaemia-derived cell lines [Santegoets et al. 2008; van Helden et al. 2008]. The human monocytic THP1 cell line can be differentiated into immature dendritic-like cells (THP1DC) in a process that mimics the protocol for in vitro differentiation of $CD14^+$ peripheral blood monocytes, consisting of culturing THP1 cells in complete culture media with FCS for 5 days in the presence of IL4 and GMCSF [Berges et al. 2005]. The resulting cells display phenotypic, molecular and functional characteris-

tics of DC generated from $CD14^+$ monocytes. Namely, differentiated cells present *de novo* expression of CD80, CD86, CD40, and CD209 surface markers, increased expression of CD11c and lack of expression of CD83 [Berges et al. 2005]. THP1DC have also been shown to have strong antigen uptake capacity using FITC-labelled dextran and only weak T-cell stimulatory capacity, consistent with an immature DC phenotype [Berges et al. 2005]. In this thesis, THP1 cells were differentiated into immature THP1DC and analysed by flow cytometry. THP1DC presented increased expression of CD11c, CD86 and HLADR surface markers and the expression of β_1 and β_2 integrins was also confirmed (Supplemental Data Figure S.2). A slight decrease in proliferation was noticed (data not shown), consistent with a more differentiated state [Berges et al. 2005].

When plated on 2D surfaces, immature human monocyte-derived DC form podosomes which can be identified by immunofluorescence microscopy as dense actin cores surrounded by rings of vinculin (Figure 4.1 A and Supplemental Data Figure S.3). It has been shown that when THP1 cells are stimulated with a combination of IL4 and PMA or PMA alone most of the cells adhere and readily form podosomes similar to those observed in primary human myeloid cells [Monypenny et al. 2011; van Helden et al. 2008]. Following differentiation from THP1, THP1DC were plated on ICAM-coated glass slides and imaged by confocal microscopy after being stained for actin and vinculin.

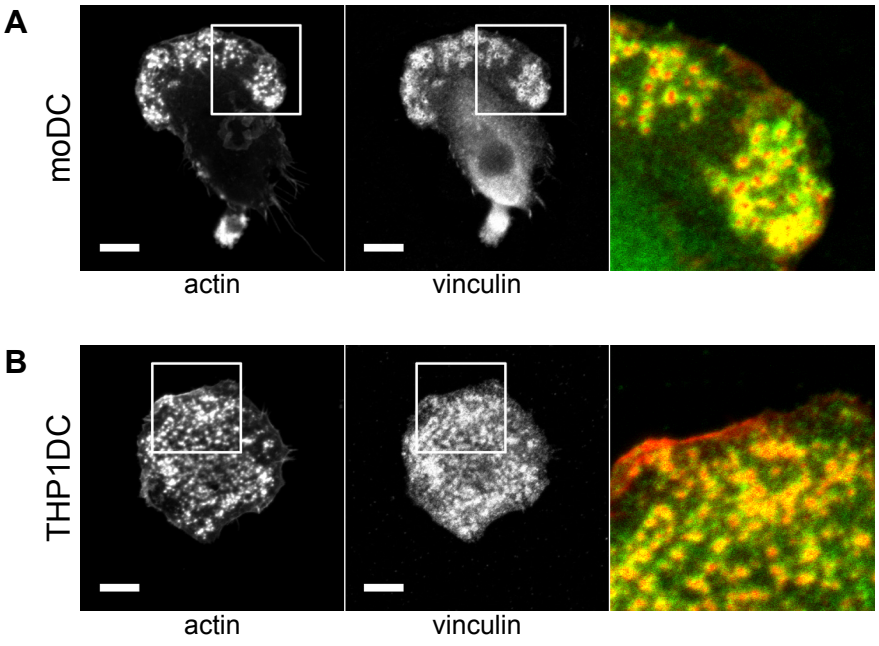

Figure 4.1. Podosomes of moDC and THP1DC.
A Human monocyte-derived DC were plated onto ICAM-coated glass slides overnight and fixed, permeabilised and stained for actin (red in the merged image) and vinculin (green in the merged image). **B** THP1 cells were differentiated into THP1DC and then plated onto ICAM-coated slides. After 48h they were fixed and prepared as above. Podosomes are clearly identified as dense F-actin cores surrounded by rings of vinculin.

Podosomes were also identified in this cell line model of immature DC (Figure 4.1 B). A similar pattern was observed in THP1DC plated on fibronectin-coated surfaces (Supplemental Data Figure S.3).

4.3 Identification of podosome components

Human monocyte-derived DC have been shown by different groups to either concentrate β_1 or β_2 integrins in their podosomes [Burns et al. 2004; van Helden et al. 2006]. I first sought to reproduce those early experiments. Immature moDC were plated on ICAM and on fibronectin and analysed by immunofluorescence confocal microscopy, using antibodies against the β chains of β_1 and β_2 integrins (CD29 and CD18 respectively) (Figure 4.2). moDC podosomes are specifically enriched in β_2 integrins. These are concentrated in areas of podosome patches and are excluded from the podosome cores, resulting in a honeycomb pattern particularly obvious in the micrograph of a moDC plated on fibronectin (Figure 4.2 A). Staining for β_1 integrins did not indicate a concentration of these proteins at podosome areas. Instead CD29 appeared to localise to the edge of lamellipodia and to membrane ruffles (Figure 4.2 B). The same results were obtained using two other anti-CD29 antibody clones, one specific against the active conformation of CD29 (Supplemental Data Figure S.4). THP1DC were also plated on ICAM and on fibronectin-coated slides and the localization of β_1 and β_2 integrins was also analysed. The same localisation pattern was observed. Even though not as clear as in the micrographs of moDC, CD18 localises to podosome areas whereas CD29 is concentrated elsewhere, in particular in lamellipodial edges and membrane ruffles (Supplemental Data Figure S.5).

WASp has been extensively shown to localise to the DC podosome actin cores and to be required for podosome assembly [Burns et al. 2001; Calle et al. 2004]. WIP has been demonstrated to be recruited to murine splenic DC podosomes and also to be required for podosome formation by acting as WASp chaperone [Chou et al. 2006]. Reports of WIP localization to podosomes in the human context are limited to THP1 cells expressing WIP fused to the fluorescent protein mCherry [Monypenny et al. 2011]. A similar strategy was attempted here by transducing immature monocyte-derived DC with a lentivector harbouring an mCherry-WIP fusion construct (kind gift from Dr Austen Worth, Clinical Lecturer, Molecular Immunology Unit, UCL-Institute of Child Health). However, due to the low transduction efficiency achieved, it was not possible to demonstrate the localization of WIP to human DC podosomes. Immunostaining for WIP was not considered here as extensive experience in our laboratory has demonstrated very poor localisation results with currently available WIP antibodies.

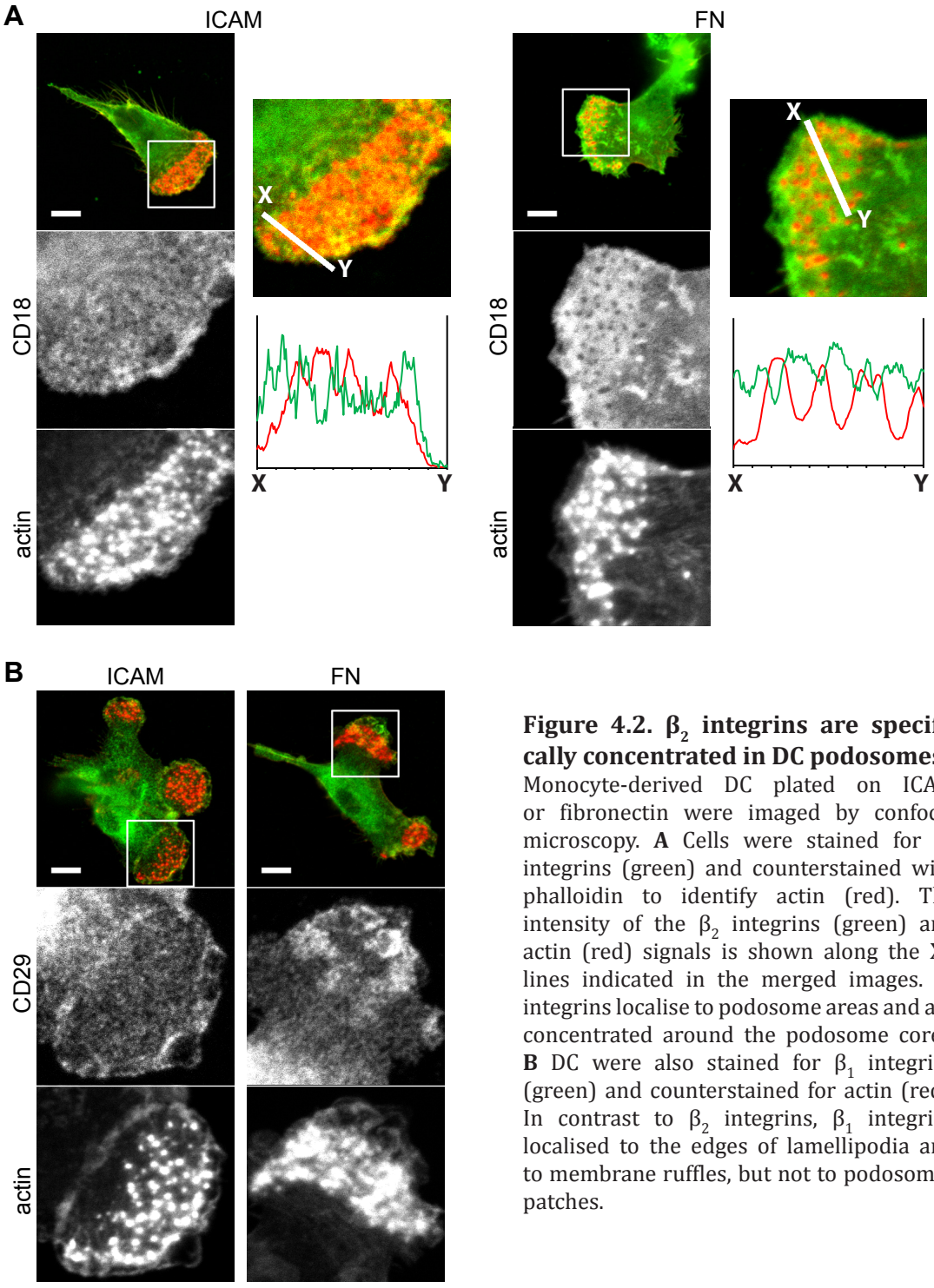

Figure 4.2. β_2 integrins are specifically concentrated in DC podosomes. Monocyte-derived DC plated on ICAM or fibronectin were imaged by confocal microscopy. **A** Cells were stained for β_2 integrins (green) and counterstained with phalloidin to identify actin (red). The intensity of the β_2 integrins (green) and actin (red) signals is shown along the XY lines indicated in the merged images. β_2 integrins localise to podosome areas and are concentrated around the podosome cores. **B** DC were also stained for β_1 integrins (green) and counterstained for actin (red). In contrast to β_2 integrins, β_1 integrins localised to the edges of lamellipodia and to membrane ruffles, but not to podosomes patches.

Cortactin and HS1 have been involved in podosome formation and function in a variety of cell types. Expression of cortactin is generally acknowledged to be restricted to non-haematopoietic cells and HS1 to be exclusive of haematopoietic cells [Kitamura et al. 1989]. However, a few exceptions have been reported: murine platelets express both proteins [Thomas et al. 2007]; chicken and murine monocytes do not express cortactin but differentiation into osteoclasts induces cortactin expression [Hiura et al. 1995; Tehrani et al. 2006]; and murine splenic DC have been reported to only express cortactin [Banon-Rodriguez et al. 2011; Chou et al. 2006]. Interestingly, murine bone-marrow derived DC

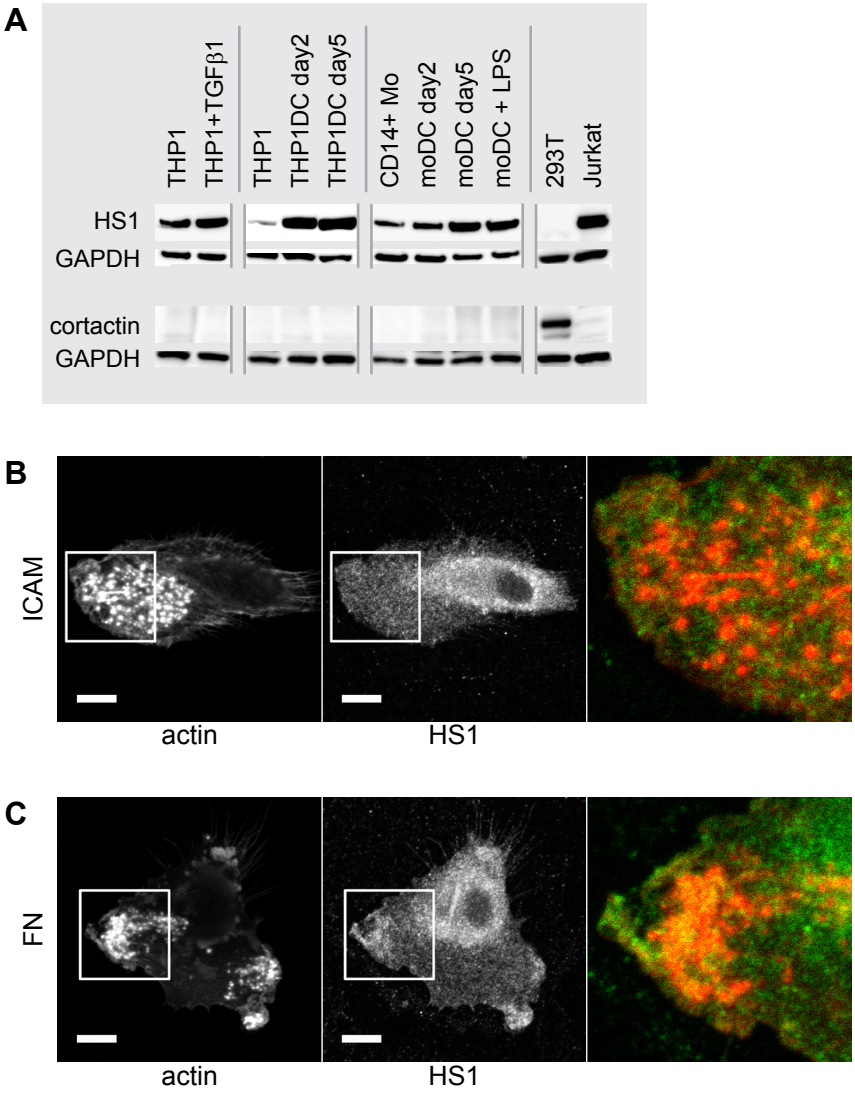

Figure 4.3. Cortactin and HS1 expression and localization to podosomes.
A The expression of cortactin and HS1 was analysed by Western blot in lysates from THP1 cells, THP1-derived macrophages (THP1+TGFβ1), THP1-derived DC in different days along the differentiation culture (THP1DC on day 2 and day 5), human primary monocytes ($CD14^+$ Mo), monocyte-derived DC in different days along the differentiation culture (moDC on day 2 and day 5), mature DC (moDC+LPS), the human embryonic kidney 293T cell line and Jurkat T-cells. GAPDH expression was also determined as loading control. Human monocyte-derived DC were plated on **B** ICAM- or **C** fibronectin-coated slides and imaged by confocal microscopy to identify actin (red in the merged images) and HS1 (green in the merged images).

have been shown to only express HS1 [Dehring et al. 2011], suggesting expression in DC may be subset-specific. The expression profiles of cortactin and HS1 are not completely understood but current data suggests variability between species, cell type and cell subsets. To our knowledge, the expression pattern of either of these proteins has not been investigated in human DC. We analysed cortactin and HS1 expression in a variety of human cells and cell lines by Western blot. Cortactin was only expressed by 293T human embryonic kidney cells and not by any of the human haematopoietic cells tested, in particular THP1 and Jurkats, as previously decribed [Banon-Rodriguez et al. 2011;

Gomez et al. 2006], or by THP1-derived cells, primary monocytes and monocyte-derived DC (Figure 4.3 A). HS1, on the other hand, was not detected in the non-haematopoietic cell line 293T but it was expressed by all other haematopoietic cells (Figure 4.3 A). Additionally, differentiation into DC, either from the THP1 cell line or from primary human monocytes, resulted in an upregulation of HS1 expression with no detection of cortactin expression (Figure 4.3 A). The localisation of HS1 in relation with the immature DC cytoskeleton was analysed by immunofluorescence. HS1 concentrated in lamellipodial edges and actin-rich membrane ruffles and no clear localisation to podosomes was noted (Figure 4.3 B and C).

4.4 Testing different shRNA sequences against CD18 and CD29

No previous reports were found where CD18 and CD29 had been knocked-down using shRNA. Therefore, an shRNA expression system and shRNA sequences were chosen and tested. shRNA sequences specific for any protein can be designed using one of the several publicly available algorithms. In this case we took advantage of an existing library of shRNA constructs. The RNAi consortium (TRC, Broad Institute in Cambridge) was the first and is currently the most widely used lentiviral shRNA library [Pan et al. 2011]. The TRC library was developed primarily to enable for genome wide loss-of-function screenings and it is based on the second generation pLKO.1 lentivector and uses multiple different shRNA sequences to cover most of the known human and mouse genes assuring that more than 70% knock-down can be achieved with at least one of the provided constructs [Root et al. 2006]. The library includes 5 different shRNA sequences for both CD18 and CD29 (Figure 4.4). A scrambled control shRNA construct with no homology to any known mouse or human gene is also part of the library and was used in this study (Figure 4.4). The library constructs have been tested and no induction of interferon response was observed [Root et al. 2006]. The shRNA expression cassette comprises the human RNA Polymerase III promoter U6. The original vector also harboured a puromycin resistance gene (puromycin n-acetil transferase) driven by the phosphoglycerate kinase (PGK) promoter element for selection of transduced cells. In order for easy detection of the transduced populations, the puromycin resistance gene was replaced by a visual marker (eGFP). The WPRE element was also introduced for improved expression, as discussed in the previous chapter.

The two sets of five shRNA sequences targeting CD18 (CD18_1 to CD18_5) and targeting CD29 (CD29_1 to CD29_5) were tested for their ability to induce knock-down of the expression of these proteins, alongside with the scrambled control sequence (CTRS). Lentivectors pseudotyped with VSVg were generated for all shRNA contructs and used to

pLKO.1-GFPW

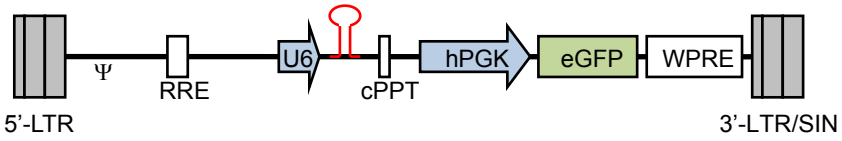

sense strand loop antisense strand stop

CCGG NNN.....NNN CTCGAG NNN.....NNN TTTTT
GGCC NNN.....NNN GAGCTC NNN.....NNN AAAAA

Name	TRC number	Antisense sequence
CD18_1	TRCN0000029643	ATTGTGGTCTTCCTGGGTTTC
CD18_2	TRCN0000029642	ATGGGTAGTCGAATTCGTTGC
CD18_3	TRCN0000029641	TACTGCCCGTATATCAGCTTG
CD18_4	TRCN0000029640	TTTCGCAGCTTATCAGGGTGC
CD18_5	TRCN0000029639	TAAGCATTCTTAATGAGATGG
CD29_1	TRCN0000029644	TTTCAGCTCCTTGTAAACAGG
CD29_2	TRCN0000029645	ATATCAGCAGTAATGCAAGGC
CD29_3	TRCN0000029646	TACATTCTCCACATGATTTGG
CD29_4	TRCN0000029647	TTACTCCTTCTGACAATTTGC
CD29_5	TRCN0000029648	TTTCTATGTCATCTGGAGGGC
CTRS	SHC0002	TTGGTGCTCTTCATCTTGTTG

Figure 4.4. shRNA expression plasmid and sequences against β_1 and β_2 integrins. Schematic representation of the lentiviral genome of pLKO.1-GFPW and structure of the shRNA. Antisense sequences of the shRNA constructs from the TRC library targeting β_2 integrin (CD18_1 to CD18_5), β_1 integrin (CD29_1 to CD29_5) and non-targeting shRNA control (CTRS) are also shown. 5'-LTR: HIV-1 long terminal repeat. 3'-LTR/SIN: HIV-1 long terminal repeat with deleted U3 region. Ψ: packaging signal. RRE: reverse responsive element. cPPT: HIV-1 central polypurine tract and central termination sequence. U6: RNA Polymerase III promoter, driving shRNA expression. hPGK: human phosphoglycerate kinase promoter. eGFP: enhanced green fluorescent protein. WPRE: woodchuck hepatitis virus post-transcriptional regulatory element.

transduce THP1 cells. Transduced cells were sorted by fluorescence assisted cell sorting (FACS) based on GFP expression, thus generating THP1 cultures stably expressing all shRNA sequences. The efficiency of the different shRNA sequences was tested by measuring the mRNA levels of their targets by RT-qPCR, relative to the house-keeping gene β-actin (Figure 4.5 A and B). Only two CD18-targeting shRNA sequences resulted in more than 50% reduction in CD18 mRNA, with CD18_1 being the most efficient with a 75% reduction and CD18_2 resulting in 54% knock-down (Figure 4.5 A). CD29 sequences induced stronger knock-down, with two constructs above 80%: CD29_2 induced 93% and CD29_3 resulted in 88% reduction in mRNA levels (Figure 4.5 B). The production of lentivectors for the CD29 sequences, the generation of THP1 lines for screening of the constructs and CD29 mRNA analysis was performed by João Nunes (Research Assistant, Molecular Immunology Unit, UCL-Institute of Child Health).

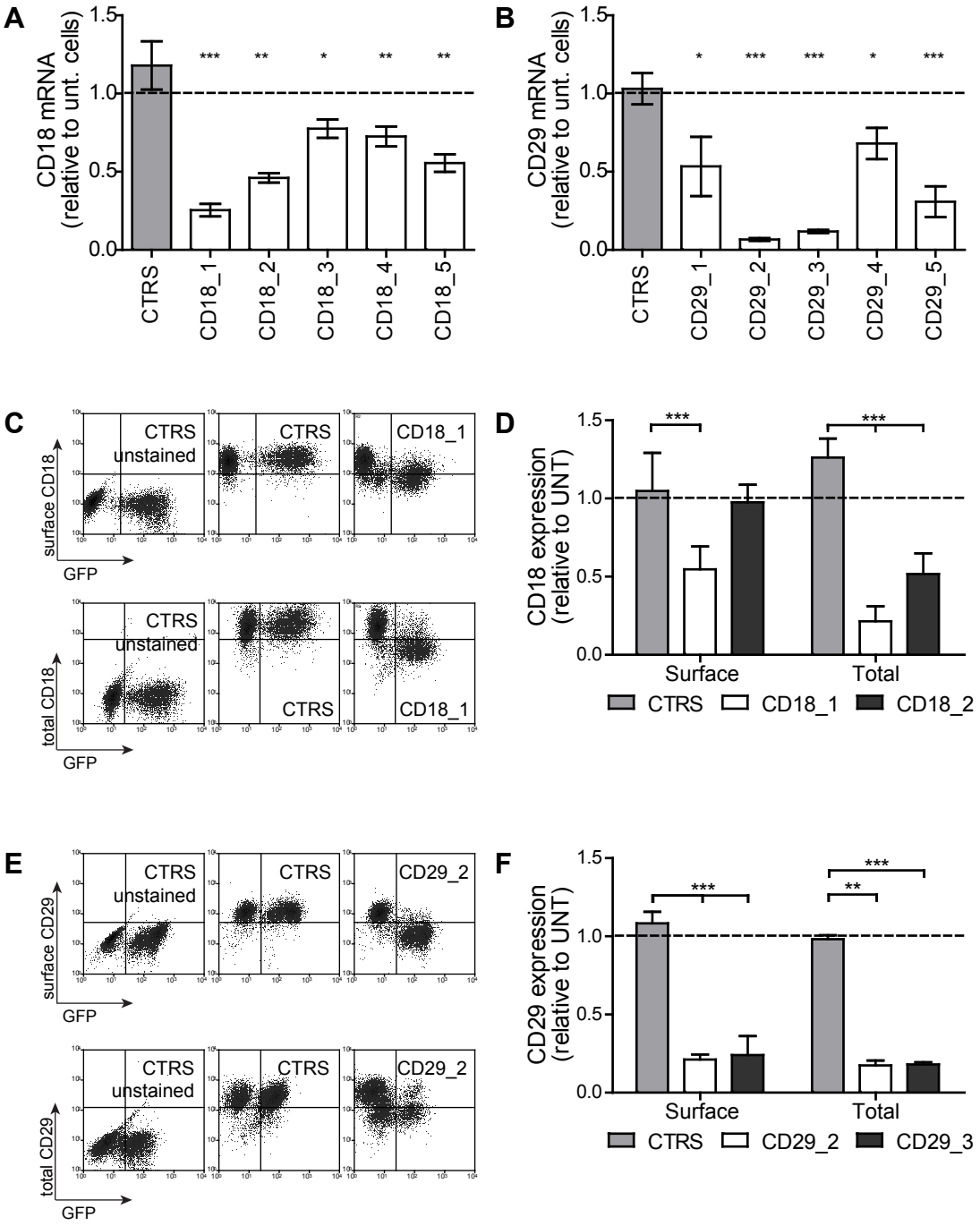

Figure 4.5. Testing shRNA sequences in knocking-down CD18 and CD29 expression. THP1 cells were transduced with lentivectors bearing shRNA sequences against CD18 and CD29 (CD18_1 to CD18_5 and CD29_1 to CD29_5) as well as a scrambled shRNA control sequence (CTRS). The levels of **A** CD18 and **B** CD29 mRNA in those cells were measured by RT-qPCR against actin and are presented relative to untransduced cells (UNT). Error bars represent one SD from triplicates from one experiment (* $p<0.05$, ** $p<0.01$, *** $p<0.001$, *t*-test). **C** The surface and total CD18 expression was measured by flow cytometry for all the THP1 cultures. Representative dot-plots are presented for the control and for one shRNA construct. **D** CD18 expression (MFI) relative to untransduced cells is presented for the control and the two shRNA constructs that resulted in the strongest knock-down (mean ± SD from at least 6 independent experiments; *** $p<0.001$, *t*-test). **E** The expression of CD29 was measured in control and CD29 shRNA THP1 cultures and representative flow cytometry results are presented for the control and the shRNA construct that resulted in the best CD29 knock-down. **F** Expression of CD29 (MFI) relative to untransduced cells for CTRS and the two constructs that resulted in the best knock-down is shown (mean ± SD from

Integrin expression in the shRNA THP1 cultures was measured by flow cytometry. Both surface and total protein expression was determined, the later by permeabilising the cells prior to antibody staining so that both surface and internal protein would be detected (Figure 4.5 C and E). Untransduced THP1 were mixed with transduced cultures before antibody staining in order to act as an internal control for both the staining and the flow cytometry analysis (Figure 4.5 C and E). The integrin expression was calculated as the difference between the MFI of stained and unstained/isotype-control transduced (GFP^+) cells relative to that of untransduced cells (Figure 4.5 D and F). Protein expression was assessed for all shRNA constructs and higher levels of expression were consistent with higher mRNA levels (data not shown). shRNA construct CD18_1, for which CD18 mRNA was 25% of untransduced cells, lead to a total CD18 expression of 22±9% and a surface expression of 55±15% of untransduced cells. CD18_2 resulted in no detectable change in surface expression and 52±13% total CD18 expression (Figure 4.5 D). Knock-down of CD29 protein expression was again stronger, consistent with the mRNA results: CD29_2 cells presented 21±7% surface and 18±3% total CD29 expression and CD29_3 24±12% surface and 18±1% total expression (Figure 4.5 F).

The kinetics of knock-down was investigated by transducing THP1 cells with CD18_1 and CD29_2 constructs and measuring protein expression over time by flow cytometry. A stable knock-down was achieved 5 days after transduction for both constructs (Figure 4.6 A). The knock-down was maintained for several months and after repeated freeze-thaw cycles (data not shown).

THP1 cells retained their normal integrin expression regardless of the reduction in the expression of the other integrin. The CD29 surface expression in CD18_1 THP1 cells remained the same as in untransduced cultures and, in a similar fashion, CD18 surface expression in CD29_2 cultures was comparable to that of untransduced cells (Figure 4.6 B).

4.5 Strategies to improve CD18 knock-down

The strongest CD18 knock-down achieved in THP1 cells, with sequence CD18_1, resulted in 55% CD18 surface expression. Other cell lines were used to test the CD18_1 and CD18_2 sequences, so as to understand whether THP1 were particularly refractory to RNAi. CD18_2 did not result in any knock-down on either PLB or Jurkat cells. CD18_1

---

at least 6 independent experiments; ** $p<0.01$, *** $p<0.001$, *t*-test).

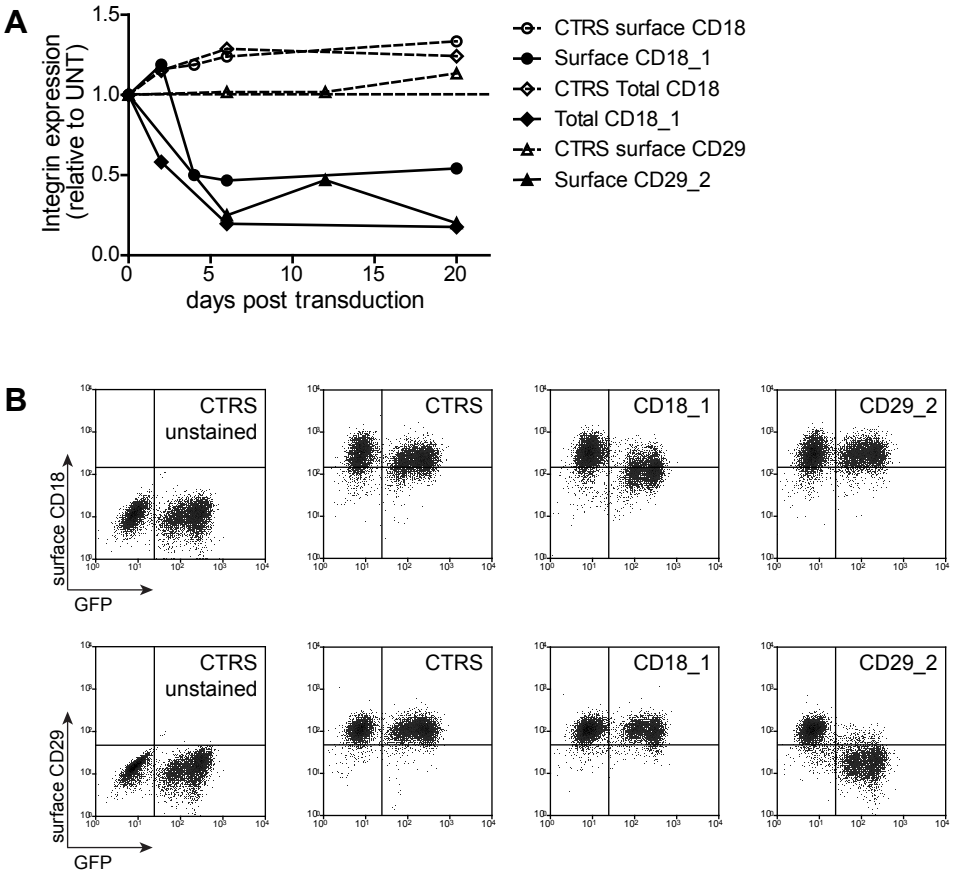

Figure 4.6. Stable knock-down of CD18 and CD29 is achieved after 5 days of transduction and knock-down of one integrin does not induce up-regulation of the other. **A** THP1 cells were transduced with control (CTRS), CD18_1 and CD29_2 shRNA constructs and the expression of the respective integrin in transduced cells was measured by flow cytometry over a period of 20 days. **B** The surface expression of both CD18 and CD29 in THP1 transduced with shRNA against these integrins was assessed and flow cytometry plots representative of 3 independent experiments are presented.

induced a small reduction of both surface and total CD18 expression in both PLB and Jurkat cells. This was only statistically significant for total CD18 expression in PLB cells (42% knock-down) (Figure 4.7).

In an attempt to try and improve the CD18 knock-down achieved with the two constructs that yielded the strongest effect individually (CD18_1 and CD18_2), THP1 were transduced with increasing viral loads. This corresponds to an increase in the proviral copy number, which was reported to result in enhanced expression of the shRNA sequence and in a stronger knock-down [Jeanson-Leh et al. 2007]. THP1 cells were transduced with increasing MOI (10 to 200) and although there was an increase in GFP MFI, which has been demonstrated to correlate with copy number [Jeanson-Leh et al. 2007], there was no detectable improvement in CD18 knockdown (Figure 4.7 C). The two sequences CD18_1 and CD18_2 were further combined by transducing THP1 cells with both constructs. In this experiment both constructs have GFP as the transduction

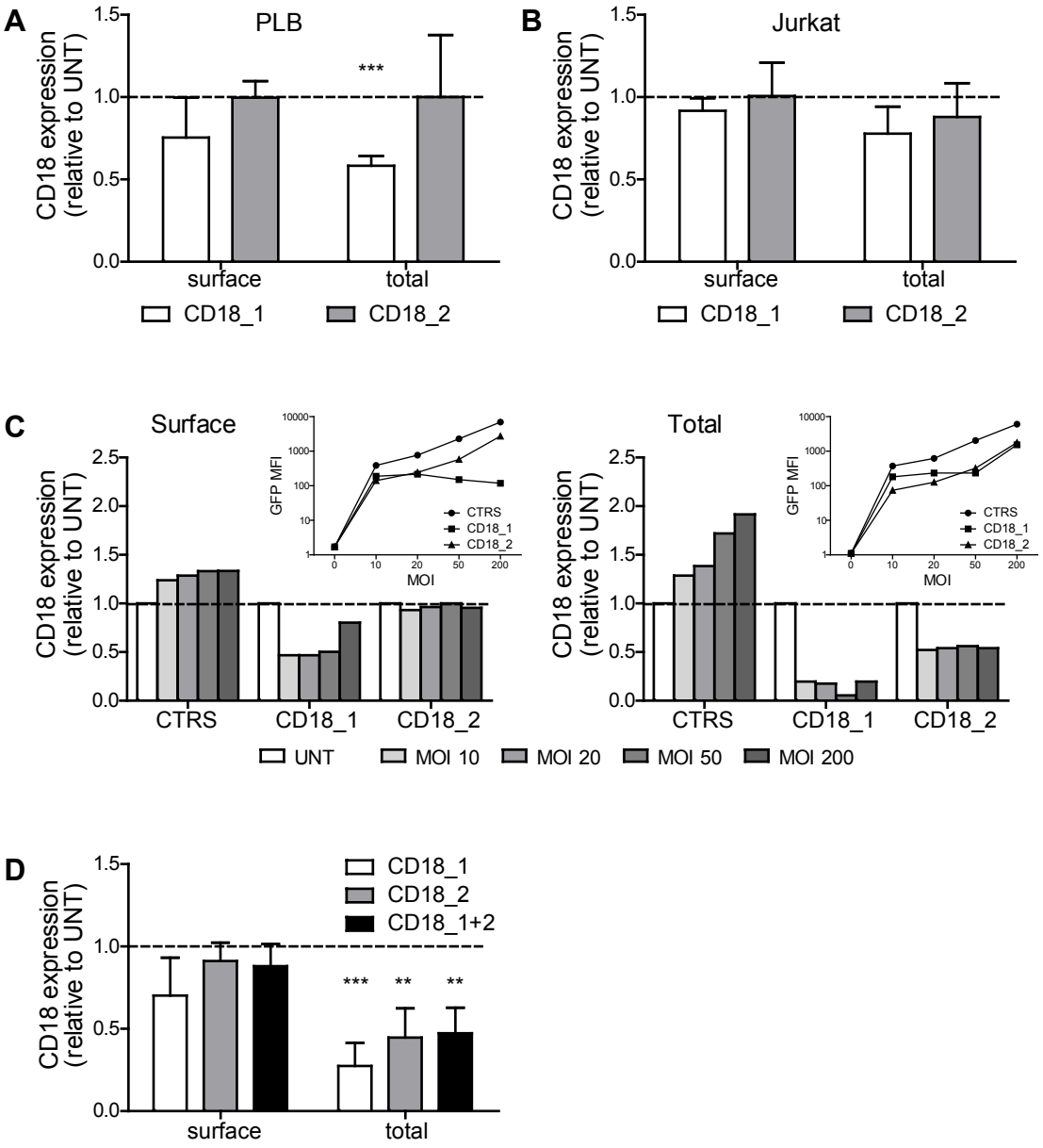

Figure 4.7. Attempts at improving CD18 knock-down with shRNA.
A CD18_1 and CD18_2 constructs were transduced into PLB cells and **B** Jurkat cells. Both the surface and total CD18 expression was measured by flow cytometry and is presented relative to untransduced cells (UNT) (mean ± SD from 3 independent experiments; *** p<0.001, *t*-test). **C** THP1 cells were transduced with increasing MOI of CTRS, CD18_1 and CD18_2 shRNA constructs and their CD18 expression was assessed by flow cytometry. The insets show increasing GFP expression in the transduced cells with increasing MOI. **D** THP1 cells were transduced with CD18_1 and CD18_2 alone and with both the constructs together and the resulting CD18 expression is presented (mean ± SD from 3 experiments; ** p<0.01, ***p<0.001, *t*-test).

marker, so it was not possible to distinguish single transduced form double transduced cells. Nevertheless, since the MOI used for each construct (MOI 50) should result in more than 90% transduction (data not shown) the majority of transduced THP cells should express both shRNA constructs. However, no additional effect was observed. In fact, the knock-down levels resembled that of CD18_2 and not the sum of the individual shRNA constructs (Figure 4.7 D).

4.6 Single-cell cloning to optimise CD18 and CD29 knock-down

The THP1 cultures expressing CD18_1 and CD29_2 shRNA constructs were heterogeneous populations as they had been sorted based only on expression of the transduction marker GFP. Therefore, they necessarily included cells with different levels of shRNA expression resulting in a variety of CD18 and CD29 knock-down. Not only would there have been different numbers of integrated proviral copies but, most importantly, these would have integrated in different parts of the genome, leading to different levels of transcription of both the reporter gene (GFP) and the shRNA cassette. To try and optimise the knock-down in CD18_1 and CD29_2 THP1 cultures, clonal cell lines were generated by single-cell sorting by FACS.

Forty CD18_1 clones were analysed by flow cytometry for CD18 surface expression. As hypothesised, a variety of CD18 surface expression was found in these lines, ranging from 21% (clone 18-4) to 150% (clone 18-34) (Figure 4.8 A). The thirteen clones with CD18 surface expression below 50% were further analysed by measuring total CD18 expression (Figure 4.8 B). The clones with total CD18 knock-down above 90% in this screening experiment were identified and their CD18 expression, both surface and total, was characterised (Figure 4.8 C-E). Severe LAD patients present virtually no CD18 surface expression and in the mild form of LAD only up to 31% surface expression is observed [Anderson et al. 1985; Anderson and Springer 1987]. Out of these four CD18_1 clones, 18-4 and 18-37 present CD18 surface expression within the range found in cells from patients with the mild form of LAD (22±2% and 23±2%, respectively).

Thirty two CD29_2 THP1 clones were screened by flow cytometry for CD29 surface expression and clones with CD29 expression from 4% (29-29) to 34% (29-25) were detected (Figure 4.9 A). The two clones with knock-down above 95% were selected for further characterisation together with the clone 29-20 (Figure 4.9 B and C), which presented a knock-down level of 77%, similar to that of CD18 in the 18-37 clone, the best CD18_1 clone.

The CD18 and CD29 expression of two control cell lines (CTRS and CTRW) was analysed in these experiments alongside that of the CD18_1 and CD29_2 clones (Figures 4.8 and 4.9). CTRW corresponds to another scrambled shRNA control sequence which is described below (Section 4.8, Figure 4.11). Both control cell lines presented normal integrin expression.

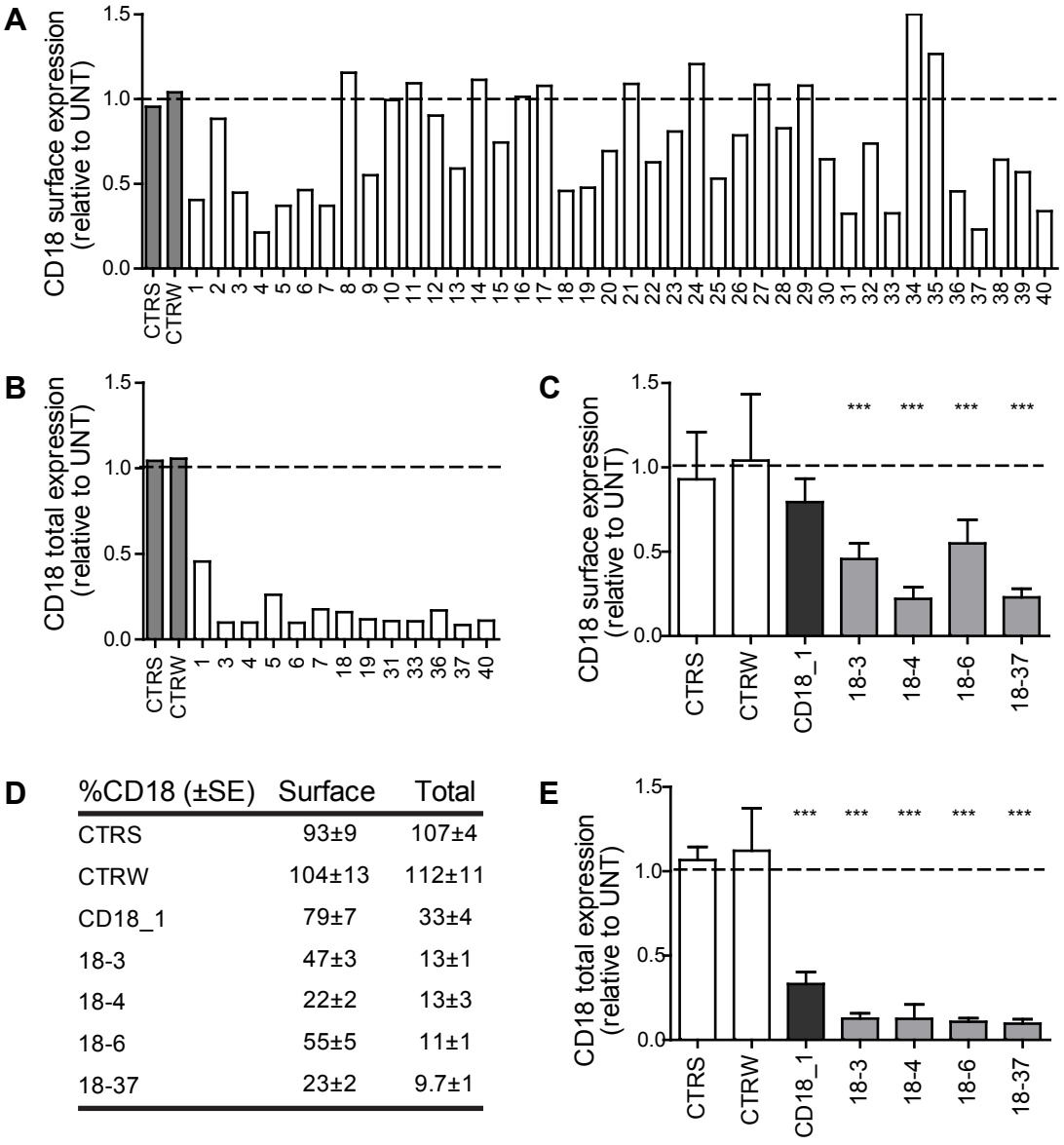

Figure 4.8. Screening of CD18_1 shRNA clonal cell lines.
A THP1 culture stably expressing CD18_1 shRNA contruct was single-cell sorted and CD18 surface expression of clonal cultures was measured once by flow cytometry for screening purposes and is presented relative to untransduced cells (UNT). **B** Total CD18 expression was also determined for the clones presenting surface expression below 50% of UNT. **C-E** Surface and total CD18 expression is presented for four selected clones together with the bulk CD18_1 culture and the controls CTRS and CTRW (mean ± SD from at least 4 experiments; *** $p<0.001$, *t*-test).

4.7 Using shRNA to knock-down CD18 and CD29 in human primary DC

Primary human monocyte derived DC were transduced with the VSVg-pseudotyped lentivectors containing the CD18_1, CD29_2 and CTRS constructs. Transduction achieved

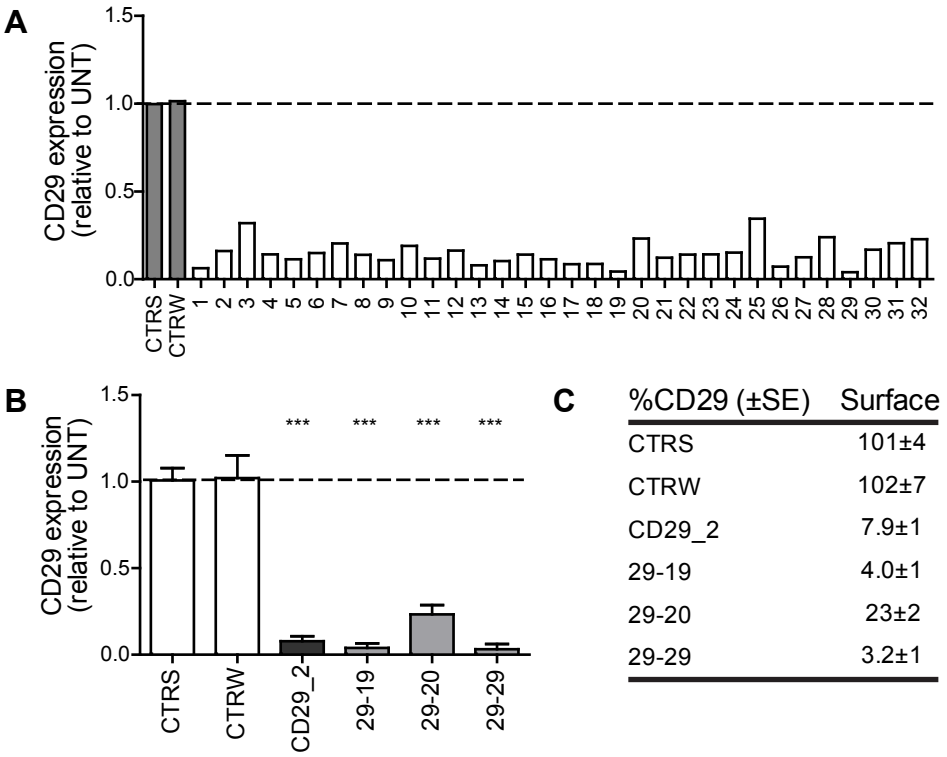

Figure 4.9. Screening of CD29_2 shRNA clonal cell lines.
A THP1 culture stably expressing CD29_2 shRNA contruct was single-cell sorted and CD29 expression of clonal cultures was measured once by flow cytometry for screening purposes and is presented relative to untransduced cells (UNT). **B, C** CD29 expression results are presented for three chosen clones alongside the bulk CD29_2 population and the controls CTRS and CTRW (mean ± SD from at least 4 experiments; *** $p<0.001$, *t*-test).

only a moderate increase in GFP MFI, resulting in difficult identification of the GFP^+ cell population, as both the GFP^+ and GFP^- populations overlapped (Figure 4.10 A and B). The cells were transduced with an MOI of 50. As shown in the previous chapter of this thesis, using an MOI of 50 of VSVg-pseudotyped vectors is expected to result in close to 60% transduction (Figure 3.3, Chapter 3 - Lentivectors as potential tools for manipulating of the immature DC cytoskeleton). However, in this experiment transduction efficiency was lower than predicted. The CD18_1 construct resulted in 30% transduced cells; CTRS resulted in 36% transduced cells in the CD18 experiment and 17% in the CD29 experiment; and CD29_2 resulted in 20% transduced DC (Figure 4.10 B). This demonstrates a degree of inter-experiment variability and the need for various attempts at experiments using primary cells. Integrin expression was measured by flow cytometry. The CD18_1 construct resulted in a decrease in CD18 surface expression of only 15%, resulting in 86.5% surface CD18 expression and a total CD18 expression of 45.2% (Figure 4.9 A). DC transduced with the CD29_2 construct retained 77.7% CD29 expression (Figure 4.10 B).

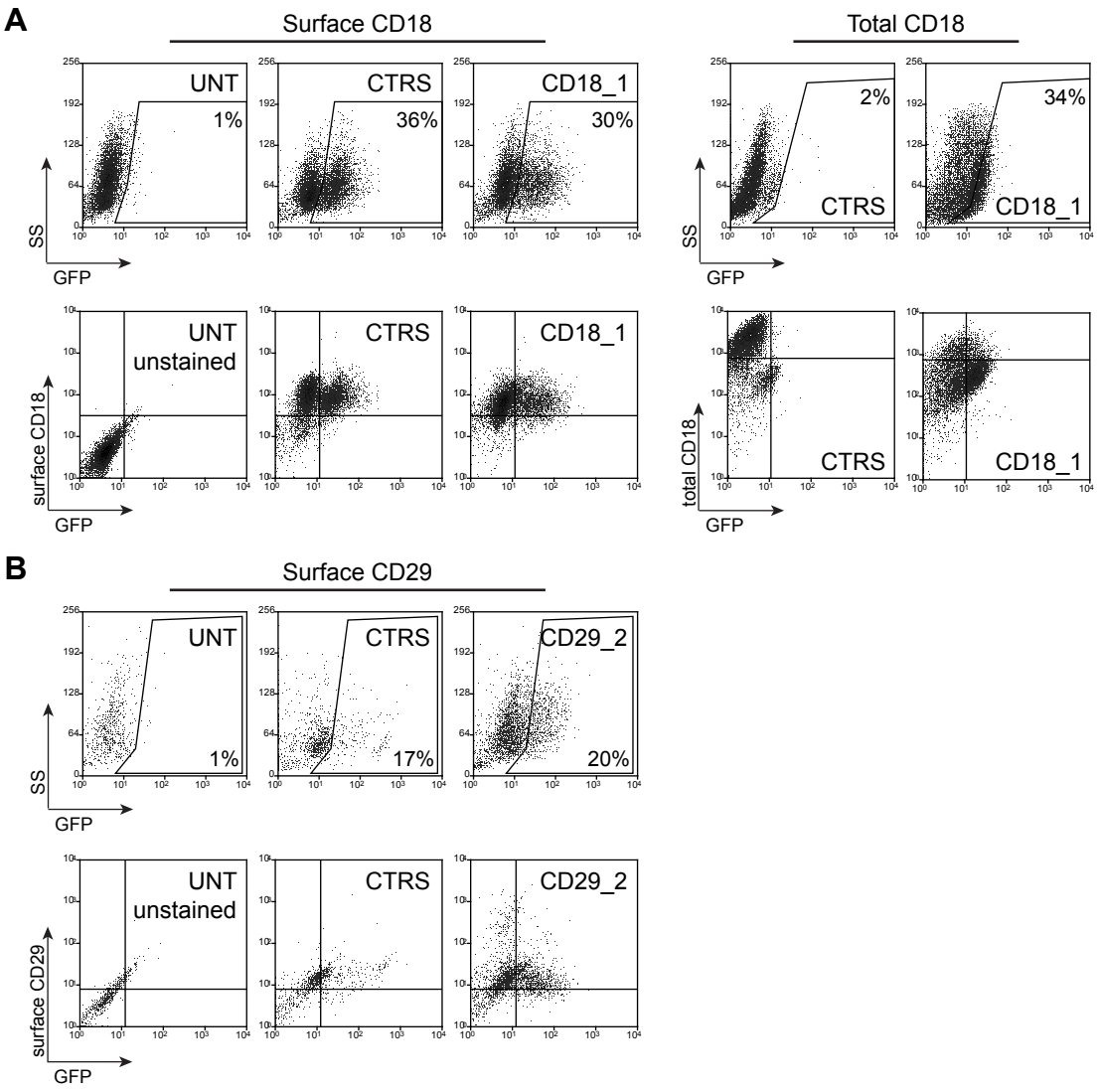

Figure 4.10. Knocking-down CD18 and CD29 in primary DC using shRNA.
A Monocyte derived DC were transduced with lentivectors pseudotyped with VSVg and harbouring the shRNA control CTRS and CD18_1 constructs. The surface and total CD18 expression were assessed and the flow cytometry results are presented. **B** DC were also transduced with CD29_2 shRNA construct and the flow cytometry results for CD29 expression are presented.

4.8 shRNA expression system and shRNA sequences for WASp, WIP and HS1

The expression of WASp, WIP and HS1 has been previously knocked-down in human cells using shRNA in a lentivector context. Therefore, to avoid the process of testing shRNA sequences, sequences that had been previously tested and validated were used. The shRNA expression lentivector pLN-SEW-TH was constructed (Figure 4.11). It presents a GFP transduction marker driven by the strong SFFV promoter. The DNA Polymerase III promoter H1 controls expression of the shRNA. This construct is harboured within the 3'-LTR of the vector genome, which is replicated into the 5'-LTR of the integrated provirus, therefore resulting in a duplication of the shRNA expression cassette [Wiznerowicz and Trono 2003]. The unique endonuclease restriction sites MluI and XhoI, located immediately after the H1 promoter sequence, allow for cloning of shRNA oligonucleotides. Constructs were generated with shRNA sequences against WASp [Olivier et al. 2006], WIP [Krzewski et al. 2008] and HS1 [Gomez et al. 2006], as well as a scrambled

pLN-SEW-TH

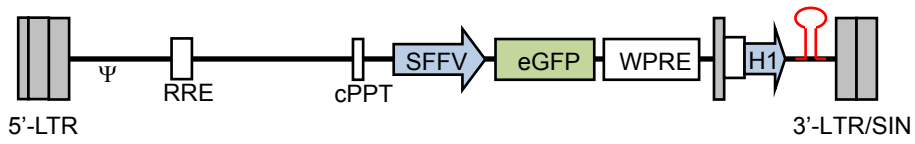

MluI sense strand loop antisense strand stop XhoI

CGCT CCCC NNN.....NNN TTCAAGAGA NNN.....NNN TTTTT GGAA C
A GGGG NNN.....NNN AAGTTCTCT NNN.....NNN AAAAA CCTT GAGCT

Name	Target gene	Antisense sequence
W7	WASp	TGAGATGCTTGGACGAAAA
Wi	WIP	GGGTGGGAATCGGTAAGAAAT
Hs	HS1	GACTACAAGGGAGAGACGGAG
CTRW	Non-targeting	TGTTTTAAGGGCCCCCCGT

Figure 4.11. shRNA expression plasmid and sequences against WASp, WIP and HS1. Schematic representation of the lentiviral genome of pLN-SEW-TH and structure of the shRNA oligonucleotides. These were flanked by MluI and XhoI endonuclease restriction sequences for cloning into the MluI and XhoI unique restriction sites of the pLN-SEW-TH plasmid. This plasmid was used for expression of the shRNA sequences targeting WASp [Olivier et al. 2006], WIP [Krzewski et al. 2008] and HS1 [Gomez et al. 2006] and the non-targeting control sequence CTRW [Olivier et al. 2006]. 5'-LTR: HIV-1 long terminal repeat. 3'-LTR/SIN: HIV-1 long terminal repeat with deleted U3 region. Ψ: packaging signal. RRE: reverse responsive element. cPPT: HIV-1 central polypurine tract and central termination sequence. SFFV: 3' LTR of the spleen focus forming virus (promoter). eGFP: enhanced green fluorescent protein. WPRE: woodchuck hepatitis virus post-transcriptional regulatory element. H1: RNA Polymerase III promoter, driving shRNA expression.

non-targeting control [Olivier et al. 2006].

4.9 Establishing knock-down cell lines for WASp, WIP and HS1

In order to knock-down WASp in THP1 cells, these were transduced with VSVg-pseudotyped lentivectors with the W7 shRNA construct. WASp expression was analysed by Western blot, where one unspecific band is detected just above the WASp band, as previously observed in our laboratory (Figure 4.12 A and B). Densitometry of the Western blots showed the W7 THP1 culture retained 28% of WASp expression (Figure 4.12 C, D). The W7 THP1 culture was single-cell sorted by FACS and ten clones were analysed for WASp expression by Western blot (Figure 4.12 A). The two clonal cell lines W7-3 and W7-6 were selected, with WASp expression 7.3% and 8.0% of untransduced cells (Figure 4.12 B-D).

THP1 cell lines expressing the WIP shRNA construct were similarly assessed. The bulk Wi THP1 population retained 57% WIP expression as measured by densitometry of Western blots (Figure 4.13 A-D). In order to generate cell lines with lower levels of WIP expression, the Wi culture was single-cell sorted as explained before and eleven clones were screened (Figure 4.13 A). Two clones were selected: Wi-3 with 13% WIP expression and Wi-10 with 24% WIP expression (Figure 4.13 B-D). WIP is necessary for WASp stabilisation. Cells from WIP null mice have been shown to lack WASp expression because of reduced WASp half-life due to enhanced degradation [Konno et al. 2007]. This was confirmed in the Wi lines by measuring the expression of both WASp and WIP in the Wi and W7 (WASp knock-down) lines (Figure 4.13 E). WIP is shown to be decreased in the Wi but not in the W7 lines. On the other hand, WASp expression is reduced in both the W7 and the Wi lines.

Finally, the HS1 shRNA construct (Hs) was transduced into THP1 cells. HS1 expression in the bulk Hs THP1 culture was analysed by Western blot and quantified by densitometry and was determined to be 41% of untransduced THP1 (Figure 4.14 A, C, D). Twenty two Hs clones were screened (Figure 4.14 A) and clones Hs-11, HS-13, Hs-16 and Hs-20 were selected with HS1 expression 8.3%, 24%, 7.3% and 6.8% respectively (Figure 4.14 B-D).

HS1 knock-down did not alter WIP or WASp expression and HS1 expression was also not affected by knock-down of either WIP or WASp (data not shown), similar to previous reports of HS1 and WASp expression in murine BMDC [Dehring et al. 2011]. Also, as previously demonstrated, cortactin expression was not induced by down-regulation of HS1 [Gomez et al. 2006], WIP or WASp (data not shown).

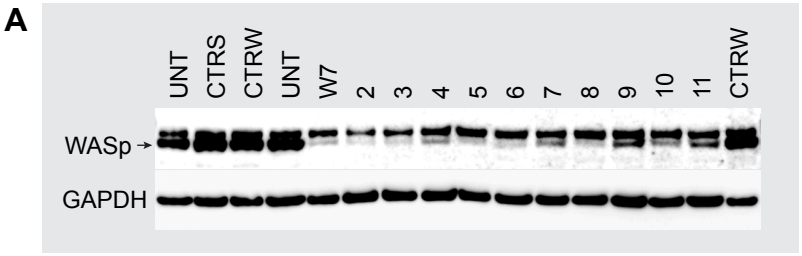

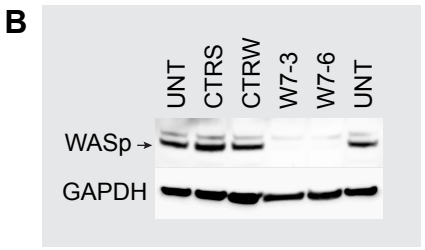

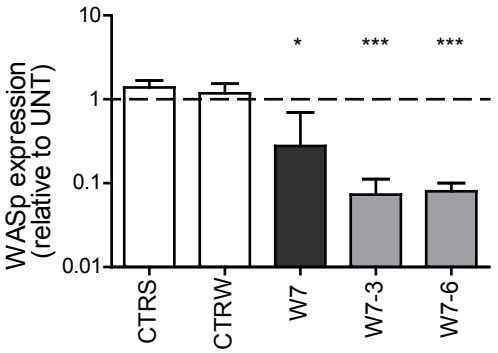

D

%WASp (±SE)	
CTRS	139±14
CTRW	118±16
W7	28±21
W7-3	7.3±2
W7-6	8.0±1

Figure 4.12. Generating WASp shRNA knock-down THP1 cell lines.
THP1 cells were transduced with CTRS and CTRW constructs as well as with the W7 shRNA construct targeting WASp. The latter were and single-cell sorted. **A** The expression of WASp in untransduced THP1 cells (UNT) and cells transduced with CTRS, CTRW and W7 constructs as well as in W7 clonal cultures was analysed by Western blot. **B** A representative Western blot is shown with two W7 clones side-by-side untransduced THP1 (UNT) and the two controls CTRS and CTRW. **C, D** WASp expression was calculated by densitometry analysis of 3 independent Western blots and is presented relative to untransduced cells (mean ± SD; * $p<0.05$, *** $p<0.001$, *t*-test).

4.10 Discussion

In this chapter I describe the generation of THP1 cell lines with expression of different proteins involved in DC podosomes knocked-down by shRNA. The targets chosen were β_1 and β_2 integrins and the actin regulators WASp, WIP and HS1.

Monocyte-derived DC express both β_1 and β_2 integrins [Ammon et al. 2000]. β_2 integrins have been shown to localise to podosomes in human monocytes and monocyte-derived DC [Burns et al. 2004; Gregoretti et al. 1994]. Moreover, β_2 integrin expression is necessary for podosome formation as podosomes are absent in monocyte-derived DC

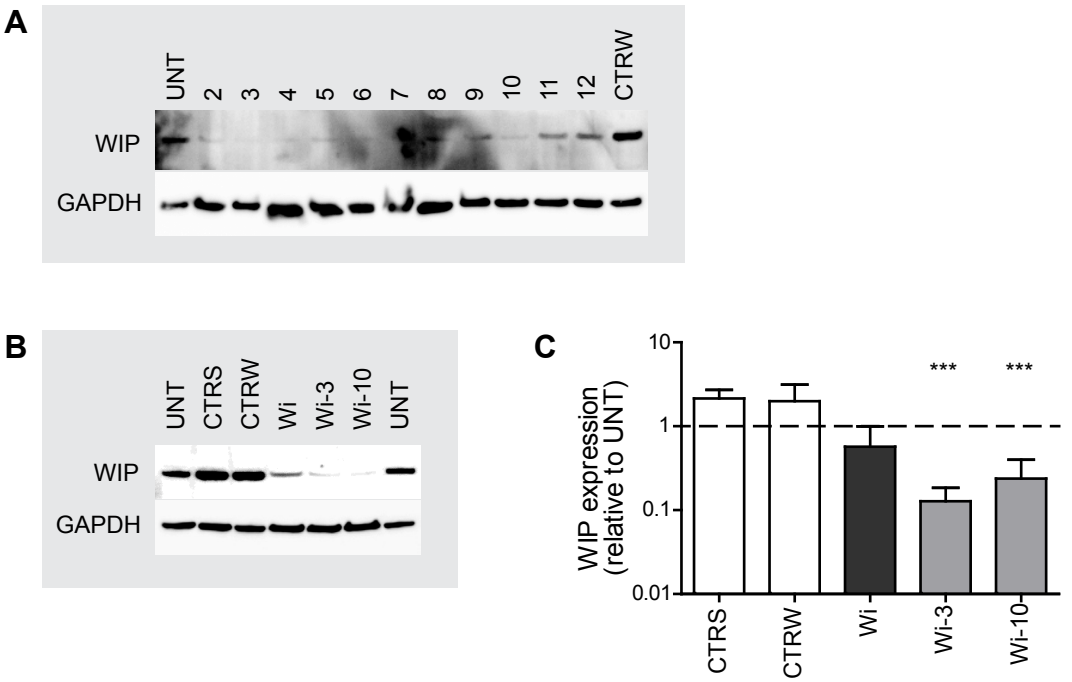

Figure 4.13. Generating WIP shRNA knock-down THP1 cell lines.
THP1 cells were transduced with shRNA construct Wi targeting WIP and single-cell sorted. **A** The expression of WIP in the clonal cultures was analysed by Western blot together with untransduced (UNT) and THP1 transduced with control shRNA sequences. **B** A representative Western blot is shown with two Wi clones side-by-side the bulk unsorted Wi culture, untransduced THP1 (UNT) and the two control cultures CTRS and CTRW. **C, D** WIP expression was calculated relative to untransduced cells by densitometry analysis of 3 independent Western blots (mean ± SD; *** $p<0.001$, *t*-test). **E** The expression of WIP and WASp in WIP and WASp knock-down cell lines (Wi-3, Wi-10 and W7-3, W7-6, respectively) was assessed and the corresponding Western blots are presented.

from LAD patients, lacking CD18 expression (Siobhan Burns, unpublished results). To further investigate the role of CD18 in human DC podosomes we decided to generate

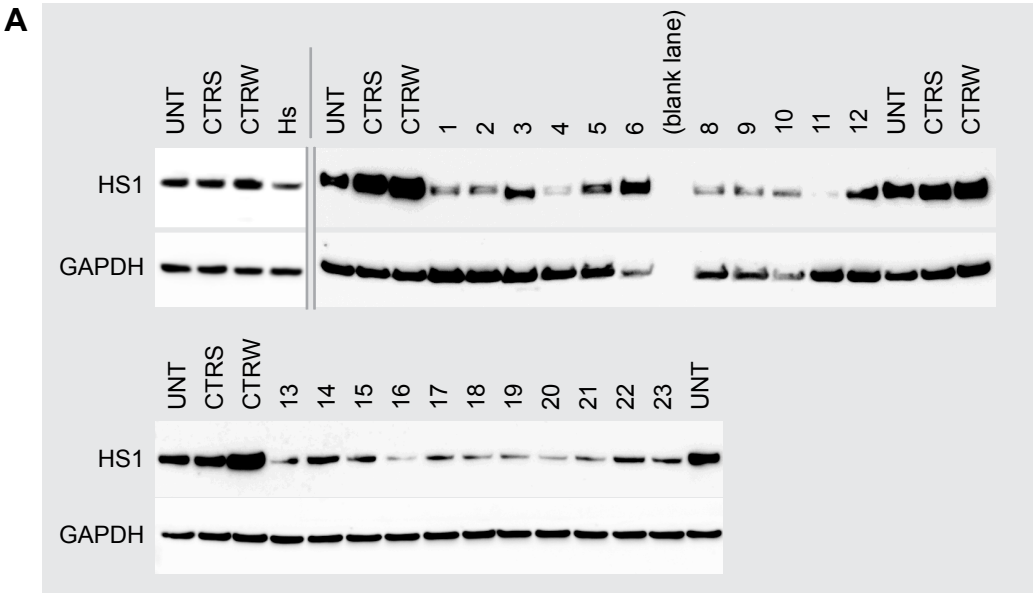

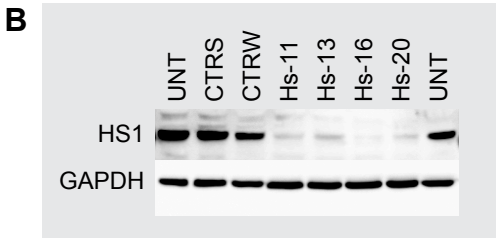

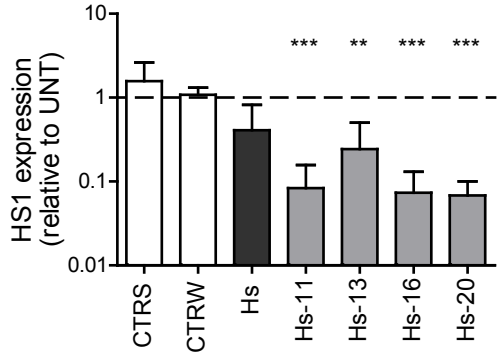

D

%HS1 (±SE)	
CTRS	156±37
CTRW	108±23
Hs	41±29
Hs-11	8.3±4
Hs-13	24±15
Hs-16	7.3±3
Hs-20	6.8±1

Figure 4.14. Generating HS1 shRNA knock-down THP1 cell lines.
THP1 cells were transduced with Hs shRNA construct targeting HS1 and single-cell sorted. **A** The expression of HS1 in the Hs bulk population, clonal cultures and in untransduced (UNT) THP1 and in control CTRS and CTRW cultures was analysed by Western blot. **B** A representative Western blot is shown with four Hs clones together with untransduced THP1 (UNT) and the two controls CTRS and CTRW. **C, D** HS1 expression in the controls, bulk Hs culture and the four clones was calculated relative to untransduced cells by densitometry analysis of 3 independent Western blots (mean ± SD; ** p<0.01, *** p<0.001, *t*-test).

a CD18 knock-down cell line. Available data regarding localization of β_1 integrins to podosomes is conflicting: while CD29 had been shown to be diffusely distributed on

moDC assembling podosomes on a variety of substrates [Burns et al. 2004], a subsequent report has demonstrated co-localisation of CD29 to human DC podosomes where it mediates adhesion to fibronectin [van Helden et al. 2006]. It has also been suggested that THP1-derived macrophages cluster β_1 and β_3 integrins in their podosomes (localisation of β_2 integrins was not analysed in that study) [Akimov and Belkin 2001]. I was unable to demonstrate localisation of β_1 integrins to DC or THP1DC podosomes. Using two different antibody clones against CD29 as well one antibody against the active CD29 conformation I observed diffuse staining together with integrin concentration at leading edge lamellipodia and membrane ruffles, but no specific recruitment to podosome rings or podosome patches. Nevertheless, it was decided to generate a cell line with reduced expression of CD29 as well, to address the functional need for β_1 integrins in human podosome formation and function.

WASp and WIP are acknowledged to be necessary for podosome formation, dynamics and function. In order to further characterise the function of these proteins in podosome biology, we generated knock-down cell lines for these proteins. The other actin regulators that have been implicated in podosome and invadopodia formation are cortactin and, very recently, HS1. I demonstrated that cortactin is not expressed in primary human monocytes, moDC or in the monocytic THP1 cell line or THP1-derived macrophages and immature DC. This data strengthens the understanding of HS1 as a haematopoietic-restricted protein in human cells. This is in contrast with the murine system, where cortactin expression has been demonstrated in murine splenic DC, but not in BMDC, for example [Chou et al. 2006; Dehring et al. 2011]. It was therefore hypothesised that HS1, the cortactin homolog, could have a similar function in human DC as has been proposed for cortactin in splenic murine DC, which do not express HS1 and where cortactin has recently been suggested to be important for podosome function [Banon-Rodriguez et al. 2011]. HS1 was, thus, chosen as target for the generation of knock-down cell lines.

The myeloid THP1 cell line was used to generate knock-down cell lines using shRNA expressed by integrating lentivectors. THP1 can be derived into immature DC-like cells that assemble podosomes. These structures were shown to also concentrate vinculin in a ring around the dense F-actin core and to recruit CD18, but nor CD29, in a similar fashion to moDC podosomes. Even though using a cell line approach to study DC podosomes has the disadvantage of the cell line constituting only a model of the primary cells, a cell line presents several advantages: the cells are immortalized and therefore they are unlimitedly available; isolation and enrichment of transduced populations is feasible; generation of clonal populations is available as a strategy to optimize knock-down.

In the case of β_1 or β_2 integrins, there are no published reports where shRNA has been used to knock-down their expression in human cells. Therefore, shRNA sequences had to be tested. It was decided to use the TRC library (Board Institute, Cambridge) as a source for shRNA sequences. This was the first and is currently the most widely used

lentiviral shRNA library [Pan et al. 2011]. Five shRNA sequences were tested for CD18 and CD29 in THP1 cells. One sequence (CD18_1) resulted in a CD18 mRNA knockdown of 75% and corresponding 78% total protein knockdown and reduction of 45% in surface expression. Sequence CD29_2 induced a decrease of 93% of CD29 mRNA and knockdown in total protein expression of 82% and surface protein expression of 79%.

For both β_1 and β_2 integrin knockdown cells, there was a difference between surface and total protein expression, remarkably larger for β_2 integrins. This is due to the presence of intracellular stores of the integrins, particularly important for CD18. This has been demonstrated for monocytes and neutrophils, where more than 75% of Mac-1 (CD11b/CD18) and p150,95 (CD11c/CD18) are present in intracellular granules. In response to stimuli, these cells are able to rapidly augment the surface expression of the integrins [Miller et al. 1987; Sengelov et al. 1993; Todd et al. 1984]. The results presented suggest that the shRNA-induced protein knock-down first affects the intracellular stores and only when those are depleted will surface expression become reduced, demonstrating the cell's attempt to maintain the surface level of expression of the integrins. β_1 integrins can also be present in intracellular stores, for example, in baby hamster kidney cells where about 50% of β_1 is localised intracellularly [McAbee and Grinnell 1985], or in human skin fibroblasts where this percentage is close to 60% [Destrooper et al. 1991]. However, in haematopoietic cells, where β_2 is the most important family of integrins, the intracellular reserve of β_1 integrins is much smaller. For example, macrophages and T-cells do not augment their β_1 surface expression upon activation [Molnar et al. 1987; Shimizu et al. 1990] and only a small percentage of these integrins are localised intracellularly as a result of recycling [Molnar et al. 1987].

The knockdown of expression of one integrin did not result in upregulation of the other. In particular, β_1 knock-down THP1 cells presented normal levels of expression of β_2 integrins and vice versa. This indicates independent regulation of expression between these two integrin families.

The ability of DC to assemble podosomes is connected with the level of CD18 expression. While cells from severe LAD patients, virtually lacking CD18 expression, are completely unable to assemble podosomes, DC from mild LAD patients (CD18 expression up to 31%) present actin structures reminiscent of podosomes, where β_2 integrins are clustered, but with poorly condensed and defined actin cores (Burns, unpublished data). The residual CD18 surface expression achieved in the knockdown CD18_1 line (55%) was considerably higher than that observed in mild LAD patients [Anderson et al. 1985] and resembled the expression level of individuals that are heterozygous carriers of LAD-causing mutations (about 60% of normal), which show no clinical manifestations of the disease [Anderson et al. 1985; Springer et al. 1984]. This prompted us to attempt to improve the knockdown levels in the THP1 lines for both β_1 and β_2 integrins. This was done by generating individual clonal cell lines from the CD18_1 and CD29_2 cultures. There was a high variability in integrin expression within the bulk THP1 cultures, most likely denoting a mix of copy number and integration sites, which would induce a variety

of transcription efficiency of both the reporter gene cassette and the shRNA expression cassette. Four CD18_1 clones were chosen, of which clone 18-37 (strongest knock-down, with only 23% surface expression, corresponding to 10% total expression) had surface CD18 expression within the moderate LAD phenotype. Three CD29_2 clones were identified with CD29 surface expression ranging from 3% to 23%. The clones 18-37 and 29-19 (4% CD29 surface expression) were taken forward to perform functional assays as described in the next chapter of this thesis, Chapter 5.

WASp has previously been knocked-down in human monocyte-derived DC [Olivier et al. 2006]. The same W7 shRNA sequence was used in THP1 cells, which resulted in a knock-down of 72% of WASp expression. This level of WASp knock-down has been shown to result in reduced numbers of podosomes in moDC, although not a complete absence of these structures [Olivier et al. 2006]. Several clones from the W7 THP1 culture were screened and a clonal cell line with 7.3% WASp expression (W7-3) was identified for further analysis (see Chapter 5). In order to knock-down WIP, an shRNA sequence which had been previously applied to knocking-down WIP expression in human NK cell lines was used [Krzewski et al. 2008]. THP1 cells expressing this construct presented 57% WIP expression. After clone isolation 87% knock-down was achieved in clone Wi-3, which was used in functional experiments described in Chapter 5 of this thesis. The shRNA sequence used against HS1 has also been previously published [Gomez et al. 2006]. In this study I was able to achieve 41% HS1 expression in the bulk THP1 culture. After clone isolation, expression below 10% was reached. Clone Hs-16 was chosen to use in functional assays (Chapter 5).

When using shRNA several control measures should be observed in order to control for off-target effects. The use of scrambled non-targeting sequences can control for non-sequence specific effects, such as the saturation of the RNAi machinery of the cell, naturally set to regulate several biological processes. In this project I used two non-targeting sequences. Both resulted in expression levels of the proteins tested in line with that of untransduced cells. There was a notable exception to this case. When increasing MOI of the CTRS construct were applied to THP1 cells, an increase in CD18 was detected, suggesting a dose response effect between the amount of control shRNA expressed and total CD18 expression. Recent reports have suggested that higher copy numbers of shRNA cassettes may result in saturation of the RNAi machinery, resulting in unpredicted off-target effects. This may be more of a problem for the type of shRNA construct used here compared with the newer amiRNA design [Beer et al. 2010; Grimm et al. 2006; McBride et al. 2008]. The CTRS cell line further used in the following experiments, detailed in Chapter 5 of this thesis, was generated with a low MOI (the same MOI as for the targeting shRNA constructs) and retained not only normal levels of CD18 expression but expression of all other proteins tested comparable to that of untransduced cells.

A stable knockdown was achieved after 5 days of transduction and maintained throughout months using the shRNA constructs against CD18 and CD29. The rapid rate of knock-down makes this system feasible to use in primary monocyte-derived DC. DC take 5-7 days to differentiate from monocytes and therefore if transduction is performed at the beginning of the culture period, following the conclusions from the previous chapter of this thesis, the final knock-down level will have been achieved by the end of the differentiation process, minimising manipulation and time in culture. Indeed, shRNA had previously been used in primary human monocyte-derived DC [Olivier et al. 2006], demonstrating the RNAi machinery is functional in these cells. CD18_1 and CD29_2 shRNA constructs were tested on primary moDC in one experiment. Not only was transduction efficiency low (ranging from 17 to 36% for MOI of 50) but the GFP MFI was low as well, making it difficult to clearly isolate the transduced population. This was particularly hard by fluorescence microscopy without using anti-GFP antibody, which itself is prone to resulting in background staining (data not shown). A future improvement would be to replace the PGK promoter driving GFP expression in these vectors by the stronger SFFV promoter used in the previous chapter and present in the pLN-SEW-TH system used to knock-down WASp, WIP and HS1. Only weak knockdown of integrin expression was detected: 14% of surface and 55% of total CD18 levels and 23% knockdown of CD29 surface expression. Such levels of surface expression of both integrins were not expected to result in any functional deficiency. For practicality reasons, as experiments with primary DC are very time-consuming and require more attempts due to higher inherent variability between experiments, it was elected to proceed to functional experiments, as detailed in Chapter 5 of this thesis, using the cell lines. Findings with the THP1 cell lines should then be validated on primary moDC.

Chapter

5

FUNCTIONAL CHARACTERISATION OF KNOCK-DOWN DENDRITIC CELL LINES

5.1 Introduction

In the previous chapter of this thesis, THP1 cell lines with decreased expression of β_1 and β_2 integrins as well as the actin regulators WASp, WIP and HS1 were established. The knock-down of expression was achieved by RNAi technology by introducing shRNA expression cassettes into THP1 cells using integrating SIN lentiviral vectors. The knock-down was characterised in biochemical terms, by measuring mRNA levels and protein expression levels, either by flow cytometry for the integrins or by Western blot for the actin regulators. A summary of the expression results for the lines used for further experiments is presented in Figure 5.1 A. In this chapter the phenotype of these cell lines was investigated at a cellular level.

Human DC from LAD patients, lacking CD18 expression, show impaired chemotaxis and transendothelial migration [Fiorini et al. 2002]. Moreover, they are unable to assemble podosomes and stabilise the leading edge lamellipodia (Burns, unpublished data). There is little literature investigating the effect of a lack of β_1 integrins on DC biology, particularly in regards to the immature DC cytoskeleton. The functional defects of cells lacking WASp have been extensively characterised. DC from WASp patients fail to assemble

podosomes, present defective directed migration and their adhesion to ICAM (β_2 ligand), but not to fibronectin (β_1 ligand), is weaker than for normal DC [Burns et al. 2004; Burns et al. 2001]. WIP function in immature DC and podosomes has been investigated but only in the murine model [Chou et al. 2006]. Finally, there is only one very recent report investigating the function of HS1 in myeloid cells, limited to murine BMDC [Dehring et al. 2011].

Here we present functional analysis of the THP1 cell lines generated. THP1 are myeloid leukaemia cells which can be differentiated into immature DC-like cells (THP1DC) proficient at antigen capture and expressing DC surface markers [Berges et al. 2005]. Additionally, THP1DC assemble podosomes, as demonstrated in Chapter 4 of this thesis. The THP1 cell lines previously generated were subjected to an adhesion assay. The morphology of adherent THP1DC was characterised, their ability to assemble podosomes was investigated as well as the characterisation of podosomes and podosome arrays. Furthermore, the dynamics of adhesive areas was examined by interference reflection microscopy (IRM).

5.2 Analysis of adhesion to β_1 and β_2 integrin ligands

Integrins are adhesion molecules involved in cell-cell and cell-substrate adhesion. The ECM component fibronectin is recognised by CD49d/CD29 and CD49e/CD29 integrins and although DC express both these integrins, it has been shown that DC adhesion to fibronectin is mediated by the CD49e/CD29 ($\alpha_5\beta_1$) integrin [D'Amico et al. 1998; Jancic et al. 1998]. Adhesion to ICAM is specifically mediated by β_2 integrins, namely the CD11a/CD18 and CD11b/CD18 heterodimers. Therefore, THP1 cell lines expressing shRNA against CD18 and CD29 were expected to have a defect in adhesion to fibronectin and ICAM. HS1 has been shown to mediate β_2 integrin activation in NK cells [Butler et al. 2008]. Thus, adhesion of THP1 cells with reduced HS1 expression could also be affected. WAS cells have been shown to have defective adhesion to ICAM, but not fibronectin, in a dynamic adhesion assay [Burns et al. 2004]. WIP reduction has not been reported to result in adhesion defects. However, a similar phenotype to WASp depleted cells could be foreseen due to the reduced levels of WASp expression in the WIP knock-down cell lines.

A simple static adhesion assay was devised whereby THP1 clonal cell lines expressing different shRNA constructs (GFP^+ cells) were mixed with untransduced THP1 (GFP^-) and then plated on glass slides previously coated with fibronectin or ICAM. Because of the use of differential substrates, this assay allows the detection of integrin-specific adhesion defects. The proportion of transduced adherent cells was determined relying on expression

of GFP, by fluorescence microscopy, and compared to the ratio of transduced to untransduced cells in the initial cell suspension, which was determined by flow cytometry. Mixing transduced and untransduced cells in the same slide minimised variability in washing off non-adherent cells prior to determining adherent cells. Moreover, while other methods rely on accurately counting the absolute number of plated cells, this method results in a comparative measure of adhesion, relative to untransduced cells which act as an internal control.

The clonal cell lines expressing shRNA sequences against CD18 (18-37), CD29 (29-19), HS1 (Hs-16), WIP (Wi-3) and WASp (W7-3) were used in the adhesion assay, as well as THP1 cells expressing two non-targeting shRNA sequences (CTRS and CTRW). A summary of the expression levels of these proteins in the THP1 shRNA cell lines is presented in Figure 5.1 A. The cell line 18-37, with reduced expression of CD18, presented normal adhesion to fibronectin but a significant reduction in its ability to bind ICAM (Figure 5.1 B). On the contrary, the cell line 29-19, whose CD29 expression is reduced, presents no alteration in its ability to bind ICAM but a significant defect in adhesion to fibronectin (Figure 5.1 B). Cells where HS1 expression has been knocked-down present a small, although statistically significant, reduction in adhesion to fibronectin and a larger and significant defect in adhesion to ICAM, comparable to that observed for CD18 knock-down cells (18-37 cell line) (Figure 5.1 B). The Wi-3 cell line presented only a minor, although statistically significant, reduction in adhesion to ICAM and the W7-3 line did not result in any defect in adhesion to either integrin ligand (Figure 5.1 B).

5.3 Characterisation of the morphology and polarization of the knock-down cell lines

THP1 clonal cell lines were differentiated into THP1DC and characterized regarding their morphology. After plating on fibronectin or ICAM the cells were allowed to adhere and spread for 48h and were then fixed and stained with the fluorescently labelled actin probe phalloidin. Fluorescence microscopy images were automatically processed (as described in Chapter 2 – Materials and methods) so as to identify cells in random fields (Figure 5.2 A) and calculate the area of spreading of each cell and the cell's shape, characterised by circularity and aspect radio (Figure 5.2 B and C). Circularity measures how much a shape resembles a perfect circle. While the perfect circle would present a circularity of 1, very elongated shapes or with multiple projections (increasing perimeter for the same area) would bring this parameter closer to 0. The aspect ratio is the ratio between the major axis and the minor axis of the cell. The percentage of polarised cells was also determined, by considering a cell as polarised if its longer axis was 1.6 times longer than the shortest

A

	%CD18(±SE) Surface	%CD18(±SE) Total	%CD29(±SE) Surface
CTRS	93±9	107±4	101±4
CTRW	104±13	112±11	102±7
18-37	23±2	9.7±1	
29-19			4.0±1

	%HS1(±SE)	%WIP(±SE)	%WASp(±SE)
CTRS	156±37	215±33	139±14
CTRW	108±23	199±66	118±16
Hs-16	7.3±3		
Wi-3		13±3	
W7-3			7.3±2

B

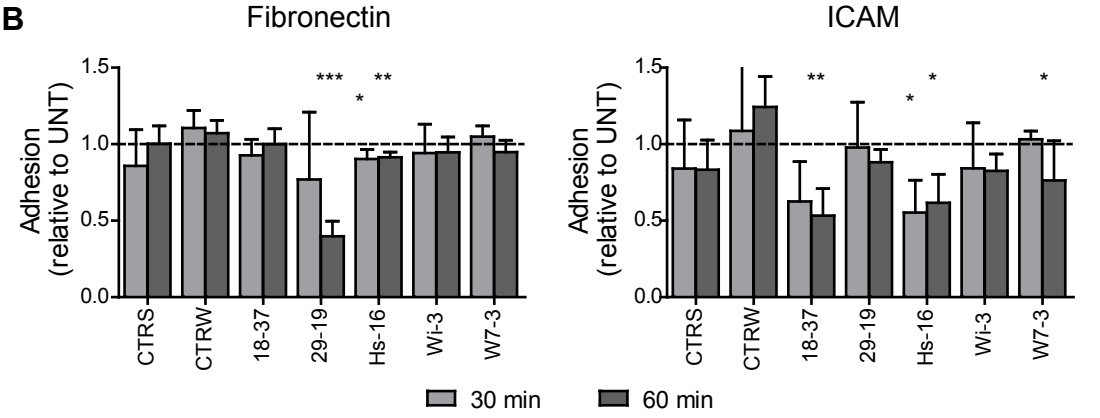

Figure 5.1. CD18 and CD29 knock-down cells show defective adhesion to the relevant integrin ligand and HS1 knock-down cells present defective adhesion to ICAM.

THP1 clonal cell lines expressing different shRNA constructs targeting CD18 (18-37), CD29 (29-19), HS1 (Hs-16), WIP (Wi-3) and WASp (W7-3) were subjected to a static adhesion assay. **A** The percentage of expression of those proteins in the THP1 lines relative to untransduced cells is summarised, as determined in Chapter 4. **B** The THP1 shRNA cell lines expressing GFP as a transduction marker were mixed with untransduced cells and plated onto fibronectin- or ICAM-coated glass slides. After 30min and 60min the non-adherent cells were washed off and the percentage of GFP^+ adherent cells was counted by fluorescence microscopy and compared to the initial ratio of transduced and untransduced cells (determined by flow cytometry), resulting in a measurement of adhesion ability relative to untransduced cells. CTRS and CTRW scrambled shRNA cells were used as controls (mean ± SD from 3-5 independent experiments; * $p<0.05$, ** $p<0.01$, *** $p<0.001$, *t*-test).

axis, that is, for aspect ratio larger than 1.6 (Figure 5.2 D).

All cell lines present very similar cell size and shape. The majority of cells presented a round morphology with only a small percentage having polarised. Wi-3 cells were slightly more spread (larger area) than the other clones, reaching statistical significance when plated on ICAM (Figure 5.2 C). The control shRNA contruct CTRS THP1DC cells were more circular, as indicated by average circularity significantly closer to 1 on both substrates (Figure 5.2 B and C) and a smaller aspect ratio and percentage polarised cells than untransduced cells (Figure 5.2 D), although the latter two not being statistically significant. There were no other significant differences compared with untransduced

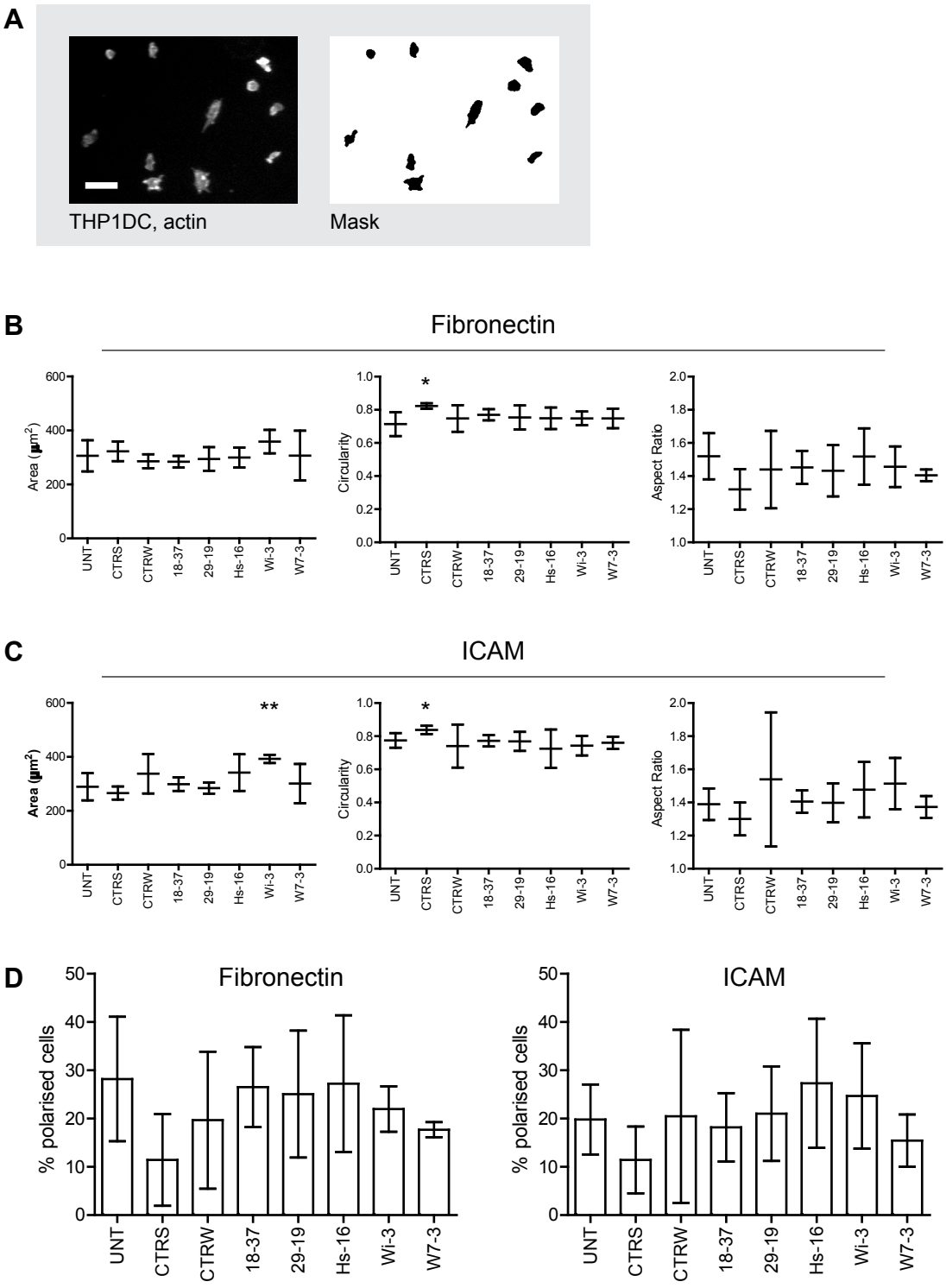

Figure 5.2. Morphological characterisation of THP1DC shRNA lines.
THP1 cell lines expressing shRNA aginst CD18 (18-37), CD29 (29-29), HS1 (Hs-16), WIP (Wi-3) and WASp (W7-3) as well as untransduced (UNT) cells and shRNA control cells (CTRS and CTRW) were differentiated into THP1DC and plated on fibronectin- and ICAM-coated glass slides and imaged by fluorescence microscopy after F-actin staining with rhodamine-phalloidin. **A** A fluorescence microscope micrograph of 18-37 THP1DC cells plated on fibronectin and stained with rhodamine-phalloidin alongside the mask resulting from image processing is presented to illustrate the result of the automated image processing. Scale bar: 50μm. **B** The area of individual cells, the circularity and the aspect ratio were determined from the image masks for cells plated on fibronectin and **C** ICAM. **D** The percentage of polarised cells was also calculated considering

cells for area, circularity, aspect ratio or percentage polarised cells for any of the other constructs.

5.4 Characterization of podosomes in the knock-down cell lines

A closer examination was made of more specific aspects of the actin cytoskeleton of THP1DC. In particular, the assembly of podosomes, the organisation of podosome arrays and podosome size and shape were analysed. In order to identify podosomes, the shRNA THP1DC lines were plated on fibronectin- or ICAM-coated glass slides for 48h, fixed and stained for actin and vinculin (Figure 5.3 A). The number of cells with podosomes was determined. Podosome formation was impaired in both Wi-3 and W7-3 cells, with deficient expression of WIP and WASp respectively (Figure 5.3 B). Significantly reduced numbers of cells presenting podosomes were also observed for the 18-37 cell line (Figure 5.3 B). This was independent of the substrate. In contrast, the ability of Hs-16 cells to form podosomes appeared unaffected when plated on fibronectin but, when cells where plated on ICAM, a significant reduction of the number of cells presenting podosomes was observed (Figure 5.3 B). Finally, the 29-19 THP1DC showed no defect in podosome assembly (Figure 5.3 B).

Further analysis into the podosomes from the THP1DC shRNA lines was conducted. Wi-3 and W7-3 cells were not used in these experiments since only very few cells presented podosomes (Figure 5.3 B). THP1DC plated onto fibronectin or ICAM and presenting podosomes were imaged by confocal microscopy and images were all coded and randomised to blind for both the shRNA construct and the substrate. Images were then processed in order to enhance the contrast of podosomes (see Chapter 2 – Materials and methods) and podosome array borders were drawn manually. The podosome arrays were then scored according to their distribution within the cell as being in the middle of the cell, behind the leading edge, touching the leading edge or on the side of the cell. As determined in the previous section, only a small percentage of THP1DC were polarised, while most of the cells were round and with no defined leading edge. Accordingly, the majority of podosome arrays were found to be located in the middle of the cells in all THP1DC lines (data not shown). Individual podosomes were identified automatically within the previously defined podosome array border (Figure 5.4 A). All the automati-

---

cells with aspect ratio bigger than 1.6. All results presented (means ± SD; * $p<0.05$, ** $p<0.01$, compared to untransduced (UNT) cells, *t*-test) correspond to 4 independent experiments, with a minimum of 50 cells considered per experiment.

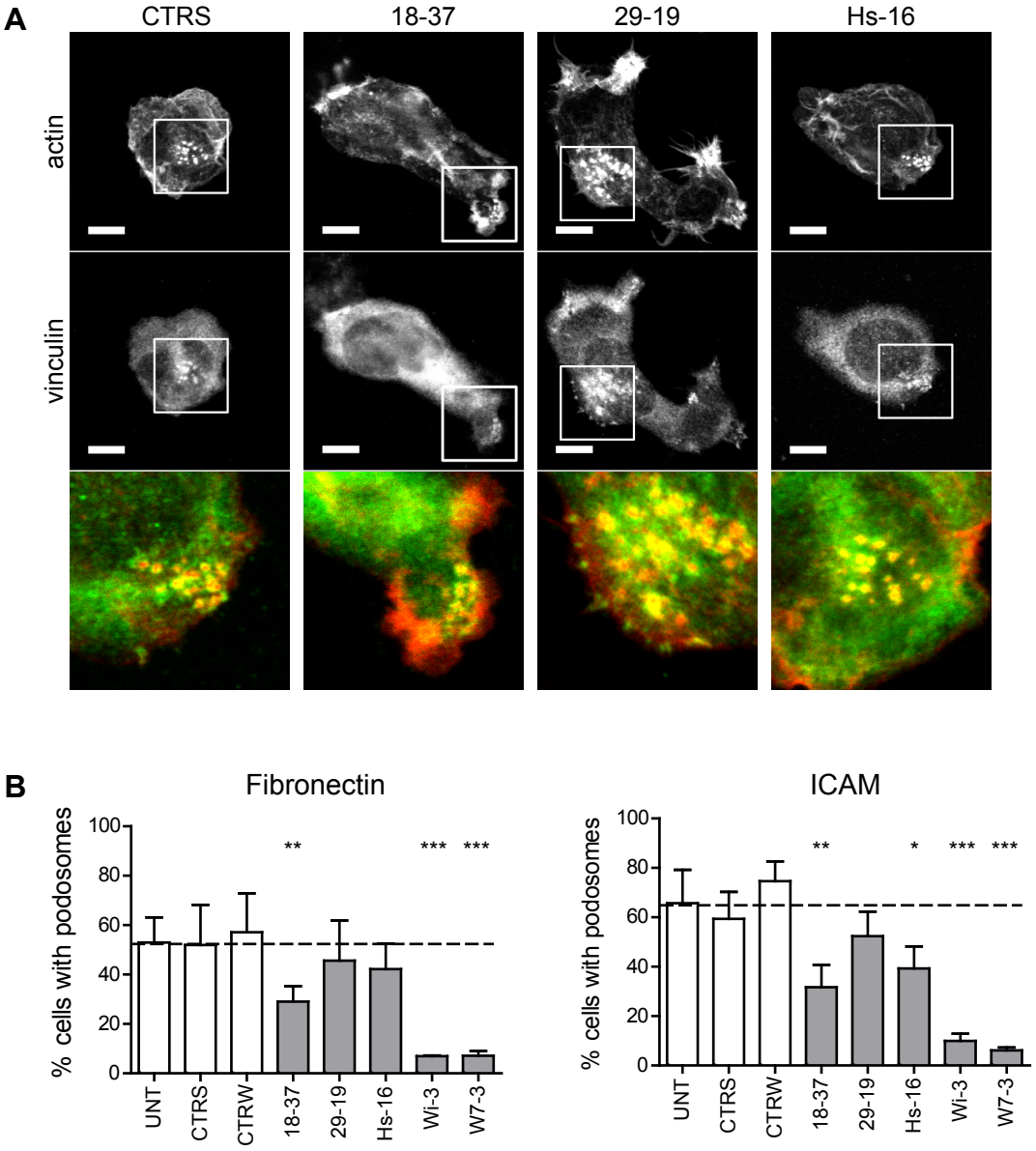

Figure 5.3. Knock-down of CD29 does not affect podosome formation, whereas CD18, WIP and WASp knock-down impairs podosome formation and HS1 expression is necessary for podosome formation on ICAM.

THP1 cell lines expressing different shRNA constructs were differentiated into THP1DC and plated for 48h, after which they were fixed, permeabilised and stained for actin and vinculin. **A** Confocal micrographs of THP1DC from CTRS, 18-37, 29-19 and Hs-16 cultures plated onto fibronectin are presented. Podosomes are readily identified as dense F-actin dots (red in the merged image) enriched in vinculin (green in the merged image). Scale bars: 10μm. **B** The percentage of THP1DC presenting podosomes was determined. A minimum of 100 cells per cell line was scored for the presence of podosomes for each experiment and aggregated results of 4 experiments are presented (mean ± SD; * $p<0.05$, ** $p<0.01$, *** $p<0.001$).

cally identified podosomes were manually confirmed as podosomes. This was necessary because small bright actin signals were sometimes being considered podosomes whereas by eye they would not be counted as such. The number of podosomes per cell was, thus, calculated, as well as the size distribution of the individual podosomes (Figure 5.4 B

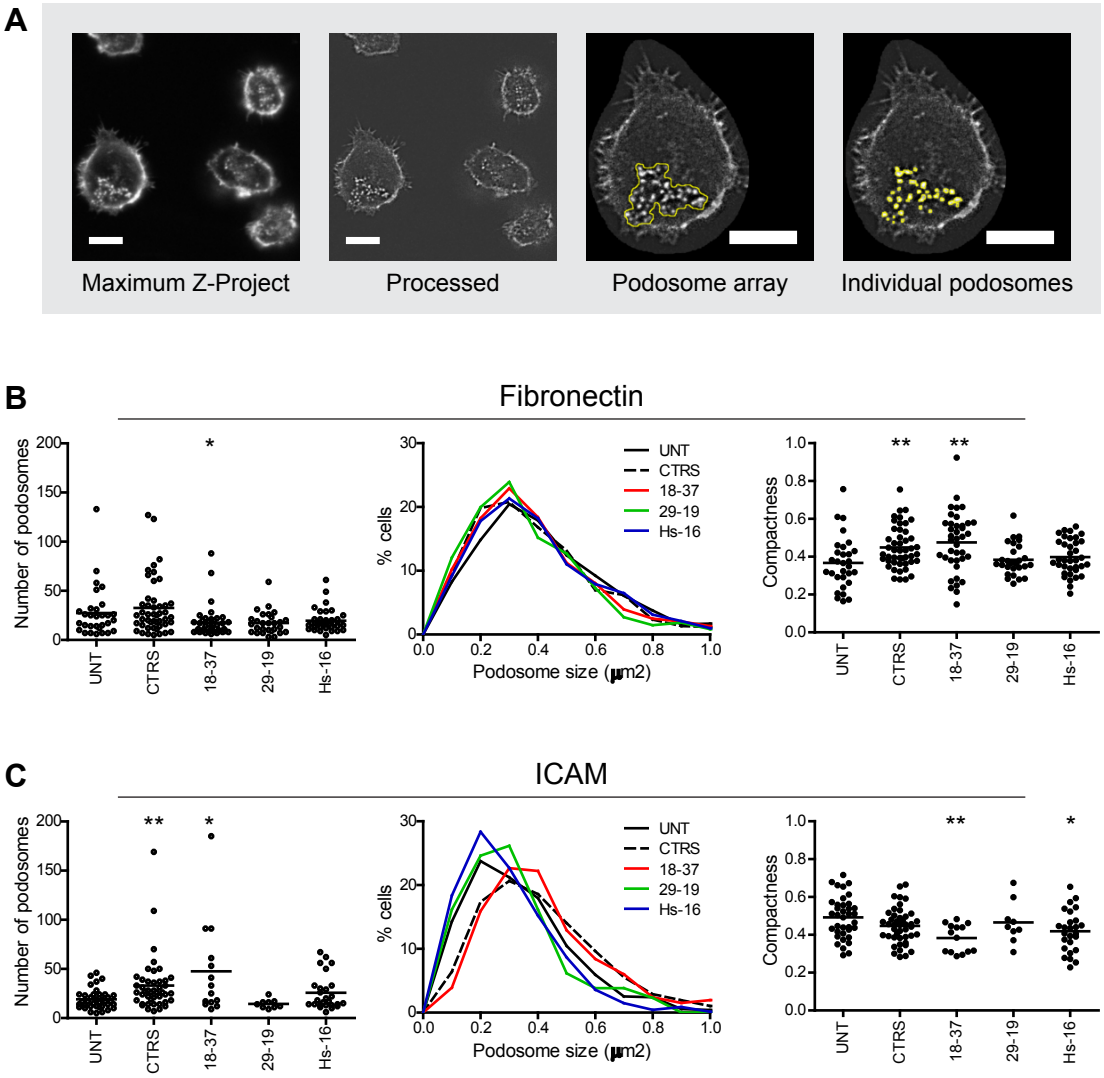

Figure 5.4. Characterisation of podosomes and podosome arrays in shRNA THP1DC cell lines.

THP1DC plated on fibronectin- or ICAM-coated glass slides were imaged by confocal microscopy for identification of podosomes. The cells were stained with rhodamine-phalloidin for actin identification and with anti-vinculin antibody. **A** The maximum Z-projection of a confocal Z-stack of THP1DC expressing CTRS shRNA is presented. The confocal images were processed as detailed in the Materials and Methods section to enable easier identification of podosomes. The podosome arrays' limits were defined manually (yellow border) and the individual podosomes were then identified automatically (yellow borders). Scale bars: 10µm. **B** 28-47 cells plated on fibronectin were analysed for the different constructs and the number of podosomes per cell, the size distribution of the podosomes (481-1535 podosomes) and the compactness of the podosome arrays, defined as the number of podosomes divided by the area of the podosome array, were determined. **C** The same parameters were calculated for cells plated on ICAM; 9-44 cells and 130-1453 podosomes were analysed. * $p<0.05$, ** $p<0.01$, compared to untransduced cells (UNT), Mann Whitney *U*-test.

and C). Another parameter calculated to characterise the podosome arrays was their compactness, defined as the inverse of the area occupied by each podosome in the array. This was calculated by dividing the number of podosomes in one array by the area of

that podosome array, as defined by the manually drawn border (Figure 5.4 B and C). The higher the value of compactness, the more compact the podosome array.

When THP1DC were plated on fibronectin, there were fewer podosomes per cell for all shRNA constructs compared to untransduced or CTRS expressing cells, reaching statistical significance for the 18-37 line. The 18-37 clone also presented significantly more compact podosome arrays. In contrast, when plated on ICAM, this clone appeared to have more and larger podosomes per cell and the podosome arrays of the 18-37 clone were less compact than those of untransduced THP1DC. Cells with reduced expression of HS1 plated on fibronectin assembled podosomes that were indistinguishable from control cells for the parameters tested. In contrast, when plated on ICAM, cells with reduce levels of HS1appeared to assemble more podosomes per cell in less compact podosome arrays. Unexpectedly, the control CTRS cells presented statistically significantly more compact podosomes arrays than untransduced cells when plated on fibronectin. On ICAM these cells presented an average higher number of podosomes per cell as well as larger podosomes compared to untransduced cells.

The shape of individual podosomes was also measured (circularity and aspect ratio) but no difference was found between constructs regardless of substrate (data not shown).

5.5 Analysis of adhesions turnover in the knock-down cell lines

We wished to investigate in more detail the effect of the knock-downs in integrin-mediated adhesions made by these cells. THP1DC were plated onto fibronectin or ICAM and imaged by time-lapse interference reflection microscopy (IRM) using a laser scanning confocal microscope in order to study the dynamics of such adhesions.

IRM is an optical technique which allows to image sites of close contact between a cell and the substrate. IRM relies on reflections of a polarised monochromatic light beam (such as a laser line in a confocal microscope) as it passes through materials with different refraction indexes, specifically from the glass coverslip into the aqueous medium where a cell is cultured and from there into the cell [Curtis 1964]. As the specimen is illuminated with a polarised monochromatic light beam, using an oil immersion objective, the first reflection occurs at the glass-aqueous medium interphase. Light is reflected back into the objective with a half wavelength shift because it is passing into a medium with a lower refraction index. A second reflection will occur at the medium-cell surface interface (reflected light will not undergo a phase reversal because the refraction index of the cell is higher than that of the aqueous medium). The signal detected by the microscope will be a sum of these two major reflections, which will have different optical paths. The

optical path of the first reflection is half a wavelength due to the phase reversal. The second reflection has an optical path corresponding to the distance travelled by the light between the glass coverslip and the cell surface, where it was reflected, and back into the glass coverslip (twice the distance between the cell surface and the coverslip). The interference between the two reflections will either be constructive or destructive depending on the distance between the two reflection surfaces, that is, the distance between the glass coverslip and the cell membrane. The IRM intensity is a function of this distance [Barr and Bunnell 2009]. Using a 488nm laser light, which has a wavelength in water of approximately 400nm, if the cell surface is at 100nm from the glass coverslip, the second reflection will have a 200nm optical path. As the reflected beam from the first reflexion has half wavelength shift (200nm) the two waves are in phase and will result in constructive interference, having the brightest signal. If the membrane is very close to the glass surface, then the second reflection will have a very small optical path and the difference between the two reflections will be close to half wavelength, resulting in destructive interference, and a dark signal. In the IRM image, white occurs when the distance from the coverslip is about 100nm, greys at intermediate distances and black at distances below 15nm, indicating adhesion areas. The coating of coverslips with substrates does not constitute a problem for this type of analysis [Barr and Bunnell 2009]. Focusing on the glass-medium interface is critical as the IRM signal will only be obtained for a very narrow focusing window. Constant manual adjustment of the focus plane during image acquisition had to be done as autofocus routines would have added considerable time between images.

The use of a laser scanning confocal microscope resulted in scanning line background noise, the horizontal lines seen in the time-lapse videos (Figure 5.5 A). Because of the constant frequency of these horizontal lines, it is possible to use Fourier Transform (FT) analysis to remove this background noise (Figure 5.5 B). In FT analysis an image (special domain) is decomposed into its sine and cosine components, resulting in two images: the frequency or magnitude domain and the phase domain. The former contains most of the information on the geometric structure of the spatial domain (Figure 5.5 A). The majority of the information in the spatial domain is found for lower frequencies, at the centre of the frequency image (brighter pixels). Less information is associated with higher frequencies (darker pixels on the edges of the FT frequency domain). However, if there are geometric structures in the original image, they will appear as higher frequencies with larger magnitude. Horizontal structures in the spatial domain, such as the confocal scanning lines, result in high magnitudes over the vertical axis of the frequency domain (Figure 5.5 A). FT analysis allows the identification of these horizontal scanning lines in the frequency image, their removal, and the generation of a new spatial domain by performing an inverse FT. By analysing the spatial domain (Figure 5.5 A) we can identify the frequency of the scanning lines between 1/16th and 1/8th of the maximum frequency (1/2 pixels) and apply a filter designed to block these frequencies (Figure 5.5 B). The inverse FT creates an image where the regular scanning lines have been considerably attenuated (Figure 5.5 B).

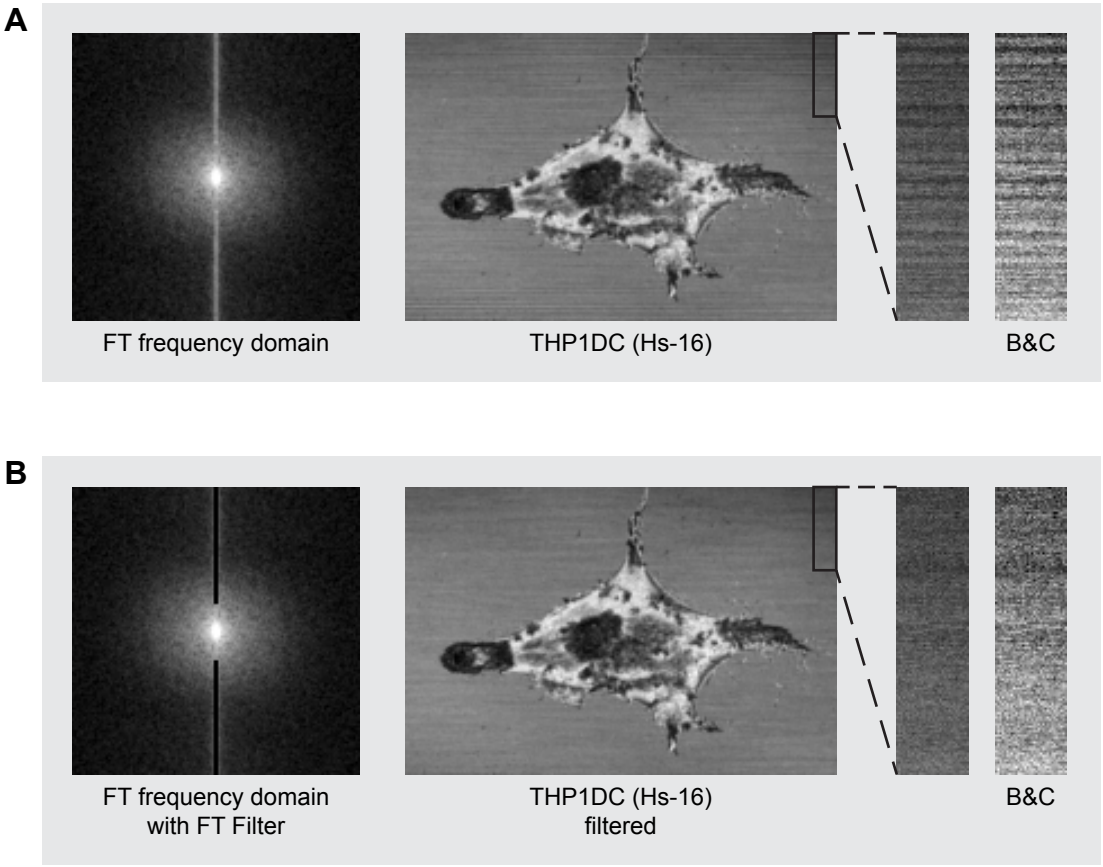

Figure 5.5. FT filtering to remove noise from scanning microscope IRM videos.
THP1DC were plated on fibronectin- and ICAM-coated glass slides and imaged by interference reflection microscopy (IRM) with a scanning confocal microscope using the 488 laser line and images were collected every 0.5 seconds for 1-5 minutes. Image sequences with 2 frame per second and duration of 16 seconds where there was no change in focusing were identified. **A** A frame from one of such videos is shown for THP1DC from the Hs-16 clone plated on fibronectin. The detail of the top-right corner of the image shows the regular noise originated from the scanning confocal microscope, clearer after brightness and contrast enhancement (B&C). Left from the main image is the corresponding Fourier Transform (FT) frequency domain. **B** A FT filter was applied to the IRM videos to remove the horizontal regular noise. The frequency domain of the image in A is shown with the FT filter blocking horizontal lines with frequencies up to $1/8^{th}$ of the maximum frequency and the corresponding filtered image is presented, again with the top-right corner blown-up for comparison.

Adhesion areas were cropped form the IRM videos (1 frame per second) and were processed in order to increase contrast and sharpness as detailed in Chapter 2 - Materials and methods (Figure 5.6 A). An Adhesion Index was calculated which measures the stability of adhesions. This index, developed for analysis of focal adhesions and podosome turnover [Ancliff et al. 2006; Blundell et al. 2009; Chou et al. 2006; Holt et al. 2008] and also used to assess membrane contact dynamics in lymphocytes [Burns et al. 2010], was adapted for this study. Individual frames were thresholded at 50% to identify stronger adhesive areas and four consecutive frames were overlaid and averaged into

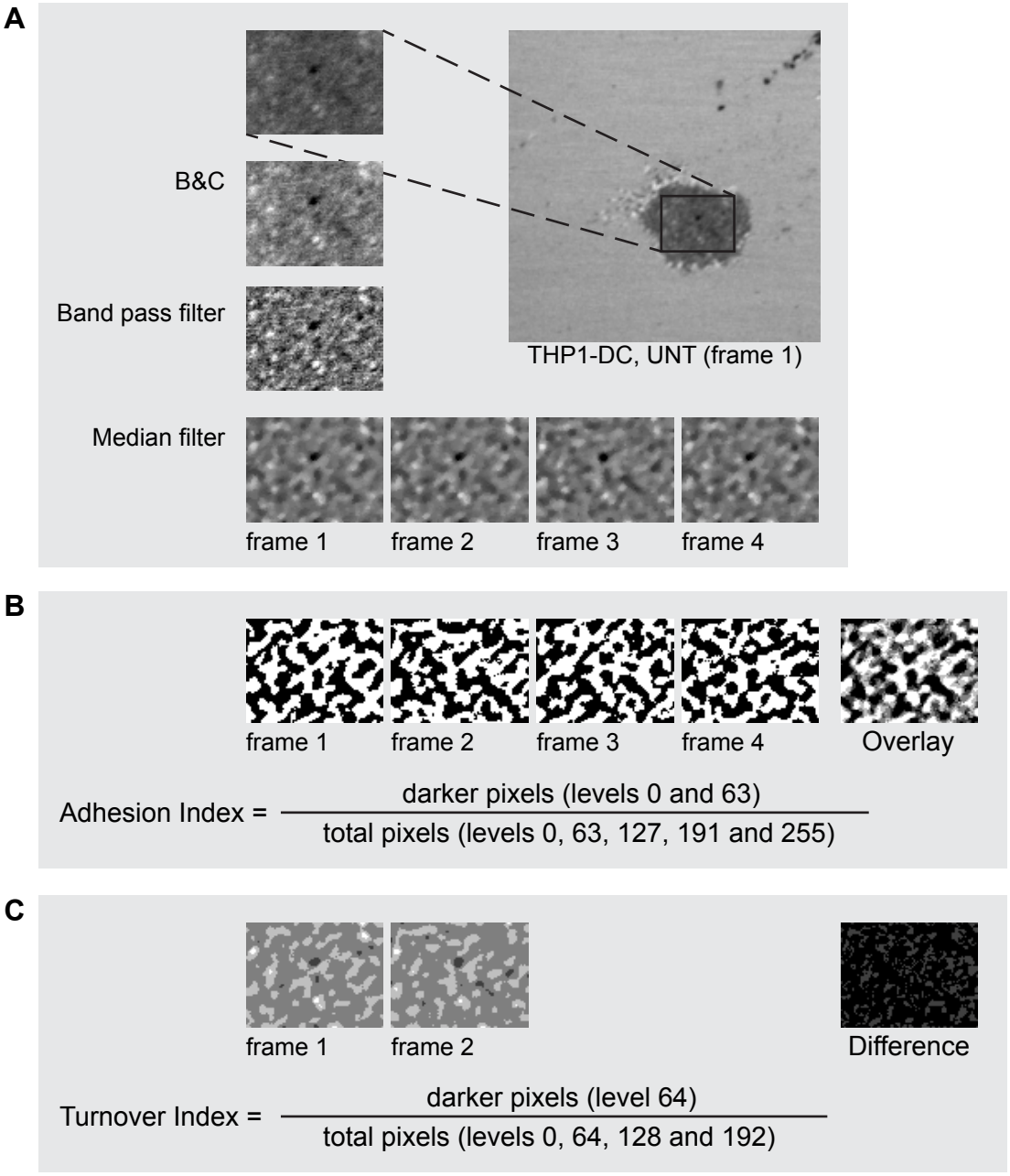

Figure 5.6. Processing of IRM videos and Adhesion and Turnover Index calculation. **A** Interference Reflection Microscopy videos of THP1DC with duration 16 seconds and 1 frame per second were cropped to isolate adhesion areas, as shown for the first frame of a video of an untransduced cell (UNT). Adhesion areas videos were processed automatically by enhancing bringhtness and contrast (B&C) and filtering with a band pass filter and a median filter. The first four frames of the video are shown. **B** Each frame was then transformed into a binary image and every 4 consecutive frames were overlaid and averaged. An Adhesion Index was calculated from the histogram values of the overlaid image, as indicated. **C** In order to calculate a Turnover Index, the look-up table (LUT) of each frame was transformed into a 4 grey levels LUT. The difference between each 2 consecutive frames was determined and the turnover index was calculated from the histogram values of the difference image.

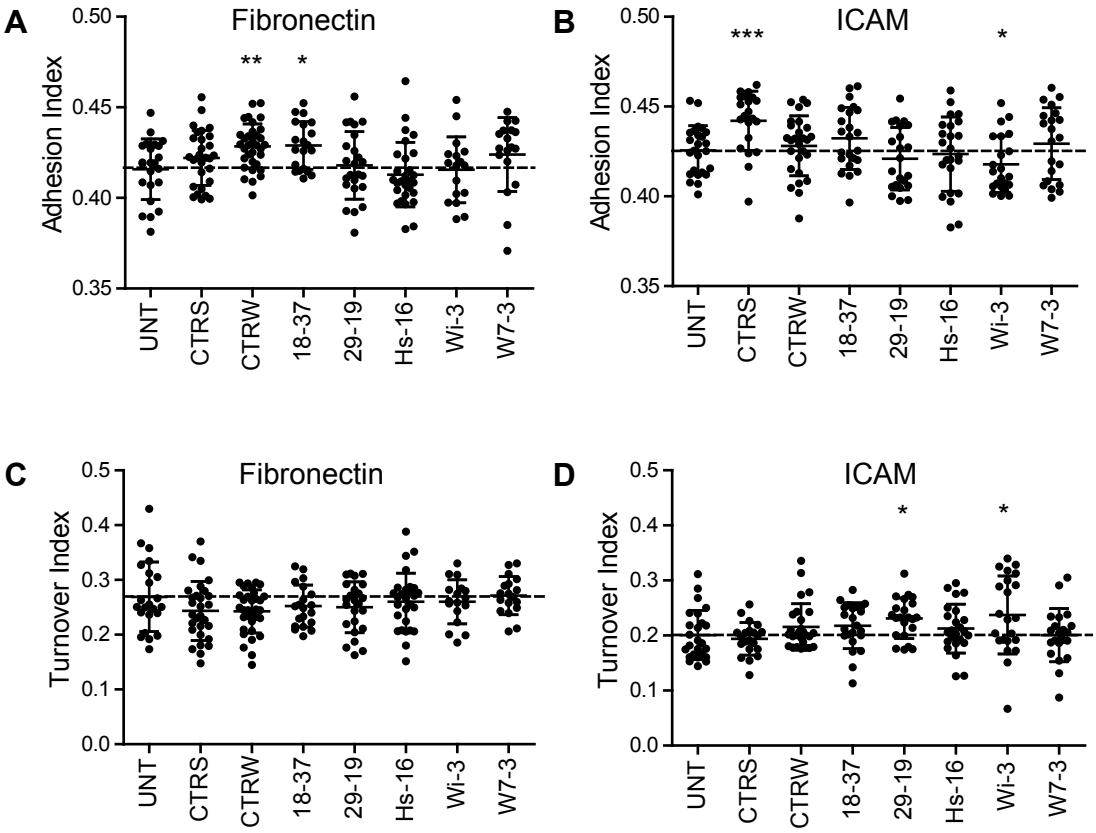

Figure 5.7. Adhesion Index and Turnover Index of shRNA THP1DC lines.
The Adhesion Index was calculated for THP1DC cell lines 18-37, 29-19, Hs-16, Wi-3 and W7-3, the controls CTRS and CTRW and for untransduced (UNT) cells plated on **A** fibronectin- and **B** ICAM-coated glass slides. The Turnover Index was calculated for the same cells, also on **C** fibronectin- and on **D** ICAM-coated glass slides. Depending on the constructs, 17-33 cells plated on fibronectin and 21-27 cells plated on ICAM were analysed. * $p<0.05$, ** $p<0.01$, *** $p<0.001$, compared to UNT, Mann Whitney *U*-test.

an adhesion map which reveals spatial and dynamic changes in adhesions (Figure 5.6 B). The Adhesion Index reflects the extent of coincidence of adhesions at different time points, that is, the persistence of adhesion points. A Turnover Index was also calculated, measuring the change in adhesions from on frame to the next. Each frame was converted into a 4 grey levels image, creating a map of adhesion strength. The difference between two consecutive frames was calculated and its histogram values used to calculate the Turnover Index (Figure 5.6 C). This index is a measurement of pixels that changed by one level of grey between the two frames.

Both the Adhesion Index and the Turnover Index calculated resulted in very similar results for all cell lines plated either on fibronectin or on ICAM (Figure 5.7). Exceptions were CTRW and 18-37 lines, whose adhesions appeared more stable on fibronectin than those from untransduced THP1DC. Also CTRS presented more stable adhesions on ICAM. Clone Wi-3 had slightly less stable adhesions to ICAM and a small but significantly higher adhesion turnover on ICAM, similarly to 29-19, when compared to untransduced cells.

The Turnover Index presented accounts for the number of pixels which have changed by one level of grey between two consecutive frames. From the pixels which had their grey value changing, the vast majority demonstrated a change by only one level of grey. This was noted across all the experimental conditions, making it irrelevant to calculate turnover indexes accounting for more drastic change in adhesion strength between consecutive frames, such as a change of 2, 3 or 4 levels. Another variation of this Turnover Index was calculated by using 8 levels of grey. However, this approach did not make the analysis more sensitive. In fact, the opposite became apparent as this new Turnover Index, calculated for 1 grey level change, resulted in virtually the same value for all constructs and with very narrow standard deviations (data not shown). Additionally, the new Turnover Index calculated for 2 levels change resulted in essentially the same results as the ones presented in Figure 5.7 B for the initial Turnover Index. Finally, the Adhesion Index and the Turnover Index were calculated taking consecutive frames every 0.5sec instead of every 1sec, but results were effectively the same as those originally calculated (data not shown).

5.6 Discussion

The generation and biochemical characterization of a panel of knock-down myeloid cell lines was described in the previous chapter of this thesis (Chapter 4 – Generation of knock-down human myeloid cell lines for integrins and actin regulators). Briefly, THP1 cell lines stably expressing shRNA targeting the integrins CD18 and CD29 and the actin regulators HS1, WASp and WIP were generated using a lentiviral vector system and the expression of the target proteins was characterised. A knock-down level between 96% and 87% was achieved. The present chapter concerns the functional characterization of the cell lines, namely their adhesion to ICAM and fibronectin, the morphology of adherent cells, the ability to assemble podosomes, podosome architecture and adhesion dynamics.

The 18-37 cell line retained 9.7% total CD18 expression and 23% CD18 surface expression and normal CD29 expression. Accordingly, these cells presented a specific adhesion defect to ICAM, the β_2 integrin ligand, but not to fibronectin, the β_1 ligand. CD18 has been shown to be recruited to human DC podosomes, as discussed in Chapter 4 – Generation of knock-down human myeloid cell lines for integrins and actin regulators. In this chapter I have additionally demonstrated that knock-down CD18 expression in THP1DC results in a defect in podosome formation as significantly fewer cells from this line presented podosomes compared to untransduced THP1DC, regardless of the substrate (fibronectin

or ICAM). This is in line with results obtained using DC from severe LAD patients, which lack CD18 expression and present a selective adhesive defect to ICAM and are incompetent at assembling podosomes (Siobhan Burns, unpublished data). Moreover, those results are also in concurrence with results obtained with DC from WAS patients, where CD18 is present but does not cluster as podosomes are absent, and which present an adhesion defect to ICAM but normal adhesion to fibronectin [Burns et al. 2004; Burns et al. 2001]. A study using DC from LAD patients suggests that podosome architecture in these cells correlates with the level of CD18 expression: residual levels of CD18 (in severe LAD patients) result in diffuse F-actin plaques and absence of normal podosome cores; intermediate levels of CD18 (DC from mild LAD patients, who have up to 30% CD18 surface expression) support podosome-like structures that highly resemble podosomes from normal DC but with less defined fuzzier actin cores; normal levels of CD18, in DC from normal individuals, result in assembly of podosomes with individualised actin cores clearly surrounded by integrin-rich rings (Siobhan Burns, unpublished data). Both the observations from DC from LAD patients and the results presented regarding the 18-37 THP1DC cell line indicate a correlation between CD18 expression and podosome formation. However, whereas in primary DC reduced expression of the integrin resulted in failure to condense the F-actin into defined cores, no consistent different was observed in 18-37 THP1DC podosome morphology. Despite this fact, the THP1DC generated here represent a useful model of human LAD DC.

The importance of CD29 in DC podosomes is not clear. There is one report showing concentration of total and active β_1 integrins in podosome rings of human DC [van Helden et al. 2006]. However, another study had suggested specific recruitment of β_2 integrins only [Burns et al. 2004]. In the previous chapter, I was also unable to identify recruitment of CD29 to podosome areas, using either anti-CD29 or anti-active CD29 antibodies. On the contrary, CD29 appeared excluded form podosome areas. The results presented in this chapter demonstrate the requirement for CD29 in THP1 cells for efficient adhesion to fibronectin, as cells from the 29-19 cell line present reduced adhesion to this substrate, but normal CD18 expression and corresponding normal adhesion to ICAM. However, no defect in podosome formation was detected for this cell line as the number of 29-19 THP1DC presenting podosomes was comparable to that of untransduced or control cells. There were fewer podosomes per cell when cells were plated on fibronectin, but no other difference in size of podosomes or compactness of arrays on either fibronectin or ICAM. Therefore, these results suggest that CD29 is redundant in DC podosome formation. It had been suggested that β_1-enriched DC podosomes mediated adhesion to fibronectin [van Helden et al. 2006]. However, the THP1 line with only 4% CD29 surface expression had a defect in static adhesion to fibronectin despite presenting normal podosome numbers, suggesting that even though static adhesion to fibronectin is mediated by CD29, it is not via DC podosomes. To further confirm the irrelevance of CD29 in podosome formation, it would be interesting to analyse the localisation of CD29 in the 18-37 THP1DC podosomes and knockdown CD29 expression in the 18-37 THP1 line to assess whether there would be a further reduction in the number of cells able to assemble podosomes.

The Hs-16 cell line, with reduced expression of HS1 (to 7% of control values), presented a clear adhesion defect to ICAM, the β_2 ligand. The magnitude of the adhesion defect was similar to that of cells where CD18 expression had been knocked-down – the 18-37 line. This result suggests the possible involvement of HS1 in the regulation of CD18 avidity. HS1 is an actin regulator whose function has only recently started to be investigated. There is only one published study looking at HS1 in myeloid cells, in particular in murine BMDC [Dehring et al. 2011], which reported no defect in adhesion or spreading on fibronectin, in agreement with the results presented here. However, the use of ICAM, the CD18 ligand, was not reported. Nevertheless, there is one study which links HS1 and CD18 activation in NK cells. When human NK cells are plated on ICAM or form a conjugate with a target cell, HS1 is recruited to the F-actin rich interface. However, HS1 remains diffuse throughout the cell when these are plated on fibronectin. Moreover, NK cells depleted of HS1, using shRNA, present reduced staining of active β_2 integrin at their surface, which is suggested to cause the reduced conjugate formation, defective adhesion to ICAM, but not to fibronectin, as well as reduced spreading and abolished chemotaxis [Butler et al. 2008]. Additionally, whereas THP1DC from the Hs-16 line presented no significant defect in podosome formation when plated on fibronectin, they assembled significantly fewer podosomes when plated on ICAM when compared to control cells. Once more, the Hs-16 cell line presented results comparable to the 18-37 line, where CD18 expression had been knocked-down. Together, these results indicate a role for HS1 in a CD18 activation pathway possibly shared between myeloid cells and lymphocytes. It would be interesting to analyse the surface expression of active CD18 in the Hs-16 line after cell activation to see whether HS1 depletion also results in reduced CD18 activation in human myeloid cells.

The importance for HS1 in podosome formation and dynamics has been analysed in the study using BMDC referred to above but only cells plated on fibronectin were tested [Dehring et al. 2011] When plated on fibronectin, the number of BMDC from HS1 null mice presenting podosomes was comparable to that of cells from normal animals but podosome arrays were more loosely packed and improperly localised within the cell. In line with these results, I also found that THP1DC from the Hs-16 line presented no significant defect in podosome formation when plated on fibronectin. There were slightly, although not statistically significant, fewer podosomes per cell in the Hs-16 THP1DC line. However, no altered podosome array distribution was observed. This could simply reflect the fact that only very few THP1DC were polarised under the conditions used here. This was intrinsic to the cell model and conditions used, as the vast majority of THP1DC were round and not polarised, resulting in the majority of podosome arrays localising to the centre of the cells. Activation of THP1DC could be attempted in order to induce their polarization and possibly reveal aberrant podosome array localization.

In human T-cells, although HS1 is not required for conjugate formation or initial immune synapse formation, it is required for the stabilisation of associated actin structures, as T-cells with reduced HS1 expression are able to form actin-rich lamellipodia after TCR

engagement but these collapse rapidly [Carrizosa et al. 2009; Gomez et al. 2006]. In contrast, in murine BMDC HS1 did not affect podosome turnover or stability but was involved in podosome early biogenesis, accelerating it (HS1 null podosomes take longer to be formed) [Dehring et al. 2011]. In this study I did not investigate the dynamics of podosome formation. Nevertheless, the defect in podosome formation observed when HS1 knock-down cells were plated on ICAM could result from deregulation of podosome core assembly/disassembly dynamics the absence of HS1.

Phosphorylation of HS1 remains to be explored in DC and in particular in podosome formation and function. Work done in NK-cells and T-cells has shown that HS1 is rapidly and transiently phosphorylated following cell activation [Brunati et al. 2005; Butler et al. 2008; Carrizosa et al. 2009; Gomez et al. 2006; Huang et al. 2008; Yamanashi et al. 1993]. HS1 can be phosphorylated in two tyrosine residues. Phosphorylation on Y397 has been demonstrated to be required for normal NK-cell adhesion to ICAM as well as lytic synapse formation; phosphorylation at Y378 is required for NK cells chemotaxis [Butler et al. 2008]. Furthermore, HS1 phosphorylation is essential for Vav1 stabilisation and integrin activation [Butler et al. 2008; Gomez et al. 2006]. Future work on the investigation of HS1 function in myeloid cells should explore HS1 phosphorylation. For this, expression of HS1 in the Hs-16 line could be rescued using shRNA resistant phospho-dead and phospho-mimicking HS1 mutants.

DC from WAS patients are unable to assemble podosomes and present defective adhesion to ICAM but not fibronectin, presumably due to the inability to cluster β_2 integrins at podosomes [Burns et al. 2004]. Results presented here show that THP1DC with reduced WASp expression were also defective in podosome formation as significantly fewer cells presented podosomes compared to untransduced or control cell lines. Adhesion to fibronectin was also normal and adhesion to ICAM was significantly reduced, although the effect observed was considerably weaker than previously reported. This is most likely due to the specific adhesion assay used here, which is a static adhesion assay, whereas the study mentioned applied a dynamic adhesion assay, where the actual strength of adhesion can be measured with increasing levels of shear force applied.

THP1 with reduced expression of WIP (Wi cell line) were expected to mimic at least in part the phenotype of the W7 cell line (WASp knock-down) because WIP knock-down also results in reduced WASp expression, as demonstrated in Chapter 4 – Generation of knock-down human myeloid cell lines for integrins and actin regulators – as WIP is required for WASp functional expression [Konno et al. 2007]. In fact, WIP depletion resulted in a decrease in the number of cells presenting podosomes to similar levels as those observed for the W7 line. No adhesion defect was detected on either fibronectin or ICAM. However, the defect detected for the W7 line was very mild, and although statistically significant of doubtful physiological significance. WIP has been implicated in podosome degradative function of murine splenic DC by regulating MMP secretion at

podosome sites via its interaction with cortactin [Banon-Rodriguez et al. 2011; Chou et al. 2006]. In BMDC, which do not express cortactin but its homolog HS1, HS1 does not appear to influence MMP secretion by murine BMDC [Dehring et al. 2011]. Nevertheless, a function for HS1 in podosome-mediated ECM degradation, possibly in conjunction with WIP, has not been addressed in human cell lines or primary DC.

The turnover of adhesions in THP1DC was analysed by IRM. The IRM technique and processing had been developed to analyse focal adhesion turnover and used for podosome turnover and B-cell membrane dynamics [Ancliff et al. 2006; Blundell et al. 2009; Burns et al. 2010; Chou et al. 2006; Holt et al. 2008]. Here, I was unable to identify podosomes by IRM and attempted at measuring adhesion dynamics in an integrin-dependent adhesion system in the THP1DC lines. FT filtering of the IRM videos was required to remove scanning line background noise, after which an Adhesion and a Turnover Index were calculated. The results obtained for the different THP1DC lines were all very similar. The adhesion areas analysed showed very little change in terms of adhesion dynamics, even though some of those cell lines have been shown to present defective adhesion to integrin ligands and defective podosome formation. On one hand, analysing more cells could improve the power of the results. On the other hand, improving the sensitivity of the analysis may be required. The latter was tried by calculating variations of the Turnover Index, either by changing the time between frames or the levels of grey differentiating different strength adhesions, but with no success. Additionally, total internal reflection fluorescence microscopy (TIRF) could be used in order to specifically measure turnover of fluorescently labelled podosomes, for example using fluorescently labelled actin or actin probe.

The controls used in the experiments presented were untransduced cells and cells transduced with non-targeting shRNA sequences (CTRS and CTRW). Data presented in the previous chapter demonstrates that the expression of the proteins of interest in this study in the control lines were not significantly different from untransduced cells. However, a few differences were found in the functional assays performed and presented in the present chapter. CTRS THP1DC were morphologically significantly more round and less polarised than any other cell line, in particular untransduced or CTRW cells. This did not reflect any adhesion defect. Podosome formation was normal. However, when plated on ICAM, CTRS presented significantly more podosomes per cell and these were slightly larger. On fibronectin, podosome arrays were slightly less compact than untransduced cells.

Furthermore, reconstitution experiments should be performed in order to demonstrate the observed phenotype is, in fact, due to the knock-down induced by the shRNA. Expression of CD18, CD29, HS1, WASp and WIP should be rescued, for example using

a lentivector system to deliver cDNA for these proteins which is resistant to the shRNA the cells are expressing, and those cells should be tested as to whether their abnormal behaviour is reverted to the normal phenotype. This is particular important for the results obtained for the HS1 and CD29 knock-down cell lines, for which results are novel and not corroborated by knock-out models.

In this chapter an adhesion defect to fibronectin and ICAM was demonstrated for the integrin knock-down cell lines, as expected from the specificity of the integrin ligands. Additionally, defective podosome formation was observed for the CD18, WAS and WIP knock-down cell lines, as would have been predicted from previous work using knock-out models. Additionally, despite resulting in reduced adhesion to fibronectin, the CD29 knock-down cell line presented no defect in podosome formation when plated either on fibronectin or ICAM, suggesting CD29 is not necessary for podosome formation. Finally, the knock-down of HS1 resulted in reduced capacity to adhere to ICAM, but not to fibronectin, as well as reduced numbers of cells presenting podosomes when plated on ICAM, with results comparable to those obtained with the CD18 knock-down cell line. These observations strengthen the idea of HS1 being involved in a CD18 activation pathway, as has been suggested in lymphocytes. The lack of effect of the knock-downs in podosome architecture and adhesion dynamics may be due to the fact that those molecules do not influence these functions or it may reflect the sensitivity of the functional assays used for their assessment.

Chapter

6

GENERAL DISCUSSION

Podosomes are actin adhesive structures considered to be important for adhesion-dependent migration. Podosomes are comprised of a dense F-actin core, dependent on the WASp-mediated Arp2/3 actin polymerisation machinery, surrounded by a ring of integrins and associated proteins. Podosomes are the prominent actin structures in immature DC. Migration is critical for the DC life-cycle and function and podosomes are thought to play a role in immature DC migration in extravascular tissues as immune sentinels and in the onset of maturation when migrating to afferent lymphatics to home to lymph nodes. Initiation of DC maturation is accompanied by a transient upregulation of podosomes followed by complete loss of these structures in mature DC.

Podosomes and the related structures invadopodia have been the focus of increasing research, in particular related with cancer biology. However, a comprehensive view of these structures is hampered by the use of several different cellular models and transgenic animals, making it difficult to extrapolate results to the human context, the ultimate goal when studying the immune system or cancer biology. In this project I wished to study DC podosomes in a human system.

Manipulation of the DC cytoskeleton

The potential of lentivectors to genetically manipulate monocyte-derived DC was addressed. Different viral envelopes were tested and VSVg-pseudotyped vectors were

found to be the most efficient. The use of MACS CD14 bead selection for monocyte isolation as well as the use of FCS in the culture media are suggested to have contributed to the high transduction efficiency observed without the use of polycationic adjuvants, co-centrifugation or multiple exposures to the virus [Breckpot et al. 2004; Neil et al. 2001; Rouas et al. 2002].

Manipulation of immature DC may induce their activation and result in undesirable changes to their cytoskeleton and function. There is controversy in the literature regarding whether lentivectors inherently induce DC cellular activation and maturation [Breckpot et al. 2007; Chinnasamy et al. 2000; Esslinger et al. 2002; Gruber et al. 2000; Rouas et al. 2002; Tan et al. 2005]. Here I have shown that the immature phenotype and function was retained in transduced DC. Transduction was performed on monocytes, the DC precursors. This may enabled avoiding lentivector pattern recognition by TLR3, 7 and 8 and consequent DC activation [Breckpot et al. 2007; Breckpot et al. 2010] since monocytes express no or very low basal levels of TLR 3 and 7 [Bekeredjian-Ding et al. 2006; Iwasaki and Medzhitov 2004; Kadowaki et al. 2001; Matsumoto et al. 2003; Muzio et al. 2000; Schreibelt et al.]. No significant upregulation of the maturation surface markers MHCII and CD86 co-stimulatory molecule was observed in transduced cells. Moreover, similarly to untransduced iDC, transduced cells retained their antigen uptake capacity and were deficient in generating an allogeneic T-cell response. Maturation was also not affected by lentivector transduction since cell activation by LPS, via TLR4, resulted in upregulation of maturation surface markers, down-regulation of antigen uptake and increased T-cell stimulatory capacity, in an indistinguishable way to untransduced DC.

The actin cytoskeleton of transduced DC was also analysed and only negligible differences were found between transduced and untransduced cells. A slight decrease in the number of transduced iDC presenting podosomes was observed, compared to untransduced cells, but this was not reflected in differences in migratory behaviour, including speed of migration. Therefore, results presented demonstrate lentivectors to be effective tools for the genetic manipulation of moDC for cytoskeletal studies.

Generation of a panel of knock-down cell lines

There are only two human conditions that are known to affect DC podosome formation: LAD, due to reduced levels of β_2 integrin expression (Siobhan Burns, unpublished results); and WAS, due to defective WASp expression or function [Burns et al. 2001]. Cells from these patients are a very scarce biological resource even at a national centre for paediatric primary immunodeficiencies such as ours. Additionally, there are no other human conditions characterised by defects in expression or function of other podosome associated proteins. Moreover, whereas primary DC generated from $CD34^+$ haematopoietic precursors or from $CD14^+$ circulating monocytes are subject to inter- and

intra-donor variations and have a limited life span in culture, which constitute constraints to experimental design, cell lines are a readily available homogenous unlimited resource. Therefore, a panel of knock-down human cell lines was generated using RNAi targeting proteins associated with podosome regulation.

Dendritic-like cells can be differentiated from a variety of leukaemia-derived cell lines, in particularly from the myelogenous or monocytic lineages. The potential of leukaemic cell lines for DC differentiation is likely to be determined by the stage of lineage commitment when leukemic transformation occurred [Rasaiyaah et al. 2007]. For example, whereas the Mono Mac 6, U937 and K562 cell lines are unable to differentiate into dendritic-like cells [Berges et al. 2005; Santegoets et al. 2008], probably because they had already progressed too far along the macrophage differentiation pathway to allow redirection towards DC, the THP1, HL-60, KG-1 and MUTZ-3 cell lines were blocked at an earlier stage on the monocytic lineage and have thus been shown to be able to be differentiated into dendritic-like cells displaying most of the properties of primary DC in terms of phenotype and function [Berges et al. 2005; Rasaiyaah et al. 2007; Santegoets et al. 2008; van Helden et al. 2008]. Although none of those cell lines completely presents the biological and immunological features of primary DC, they are still valuable biological tools and have been used, for example, in DC biology and differentiation studies, in immunotherapy applications, and in testing of sensitizing agents [Ackerman and Cresswell 2003; Bontkes et al. 2006; Megherbi et al. 2009; Santegoets et al. 2008; Sebastian et al. 2012; St Louis et al. 1999]. From the leukaemia cell lines that have been shown to be differentiated into DC, only THP1 and HL-60 have been suggested to be useful as models to study podosome biogenesis and turnover as these cells readily adhere and form podosomes when stimulated with IL4 and PMA or PMA alone [Launay et al. 2003; Monypenny et al. 2011; van Helden et al. 2008]. In this study, the monocytic THP1 cell line was used to generate the panel of knock-down cell lines. This cell line can easily be differentiated into immature DC (THP1DC) [Berges et al. 2005] and I have shown that, following differentiation, THP1DC are also proficient at assembling podosomes which resemble the podosomes formed by primary immature DC.

The integrins CD18 and CD29 were targeted for knock-down. CD18 has been demonstrated to be clustered in DC podosomes [Burns et al. 2004]. As for CD29 there are contradictory reports regarding its localization to DC podosomes [Burns et al. 2004; van Helden et al. 2006]. Cortactin, an actin polymerisation regulator which has been implicated in splenic murine DC podosome function but which is not expressed in BMDC [Banon-Rodriguez et al. 2011; Dehring et al. 2011], was demonstrated not to be expressed by human moDC, THP1DC, nor by their precursors, and therefore was not included in the panel. Instead, HS1, a haematopoietic-specific cortactin homolog, implicated in podosome genesis and distribution in BMDC [Dehring et al. 2011] was included. The actin polymerisation modulators WASp and WIP were also targeted for knock-down. As these have been extensively studied in leukocyte podosome formation, they constituted controls where podosome formation was abrogated.

shRNA sequences used were chosen by screening different sequences from an shRNA library or were taken from previously published studies. THP1 cell lines stably expressing shRNA against the target genes were generated using a lentivector system and mRNA and protein expression were analysed. The knock-down levels achieved in bulk transduced populations were further improved by isolation of clonal cell lines. Two scrambled non-targeting shRNA sequences were used as controls for non sequence-specific off-target effects.

CD18, but not CD29, in DC podosomes

The weakest knock-down achieved was for CD18. Although total CD18 expression was reduced to 9.7%, cells still presented 23% of surface CD18 expression. Nevertheless, this knock-down level resulted in a clear and specific adhesion defect to ICAM (but not fibronectin) and a defect in podosome formation independent of the substrate. Regarding CD29, an expression of only 4% was achieved and this resulted in a specific adhesion deficiency to fibronectin (but not ICAM) but no defect in podosome formation. This suggests CD29 is not involved in DC podosome formation. Moreover, while CD18 clearly localises to podosome patches, resulting in a honeycomb pattern due to exclusion form podosome cores, I was unable to demonstrate recruitment of CD29 to DC podosomes using 3 different CD29 antibody clones.

DC from WAS patients, which are unable to assemble podosomes, have been shown to present defective adhesion to ICAM but not to fibronectin, thus implying the need for podosomes for β_2 integrin clustering [Burns et al. 2004]. As DC podosomes are only assembled by immature DC, they are suggested to be important in extravascular migration when DC act as immune sentinels. The specific recruitment of β_2 integrins to DC podosomes, supported by the results presented here, suggests podosomes to be important particularly in cell-cell contact during the migration process rather than in adhesion to ECM components such as fibronectin of collagen fibres. The upregulation of podosomes in the onset of maturation [Burns et al. 2004; West et al. 2008] leads to further speculation over the particular importance for podosomes in lymphatic vessel approach and intravasation.

HS1 is involved in CD18 activation and DC podosome formation

HS1 is a haematopoietic-specific cortactin homolog. Very few studies have been published regarding this actin regulator. The first and only report analysing the function of HS1 in myeloid cells was published only very recently, and it particularly explores a role for HS1

in BMDC podosome assembly and podosome array organisation [Dehring et al. 2011]. A link between HS1 and CD18 activation in lymphocytes had previously been suggested [Butler et al. 2008], but that was not addressed in the referred study. In fact, in that study all experiments reported were performed on fibronectin, the CD29 ligand, rather than on ICAM, the CD18 ligand. Here I have demonstrated that HS1 expression influences both CD18-mediated adhesion and podosome formation on ICAM. HS1 knock-down resulted in a specific adhesion defect to ICAM, but not fibronectin, with cells behaving similarly to the CD18 knock-down cell line. Moreover, reduced numbers of cells presenting podosomes when plated on ICAM, but not on fibronectin, were observed. These results suggest HS1 to be involved in "outside-in" CD18 activation signalling pathway. This conclusion could be further consolidated by comparing the levels of activated CD18 in the HS1 shRNA line with the levels in control and untransduced cells in resting conditions and after induction of "inside-out" and "outside-in" integrin activation.

Limitations and future work

RNAi technology, used in this study, does not result in a complete abrogation of expression, but only reduced expression, of the targeted genes. Residual expression still remained even after selection of clones expressing lower levels of the proteins of interest. In particular for the CD18 shRNA line, despite a total protein expression of 9.7%, CD18 surface expression was still 23%. A study using DC from LAD patients suggests that podosome architecture in these cells correlates with the levels of CD18 surface expression: cells from severe LAD patients, lacking CD18 expression, present a complete absence of podosome cores; and DC from patients with the mild form of the condition, with CD18 surface expression up to 30%, present podosome-like structures with less defined fuzzier actin cores (Siobhan Burns, unpublished data). Additionally, individuals that are heterozygous carriers of LAD-causing mutations present CD18 expression of about 60% of normal but present no clinical manifestations of LAD [Anderson et al. 1985; Springer et al. 1984]. These observations suggest a threshold in CD18 expression above which no phenotype would be apparent. In the case of the CD18 shRNA cell line, the large difference between total and surface expression further suggests the cells try to compensate, in steady state, for the decrease in total amount of integrin by localising all their integrin molecules at the cell surface, and a phenotype due to decreased integrin expression is then only observed when higher integrin avidity is necessary. Therefore, a more striking phenotype would be expected in a cell line where CD18 surface expression would be further knocked-down to levels comparable to severe LAD patients. Nevertheless, in addition to the static adhesion assay performed, a dynamic adhesion assay using a flow chamber could be done. Cells would be allowed to adhere and subsequently the number of cells that would remain attached to the substrate with increasing sheer force applied by flowing media would be recorded. This is a more sensitive assay as it measures

the strength of adhesion, an indirectly measure of integrin avidity.

Using shRNA requires controlling for sequence-specific and non sequence-specific off-target effects. Two control scrambled shRNA sequences (CTRS and CTRW) were used in this study to control for non sequence-specific effects. Generally, control cells were undistinguishable from untransduced cells in the functional assays carried out. The notable exception was related with adherent THP1DC morphology, where CTRS cells were significantly more round and appeared less polarised than untransduced cells, although not reaching statistical significance. Also, when plated on ICAM, podosome arrays of CTRS cells were more compact, with more and larger podosomes per cell compared to untransduced THP1DC. Regarding sequence-specific off-target effects, cross-effect on other proteins analysed in this study was assessed by measuring the expression levels of non-target proteins. Each shRNA construct specifically reduced the expression of the target protein but had no effect on the level of expression of the other proteins analysed here. In addition, reconstitution experiments should be performed, where the knocked-down proteins would be re-expressed by transduction with shRNA-resistant cDNA. A reversal of the phenotype observed to that of untransduced THP1DC would confirm the phenotype observed was solely due to the knock-down in protein expression. This would be particularly important in the case of the results presented regarding CD29 and HS1. Whereas the results obtained with CD18, WAS and WIP shRNA can be reproduced in the murine system or using human DC from LAD or WAS patients, CD29 and HS1 results can not be corroborated using other experimental systems such as murine or, ideally, human primary cells.

Furthermore, the functional experiments performed in this project should be reproduced using human primary DC. The majority of the work presented relies on a human cell line, rather than primary cells. Most importantly, primary human moDC should be used to assess the effect of CD29 and HS1 knock-down. Results were presented for one experiment attempting the generation of integrin knock-down moDC. This was hampered by low transduction efficiency and low levels of GFP reporter gene expression, making it difficult to identify transduced cells, and poor knock-down levels. Clonal selection, as was done for the generation of the THP1 shRNA cell lines, is not an option when using primary cells. Nevertheless, after vector improvement by replacing the GFP promoter by a stronger one (for example the SFFV promoter) and further optimisation of the transduction protocol, the generation of primary DC knock-down cells could be accomplished. Regarding CD18, due to the advocated existence of a threshold of surface expression above which reduced expression would not result in any functional defects, one has to bear in mind that the specific shRNA sequence used may not allow sufficient knock-down, and therefore different shRNA sequences may have to be tested.

The analysis of THP1DC adhesion dynamics showed very little difference between knock-down cell lines, even though defective adhesion to relevant integrin ligands and defective podosome formation had been demonstrated. The assay used was adapted from an IRM technique previously developed to analyse focal adhesion turnover and used for

podosome turnover and B-cell membrane dynamics [Ancliff et al. 2006; Blundell et al. 2009; Burns et al. 2010; Chou et al. 2006; Holt et al. 2008]. This technique does not allow comparison of adhesion strength between cell lines but, instead, measures adhesion turnover. On one hand, this may suggest that adhesion turnover and integrin recycling are not affected by knock-down of the proteins studied here. On the other hand, the assay may not be sensitive enough to detect changes in adhesion turnover in this system.

As a result of time constraints, the effects of protein knock-down on cell migration were not addressed in this study. Migration is commonly addressed in cytoskeletal studies and it would be of particular interest here as podosomes are considered important in DC motility [Burns et al. 2001; Calle et al. 2006a; Calle et al. 2006b; Monypenny et al. 2011]. Additionally, adhesion is an important component of integrin- and podosome-mediated migration and HS1 expression has also been reported to be important for efficient migration of murine BMDC and B-cells [Dehring et al. 2011; Scielzo et al. 2010]. THP1 chemotaxis to MCP-1 (monocyte chemotactic protein-1) and chemokinesis or random migration could be measured, either in Dunn chamber or transwell systems. HS1 differential phosphorylation has been suggested to play a role in NK cell chemotaxis [Butler et al. 2008] and therefore the present project could be expanded by analysing the effects of phospho-dead and phospho-mimicking HS1 mutants in the migratory behaviour of THP1DC cell lines. Furthermore, there is evidence that DC podosomes may be important in transendothelial migration. Therefore, the assembly of podosomes in systems like lipid monolayers enriched with ICAM so as to simulate a cell membrane and the assembly of podosome in “soft substrates” such as on cell monolayers should be studied.

Finally, ECM degradation has now become a hallmark of podosome and podosome-like structures, even though controversy exists regarding the purpose of podosome-mediated degradation – invasive migration, as for invadopodia in cancer cells, or focalised ECM sensing and remodelling. Cortactin has been proposed to regulate protease secretion and ECM degradation in invadopodia [Clark and Weaver 2008] and it has been implicated, in conjunction with WIP, in MMP localisation to podosomes and in podosome degradative function of splenic murine DC [Banon-Rodriguez et al. 2011]. It would be interesting to explore a possible homologous function of HS1 in this context in human DC.

Extending the panel of knock-down cell lines to other targets could also be interesting. N-WASp is a ubiquitously expressed WASp homolog. In non-haematopoietic cells N-WASp is critical for podosome and invadopodia formation [Mizutani et al. 2002; Moreau et al. 2003; Osiak et al. 2005; Spinardi et al. 2004; Yamaguchi et al. 2005]. In myeloid cells WASp and N-WASp are concurrently expressed and despite not being clear whether N-WASp localises to podosomes, N-WASp has been proposed to be involved in podosome-mediated ECM degradation in a murine macrophage cell line [Calle et al. 2006a; Nusblat et al. 2011]. However, it was not possible to include N-WASp in the shRNA panel developed in the current project due to the lack of good reagents to detect N-WASp. In particular, WASp and N-WASp migrate with similar sizes in an SDS-PAGE and available antibodies for N-WASp cross react with WASp, which is about 10 times more abundant in

myeloid cells [Isaac et al. 2010]. Additionally, focusing on the ECM degradation function of podosomes, MT1MMP could be another target for the generation of a knock-down cell line. Although this protein has not been so far shown to localise to DC podosomes, ECM degradation by murine DC has been demonstrated to be catalysed by MT1MMP [Gawden-Bone et al. 2010; West et al. 2008]. Again, no studies using human DC have been reported.

Conclusion

In conclusion, the results presented in this thesis contribute to a more comprehensive understanding of human DC podosome biology. Lentivectors were proposed and validated as an effective tool for the genetic manipulation of the immature DC cytoskeleton. DC podosome formation was found to be independent of β_1 integrins, but dependent on β_2 integrins. Indirect evidence has been presented for the importance of HS1 in CD18 activation, possibly taking part in "outside-in" CD18 activation pathway. Finally, the shRNA human THP1 cell lines generated constitute potentially very interesting biological reagents to expand the work developed in this project.

REFERENCES

Abinun M, Mikuska M, Filipovic B. 1988. INFANTILE CORTICAL HYPEROSTOSIS ASSOCIATED WITH THE WISKOTT-ALDRICH SYNDROME. European Journal of Pediatrics 147(5):518-519.

Ackerman AL, Cresswell P. 2003. Regulation of MHC class I transport in human dendritic cells and the dendritic-like cell line KG-1. Journal of Immunology 170(8):4178-4188.

Akimov SS, Belkin AM. 2001. Cell surface tissue transglutaminase is involved in adhesion and migration of monocytic cells on fibronectin. Blood 98(5):1567-1576.

Ammon C, Meyer SP, Schwarzfischer L, Krause SW, Andreesen R, Kreutz M. 2000. Comparative analysis of integrin expression on monocyte-derived macrophages and monocyte-derived dendritic cells. Immunology 100(3):364-369.

Ancliff PJ, Blundell MP, Cory GO, Calle Y, Worth A, Kempski H, Burns S, Jones GE, Sinclair J, Kinnon C and others. 2006. Two novel activating mutations in the Wiskott-Aldrich syndrome protein result in congenital neutropenia. Blood 108(7):2182-2189.

Andersen CAS, Handley M, Pollara G, Ridley AJ, Katz DR, Chain BM. 2006. beta 1-integrins determine the dendritic morphology which enhances DC-SIGN-mediated particle capture by dendritic cells. International Immunology 18(8):1295-1303.

Anderson DC, Schmalsteig FC, Finegold MJ, Hughes BJ, Rothlein R, Miller LJ, Kohl S, Tosi MF, Jacobs RL, Waldrop TC and others. 1985. THE SEVERE AND MODERATE PHENOTYPES OF HERITABLE MAC-1, LFA-1 DEFICIENCY - THEIR QUANTITATIVE DEFINITION AND RELATION TO LEUKOCYTE DYSFUNCTION AND CLINICAL-FEATURES. Journal of Infectious Diseases 152(4):668-689.

Anderson DC, Springer TA. 1987. LEUKOCYTE ADHESION DEFICIENCY - AN INHERITED DEFECT IN THE MAC-1, LFA-1, AND P150,95 GLYCOPROTEINS. Annual Review of Medicine 38:175-194.

Anton IM, Lu WG, Mayer BJ, Ramesh N, Geha RS. 1998. The Wiskott-Aldrich syndrome protein-interacting protein (WIP) binds to the adaptor protein Nck. Journal of Biological Chemistry 273(33):20992-20995.

Artym VV, Zhang Y, Seillier-Moiseiwitsch FO, Yamada KM, Mueller SC. 2006. Dynamic interactions of cortactin and membrane type 1 matrix metalloproteinase at invadopodia: Defining the stages of invadopodia formation and function. Cancer Research 66(6):3034-3043.

Aspenstrom P. 2002. The WASP-Binding protein WIRE has a role in the regulation of the actin filament system downstream of the platelet-derived growth factor receptor. Experimental Cell Research 279(1):21-33.

Badolato R, Sozzani S, Malacarne F, Bresciani S, Fiorini M, Borsatti A, Albertini A, Mantovani A, Ugazio AG, Notarangelo LD. 1998. Monocytes from Wiskott-Aldrich patients display reduced chemotaxis and lack of cell polarization in response to monocyte chemoattractant protein-1 and formyl-methionyl-leucyl-phenylalanine. Journal of Immunology 161(2):1026-1033.

Bajenoff M, Egen JG, Koo LY, Laugier JP, Brau F, Glaichenhaus N, Germain RN. 2006. Stromal cell networks regulate lymphocyte entry, migration, and territoriality in lymph nodes. Immunity 25(6):989-1001.

Baldassarre M, Pompeo A, Beznoussenko G, Castaldi C, Cortellino S, McNiven MA, Luini A, Buccione R. 2003. Dynamin participates in focal extracellular matrix degradation by invasive cells. Molecular Biology of the Cell 14(3):1074-1084.

Banchereau J, Briere F, Caux C, Davoust J, Lebecque S, Liu YT, Pulendran B, Palucka K. 2000. Immunobiology of dendritic cells. Annual Review of Immunology 18:767-+.

Banon-Rodriguez I, Monypenny J, Ragazzini C, Franco A, Calle Y, Jones GE, Anton IM. 2011. The cortactin-binding domain of WIP is essential for podosome formation and extracellular matrix degradation by murine dendritic cells. European Journal of Cell Biology 90(2-3):213-223.

Barr VA, Bunnell SC. 2009. Interference reflection microscopy. Current protocols in cell biology / editorial board, Juan S. Bonifacino ... [et al.] Chapter 4:Unit 4.23.

Bartel DP. 2004. MicroRNAs: Genomics, biogenesis, mechanism, and function. Cell 116(2):281-297.

Beel K, Cotter MM, Blatny J, Bond J, Lucas G, Green F, Vanduppen V, Leung DW, Rooney S, Smith OP and others. 2009. A large kindred with X-linked neutropenia with an I294T mutation of the Wiskott-Aldrich syndrome gene. British Journal of Haematology 144(1):120-126.

Beer S, Bellovin DI, Lee JS, Komatsubara K, Wang LS, Koh H, Boerner K, Storm TA, Davis CR, Kay MA and others. 2010. Low-level shRNA Cytotoxicity Can Contribute to MYC-induced Hepatocellular Carcinoma in Adult Mice. Molecular Therapy 18(1):161-170.

Bekeredjian-Ding I, Roth SI, Gilles S, Giese T, Ablasser A, Hornung V, Endres S, Hartmann G. 2006. T cell-independent, TLR-induced IL-12p70 production in primary human monocytes. Journal of Immunology 176(12):7438-7446.

Benvenuti F, Hugues S, Walmsley M, Ruf S, Fetler L, Popoff M, Tybulewicz VLJ, Amigorena S. 2004. Requirement of Rac1 and Rac2 expression by mature dendritic cells for T cell priming. Science 305(5687):1150-1153.

Berges C, Naujokat C, Tinapp S, Wieczorek H, Hoh A, Sadeghi M, Opelz G, Daniel V. 2005. A cell line model for the differentiation of human dendritic cells. Biochemical and Biophysical Research Communications 333(3):896-907.

Binks M, Jones GE, Brickell PM, Kinnon C, Katz DR, Thrasher AJ. 1998. Intrinsic dendritic cell abnormalities in Wiskott-Aldrich syndrome. European Journal of Immunology 28(10):3259-3267.

Blundell MP, Bouma G, Calle Y, Jones GE, Kinnon C, Thrasher AJ. 2008. Improvement of migratory defects in a murine model of Wiskott-Aldrich syndrome gene therapy. Molecular Therapy 16(5):836-844.

Blundell MP, Bouma G, Metelo J, Worth A, Calle Y, Cowell LA, Westerberg LS, Moulding DA, Mirando S, Kinnon C and others. 2009. Phosphorylation of WASp is a key regulator of activity and stability in vivo. Proceedings of the National Academy of Sciences of the United States of America 106(37):15738-15743.

Blundell MP, Worth A, Bouma G, Thrasher AJ. 2010. The Wiskott-Aldrich syndrome: The actin cytoskeleton and immune cell function. Disease Markers 29(3-4):157-175.

Boissonnas A, Fetler L, Zeelenberg IS, Hugues S, Amigorena S. 2007. In vivo imaging of cytotoxic T cell infiltration and elimination of a solid tumor. Journal of Experimental Medicine 204(2):345-356.

Bonasio R, Tu SJ, Reinberg D. 2010. Molecular Signals of Epigenetic States. Science 330(6004):612-616.

Bontkes HJ, Ruizendaal JJ, Kramer D, Santegoets S, Scheper RJ, de Gruijl TD, Meijer C, Hooijberg E. 2006. Constitutively active STAT5b induces cytokine-independent growth of the acute myeloid leukemia-derived MUTZ-3 cell line and accelerates its differentiation into mature dendritic cells. Journal of Immunotherapy 29(2):188-200.

Bouma G, Ancliff PJ, Thrasher AJ, Burns SO. 2010. Recent advances in the understanding of genetic defects of neutrophil number and function. British Journal of Haematology 151(4):312-326.

Bouma G, Mendoza-Naranjo A, Blundell MP, de Falco E, Parsley KL, Burns SO, Thrasher AJ. 2011. Cytoskeletal remodeling mediated by WASp in dendritic cells is necessary for normal immune synapse formation and T-cell priming. Blood 118(9):2492-501.

Bowden ET, Barth M, Thomas D, Glazer RI, Mueller SC. 1999. An invasion-related complex of cortactin, paxillin and PKC mu associates with invadopodia at sites of extracellular matrix degradation. Oncogene 18(31):4440-4449.

Bowden ET, Onikoyi E, Slack R, Myoui A, Yoneda T, Yamada KM, Mueller SC. 2006. Co-localization of cortactin and phosphotyrosine identifies active invadopodia in human breast cancer cells. Experimental Cell Research 312(8):1240-1253.

Breckpot K, Corthals J, Heirman C, Bonehill A, Michiels A, Tuyaerts S, De Greef C, Thielemans K. 2004a. Activation of monocytes via the CD14 receptor leads to the enhanced lentiviral transduction of immature dendritic cells. Human Gene Therapy 15(6):562-573.

Breckpot K, Dullaers M, Bonehill A, Van Meirvenne S, Heirman C, De Greef C, van der Bruggen P, Thielemans K. 2003. Lentivirally transduced dendritic cells as a tool for cancer immunotherapy. Journal of Gene Medicine 5(8):654-667.

Breckpot K, Emeagi P, Dullaers M, Michiels A, Heirman C, Thielemansi K. 2007. Activation of immature monocyte-derived dendritic cells after transduction with high doses of lentiviral vectors. Human Gene Therapy 18(6):536-546.

Breckpot K, Escors D, Arce F, Lopes L, Karwacz K, Van Lint S, Keyaerts M, Collins M. 2010. HIV-1 Lentiviral Vector Immunogenicity Is Mediated by Toll-Like Receptor 3 (TLR3) and TLR7. Journal of Virology 84(11):5627-5636.

Breckpot K, Heirman C, Neyns B, Thielemans K. 2004b. Exploiting dendritic cells for cancer immunotherapy: genetic modification of dendritic cells. Journal of Gene Medicine 6(11):1175-1188.

Bridge AJ, Pebernard S, Ducraux A, Nicoulaz AL, Iggo R. 2003. Induction of an interferon response by RNAi vectors in mammalian cells. Nature Genetics 34(3):263-264.

Briggs JAG, Wilk T, Welker R, Krausslich HG, Fuller SD. 2003. Structural organization of authentic, mature HIV-1 virions and cores. Embo Journal 22(7):1707-1715.

Brown AF. 1982. NEUTROPHIL GRANULOCYTES - ADHESION AND LOCOMOTION ON COLLAGEN SUBSTRATA AND IN COLLAGEN MATRICES. Journal of Cell Science 58(DEC):455-467.

Brunati AM, Deana R, Folda A, Massimino ML, Marin O, Ledro S, Pinna LA, Donella-Deana AD. 2005. Thrombin-induced tyrosine phosphorylation of HS1 in human platelets is sequentially catalyzed by Syk and Lyn tyrosine kinases and associated with the cellular migration of the protein. Journal of Biological Chemistry 280(22):21029-21035.

Brunati AM, Donella-Deana A, James P, Quadroni M, Contri A, Marin O, Pinna LA. 1999. Molecular features underlying the sequential phosphorylation of HS1 protein and its association with c-Fgr protein-tyrosine kinase. Journal of Biological Chemistry 274(11):7557-7564.

Buccione R, Orth JD, McNiven MA. 2004. Foot and mouth: Podosomes, invadopodia and circular dorsal ruffles. Nature Reviews Molecular Cell Biology 5(8):647-657.

Burgstaller G, Gimona M. 2005. Podosome-mediated matrix resorption and cell motility in vascular smooth muscle cells. American Journal of Physiology-Heart and Circulatory Physiology 288(6):H3001-H3005.

Burns JC, Friedmann T, Driever W, Burrascano M, Yee JK. 1993. Vesicular Stomatitis-Virus G Glycoprotein Pseudotyped Retroviral Vectors - Concentration to Very High-Titer and Efficient Gene-Transfer into Mammalian and Nonmammalian Cells. Proceedings of the National Academy of Sciences of the United States of America 90(17):8033-8037.

Burns S, Cory GO, Vainchenker W, Thrasher AJ. 2004a. Mechanisms of WASp-mediated hematologic and immunologic disease. Blood 104(12):3454-3462.

Burns S, Hardy SJ, Buddle J, Yong KL, Jones GE, Thrasher AJ. 2004b. Maturation of DC is associated with changes in motile characteristics and adherence. Cell Motility and the Cytoskeleton 57(2):118-132.

Burns S, Thrasher AJ, Blundell MP, Machesky L, Jones GE. 2001. Configuration of human dendritic cell cytoskeleton by Rho GTPases, the WAS protein, and differentiation. Blood 98(4):1142-1149.

Burns SO, Killock DJ, Moulding DA, Metelo J, Nunes J, Taylor RR, Forge A, Thrasher AJ, Ivetic A. 2010. A congenital activating mutant of WASp causes altered plasma membrane topography and adhesion under flow in lymphocytes. Blood 115(26):5355-5365.

Butler B, Kastendieck DH, Cooper JA. 2008. Differently phosphorylated forms of the cortactin homolog HS1 mediate distinct functions in natural killer cells. Nature Immunology 9(8):887-897.

Calderwood DA, Shattil SJ, Ginsberg MH. 2000. Integrins and actin filaments: Reciprocal regulation of cell adhesion and signaling. Journal of Biological Chemistry 275(30):22607-22610.

Calle Y, Burns S, Thrasher AJ, Jones GE. 2006a. The leukocyte podosome. European Journal

of Cell Biology 85(3-4):151-157.

Calle Y, Carragher NO, Thrasher AJ, Jones GE. 2006b. Inhibition of calpain stabilises podosomes and impairs dendritic cell motility. Journal of Cell Science 119(11):2375-2385.

Calle Y, Chou HC, Thrasher AJ, Jones GE. 2004a. Wiskott-Aldrich syndrome protein and the cytoskeletal dynamics of dendritic cells. Journal of Pathology 204(4):460-469.

Calle Y, Jones GE, Jagger C, Fuller K, Blundell MP, Chow J, Chambers T, Thrasher AJ. 2004b. WASp deficiency in mice results in failure to form osteoclast sealing zones and defects in bone resorption. Blood 103(9):3552-3561.

Cameron P, Pope M, GranelliPiperno A, Steinman RM. 1996. Dendritic cells and the replication of HIV-1. Journal of Leukocyte Biology 59(2):158-171.

Campellone KG, Webb NJ, Znameroski EA, Welch MD. 2008. WHAMM is an Arp2/3 complex activator that binds microtubules and functions in ER to Golgi transport. Cell 134(1):148-161.

Caplen NJ. 2004. Gene therapy progress and prospects. Downregulating gene expression: the impact of RNA interference. Gene Therapy 11(16):1241-1248.

Carlier MF, Nioche P, Broutin-L'Hermite I, Boujemaa R, Le Clainche C, Egile C, Garbay C, Ducruix A, Sansonetti P, Pantaloni D. 2000. GRB2 links signaling to actin assembly by enhancing interaction of neural Wiskott-Aldrich syndrome protein (N-WASp) with actin-related protein (ARP2/3) complex. Journal of Biological Chemistry 275(29):21946-21952.

Carman CV, Sage PT, Sciuto TE, de la Fuente MA, Geha RS, Ochs HD, Dvorak HF, Dvorak AM, Springer TA. 2007. Transcellular diapedesis is initiated by invasive podosomes. Immunity 26(6):784-797.

Carman CV, Springer TA. 2003. Integrin avidity regulation: are changes in affinity and conformation underemphasized? Current Opinion in Cell Biology 15(5):547-556.

Carrizosa E, Gomez TS, Labno CM, Dehring DAK, Liu XH, Freedman BD, Billadeau DD, Burkhardt JK. 2009. Hematopoietic Lineage Cell-Specific Protein 1 Is Recruited to the Immunological Synapse by IL-2-Inducible T Cell Kinase and Regulates Phospholipase C gamma 1 Microcluster Dynamics during T Cell Spreading. Journal of Immunology 183(11):7352-7361.

Caux C, Dezutterdambuyant C, Schmitt D, Banchereau J. 1992. GM-CSF AND TNF-ALPHA COOPERATE IN THE GENERATION OF DENDRITIC LANGERHANS CELLS. Nature 360(6401):258-261.

Cella M, Jarrossay D, Facchetti F, Alebardi O, Nakajima H, Lanzavecchia A, Colonna M. 1999. Plasmacytoid monocytes migrate to inflamed lymph nodes and produce large amounts of type I interferon. Nature Medicine 5(8):919-923.

Cella M, Sallusto F, Lanzavecchia A. 1997. Origin, maturation and antigen presenting function of dendritic cells. Current Opinion in Immunology 9(1):10-16.

Chabadel A, Banon-Rodriguez I, Cluet D, Rudkin BB, Wehrle-Haller B, Genot E, Jurdic P, Anton IM, Saltel F. 2007. CD44 and beta 3 integrin organize two functionally distinct actin-based domains in osteoclasts. Molecular Biology of the Cell 18(12):4899-4910.

Chandrakasan S, Singh S, Dogra S, Delaunay J, Proust A, Minz RW. 2011. Wiskott-Aldrich Syndrome Presenting With Early Onset Recurrent Acute Hemorrhagic Edema and Hyper-

ostosis. Pediatric Blood & Cancer 56(7):1130-1132.

Chang C, Werb Z. 2001. The many faces of metalloproteases: cell growth, invasion, angiogenesis and metastasis. Trends in Cell Biology 11(11):S37-S43.

Charrier S, Stockholm D, Seye K, Opolon P, Taveau M, Gross DA, Bucher-Laurent S, Delenda C, Vainchenker W, Danos O and others. 2005. A lentiviral vector encoding the human Wiskott Aldrich syndrome protein corrects immune and cytoskeletal defects in WASP knockout mice. Gene Therapy 12(7):597-606.

Chellaiah M, Fitzgerald C, Alvarez U, Hruska K. 1998. c-Src is required for stimulation of gelsolin-associated phosphatidylinositol 3-kinase. Journal of Biological Chemistry 273(19):11908-11916.

Chellaiah M, Kizer N, Silva M, Alvarez U, Kwiatkowski D, Hruska KA. 2000. Gelsolin deficiency blocks podosome assembly and produces increased bone mass and strength. Journal of Cell Biology 148(4):665-678.

Chen M, She HY, Davis EM, Spicer CM, Kim L, Ren RB, Le Beau MM, Li W. 1998. Identification of Nck family genes, chromosomal localization, expression, and signaling specificity. Journal of Biological Chemistry 273(39):25171-25178.

Chen WT. 1989. PROTEOLYTIC ACTIVITY OF SPECIALIZED SURFACE PROTRUSIONS FORMED AT ROSETTE CONTACT SITES OF TRANSFORMED-CELLS. Journal of Experimental Zoology 251(2):167-185.

Chinnasamy N, Chinnasamy D, Toso JF, Lapointe R, Candotti F, Morgan RA, Hwu P. 2000. Efficient gene transfer to human peripheral blood monocyte-derived dendritic cells using human immunodeficiency virus type 1-based lentiviral vectors. Human Gene Therapy 11(13):1901-1909.

Chinnasamy N, Treisman JS, Oaks MK, Hanson JP, Chinnasamy D. 2005. Ex vivo generation of genetically modified dendritic cells for immunotherapy: implications of lymphocyte contamination. Gene Therapy 12(3):259-271.

Chou HC, Anton IM, Holt MR, Curcio C, Lanzardo S, Worth A, Burns S, Thrasher AJ, Jones GE, Calle Y. 2006. WIP regulates the stability and localization of WASP to podosomes in migrating dendritic cells. Current Biology 16(23):2337-2344.

Clark EA, Grabstein KH, Shu GL. 1992. CULTURED HUMAN FOLLICULAR DENDRITIC CELLS - GROWTH-CHARACTERISTICS AND INTERACTIONS WITH LYMPHOCYTES-B. Journal of Immunology 148(11):3327-3335.

Clark ES, Weaver AM. 2008. A new role for cortactin in invadopodia: Regulation of protease secretion. European Journal of Cell Biology 87(8-9):581-590.

Constantin G, Majeed M, Giagulli C, Piccio L, Kim JY, Butcher EC, Laudanna C. 2000. Chemokines trigger immediate beta 2 integrin affinity and mobility changes: Differential regulation and roles in lymphocyte arrest under flow. Immunity 13(6):759-769.

Cory GOC, Cramer R, Blanchoin L, Ridley AJ. 2003. Phosphorylation of the WASP-VCA domain increases its affinity for the Arp2/3 complex and enhances actin polymerization by WASP. Molecular Cell 11(5):1229-1239.

Cory GOC, Garg R, Cramer R, Ridley AJ. 2002. Phosphorylation of tyrosine enhances the ability of WASp to stimulate actin polymerization and filopodium formation. Journal of

Biological Chemistry 277(47):45115-45121.

Cote JF, Chung PL, Theberge JF, Halle M, Spencer S, Lasky LA, Tremblay ML. 2002. PSTPIP is a substrate of PTP-PEST and serves as a scaffold guiding PTP-PEST toward a specific dephosphorylation of WASP. Journal of Biological Chemistry 277(4):2973-2986.

Cullen BR. 2006. Enhancing and confirming the specificity of RNAi experiments. Nature Methods 3(9):677-681.

Curtis ASG. 1964. MECHANISM OF ADHESION OF CELLS TO GLASS - STUDY BY INTERFERENCE REFLECTION MICROSCOPY. Journal of Cell Biology 20(2):199-&.

D'Amico G, Bianchi G, Bernasconi S, Bersani L, Piemonti L, Sozzani S, Mantovani A, Allavena P. 1998. Adhesion, transendothelial migration, and reverse transmigration of in vitro cultured dendritic cells. Blood 92(1):207-214.

Davidpfeuty T, Singer SJ. 1980. ALTERED DISTRIBUTIONS OF THE CYTOSKELETAL PROTEINS VINCULIN AND ALPHA-ACTININ IN CULTURED FIBROBLASTS TRANSFORMED BY ROUS-SARCOMA VIRUS. Proceedings of the National Academy of Sciences of the United States of America-Biological Sciences 77(11):6687-6691.

de la Fuente MA, Sasahara Y, Calamito M, Anton IM, Elkhal A, Gallego MD, Suresh K, Siminovitch K, Ochs HD, Anderson KC and others. 2007. WIP is a chaperone for Wiskott-Aldrich syndrome protein (WASP). Proceedings of the National Academy of Sciences of the United States of America 104(3):926-931.

de Noronha S, Hardy S, Sinclair J, Blundell MP, Strid J, Schulz O, Zwirner J, Jones GE, Katz DR, Kinnon C and others. 2005. Impaired dendritic-cell homing in vivo in the absence of Wiskott-Aldrich syndrome protein. Blood 105(4):1590-1597.

Dehring DAK, Clarke F, Ricart BG, Huang YP, Gomez TS, Williamson EK, Hammer DA, Billadeau DD, Argon Y, Burkhardt JK. 2011. Hematopoietic Lineage Cell-Specific Protein 1 Functions in Concert with the Wiskott-Aldrich Syndrome Protein To Promote Podosome Array Organization and Chemotaxis in Dendritic Cells. Journal of Immunology 186(8):4805-4818.

Delaisse JM, Engsig MT, Everts V, Ovejero MD, Ferreras M, Lund L, Vu TH, Werb Z, Winding B, Lochter A and others. 2000. Proteinases in bone resorption: obvious and less obvious roles. Clinica Chimica Acta 291(2):223-234.

Demaison C, Parsley K, Brouns G, Scherr M, Battmer K, Kinnon C, Grez M, Thrasher AJ. 2002. High-level transduction and gene expression in hematopoietic repopulating cells using a human imunodeficiency virus type 1-based lentiviral vector containing an internal spleen focus forming virus promoter. Human Gene Therapy 13(7):803-813.

DeMali KA, Barlow CA, Burridge K. 2002. Recruitment of the Arp2/3 complex to vinculin: coupling membrane protrusion to matrix adhesion. Journal of Cell Biology 159(5):881-891.

Derry JMJ, Ochs HD, Francke U. 1994. ISOLATION OF A NOVEL GENE MUTATED IN WISKOTT-ALDRICH SYNDROME. Cell 78(4):635-644.

Destaing O, Saltel F, Geminard JC, Jurdic P, Bard F. 2003. Podosomes display actin turnover and dynamic self-organization in osteoclasts expressing actin-green fluorescent protein. Molecular Biology of the Cell 14(2):407-416.

Destrooper B, Vanleuven F, Carmeliet G, Vandenberghe H, Cassiman JJ. 1991. CULTURED HUMAN FIBROBLASTS CONTAIN A LARGE POOL OF PRECURSOR BETA-1-INTEGRIN BUT LACK AN INTRACELLULAR POOL OF MATURE SUBUNIT. European Journal of Biochemistry 199(1):25-33.

Devriendt K, Kim AS, Mathijs G, Frints SGM, Schwartz M, Van den Oord JJ, Verhoef GEG, Boogaerts MA, Fryns JP, You DQ and others. 2001. Constitutively activating mutation in WASP causes X-linked severe congenital neutropenia. Nature Genetics 27(3):313-317.

Dewey RA, Avedillo Diez I, Ballmaier M, Filipovich A, Greil J, Gungor T, Happel C, Maschan A, Noyan F, Pannicke U and others. 2006. Retroviral WASP gene transfer into human hematopoietic stem cells reconstitutes the actin cytoskeleton in myeloid progeny cells differentiated in vitro. Experimental Hematology 34(9):1161-9.

Donello JE, Loeb JE, Hope TJ. 1998. Woodchuck hepatitis virus contains a tripartite post-transcriptional regulatory element. Journal of Virology 72(6):5085-5092.

Donnelly SFH, Pocklington MJ, Pallotta D, Orr E. 1993. A PROLINE-RICH PROTEIN, VERPROLIN, INVOLVED IN CYTOSKELETAL ORGANIZATION AND CELLULAR GROWTH IN THE YEAST SACCHAROMYCES-CEREVISIAE. Molecular Microbiology 10(3):585-596.

Dovas A, Gevrey JC, Grossi A, Park H, Abou-Kheir W, Cox D. 2009. Regulation of podosome dynamics by WASp phosphorylation: implication in matrix degradation and chemotaxis in macrophages. Journal of Cell Science 122(21):3873-3882.

Du Q, Thonberg H, Wang J, Wahlestedt C, Liang ZC. 2005. A systematic analysis of the silencing effects of an active siRNA at all single-nucleotide mismatched target sites. Nucleic Acids Research 33(5):1671-1677.

Duong LT, Rodan GA. 2000. PYK2 is an adhesion kinase in macrophages, localized in podosomes and activated by beta(2)-integrin ligation. Cell Motility and the Cytoskeleton 47(3):174-188.

Dupre L, Aiuti A, Trifari S, Martino S, Saracco P, Bordignon C, Roncarolo MG. 2002. Wiskott-Aldrich syndrome protein regulates lipid raft dynamics during immunological synapse formation. Immunity 17(2):157-166.

Echeverri CJ, Beachy PA, Baum B, Boutros M, Buchholz F, Chanda SK, Downward J, Ellenberg J, Fraser AG, Hacohen N and others. 2006. Minimizing the risk of reporting false positives in large-scale RNAi screens. Nature Methods 3(10):777-779.

Eddy RJ, Pierini LM, Matsumura F, Maxfield FR. 2000. Ca2+-dependent myosin II activation is required for uropod retraction during neutrophil migration. Journal of Cell Science 113(7):1287-1298.

Elbashir SM, Harborth J, Lendeckel W, Yalcin A, Weber K, Tuschl T. 2001. Duplexes of 21-nucleotide RNAs mediate RNA interference in cultured mammalian cells. Nature 411(6836):494-498.

Ellis J. 2005. Silencing and variegation of gammaretrovirus and lentivirus vectors. Human Gene Therapy 16(11):1241-1246.

Escors D, Lopes L, Lin RT, Hiscott J, Akira S, Davis RJ, Collins MK. 2008. Targeting dendritic cell signaling to regulate the response to immunization. Blood 111(6):3050-3061.

Esslinger C, Romero P, MacDonald HR. 2002. Efficient transduction of dendritic cells and

induction of a T-cell response by third-generation lentivectors. Human Gene Therapy 13(9):1091-1100.

Etzioni A, Frydman M, Pollack S, Avidor I, Phillips ML, Paulson JC, Gershonibaruch R. 1992. RECURRENT SEVERE INFECTIONS CAUSED BY A NOVEL LEUKOCYTE ADHESION DEFICIENCY. New England Journal of Medicine 327(25):1789-1792.

Fiorini M, Vermi W, Facchetti F, Moratto D, Alessandri G, Notarangelo L, Caruso A, Grigolato P, Ugazio AG, Notarangelo LD and others. 2002. Defective migration of monocyte-derived dendritic cells in LAD-1 immunodeficiency. Journal of Leukocyte Biology 72(4):650-656.

Fire A, Xu SQ, Montgomery MK, Kostas SA, Driver SE, Mello CC. 1998. Potent and specific genetic interference by double-stranded RNA in Caenorhabditis elegans. Nature 391(6669):806-811.

Flores-Romo L. 2001. In vivo maturation and migration of dendritic cells. Immunology 102(3):255-262.

Follenzi A, Ailles LE, Bakovic S, Geuna M, Naldini L. 2000. Gene transfer by lentiviral vectors is limited by nuclear translocation and rescued by HIV-1 pol sequences. Nature Genetics 25(2):217-+.

Fonteneau JF, Gilliet M, Larsson M, Dasilva I, Munz C, Liu YJ, Bhardwaj N. 2003. Activation of influenza virus-specific CD4(+) and CD8(+) T cells: a new role for plasmacytoid denchitic cells in adaptive immunity. Blood 101(9):3520-3526.

Franitza S, Alon R, Lider O. 1999. Real-time analysis of integrin-mediated chemotactic migration of T lymphocytes within 3-D extracellular matrix-like gels. Journal of Immunological Methods 225(1-2):9-25.

Friedl P. 2004. Prespecification and plasticity: shifting mechanisms of cell migration. Current Opinion in Cell Biology 16(1):14-23.

Friedl P, Entschladen F, Conrad C, Niggemann B, Zanker KS. 1998. CD4(+) T lymphocytes migrating in three-dimensional collagen lattices lack focal adhesions and utilize beta 1 integrin-independent strategies for polarization, interaction with collagen fibers and locomotion. European Journal of Immunology 28(8):2331-2343.

Friedl P, Noble PB, Zanker KS. 1995. T-LYMPHOCYTE LOCOMOTION IN A 3-DIMENSIONAL COLLAGEN MATRIX - EXPRESSION AND FUNCTION OF CELL-ADHESION MOLECULES. Journal of Immunology 154(10):4973-4985.

Fukamachi H, Yamada N, Miura T, Kato T, Ishikawa M, Gulbins E, Altman A, Kawakami Y, Kawakami T. 1994. IDENTIFICATION OF A PROTEIN, SPY75, WITH REPETITIVE HELIX-TURN-HELIX MOTIFS AND AN SH3 DOMAIN AS A MAJOR SUBSTRATE FOR PROTEIN-TYROSINE KINASE(S) ACTIVATED BY FC-EPSILON-RI CROSS-LINKING. Journal of Immunology 152(2):642-652.

Gawden-Bone C, Zhou ZJ, King E, Prescott A, Watts C, Lucocq J. 2010. Dendritic cell podosomes are protrusive and invade the extracellular matrix using metalloproteinase MMP-14. Journal of Cell Science 123(9):1427-1437.

Geissmann F, Manz MG, Jung S, Sieweke MH, Merad M, Ley K. 2010. Development of Monocytes, Macrophages, and Dendritic Cells. Science 327(5966):656-661.

Giagulli C, Ottoboni L, Caveggion E, Rossi B, Lowell C, Constantin G, Laudanna C, Berton

G. 2006. The Src family kinases Hck and Fgr are dispensable for inside-out, chemoattractant-induced signaling regulating beta(2) integrin affinity and valency in neutrophils, but are required for beta(2) integrin-mediated outside-in signaling involved in sustained adhesion. Journal of Immunology 177(1):604-611.

Giger U, Boxer LA, Simpson PJ, Lucchesi BR, Todd RF. 1987. DEFICIENCY OF LEUKOCYTE SURFACE GLYCOPROTEINS MO1, LFA-1, AND LEU M5 IN A DOG WITH RECURRENT BACTERIAL-INFECTIONS - AN ANIMAL-MODEL. Blood 69(6):1622-1630.

Gilmore AP, Burridge K. 1996. Regulation of vinculin binding to talin and actin by phosphatidyl-inositol-4-5-bisphosphate. Nature 381(6582):531-535.

Gimona M, Buccione R. 2006. Adhesions that mediate invasion. International Journal of Biochemistry & Cell Biology 38(11):1875-1892.

Gimona M, Buccione R, Courtneidge SA, Linder S. 2008. Assembly and biological role of podosomes and invadopodia. Current Opinion in Cell Biology 20(2):235-241.

Gismondi A, Cifaldi L, Mazza C, Giliani S, Parolini S, Morrone S, Jacobelli J, Bandiera E, Notarangelo L, Santoni A. 2004. Impaired natural and CD16-mediated NK cell cytotoxicity in patients with WAS and XLT: ability of IL-2 to correct NK cell functional defect. Blood 104(2):436-443.

Gomez TS, McCarney SD, Carrizosa E, Labno CM, Comiskey EO, Nolz JC, Zhu PM, Freedman BD, Clark MR, Rawlings DJ and others. 2006. HS1 functions as an essential actin-regulatory adaptor protein at the immune synapse. Immunity 24(6):741-752.

Goto T, Maeda H, Tanaka T. 2002. A selective inhibitor of matrix metalloproteinases inhibits the migration of isolated osteoclasts by increasing the life span of podosomes. Journal of Bone and Mineral Metabolism 20(2):98-105.

Granelli-Piperno A, Delgado E, Finkel V, Paxton W, Steinman RM. 1998. Immature dendritic cells selectively replicate macrophagetropic (M-tropic) human immunodeficiency virus type 1, while mature cells efficiently transmit both M- and T-Tropic virus to T cells. Journal of Virology 72(4):2733-2737.

GranelliPiperno A, Chen DL, Moser B, Steinman RM. 1997. The HIV-1 life cycle is blocked at two different points in mature dendritic cells. Dendritic Cells in Fundamental and Clinical Immunology, Vol 3 417:415-419.

Gregoretti MG, Gottardi D, Ghia P, Bergui L, Merico F, Marchisio PC, Caligariscappio F. 1994. CHARACTERIZATION OF BONE-MARROW STROMAL CELLS FROM MULTIPLE-MYELOMA. Leukemia Research 18(9):675-682.

Grimm D, Streetz KL, Jopling CL, Storm TA, Pandey K, Davis CR, Marion P, Salazar F, Kay MA. 2006. Fatality in mice due to oversaturation of cellular microRNA/short hairpin RNA pathways. Nature 441(7092):537-541.

Gruber A, Kan-Mitchell J, Kuhen KL, Mukai T, Wong-Staal F. 2000. Dendritic cells transduced by multiply deleted HIV-1 vectors exhibit normal phenotypes and functions and elicit an HIV-specific cytotoxic T-lymphocyte response in vitro. Blood 96(4):1327-1333.

Hai CM, Hahne P, Harrington EO, Gimona M. 2002. Conventional protein kinase C mediates phorbol-dibutyrate-induced cytoskeletal remodeling in A7r5 smooth muscle cells. Experimental Cell Research 280(1):64-74.

Hammarfjord O, Falet H, Gurniak C, Hartwig JH, Wallin RPA. 2011. Gelsolin-Independent Podosome Formation in Dendritic Cells. Plos One 6(7).

Hanawa H, Kelly PF, Nathwani AC, Persons DA, Vandergriff JA, Hargrove P, Vanin EF, Nienhuis AW. 2002. Comparison of various envelope proteins for their ability to pseudotype lentiviral vectors and transduce primitive hematopoietic cells from human blood. Molecular Therapy 5(3):242-251.

Hao JJ, Carey GB, Zhan X. 2004. Syk-mediated tyrosine phosphorylation is required for the association of hematopoietic lineage cell-specific protein 1 with lipid rafts and B cell antigen receptor signalosome complex. Journal of Biological Chemistry 279(32):33413-33420.

Hao JJ, Zhu JW, Zhou K, Smith N, Zhan X. 2005. The coiled-coil domain is required for HS1 to bind to F-actin and activate Arp2/3 complex. Journal of Biological Chemistry 280(45):37988-37994.

Harman AN, Wilkinson J, Bye CR, Bosnjak L, Stern JL, Nicholle M, Lai J, Cunningham AL. 2006. HIV induces maturation of monocyte-derived dendritic cells and Langerhans cells. Journal of Immunology 177(10):7103-7113.

Haston WS, Shields JM, Wilkinson PC. 1982. LYMPHOCYTE LOCOMOTION AND ATTACHMENT ON TWO-DIMENSIONAL SURFACES AND IN 3-DIMENSIONAL MATRICES. Journal of Cell Biology 92(3):747-752.

Hemsath L, Dvorsky R, Fiegen D, Carlier MF, Ahmadian MR. 2005. An electrostatic steering mechanism of Cdc42 recognition by Wiskott-Aldrich syndrome proteins. Molecular Cell 20(2):313-324.

Hidalgo A, Ma SH, Peired AJ, Weiss LA, Cunningham-Rundles C, Frenette PS. 2003. Insights into leukocyte adhesion deficiency type 2 from a novel mutation in the GDP-fucose transporter gene. Blood 101(5):1705-1712.

Higgs HN, Blanchoin L, Pollard TD. 1999. Influence of the c terminus of Wiskott-Aldrich syndrome protein (WASp) and the Arp2/3 complex on actin polymerization. Biochemistry 38(46):15212-15222.

Higgs HN, Pollard TD. 2000. Activation by Cdc42 and PIP2 of Wiskott-Aldrich syndrome protein (WASp) stimulates actin nucleation by Arp2/3 complex. Journal of Cell Biology 150(6):1311-1320.

Hiura K, Lim SS, Little SP, Lin S, Sato M. 1995. DIFFERENTIATION-DEPENDENT EXPRESSION OF TENSIN AND CORTACTIN IN CHICKEN OSTEOCLASTS. Cell Motility and the Cytoskeleton 30(4):272-284.

Ho HYH, Rohatgi R, Lebensohn AM, Ma L, Li JX, Gygi SP, Kirschner MW. 2004. Toca-1 mediates Cdc42-dependent actin nucleation by activating the N-WASP-WIP complex. Cell 118(2):203-216.

Ho HYH, Rohatgi R, Ma L, Kirschner MW. 2001. CR16 forms a complex with N-WASP in brain and is a novel member of a conserved proline-rich actin-binding protein family. Proceedings of the National Academy of Sciences of the United States of America 98(20):11306-11311.

Hogg N, Bates PA. 2000. Genetic analysis of integrin function in man: LAD-1 and other syndromes. Matrix Biology 19(3):211-222.

Hogg N, Patzak I, Willenbrock F. 2011. The insider's guide to leukocyte integrin signalling and function. Nature Reviews Immunology 11(6):416-426.

Holen T, Moe SE, Sorbo JG, Meza TJ, Ottersen OP, Klungland A. 2005. Tolerated wobble mutations in siRNAs decrease specificity, but can enhance activity in vivo. Nucleic Acids Research 33(15):4704-4710.

Holmes KC, Popp D, Gebhard W, Kabsch W. 1990. ATOMIC MODEL OF THE ACTIN FILAMENT. Nature 347(6288):44-49.

Holt MR, Calle Y, Sutton DH, Critchley DR, Jones GE, Dunn GA. 2008. Quantifying cell-matrix adhesion dynamics in living cells using interference reflection microscopy. Journal of Microscopy-Oxford 232(1):73-81.

Hornung V, Guenthner-Biller M, Bourquin C, Ablasser A, Schlee M, Uematsu S, Noronha A, Manoharan M, Akira S, de Fougerolles A and others. 2005. Sequence-specific potent induction of IFN-alpha by short interfering RNA in plasmacytoid dendritic cells through TLR7. Nature Medicine 11(3):263-270.

Horwitz A, Duggan K, Buck C, Beckerle MC, Burridge K. 1986. INTERACTION OF PLASMA-MEMBRANE FIBRONECTIN RECEPTOR WITH TALIN - A TRANSMEMBRANE LINKAGE. Nature 320(6062):531-533.

Huang C, Liu JL, Haudenschild CC, Zhan X. 1998. The role of tyrosine phosphorylation of cortactin in the locomotion of endothelial cells. Journal of Biological Chemistry 273(40):25770-25776.

Huang YP, Comiskey EO, Dupree RS, Li SX, Koleske AJ, Burkhardt JK. 2008. The c-Abl tyrosine kinase regulates actin remodeling at the immune synapse. Blood 112(1):111-119.

Hynes RO. 1992. INTEGRINS - VERSATILITY, MODULATION, AND SIGNALING IN CELL-ADHESION. Cell 69(1):11-25.

Hynes RO. 2002. Integrins: Bidirectional, allosteric signaling machines. Cell 110(6):673-687.

Inui M, Martello G, Piccolo S. 2010. MicroRNA control of signal transduction. Nature Reviews Molecular Cell Biology 11(4):252-263.

Isaac BM, Ishihara D, Nusblat LM, Gevrey JC, Dovas A, Condeelis J, Cox D. 2010. N-WASP has the ability to compensate for the loss of WASP in macrophage podosome formation and chemotaxis. Experimental Cell Research 316(20):3406-3416.

Iwasaki A, Medzhitov R. 2004. Toll-like receptor control of the adaptive immune responses. Nature Immunology 5(10):987-995.

Izant JG, Weintraub H. 1984. INHIBITION OF THYMIDINE KINASE GENE-EXPRESSION BY ANTI-SENSE RNA - A MOLECULAR APPROACH TO GENETIC-ANALYSIS. Cell 36(4):1007-1015.

Jancic C, Chuluyan HE, Morelli A, Larregina A, Kolkowski E, Saracco M, Barboza M, Leiva WS. 1998. Interactions of dendritic cells with fibronectin and endothelial cells. Immunology 95(2):283-290.

Jeanson-Leh L, Blondeau J, Galy A. 2007. Optimization of short hairpin RNA for lentiviral-mediated RNAi against WAS. Biochemical and Biophysical Research Communications 362(2):498-503.

Jockusch BM, Bubeck P, Giehl K, Kroemker M, Moschner J, Rothkegel M, Rudiger M, Schluter K, Stanke G, Winkler J. 1995. The molecular architecture of focal adhesions. Annual Review of Cell and Developmental Biology 11:379-416.

Johansson MW, Lye MH, Barthel SR, Duffy AK, Annis DS, Mosher DF. 2004. Eosinophils adhere to vascular cell adhesion molecule-1 via podosomes. American Journal of Respiratory Cell and Molecular Biology 31(4):413-422.

Jones GE. 2000. Cellular signaling in macrophage migration and chemotaxis. Journal of Leukocyte Biology 68(5):593-602.

Jones GE, Zicha D, Dunn GA, Blundell M, Thrasher A. 2002. Restoration of podosomes and chemotaxis in Wiskott-Aldrich syndrome macrophages following induced expression of WASp. International Journal of Biochemistry & Cell Biology 34(7):806-815.

Judge AD, Sood V, Shaw JR, Fang D, McClintock K, MacLachlan I. 2005. Sequence-dependent stimulation of the mammalian innate immune response by synthetic siRNA. Nature Biotechnology 23(4):457-462.

Kadowaki N, Ho S, Antonenko S, Malefyt RD, Kastelein RA, Bazan F, Liu YJ. 2001. Subsets of human dendritic cell precursors express different toll-like receptors and respond to different microbial antigens. Journal of Experimental Medicine 194(6):863-869.

Kahner BN, Dorsam RT, Kim S, Shankar H, Kitamura D, Kunapuli SP. 2008. Hematopoeitic lineage cell-specific protein-1 (HS1) regulates PAR-mediated ERK activation and thromboxane generation in platelets. Platelets 19(8):614-623.

Kanehisa J, Yamanaka T, Doi S, Turksen K, Heersche JNM, Aubin JE, Takeuchi H. 1990. A BAND OF F-ACTIN CONTAINING PODOSOMES IS INVOLVED IN BONE-RESORPTION BY OSTEOCLASTS. Bone 11(4):287-293.

Kang YB, Stein CS, Heth JA, Sinn PL, Penisten AK, Staber PD, Ratliff KL, Shen H, Barker CK, Martins I and others. 2002. In vivo gene transfer using a nonprimate lentiviral vector pseudotyped with Ross River Virus glycoproteins. Journal of Virology 76(18):9378-9388.

Kanner SB, Reynolds AB, Vines RR, Parsons JT. 1990. MONOCLONAL-ANTIBODIES TO INDIVIDUAL TYROSINE-PHOSPHORYLATED PROTEIN SUBSTRATES OF ONCOGENE-ENCODED TYROSINE KINASES. Proceedings of the National Academy of Sciences of the United States of America 87(9):3328-3332.

Kato M, Miki H, Kurita S, Endo T, Nakagawa H, Miyamoto S, Takenawa T. 2002. WICH, a novel verprolin homology domain-containing protein that functions cooperatively with N-WASP in actin-microspike formation. Biochemical and Biophysical Research Communications 291(1):41-47.

Kelleher JF, Atkinson SJ, Pollard TD. 1995. SEQUENCES, STRUCTURAL MODELS, AND CELLULAR-LOCALIZATION OF THE ACTIN-RELATED PROTEINS ARP2 AND ARP3 FROM ACANTHAMOEBA. Journal of Cell Biology 131(2):385-397.

Kempiak SJ, Yamaguchi H, Sarmiento C, Sidani M, Ghosh M, Eddy RJ, DesMarais V, Way M, Condeelis J, Segall JE. 2005. A neural Wiskott-Aldrich syndrome protein-mediated pathway for localized activation of actin polymerization that is regulated by cortactin. Journal of Biological Chemistry 280(7):5836-5842.

Khvorova A, Reynolds A, Jayasena SD. 2003. Functional siRNAs and rniRNAs exhibit strand bias. Cell 115(2):209-216.

Kim AS, Kakalis LT, Abdul-Manan M, Liu GA, Rosen MK. 2000. Autoinhibition and activation mechanisms of the Wiskott-Aldrich syndrome protein. Nature 404(6774):151-158.

Kim M, Carman CV, Springer TA. 2003. Bidirectional transmembrane signaling by cytoplasmic domain separation in integrins. Science 301(5640):1720-1725.

Kinashi T. 2005. Intracellular signalling controlling integrin activation in lymphocytes. Nature Reviews Immunology 5(7):546-559.

Kinley AW, Weed SA, Weaver AM, Karginov AV, Bissonette E, Cooper JA, Parsons JT. 2003. Cortactin interacts with WIP in regulating arp2/3 activation and membrane protrusion. Current Biology 13(5):384-393.

Kirchhausen T. 1998. Wiskott-Aldrich syndrome: a gene, a multifunctional protein and the beginnings of an explanation. Molecular Medicine Today 4(7):300-304.

Kirschner MW. 1980. IMPLICATIONS OF TREADMILLING FOR THE STABILITY AND POLARITY OF ACTIN AND TUBULIN POLYMERS INVIVO. Journal of Cell Biology 86(1):330-334.

Kitamura D, Kaneko H, Miyagoe Y, Ariyasu T, Watanabe T. 1989. ISOLATION AND CHARACTERIZATION OF A NOVEL HUMAN-GENE EXPRESSED SPECIFICALLY IN THE CELLS OF HEMATOPOIETIC LINEAGE. Nucleic Acids Research 17(22):9367-9379.

Kitamura D, Kaneko H, Taniuchi I, Akagi K, Yamamura KI, Watanabe T. 1995. MOLECULAR-CLONING AND CHARACTERIZATION OF MOUSE HS1. Biochemical and Biophysical Research Communications 208(3):1137-1146.

Konno A, Kirby M, Anderson SA, Schwartzberg PL, Candotti F. 2007. The expression of Wiskott-Aldrich syndrome protein (WASP) is dependent on WASP-interacting protein (WIP). International Immunology 19(2):185-192.

Krzewski K, Chen X, Strominger JL. 2008. WIP is essential for lytic granule polarization and NK cell cytotoxicity. Proceedings of the National Academy of Sciences of the United States of America 105(7):2568-2573.

Kuijpers TW, van de Vijver E, Weterman MAJ, de Boer M, Tool ATJ, van den Berg TK, Moser M, Jakobs ME, Seeger K, Sanal O and others. 2009. LAD-1/variant syndrome is caused by mutations in FERMT3. Blood 113(19):4740-4746.

Kurisu S, Takenawa T. 2009. The WASP and WAVE family proteins. Genome Biology 10(6).

Labno CM, Lewis CM, You DQ, Leung DW, Takesono A, Kamberos N, Seth A, Finkelstein LD, Rosen MK, Schwartzberg PL and others. 2003. Itk functions to control actin polymerization at the immune synapse through localized activation of Cdc42 and WASP. Current Biology 13(18):1619-1624.

Lakkakorpi PT, Vaananen HK. 1996. Cytoskeletal changes in osteoclasts during the resorption cycle. Microscopy Research and Technique 33(2):171-181.

Lammermann T, Bader BL, Monkley SJ, Worbs T, Wedlich-Soldner R, Hirsch K, Keller M, Forster R, Critchley DR, Fassler R and others. 2008. Rapid leukocyte migration by integrin-independent flowing and squeezing. Nature 453(7191):51-+.

Lammermann T, Sixt M. 2009. Mechanical modes of 'amoeboid' cell migration. Current Opinion in Cell Biology 21(5):636-644.

Langenkamp A, Messi M, Lanzavecchia A, Sallusto F. 2000. Kinetics of dendritic cell activation: impact on priming of T(H)1, T(H)2 and nonpolarized T cells. Nature Immunology 1(4):311-316.

Langerhans P. 1868. Ueber die Nerven der menschlichen Haut. Virchows Archiv 44(2):325-337.

Lauffenburger DA, Horwitz AF. 1996. Cell migration: A physically integrated molecular process. Cell 84(3):359-369.

Leung RKM, Whittaker PA. 2005. RNA interference: from gene silencing to gene-specific therapeutics. Pharmacology & Therapeutics 107(2):222-239.

Leverrier Y, Lorenzi R, Blundell MP, Brickell P, Kinnon C, Ridley AJ, Thrasher AJ. 2001. Cutting edge: The Wiskott-Aldrich syndrome protein is required for efficient phagocytosis of apoptotic cells. Journal of Immunology 166(8):4831-4834.

Lewis PF, Emerman M. 1994. Passage through Mitosis Is Required for Oncoretroviruses but Not for the Human-Immunodeficiency-Virus. Journal of Virology 68(1):510-516.

Li YS, Tondravi M, Liu JL, Smith E, Haudenschild CC, Kaczmarek M, Zhan X. 2001. Cortactin potentiates bone metastasis of breast cancer cells. Cancer Research 61(18):6906-6911.

Linardopoulou EV, Parghi SS, Friedman C, Osborn GE, Parkhurst SM, Trask BJ. 2007. Human subtelomeric WASH genes encode a new subclass of the WASP family. Plos Genetics 3(12):2477-2485.

Linder S. 2007. The matrix corroded: podosomes and invadopodia in extracellular matrix degradation. Trends in Cell Biology 17(3):107-117.

Linder S, Aepfelbacher M. 2003. Podosomes: adhesion hot-spots of invasive cells. Trends in Cell Biology 13(7):376-385.

Linder S, Higgs H, Hufner K, Schwarz K, Pannicke U, Aepfelbacher M. 2000. The polarization defect of Wiskott-Aldrich syndrome macrophages is linked to dislocalization of the Arp2/3 complex. Journal of Immunology 165(1):221-225.

Linder S, Kopp P. 2005. Podosomes at a glance. Journal of Cell Science 118(10):2079-2082.

Linder S, Nelson D, Weiss M, Aepfelbacher M. 1999. Wiskott-Aldrich syndrome protein regulates podosomes in primary human macrophages. Proceedings of the National Academy of Sciences of the United States of America 96(17):9648-9653.

Loisel TP, Boujemaa R, Pantaloni D, Carlier MF. 1999. Reconstitution of actin-based motility of Listeria and Shigella using pure proteins. Nature 401(6753):613-616.

Launay S, Brown G, Machesky LM. 2003. Expression of WASP and Scar1/WAVE1 actin-associated proteins is differentially modulated during differentiation of HL-60 cells. Cell Motility and the Cytoskeleton 54(4):274-285.

Luo KQ, Chang DC. 2004. The gene-silencing efficiency of siRNA is strongly dependent on the local structure of mRNA at the targeted region. Biochemical and Biophysical Research Communications 318(1):303-310.

Lutz MB, Schuler G. 2002. Immature, semi-mature and fully mature dendritic cells: which signals induce tolerance or immunity? Trends in Immunology 23(9):445-449.

Machesky LM, Atkinson SJ, Ampe C, Vandekerckhove J, Pollard TD. 1994. PURIFICATION OF A CORTICAL COMPLEX CONTAINING 2 UNCONVENTIONAL ACTINS FROM ACANTHAMOEBA BY AFFINITY-CHROMATOGRAPHY ON PROFILIN-AGAROSE. Journal of Cell Biology 127(1):107-115.

Machesky LM, Insall RH. 1998. Scar1 and the related Wiskott-Aldrich syndrome protein, WASP, regulate the actin cytoskeleton through the Arp2/3 complex. Current Biology 8(25):1347-1356.

Machesky LM, Mullins RD, Higgs HN, Kaiser DA, Blanchoin L, May RC, Hall ME, Pollard TD. 1999. Scar, a WASp-related protein, activates nucleation of actin filaments by the Arp2/3 complex. Proceedings of the National Academy of Sciences of the United States of America 96(7):3739-3744.

MacKenzie TC, Kobinger GP, Kootstra NA, Radu A, Sena-Esteves M, Bouchard S, Wilson JM, Verma IM, Flake AW. 2002. Efficient transduction of liver and muscle after in utero injection of lentiviral vectors with different pseudotypes. Molecular Therapy 6(3):349-358.

Malawista SE, Chevance AD. 1997. Random locomotion and chemotaxis of human blood polymorphonuclear leukocytes (PMN) in the presence of EDTA: PMN in close quarters require neither leukocyte integrins nor external divalent cations. Proceedings of the National Academy of Sciences of the United States of America 94(21):11577-11582.

Marchisio PC, Cirillo D, Naldini L, Primavera MV, Teti A, Zamboninzallone A. 1984. CELL-SUBSTRATUM INTERACTION OF CULTURED AVIAN OSTEOCLASTS IS MEDIATED BY SPECIFIC ADHESION STRUCTURES. Journal of Cell Biology 99(5):1696-1705.

Marchisio PC, Cirillo D, Teti A, Zamboninzallone A, Tarone G. 1987. ROUS-SARCOMA VIRUS-TRANSFORMED FIBROBLASTS AND CELLS OF MONOCYTIC ORIGIN DISPLAY A PECULIAR DOT-LIKE ORGANIZATION OF CYTOSKELETAL PROTEINS INVOLVED IN MICROFILAMENT MEMBRANE INTERACTIONS. Experimental Cell Research 169(1):202-214.

Martinez-Quiles N, Rohatgi R, Anton IM, Medina M, Saville SP, Miki H, Yamaguchi H, Takenawa T, Hartwig JH, Geha RS and others. 2001. WIP regulates N-WASP-mediated actin polymerization and filopodium formation. Nature Cell Biology 3(5):484-491.

Matsumoto M, Funami K, Tanabe M, Oshiumi H, Shingai M, Seto Y, Yamamoto A, Seya T. 2003. Subcellular localization of toll-like receptor 3 in human dendritic cells. Journal of Immunology 171(6):3154-3162.

McAbee DD, Grinnell F. 1985. BINDING AND PHAGOCYTOSIS OF FIBRONECTIN-COATED BEADS BY BHK CELLS - RECEPTOR SPECIFICITY AND DYNAMICS. Journal of Cellular Physiology 124(2):240-246.

McBride JL, Boudreau RL, Harper SQ, Staber PD, Monteys AM, Martins I, Gilmore BL, Burstein H, Peluso RW, Polisky B and others. 2008. Artificial miRNAs mitigate shRNA-mediated toxicity in the brain: Implications for the therapeutic development of RNAi. Proceedings of the National Academy of Sciences of the United States of America 105(15):5868-5873.

McDowall A, Inwald D, Leitinger B, Jones A, Liesner R, Klein N, Hogg N. 2003. A novel form of integrin dysfunction involving beta 1, beta 2, and beta 3 integrins. Journal of Clinical Investigation 111(1):51-60.

McEnery G, Nash FW. 1973. WISKOTT-ALDRICH SYNDROME ASSOCIATED WITH

IDIOPATHIC INFANTILE CORTICAL HYPEROSTOSIS - (CAFFEYS DISEASE). Archives of Disease in Childhood 48(10):818-821.

Megherbi R, Kiorpelidou E, Foster B, Rowe C, Naisbitt DJ, Goldring CE, Park BK. 2009. Role of protein haptenation in triggering maturation events in the dendritic cell surrogate cell line THP-1. Toxicology and Applied Pharmacology 238(2):120-132.

Meister G, Tuschl T. 2004. Mechanisms of gene silencing by double-stranded RNA. Nature 431(7006):343-349.

Merad M, Manz MG, Karsunky H, Wagers A, Peters W, Charo I, Weissman IL, Cyster JG, Engleman EG. 2002. Langerhans cells renew in the skin throughout life under steady-state conditions. Nature Immunology 3(12):1135-1141.

Miki H, Miura K, Takenawa T. 1996. N-WASP, a novel actin-depolymerizing protein, regulates the cortical cytoskeletal rearrangement in a PIP2-dependent manner downstream of tyrosine kinases. Embo Journal 15(19):5326-5335.

Miki H, Suetsugu S, Takenawa T. 1998. WAVE, a novel WASP-family protein involved in actin reorganization induced by Rac. Embo Journal 17(23):6932-6941.

Millard TH, Sharp SJ, Machesky LM. 2004. Signalling to actin assembly via the WASP (Wiskott-Aldrich syndrome protein)-family proteins and the Arp2/3 complex. Biochemical Journal 380:1-17.

Miller LJ, Bainton DF, Borregaard N, Springer TA. 1987. STIMULATED MOBILIZATION OF MONOCYTE MAC-1 AND P150,95 ADHESION PROTEINS FROM AN INTRACELLULAR VESICULAR COMPARTMENT TO THE CELL-SURFACE. Journal of Clinical Investigation 80(2):535-544.

Mittal V. 2004. Improving the efficiency of RNA interference in mammals. Nature Reviews Genetics 5(5):355-365.

Miyauchi A, Hruska KA, Greenfield EM, Duncan R, Alvarez J, Barattolo R, Colucci S, Zamboninzallone A, Teitelbaum SL, Teti A. 1990. OSTEOCLAST CYTOSOLIC CALCIUM, REGULATED BY VOLTAGE-GATED CALCIUM CHANNELS AND EXTRACELLULAR CALCIUM, CONTROLS PODOSOME ASSEMBLY AND BONE-RESORPTION. Journal of Cell Biology 111(6):2543-2552.

Mizutani K, Miki H, He H, Maruta H, Takenawa T. 2002. Essential role of neural Wiskott-Aldrich syndrome protein in podosome formation and degradation of extracellular matrix in src-transformed fibroblasts. Cancer Research 62(3):669-674.

Molina IJ, Sancho J, Terhorst C, Rosen FS, Remoldodonnell E. 1993. T-CELLS OF PATIENTS WITH THE WISKOTT-ALDRICH SYNDROME HAVE A RESTRICTED DEFECT IN PROLIFERATIVE RESPONSES. Journal of Immunology 151(8):4383-4390.

Molnar J, Hoekstra S, Ku CSL, Vanalten P. 1987. EVIDENCE FOR THE RECYCLING NATURE OF THE FIBRONECTIN RECEPTOR OF MACROPHAGES. Journal of Cellular Physiology 131(3):374-383.

Monks CRF, Freiberg BA, Kupfer H, Sciaky N, Kupfer A. 1998. Three-dimensional segregation of supramolecular activation clusters in T cells. Nature 395(6697):82-86.

Monypenny J, Chou HC, Banon-Rodriguez I, Thrasher AJ, Anton IM, Jones GE, Calle Y. 2011. Role of WASP in cell polarity and podosome dynamics of myeloid cells. European

Journal of Cell Biology 90(2-3):198-204.

Moreau V, Tatin F, Varon C, Genot E. 2003. Actin can reorganize into podosomes in aortic endothelial cells, a process controlled by Cdc42 and RhoA. Molecular and Cellular Biology 23(19):6809-6822.

Morelli AE, Larregina AT, Ganster RW, Zahorchak AF, Plowey JM, Takayama T, Logar AJ, Robbins PD, Falo LD, Thomson AW. 2000. Recombinant adenovirus induces maturation of dendritic cells via an NF-kappa B-dependent pathway. Journal of Virology 74(20):9617-9628.

Morin NA, Oakes PW, Hyun YM, Lee DY, Chin EY, King MR, Springer TA, Shimaoka M, Tang JX, Reichner JS and others. 2008. Nonmuscle myosin heavy chain IIA mediates integrin LFA-1 de-adhesion during T lymphocyte migration. Journal of Experimental Medicine 205(1):195-205.

Mory A, Feigelson SW, Yarali N, Kilic SS, Bayhan GI, Gershoni-Baruch R, Etzioni A, Alon R. 2008. Kindlin-3: a new gene involved in the pathogenesis of LAD-III. Blood 112(6):2591-2591.

Moser M, Murphy KM. 2000. Dendritic cell regulation of T(H)1-T(H)2 development. Nature Immunology 1(3):199-205.

Mueller SC, Chen WT. 1991. CELLULAR INVASION INTO MATRIX BEADS - LOCALIZATION OF BETA-1 INTEGRINS AND FIBRONECTIN TO THE INVADOPODIA. Journal of Cell Science 99:213-225.

Mullins RD, Heuser JA, Pollard TD. 1998. The interaction of Arp2/3 complex with actin: Nucleation, high affinity pointed end capping, and formation of branching networks of filaments. Proceedings of the National Academy of Sciences of the United States of America 95(11):6181-6186.

Murphy DA, Courtneidge SA. 2011. The 'ins' and 'outs' of podosomes and invadopodia: characteristics, formation and function. Nature Reviews Molecular Cell Biology 12(7):413-426.

Muzio M, Bosisio D, Polentarutti N, D'Amico G, Stoppacciaro A, Mancinelli R, van't Veer C, Penton-Rol G, Ruco LP, Allavena P and others. 2000. Differential expression and regulation of toll-like receptors (TLR) in human leukocytes: Selective expression of TLR3 in dendritic cells. Journal of Immunology 164(11):5998-6004.

Nakahara H, Howard L, Thompson EW, Sato H, Seiki M, Yeh YY, Chen WT. 1997. Transmembrane/cytoplasmic domain-mediated membrane type 1-matrix metalloprotease docking to invadopodia is required for cell invasion. Proceedings of the National Academy of Sciences of the United States of America 94(15):7959-7964.

Naldini L, Blomer U, Gallay P, Ory D, Mulligan R, Gage FH, Verma IM, Trono D. 1996. In vivo gene delivery and stable transduction of nondividing cells by a lentiviral vector. Science 272(5259):263-267.

Neil S, Martin F, Ikeda Y, Collins M. 2001. Postentry restriction to human immunodeficiency virus-based vector transduction in human monocytes. Journal of Virology 75(12):5448-5456.

Nourshargh S, Hordijk PL, Sixt M. 2010. Breaching multiple barriers: leukocyte motility through venular walls and the interstitium. Nature Reviews Molecular Cell Biology

11(5):366-378.

Nusblat LM, Dovas A, Cox D. 2011. The non-redundant role of N-WASP in podosome-mediated matrix degradation in macrophages. European Journal of Cell Biology 90(2-3):205-212.

Olivier A, Jeanson-Leh L, Bouma G, Compagno D, Blondeau J, Seye K, Charrier S, Burns S, Thrasher AJ, Danos O and others. 2006. A partial down-regulation of WASP is sufficient to inhibit podosome formation in dendritic cells. Molecular Therapy 13(4):729-737.

Oser M, Dovas A, Cox D, Condeelis J. 2011. Nck1 and Grb2 localization patterns can distinguish invadopodia from podosomes. European Journal of Cell Biology 90(2-3):181-188.

Osiak AE, Zenner G, Linder S. 2005. Subconfluent endothelial cells form podosomes downstream of cytokine and RhoGTPase signaling. Experimental Cell Research 307(2):342-353.

Pan Q, de Ruiter PE, von Eije KJ, Smits R, Kwekkeboom J, Tilanus HW, Berkhout B, Janssen HLA, van der Laan LJW. 2011. Disturbance of the microRNA pathway by commonly used lentiviral shRNA libraries limits the application for screening host factors involved in hepatitis C virus infection. Febs Letters 585(7):1025-1030.

Panchal SC, Kaiser DA, Torres E, Pollard TD, Rosen MK. 2003. A conserved amphipathic helix in WASP/Scar proteins is essential for activation of Arp2/3 complex. Nature Structural Biology 10(8):591-598.

Pantaloni D, Carlier MF. 1993. HOW PROFILIN PROMOTES ACTIN FILAMENT ASSEMBLY IN THE PRESENCE OF THYMOSIN-BETA-4. Cell 75(5):1007-1014.

Patel AS, Schechter GL, Wasilenko WJ, Somers KD. 1998. Overexpression of EMS1/cortactin in NIH3T3 fibroblasts causes increased cell motility and invasion in vitro. Oncogene 16(25):3227-3232.

Pfaff M, Jurdic P. 2001. Podosomes in osteoclast-like cells: structural analysis and cooperative roles of paxillin, proline-rich tyrosine kinase 2 (Pyk2) and integrin alpha V beta 3. Journal of Cell Science 114(15):2775-2786.

Pichlmair A, Diebold SS, Gschmeissner S, Takeuchi Y, Ikeda Y, Collins MK, Sousa CRE. 2007. Tubulovesicular structures within vesicular stomatitis virus G protein-pseudotyped lentiviral vector preparations carry DNA and stimulate antiviral responses via toll-like receptor 9. Journal of Virology 81(2):539-547.

Prehoda KE, Lee DJ, Lim WA. 1999. Structure of the enabled VASP homology 1 domain-peptide complex: A key component in the spatial control of actin assembly. Cell 97(4):471-480.

Prehoda KE, Scott JA, Mullins RD, Lim WA. 2000. Integration of multiple signals through cooperative regulation of the N-WASP-Arp2/3 complex. Science 290(5492):801-806.

Quintavalle M, Elia L, Condorelli G, Courtneidge SA. 2010. MicroRNA control of podosome formation in vascular smooth muscle cells in vivo and in vitro. Journal of Cell Biology 189(1):13-22.

Ramesh N, Anton IM, Hartwig JH, Geha RS. 1997. WIP, a protein associated with Wiskott-Aldrich syndrome protein, induces actin polymerization and redistribution in lymphoid

cells. Proceedings of the National Academy of Sciences of the United States of America 94(26):14671-14676.

Randolph GJ, Angeli V, Swartz MA. 2005. Dendritic-cell trafficking to lymph nodes through lymphatic vessels. Nature Reviews Immunology 5(8):617-628.

Rasaiyaah J, Yong K, Katz DR, Kellam P, Chain BM. 2007. Dendritic cells and myeloid leukaemias: plasticity and commitment in cell differentiation. British Journal of Haematology 138(3):281-290.

Ratcliff FG, MacFarlane SA, Baulcombe DC. 1999. Gene silencing without DNA: RNA-mediated cross-protection between viruses. Plant Cell 11(7):1207-1215.

Reeves ME, Royal RE, Lam JS, Rosenberg SA, Hwu P. 1996. Retroviral transduction of human dendritic cells with a tumor-associated antigen gene. Cancer Research 56(24):5672-5677.

Renkawitz J, Schumann K, Weber M, Lammermann T, Pflicke H, Piel M, Polleux J, Spatz JP, Sixt M. 2009. Adaptive force transmission in amoeboid cell migration. Nature Cell Biology 11(12):1438-U121.

Rescigno M, Granucci F, Citterio S, Foti M, Ricciardi-Castagnoli P. 1999. Coordinated events during bacteria-induced DC maturation. Immunology Today 20(5):200-203.

Reynolds A, Leake D, Boese Q, Scaringe S, Marshall WS, Khvorova A. 2004. Rational siRNA design for RNA interference. Nature Biotechnology 22(3):326-330.

Ridley AJ, Schwartz MA, Burridge K, Firtel RA, Ginsberg MH, Borisy G, Parsons JT, Horwitz AR. 2003. Cell migration: Integrating signals from front to back. Science 302(5651):1704-1709.

Robert C, Fuhlbrigge RC, Kieffer JD, Ayehunie S, Hynes RO, Cheng GY, Grabbe S, von Andrian UH, Kupper TS. 1999. Interaction of dendritic cells with skin endothelium: A new perspective on immunosurveillance. Journal of Experimental Medicine 189(4):627-635.

Robinson RC, Turbedsky K, Kaiser DA, Marchand JB, Higgs HN, Choe S, Pollard TD. 2001. Crystal structure of Arp2/3 complex. Science 294(5547):1679-1684.

Rodrigo JP, Garcia LA, Ramos S, Lazo PS, Suarez C. 2000. EMS1 gene amplification correlates with poor prognosis in squamous cell carcinomas of the head and neck. Clinical Cancer Research 6(8):3177-3182.

Rogers SL, Wiedemann U, Stuurman N, Vale RD. 2003. Molecular requirements for actin-based lamella formation in Drosophila S2 cells. Journal of Cell Biology 162(6):1079-1088.

Root DE, Hacohen N, Hahn WC, Lander ES, Sabatini DM. 2006. Genome-scale loss-of-function screening with a lentiviral RNAi library. Nature Methods 3(9):715-719.

Rossi M, Young JW. 2005. Human dendritic cells: Potent antigen-presenting cells at the crossroads of innate and adaptive immunity. Journal of Immunology 175(3):1373-1381.

Rottiers P, Saltel F, Daubon T, Chaigne-Delalande B, Tridon V, Billottet C, Reuzeau E, Genot E. 2009. TGF beta-induced endothelial podosomes mediate basement membrane collagen degradation in arterial vessels. Journal of Cell Science 122(23):4311-4318.

Rouas R, Uch R, Cleuter Y, Jordier F, Bagnis C, Mannoni P, Lewalle P, Martiat P, Van den

Broeke A. 2002. Lentiviral-mediated gene delivery in human monocyte-derived dendritic cells: Optimized design and procedures for highly efficient transduction compatible with clinical constraints. Cancer Gene Therapy 9(9):715-724.

Sallusto F, Lanzavecchia A. 1994. Efficient Presentation of Soluble-Antigen by Cultured Human Dendritic Cells Is Maintained by Granulocyte-Macrophage Colony-Stimulating Factor Plus Interleukin-4 and Down-Regulated by Tumor-Necrosis-Factor-Alpha. Journal of Experimental Medicine 179(4):1109-1118.

Sallusto F, Lanzavecchia A. 1999. Mobilizing dendritic cells for tolerance, priming, and chronic inflammation. Journal of Experimental Medicine 189(4):611-614.

Sampath R, Gallagher PJ, Pavalko FM. 1998. Cytoskeletal interactions with the leukocyte integrin beta 2 cytoplasmic tail - Activation-dependent regulation of associations with talin and alpha-actinin. Journal of Biological Chemistry 273(50):33588-33594.

Sanders DA. 2002. No false start for novel pseudotyped vectors. Current Opinion in Biotechnology 13(5):437-442.

Sandrin V, Boson B, Salmon P, Gay W, Negre D, Le Grand R, Trono D, Cosset FL. 2002. Lentiviral vectors pseudotyped with a modified RD114 envelope glycoprotein show increased stability in sera and augmented transduction of primary lymphocytes and CD34(+) cells derived from human and nonhuman primates. Blood 100(3):823-832.

Santegoets S, van den Eertwegh AJM, de Loosdrecht AAV, Scheper RJ, Gruijl TD. 2008. Human dendritic cell line models for DC differentiation and clinical DC vaccination studies. Journal of Leukocyte Biology 84(6):1364-1373.

Sasahara Y, Rachid R, Byrne MJ, de la Fuente MA, Abraham RT, Ramesh N, Geha RS. 2002. Mechanism of recruitment of WASP to the immunological synapse and of its activation following TCR ligation. Molecular Cell 10(6):1269-1281.

Sato T, Ovejero MD, Hou P, Heegaard AM, Kumegawa M, Foged NT, Delaisse JM. 1997. Identification of the membrane-type matrix metalloproteinase MT1-MMP in osteoclasts. Journal of Cell Science 110:589-596.

Schafer DA, Jennings PB, Cooper JA. 1996. Dynamics of capping protein and actin assembly in vitro: Uncapping barbed ends by polyphosphoinositides. Journal of Cell Biology 135(1):169-179.

Schaller MD. 2001. Paxillin: a focal adhesion-associated adaptor protein. Oncogene 20(44):6459-6472.

Scharffetter-Kochanek K, Lu HF, Norman K, van Nood N, Munoz F, Grabbe S, McArthur M, Lorenzo I, Kaplan S, Ley K and others. 1998. Spontaneous skin ulceration and defective T cell function in CD18 null mice. Journal of Experimental Medicine 188(1):119-131.

Schauber CA, Tuerk MJ, Pacheco CD, Escarpe PA, Veres G. 2004. Lentiviral vectors pseudotyped with baculovirus gp64 efficiently transduce mouse cells in vivo and show tropism restriction against hematopoietic cell types in vitro. Gene Therapy 11(3):266-275.

Schneeberger EE, Vu Q, LeBlanc BW, Doerschuk CM. 2000. The accumulation of dendritic cells in the lung is impaired in CD18(-/-) but not in ICAM-1(-/-) mutant mice. Journal of Immunology 164(5):2472-2478.

Schreibelt G, Tel J, Sliepen K, Benitez-Ribas D, Figdor CG, Adema GJ, de Vries IJM. Toll-like

receptor expression and function in human dendritic cell subsets: implications for dendritic cell-based anti-cancer immunotherapy. Cancer Immunology Immunotherapy 59(10):1573-1582.

Schroers R, Sinha I, Segall H, Schmidt-Wolf IGH, Rooney CM, Brenner MK, Sutton RE, Chen SY. 2000. Transduction of human PBMC-derived dendritic cells and macrophages by an HIV-1-based lentiviral vector system. Molecular Therapy 1(2):171-179.

Schumann K, Lammermann T, Bruckner M, Legler DF, Polleux J, Spatz JP, Schuler G, Forster R, Lutz MB, Sorokin L and others. 2010. Immobilized Chemokine Fields and Soluble Chemokine Gradients Cooperatively Shape Migration Patterns of Dendritic Cells. Immunity 32(5):703-713.

Schuuring E. 1995. THE INVOLVEMENT OF THE CHROMOSOME 11Q13 REGION IN HUMAN MALIGNANCIES - CYCLIN D1 AND EMS1 ARE 2 NEW CANDIDATE ONCOGENES - A REVIEW. Gene 159(1):83-96.

Schuuring E, Verhoeven E, Litvinov S, Michalides R. 1993. THE PRODUCT OF THE EMS1 GENE, AMPLIFIED AND OVEREXPRESSED IN HUMAN CARCINOMAS, IS HOMOLOGOUS TO A V-SRC SUBSTRATE AND IS LOCATED IN CELL-SUBSTRATUM CONTACT SITES. Molecular and Cellular Biology 13(5):2891-2898.

Scielzo C, Bertilaccio MTS, Simonetti G, Dagklis A, ten Hacken E, Fazi C, Muzio M, Caiolfa V, Kitamura D, Restuccia U and others. 2010. HS1 has a central role in the trafficking and homing of leukemic B cells. Blood 116(18):3537-3546.

Sebastian K, Ott H, Zwadlo-Klarwasser G, Skazik-Voogt C, Marquardt Y, Czaja K, Merk HF, Baron JM. 2012. Evaluation of the sensitizing potential of antibiotics in vitro using the human cell lines THP-1 and MUTZ-LC and primary monocyte-derived dendritic cells. Toxicology and Applied Pharmacology 262(3):283-292.

Sengelov H, Kjeldsen L, Diamond MS, Springer TA, Borregaard N. 1993. SUBCELLULAR-LOCALIZATION AND DYNAMICS OF MAC-1 (ALPHA(M)BETA(2)) IN HUMAN NEUTROPHILS. Journal of Clinical Investigation 92(3):1467-1476.

Sharkey CM, North CL, Kuhn RJ, Sanders DA. 2001. Ross River virus glycoprotein-pseudotyped retroviruses and stable cell lines for their production. Journal of Virology 75(6):2653-2659.

Shimizu Y, Vanseventer GA, Horgan KJ, Shaw S. 1990. REGULATED EXPRESSION AND BINDING OF 3 VLA (BETA-1) INTEGRIN RECEPTORS ON T-CELLS. Nature 345(6272):250-253.

Shuster DE, Kehrli ME, Ackermann MR, Gilbert RO. 1992. IDENTIFICATION AND PREVALENCE OF A GENETIC-DEFECT THAT CAUSES LEUKOCYTE ADHESION DEFICIENCY IN HOLSTEIN CATTLE. Proceedings of the National Academy of Sciences of the United States of America 89(19):9225-9229.

Siegal FP, Kadowaki N, Shodell M, Fitzgerald-Bocarsly PA, Shah K, Ho S, Antonenko S, Liu YJ. 1999. The nature of the principal type 1 interferon-producing cells in human blood. Science 284(5421):1835-1837.

Sinn PL, Burnight ER, Hickey MA, Blissard GW, McCray PB. 2005. Persistent gene expression in mouse nasal epithelia following feline immunodeficiency virus-based vector gene transfer. Journal of Virology 79(20):12818-12827.

Sixt M. 2011. Interstitial locomotion of leukocytes. Immunology Letters 138(1):32-34.

Sixt M, Bauer M, Lammermann T, Fassler R. 2006. beta 1 integrins: zip codes and signaling relay for blood cells. Current Opinion in Cell Biology 18(5):482-490.

Sledz CA, Holko M, de Veer MJ, Silverman RH, Williams BRG. 2003. Activation of the interferon system by short-interfering RNAs. Nature Cell Biology 5(9):834-839.

Smith A, Bracke M, Leitinger B, Porter JC, Hogg N. 2003. LFA-1-induced T cell migration on ICAM-1 involves regulation of MLCK-mediated attachment and ROCK-dependent detachment. Journal of Cell Science 116(15):3123-3133.

Snapper SB, Meelu P, Nguyen D, Stockton BM, Bozza P, Alt FW, Rosen FS, von Andrian UH, Klein C. 2005. WASP deficiency leads to global defects of directed leukocyte migration in vitro and in vivo. Journal of Leukocyte Biology 77(6):993-998.

Snapper SB, Rosen FS, Mizoguchi E, Cohen P, Khan W, Liu CH, Hagemann TL, Kwan SP, Ferrini R, Davidson L and others. 1998. Wiskott-Aldrich syndrome protein-deficient mice reveal a role for WASP in T but not B cell activation. Immunity 9(1):81-91.

Sontheimer EJ. 2005. Assembly and function of RNA silencing complexes. Nature Reviews Molecular Cell Biology 6(2):127-138.

Spinardi L, Rietdorf J, Nitsch L, Bono M, Tacchetti C, Way M, Marchisio PC. 2004. A dynamic podosome-like structure of epithelial cells. Experimental Cell Research 295(2):360-374.

Springer TA. 1995. TRAFFIC SIGNALS ON ENDOTHELIUM FOR LYMPHOCYTE RECIRCULATION AND LEUKOCYTE EMIGRATION. Annual Review of Physiology 57:827-872.

Springer TA, Thompson WS, Miller LJ, Schmalstieg FC, Anderson DC. 1984. INHERITED DEFICIENCY OF THE MAC-1, LFA-1, P150,95 GLYCOPROTEIN FAMILY AND ITS MOLECULAR-BASIS. Journal of Experimental Medicine 160(6):1901-1918.

St Louis DC, Woodcock JB, Fransozo G, Blair PJ, Carlson LM, Murillo M, Wells MR, Williams AJ, Smoot DS, Kaushal S and others. 1999. Evidence for distinct intracellular signaling pathways in CD34(+) progenitor to dendritic cell differentiation from a human cell line model. Journal of Immunology 162(6):3237-3248.

Steinman RM, Cohn ZA. 1973. IDENTIFICATION OF A NOVEL CELL TYPE IN PERIPHERAL LYMPHOID ORGANS OF MICE. Journal of Experimental Medicine 137(5):1142-1162.

Suetsugu S, Hattori M, Miki H, Tezuka T, Yamamoto T, Mikoshiba K, Takenawa T. 2002. Sustained activation of N-WASP through phosphorylation is essential for neurite extension. Developmental Cell 3(5):645-658.

Suetsugu S, Miki H, Takenawa T. 1999. Identification of two human WAVE SCAR homologues as general actin regulatory molecules which associate with the Arp2/3 complex. Biochemical and Biophysical Research Communications 260(1):296-302.

Sullivan KE, Mullen CA, Blaese RM, Winkelstein JA. 1994. A MULTIINSTITUTIONAL SURVEY OF THE WISKOTT-ALDRICH SYNDROME. Journal of Pediatrics 125(6):876-885.

Sun CX, Downey GP, Zhu F, Koh ALY, Thang H, Glogauer M. 2004. Rac1 is the small GTPase responsible for regulating the neutrophil chemotaxis compass. Blood 104(12):3758-3765.

Svensson L, Howarth K, McDowall A, Patzak I, Evans R, Ussar S, Moser M, Metin A, Fried M, Tomlinson I and others. 2009. Leukocyte adhesion deficiency-III is caused by mutations

in KINDLIN3 affecting integrin activation. Nature Medicine 15(3):306-312.

Takagi J, Springer TA. 2002. Integrin activation and structural rearrangement. Immunological Reviews 186:141-163.

Takemoto Y, Furuta M, Li XK, Strongsparks WJ, Hashimoto Y. 1995. LCKBP1, A PROLINE-RICH PROTEIN EXPRESSED IN HEMATOPOIETIC LINEAGE CELLS, DIRECTLY ASSOCIATES WITH THE SH3 DOMAIN OF PROTEIN-TYROSINE KINASE P56(LCK). Embo Journal 14(14):3403-3414.

Tan PH, Beutelspacher SC, Xue SA, Wang YH, Mitchell P, McAlister JC, Larkin DFP, McClure MO, Stauss HJ, Ritter MA and others. 2005. Modulation of human dendritic-cell function following transduction with viral vectors: implications for gene therapy. Blood 105(10):3824-3832.

Taniuchi I, Kitamura D, Maekawa Y, Fukuda T, Kishi H, Watanabe T. 1995. ANTIGEN-RECEPTOR INDUCED CLONAL EXPANSION AND DELETION OF LYMPHOCYTES ARE IMPAIRED IN MICE LACKING HS1 PROTEIN, A SUBSTRATE OF THE ANTIGEN-RECEPTOR-COUPLED TYROSINE KINASES. Embo Journal 14(15):3664-3678.

Tarone G, Cirillo D, Giancotti FG, Comoglio PM, Marchisio PC. 1985. ROUS-SARCOMA VIRUS-TRANSFORMED FIBROBLASTS ADHERE PRIMARILY AT DISCRETE PROTRUSIONS OF THE VENTRAL MEMBRANE CALLED PODOSOMES. Experimental Cell Research 159(1):141-157.

Tatin F, Varon C, Genot E, Moreau V. 2006. A signalling cascade involving PKC, Src and Cdc42 regulates podosome assembly in cultured endothelial cells in response to phorbol ester. Journal of Cell Science 119(4):769-781.

Tehrani S, Faccio R, Chandrasekar I, Ross FP, Cooper JA. 2006. Cortactin has an essential and specific role in osteoclast actin assembly. Molecular Biology of the Cell 17(7):2882-2895.

Thomas SG, Calaminus SD, Auger JM, Watson SP, Machesky LM. 2007. Studies on the actin-binding protein HS1 in platelets. Bmc Cell Biology 8.

Thrasher AJ, Burns SO. 2010. WASP: a key immunological multitasker. Nature Reviews Immunology 10(3):182-192.

Thrasher AJ, Jones GE, Kinnon C, Brickell PM, Katz DR. 1998. Is Wiskott-Aldrich syndrome a cell trafficking disorder? Immunology Today 19(12):537-539.

Timmerman JM, Levy R. 1999. Dendritic cell vaccines for cancer immunotherapy. Annual Review of Medicine 50:507-529.

Todd RF, Arnaout MA, Rosin RE, Crowley CA, Peters WA, Babior BM. 1984. SUBCELLULAR-LOCALIZATION OF THE LARGE SUBUNIT OF MO1 (MO1-ALPHA-FORMERLY GP 110), A SURFACE GLYCOPROTEIN ASSOCIATED WITH NEUTROPHIL ADHESION. Journal of Clinical Investigation 74(4):1280-1290.

Tomari Y, Zamore PD. 2005. Perspective: machines for RNAi. Genes & Development 19(5):517-529.

Torres E, Rosen MK. 2003. Contingent phosphorylation/dephosphorylation provides a mechanism of molecular memory in WASP. Molecular Cell 11(5):1215-1227.

Tsuboi S. 2006. A complex of Wiskott-Aldrich syndrome protein with mammalian verprolins plays an important role in monocyte chemotaxis. Journal of Immunology

176(11):6576-6585.

Tsuboi S. 2007. Requirement for a complex of Wiskott-Aldrich syndrome protein (WASP) with WASP interacting protein in podosome formation in macrophages. Journal of Immunology 178(5):2987-2995.

Tuschl T. 2002. Expanding small RNA interference. Nature Biotechnology 20(5):446-448.

Uruno T, Liu JL, Zhang PJ, Fan YX, Egile C, Li P, Mueller SC, Zhan X. 2001. Activation of Arp2/3 complex-mediated actin polymerization by cortactin. Nature Cell Biology 3(3):259-266.

Uruno T, Zhang PJ, Liu JL, Hao JJ, Zhan X. 2003. Haematopoietic lineage cell-specific protein 1 (HS1) promotes actin-related protein (Arp) 2/3 complex-mediated actin polymerization. Biochemical Journal 371:485-493.

Van Goethem E, Guiet R, Balor S, Charriere GM, Poincloux R, Labrousse A, Maridonneau-Parini I, Le Cabec V. 2011. Macrophage podosomes go 3D. European Journal of Cell Biology 90(2-3):224-236.

Van Goethem E, Poincloux R, Gauffre F, Maridonneau-Parini I, Le Cabec V. 2010. Matrix Architecture Dictates Three-Dimensional Migration Modes of Human Macrophages: Differential Involvement of Proteases and Podosome-Like Structures. Journal of Immunology 184(2):1049-1061.

van Helden SFG, Krooshoop D, Broers KCM, Raymakers RAP, Figdor CG, van Leeuwen FN. 2006. A critical role for prostaglandin E-2 in podosome dissolution and induction of high-speed migration during dendritic cell maturation. Journal of Immunology 177(3):1567-1574.

van Helden SFG, van Leeuwen FN, Figdor CG. 2008. Human and murine model cell lines for dendritic cell biology evaluated. Immunology Letters 117(2):191-197.

van Hinsbergh VWM, Engelse MA, Quax PHA. 2006. Pericellular proteases in angiogenesis and vasculogenesis. Arteriosclerosis Thrombosis and Vascular Biology 26(4):716-728.

van Nierop K, de Groot C. 2002. Human follicular dendritic cells: function, origin and development. Seminars in Immunology 14(4):251-257.

Varon C, Tatin F, Moreau V, Van Obberghen-Schilling E, Fernandez-Sauze S, Reuzeau E, Kramer I, Genot E. 2006. Transforming growth factor beta induces rosettes of podosomes in primary aortic endothelial cells. Molecular and Cellular Biology 26(9):3582-3594.

Weaver AM. 2006. Invadopodia: specialized cell structures for cancer invasion. Clinical & Experimental Metastasis 23(2):97-105.

Weaver AM, Karginov AV, Kinley AW, Weed SA, Li Y, Parsons JT, Cooper JA. 2001. Cortactin promotes and stabilizes Arp2/3-induced actin filament network formation. Current Biology 11(5):370-374.

Webb BA, Eves R, Mak AS. 2006. Cortactin regulates podosome formation: Roles of the protein interaction domains. Experimental Cell Research 312(6):760-769.

Weed SA, Karginov AV, Schafer DA, Weaver AM, Kinley AW, Cooper JA, Parsons JT. 2000. Cortactin localization to sites of actin assembly in lamellipodia requires interactions with F-actin and the Arp2/3 complex. Journal of Cell Biology 151(1):29-40.

Wegner A. 1982. TREADMILLING OF ACTIN AT PHYSIOLOGICAL SALT CONCENTRATIONS - AN ANALYSIS OF THE CRITICAL CONCENTRATIONS OF ACTIN-FILAMENTS. Journal of Molecular Biology 161(4):607-615.

Welch MD, Iwamatsu A, Mitchison TJ. 1997. Actin polymerization is induced by Arp2/3 protein complex at the surface of Listeria monocytogenes. Nature 385(6613):265-269.

Werr J, Johansson J, Eriksson EE, Hedqvist P, Ruoslahti E, Lindbom L. 2000. Integrin alpha(2)beta(1) (VLA-2) is a principal receptor used by neutrophils for locomotion in extravascular tissue. Blood 95(5):1804-1809.

Werr J, Xie X, Hedqvist P, Ruoslahti E, Lindbom L. 1998. beta(1), integrins are critically involved in neutrophil locomotion in extravascular tissue in vivo. Journal of Experimental Medicine 187(12):2091-2096.

West MA, Prescott AR, Chan KM, Zhou ZJ, Rose-John S, Scheller J, Watts C. 2008. TLR ligand-induced podosome disassembly in dendritic cells is ADAM17 dependent. Journal of Cell Biology 182(5):993-1005.

Wilson RW, Ballantyne CM, Smith CW, Montgomery C, Bradley A, Obrien WE, Beaudet AL. 1993. GENE TARGETING YIELDS A CD18-MUTANT MOUSE FOR STUDY OF INFLAMMATION. Journal of Immunology 151(3):1571-1578.

Wiznerowicz M, Trono D. 2003. Conditional suppression of cellular genes: Lentivirus vector-mediated drug-inducible RNA interference. Journal of Virology 77(16):8957-8961.

Woods ML, Kivens WJ, Adelsman MA, Qiu Y, August A, Shimizu Y. 2001. A novel function for the Tec family tyrosine kinase Itk in activation of beta 1 integrins by the T-cell receptor. Embo Journal 20(6):1232-1244.

Wu H, Reynolds AB, Kanner SB, Vines RR, Parsons JT. 1991. IDENTIFICATION AND CHARACTERIZATION OF A NOVEL CYTOSKELETON-ASSOCIATED PP60SRC SUBSTRATE. Molecular and Cellular Biology 11(10):5113-5124.

Wu Y, Spencer SD, Lasky LA. 1998. Tyrosine phosphorylation regulates the SH3-mediated binding of the Wiskott-Aldrich syndrome protein to PSTPIP, a cytoskeletal-associated protein. Journal of Biological Chemistry 273(10):5765-5770.

Yamaguchi H, Lorenz M, Kempiak S, Sarmiento C, Coniglio S, Symons M, Segall J, Eddy R, Miki H, Takenawa T and others. 2005. Molecular mechanisms of invadopodium formation: the role of the N-WASP-Arp2/3 complex pathway and cofilin. Journal of Cell Biology 168(3):441-452.

Yamaguchi H, Pixley F, Condeelis J. 2006. Invadopodia and podosomes in tumor invasion. European Journal of Cell Biology 85(3-4):213-218.

Yamanashi Y, Okada M, Semba T, Yamori T, Umemori H, Tsunasawa S, Toyoshima K, Kitamura D, Watanabe T, Yamamoto T. 1993. IDENTIFICATION OF HS1 PROTEIN AS A MAJOR SUBSTRATE OF PROTEIN-TYROSINE KINASE(S) UPON B-CELL ANTIGEN RECEPTOR-MEDIATED SIGNALING. Proceedings of the National Academy of Sciences of the United States of America 90(8):3631-3635.

Yee JK, Miyanohara A, Laporte P, Bouic K, Burns JC, Friedmann T. 1994. A General-Method for the Generation of High-Titer, Pantropic Retroviral Vectors - Highly Efficient Infection of Primary Hepatocytes. Proceedings of the National Academy of Sciences of the United States of America 91(20):9564-9568.

Zamboninzallone A, Teti A, Grano M, Rubinacci A, Abbadini M, Gaboli M, Marchisio PC. 1989. IMMUNOCYTOCHEMICAL DISTRIBUTION OF EXTRACELLULAR-MATRIX RECEPTORS IN HUMAN OSTEOCLASTS - A BETA-3 INTEGRIN IS COLOCALIZED WITH VINCULIN AND TALIN IN THE PODOSOMES OF OSTEOCLASTOMA GIANT-CELLS. Experimental Cell Research 182(2):645-652.

Zennou V, Petit C, Guetard D, Nerhbass U, Montagnier L, Charneau P. 2000. HIV-1 genome nuclear import is mediated by a central DNA flap. Cell 101(2):173-185.

Zhang J, Shehabeldin A, da Cruz LAG, Butler J, Somani AK, McGavin M, Kozieradzki I, dos Santos AO, Nagy A, Grinstein S and others. 1999. Antigen receptor-induced activation and cytoskeletal rearrangement are impaired in Wiskott-Aldrich syndrome protein-deficient lymphocytes. Journal of Experimental Medicine 190(9):1329-1341.

Zicha D, Allen WE, Brickell PM, Kinnon C, Dunn GA, Jones GE, Thrasher AJ. 1998. Chemotaxis of macrophages is abolished in the Wiskott-Aldrich syndrome. British Journal of Haematology 101(4):659-665.

Zicha D, Dunn GA, Brown AF. 1991. A New Direct-Viewing Chemotaxis Chamber. Journal of Cell Science 99:769-775.

Zufferey R, Dull T, Mandel RJ, Bukovsky A, Quiroz D, Naldini L, Trono D. 1998. Self-inactivating lentivirus vector for safe and efficient in vivo gene delivery. Journal of Virology 72(12):9873-9880.

Zufferey R, Nagy D, Mandel RJ, Naldini L, Trono D. 1997. Multiply attenuated lentiviral vector achieves efficient gene delivery in vivo. Nature Biotechnology 15(9):871-875.

SUPPLEMENTAL DATA

Models of integrin deficiency

There is no human condition reported for the absence or reduced expression of β_1 integrins. In fact, a β_1 knock-out mutation in mice is lethal during early post implantation development [Fassler and Meyer 1995; Stephens et al. 1995]. Conditional knock-out murine models have been developed to investigate the effect of the lack of β_1 integrins in certain tissues, namely in the haematopoietic system, where it was shown that β_1 integrins are not essential for HSC retention in the BM, haematopoiesis or trafficking of lymphocytes [Brakebusch et al. 2002]. However, the specific effect of the lack of this family of integrins in the actin cytoskeleton, in particular in the cytoskeleton organization of immature DC and the formation of podosomes, was not addressed.

LAD is a primary immunodeficiency where patients present absent or reduced expression of β_2 integrins. DC from severe LAD patients, which lack CD18 expression, are unable to assemble podosomes (Supplemental Data Figure S.1 A, Siobhan Burns, unpublished data). The fact that LAD is a very rare disease and that prompt bone-marrow transplant is required makes it very difficult to obtain cells from such patients even at a national centre for paediatric primary immunodeficiencies, such as ours. There are two animal species with naturally occurring disorders due to lack of CD18 expression, resembling the phenotype of LAD: dog (canine LAD, CLAD) and cattle (bovine LAD, BLAD). Specific defects in DC function in these animal models have not been pursued. During this this study I was able to analyse the actin cytoskeleton of canine DC, both from normal and LAD dogs (kindly provided by Dr Dennis Hickstein, National Institutes of Health, MD) [Creevy et al. 2003]. DC were differentiated from frozen PBMC and plated on fibronectin-coated coverslips by Dr Gerben Bouma (Research Associate, Molecular Immunology Unit, UCL-Institute of Child Health). These cells were stained for immunofluorescence to reveal the actin cytoskeleton (Supplemental Data Figure S.1 B). Almost all plated WT cells presented abundant actin dots reminiscent of podosomes. CD18 and vinculin staining showed exclusion form podosome cores and uneven concentration around podosome rings. CLAD cells were generally smaller but the vast majority presented podosome actin dots (Supplemental Data Figure S.1 C), suggesting that unlike the human counterpart, canine DC are not dependent on β_2 integrins for podosome formation.

There are two murine models with reduced expression of CD18: one hypomorphic mouse,

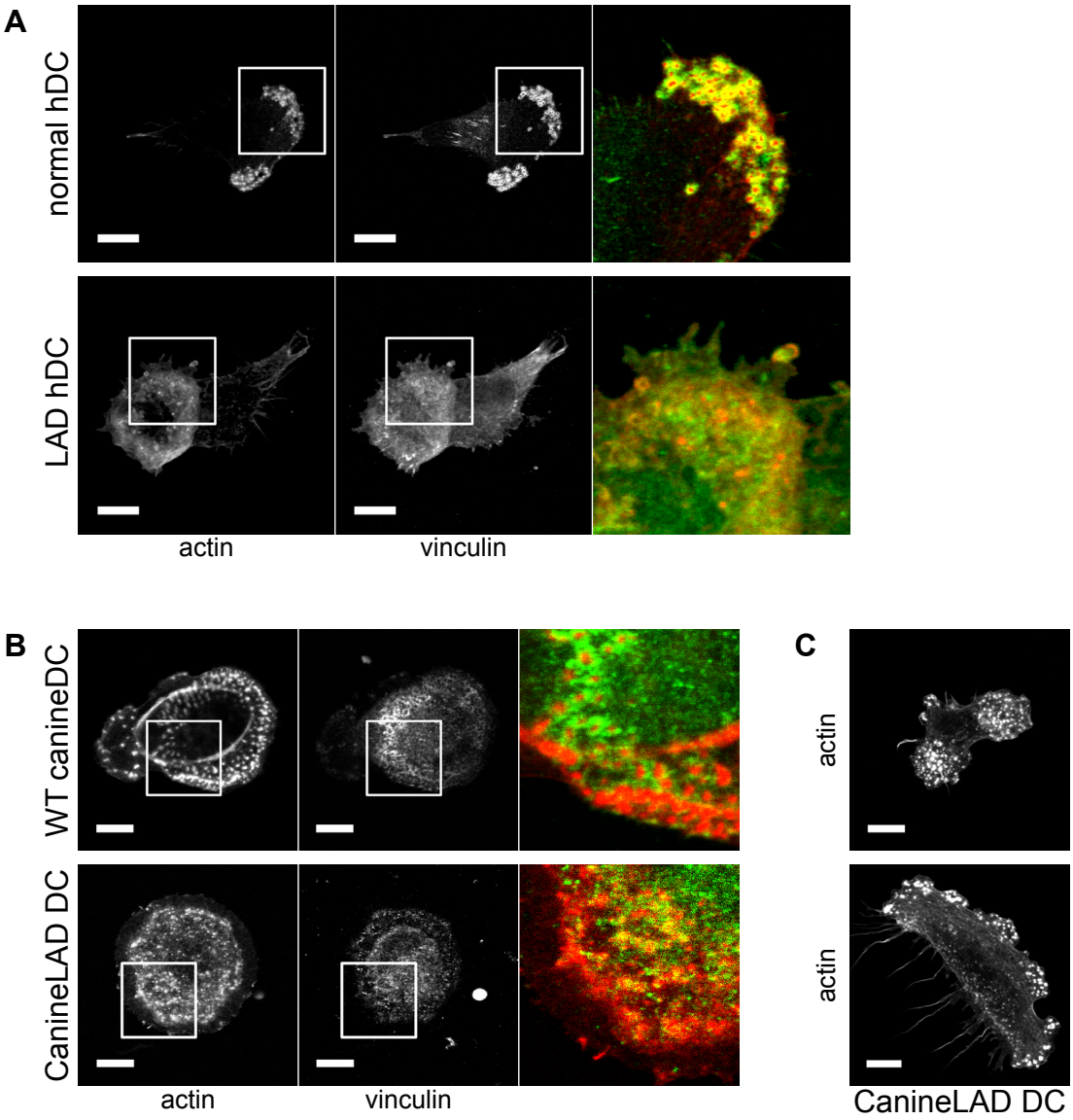

Figure S.1. DC from human LAD patients fail to assemble podosomes whereas DC from the canine LAD model are proficient at podosome formation.
A DC from LAD patients were analysed for their ability to assemble podosomes by Dr Siobhan Burns. DC from normal and severe LAD individuals were plated on fibronectin or ICAM and imaged by confocal microscopy after immune-staining for actin (red in the merged image) and vinculin (green in the merged image). Representative images for cells plated on fibronectin are presented. Whereas podosomes are readily identified in the normal DC, LAD DC fail to concentrate actin in the podosome cores and present more diffused actin staining (Siobhan Burns, unpublished data). **B and C** PBMC from the canine LAD (CLAD) disease model were differentiated from PBMC from WT and CLAD animals by Dr Gerben Bouma (Research Associate, Molecular Immunology Unit, UCL-Institute of Child Health) using the same protocol as for the generation of human monocyte-derived DC and plated onto fibronectin. These were stained by myself for immunofluorescence to reveal the actin cytoskeleton (actin in red and vinculin in green in the merged images) and imaged by confocal microscopy. Representative images are shown. Almost all plated WT cells presented abundant actin dots reminiscent of podosomes. The vast majority of CLAD cells also presented podosome actin dots. Scale bars: 10μm.

with moderate levels of CD18 expression (2-16% CD18 expression in granulocytes) [Wilson et al. 1993]; and a knock-out model [Scharffetter-Kochanek et al. 1998]. DC

podosome formation in these models has also not been previously reported. Preliminary work for the present study was done by Luísa Saraiva (Research Assistant, Molecular Immunology Unit, UCL-Institute of Child Health) using the CD18 hypomorphic mouse as the null mouse was not available. Splenic DC from these mice presented 52% CD18 expression and BMDC presented 56% CD18 expression and 60-95% expression of the α subunits (data not shown). No defect in adhesion to either fibronectin or ICAM was detected and it was found that DC from these animals were able to assemble podosomes as efficiently as cells from wild-type animals (data nor shown), suggesting the level of expression knock-down of CD18 in this model is not enough to result in podosome assembly and adhesion defects.

References

Brakebusch C, Fillatreau S, Potocnik AJ, Bungartz G, Wilhelm P, Svensson M, Kearney P, Korner H, Gray D, Fassler R. 2002. beta 1 integrin is not essential for hematopoiesis but is necessary for the T cell-dependent IgM antibody response. Immunity 16(3):465-477.

Creevy KE, Bauer TR, Tuschong LM, Embree LJ, Colenda L, Cogan K, Starost MF, Haskins ME, Hickstein DD. 2003. Canine leukocyte adhesion deficiency colony for investigation of novel hematopoietic therapies. Veterinary Immunology and Immunopathology 94(1-2):11-22.

Fassler R, Meyer M. 1995. CONSEQUENCES OF LACK OF BETA-1 INTEGRIN GENE-EXPRESSION IN MICE. Genes & Development 9(15):1896-1908.

Scharffetter-Kochanek K, Lu HF, Norman K, van Nood N, Munoz F, Grabbe S, McArthur M, Lorenzo I, Kaplan S, Ley K and others. 1998. Spontaneous skin ulceration and defective T cell function in CD18 null mice. Journal of Experimental Medicine 188(1):119-131.

Stephens LE, Sutherland AE, Klimanskaya IV, Andrieux A, Meneses J, Pedersen RA, Damsky CH. 1995. DELETION OF BETA-1 INTEGRINS IN MICE RESULTS IN INNER CELL MASS FAILURE AND PERIIMPLANTATION LETHALITY. Genes & Development 9(15):1883-1895.

Wilson RW, Ballantyne CM, Smith CW, Montgomery C, Bradley A, Obrien WE, Beaudet AL. 1993. GENE TARGETING YIELDS A CD18-MUTANT MOUSE FOR STUDY OF INFLAMMATION. Journal of Immunology 151(3):1571-1578.

Supplemental figures

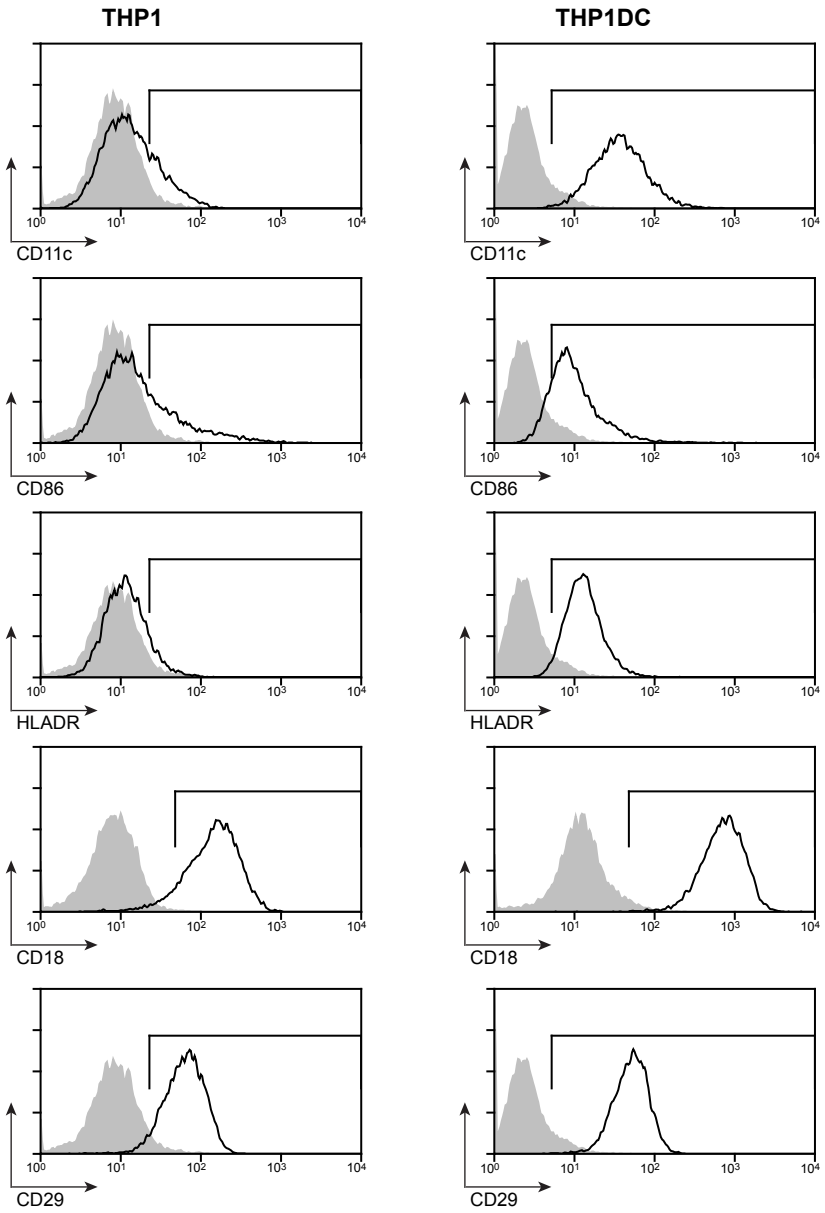

Figure S.2. THP1DC present surface marker expression consistent with an immature DC phenotype.
THP1 cells were differentiated into THP1DC and their expression of CD11c, CD86, and HLADR surface markers was assessed by flow cytometry. The expression of these surface markers was consistent with differentiation from monocytic cells (THP1) into immature dendritic-like cells (THP1DC). The surface expression of CD18 and CD29 was also confirmed in these cell lines by flow cytometry. Representative histograms are shown: filled grey histograms correspond to unstained or isotype-control stained samples; and continuous lines correspond to samples stained with the antibody against the indicated marker.

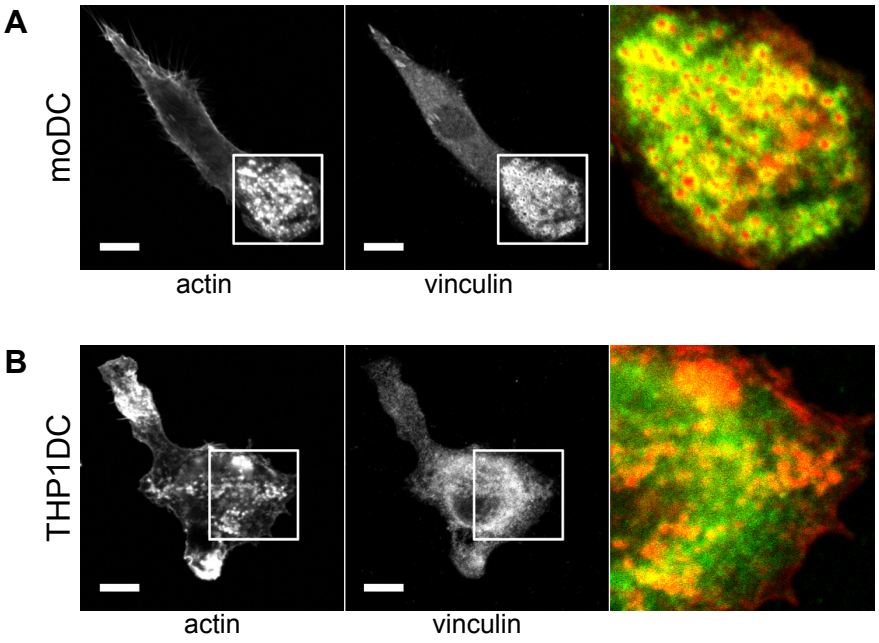

Figure S.3. Podosomes of moDC and THP1DC plated on fibronectin.
A Human monocyte-derived DC were plated onto fibronectin-coated glass slides, cultured overnight and fixed, permeabilised and stained for actin (red in the merged image) and vinculin (green in the merged image). **B** THP1 cells were differentiated into THP1DC and then plated onto fibronectin-coated slides. After 48h they were fixed and prepared as above. Podosomes are clearly identified as dense F-actin cores surrounded by rings of vinculin.

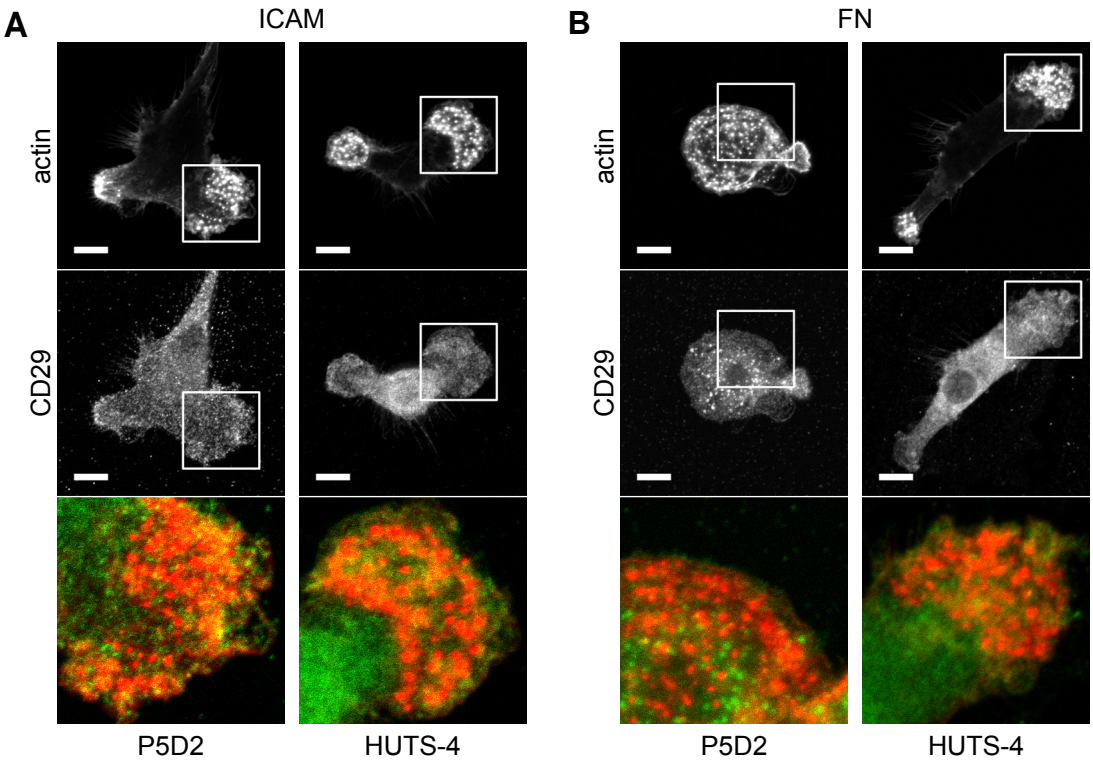

Figure S.4. β_1 integrins do not localise to moDC podosomes.
Monocyte-derived DC plated on **A** ICAM or **B** fibronectin were imaged by confocal microscopy to analyse the localization of β_1 integrins (green in the merged images). Cells were counterstained with phalloidin to identify actin (red in the merged images). Images from cells stained with two different antibody clones against CD29 are shown: clone P5D2 and clone HUTS-4, specific against the active conformation of the integrin.

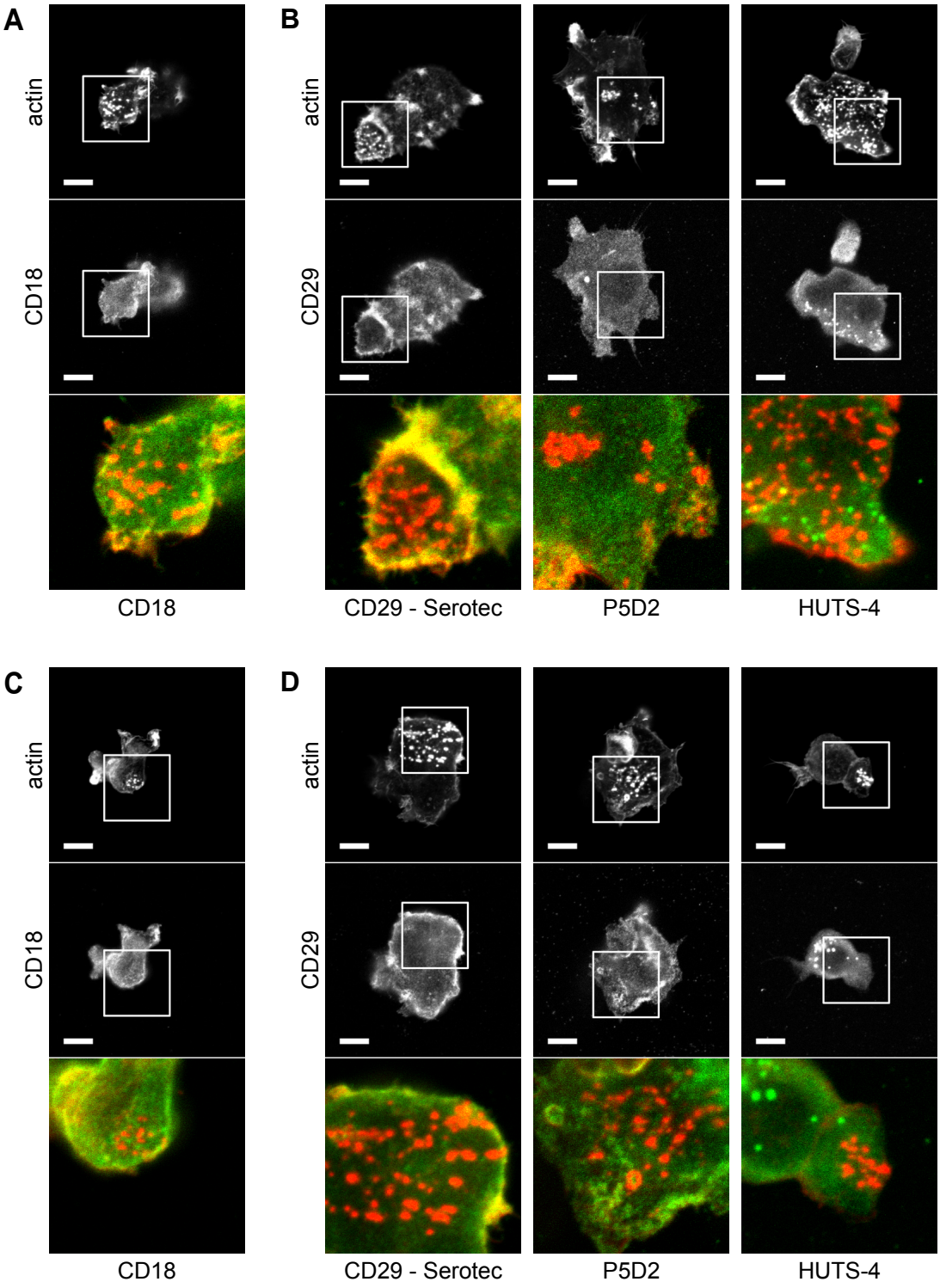

Figure S.5. Localization of β_1 and β_2 integrins in THP1DC.
THP1DC were plated onto **A and B** ICAM or **C and D** fibronectin and, 48h later, fixed and stained for actin (red in the merged images) and for **A and C** CD18 (β_2 integrin) or **B and D** CD29 (β_1 integrin). Two anti-CD29 antibody clones (4B7R and P5D2) and one anti-active CD29 clone (HUTS-4) were used.

SUPPLEMENTAL MATERIALS AND METHODS

ImageJ macros

MeasureParticles_.txt

```
//create mask
run("Make Binary");
run("Analyze Particles...", "size=100-Infinity circularity=0.00-1.00
show=Masks include");

//smooth edges of objects
run("Options...", "iterations=1 count=4 edm=Overwrite do=Dilate");
run("Options...", "iterations=1 count=4 edm=Overwrite do=Erode");

//measure number of objects, circularity and aspect ratio
run("Analyze Particles...", "size=100-Infinity circularity=0.00-1.00
show=Masks display clear include");

//copy results into excel worksheet and save mask
String.copyResults();
saveAs("Tiff");
close();
close();
close();
```

StackProcess_1.txt

```
macro "StackProcess_1" {
	run("8-bit");
	run("Bandpass Filter...", "filter_large=10 filter_small=0
suppress=None tolerance=5 process");
	run("Brightness/Contrast...");
	run("Enhance Contrast", "saturated=0.35");
	run("Apply LUT", "stack");
	run("Median...", "radius=1 stack");

//make maximum intensity Z-projection and save image
	run("Z Project...", "start=1 stop=5 projection=[Max Intensity]");
	saveAs("Tiff");
	close();
}
```

PodosomeArray_and_Podosomes_Masks.txt

```
//duplicate image
//draw by hand ROI around podosome array

roiManager(“Reset”);
run(“Add to Manager”);

run(“Make Inverse”);
run(“Clear”, “slice”);
run(“Make Inverse”);
run(“Fill”, “slice”);
run(“Make Binary”);

run(“Analyze Particles...”, “size=0.05-Infinity circularity=0.00-1.00
show=Masks summarize”);
saveAs(“Tiff”);
//save Mask of podosome array and copy summary to excel worksheet
close();
close();

roiManager(“Select”, 0);
run(“Make Inverse”);
run(“Clear”, “slice”);
run(“Make Inverse”);

setThreshold(127, 255);
run(“Convert to Mask”);
run(“Options...”, “iterations=1 count=1 edm=Overwrite do=Erode”);
run(“Watershed”);
run(“Options...”, “iterations=1 count=1 edm=Overwrite do=Dilate”);
run(“Watershed”);

run(“Analyze Particles...”, “size=0.05-Infinity circularity=0.00-1.00
show=Masks display clear include summarize add”);
String.copyResults();
//copy results (and summary) for podosomes to excel worksheet
//save ROIs.zip
saveAs(“Tiff”);
//save Mask of podosomes
close();
close();
```

Figure S.6. Filter used in FT analysis.
The image Filter6_512.tif was used to remove constant frequency background noise from IRM time-lapse videos in Fourier Transform (FT) analysis. This filter was designed so as to block horizontal frequencies up to 1/8th of the maximum frequency.

FFTFilter6512tifBatch.txt

```
macro “FFT Filter6_512.tif” {
	run(“8-bit”);
	run(“Custom Filter...”, “filter=Filter6_512.tif process”);
}
```

IRMProcess_NEW.txt

```
macro “IRM process NEW” {
//IRM processing of the stack
	run(“8-bit”);
	run(“Brightness/Contrast...”);
	run(“Enhance Contrast”, “saturated=0.35”);
	run(“Apply LUT”, “stack”);
	run(“Bandpass Filter...”, “filter_large=10 filter_small=0
suppress=None tolerance=5 autoscale saturate process”);
	run(“Median...”, “radius=2 stack”);

//Threshold individual images at 50%
//When Images are saved in batch mode the LUT is inverted resulting in:
//black (0) = adhesion
//white (255) = no adhesion
```

```
run(“Stack to Images”);
run(“Images to Stack”, “name=[] title=[]”);
run(“Stack to Images”);

selectWindow(“-0001”);
setAutoThreshold(“Percentile dark”);
run(“Convert to Mask”);
selectWindow(“-0002”);
setAutoThreshold(“Percentile dark”);
run(“Convert to Mask”);
selectWindow(“-0003”);
setAutoThreshold(“Percentile dark”);
run(“Convert to Mask”);
selectWindow(“-0004”);
setAutoThreshold(“Percentile dark”);
run(“Convert to Mask”);
selectWindow(“-0005”);
setAutoThreshold(“Percentile dark”);
run(“Convert to Mask”);
selectWindow(“-0006”);
setAutoThreshold(“Percentile dark”);
run(“Convert to Mask”);
selectWindow(“-0007”);
setAutoThreshold(“Percentile dark”);
run(“Convert to Mask”);
selectWindow(“-0008”);
setAutoThreshold(“Percentile dark”);
run(“Convert to Mask”);
selectWindow(“-0009”);
setAutoThreshold(“Percentile dark”);
run(“Convert to Mask”);
selectWindow(“-0010”);
setAutoThreshold(“Percentile dark”);
run(“Convert to Mask”);
selectWindow(“-0011”);
setAutoThreshold(“Percentile dark”);
run(“Convert to Mask”);
selectWindow(“-0012”);
setAutoThreshold(“Percentile dark”);
run(“Convert to Mask”);
selectWindow(“-0013”);
setAutoThreshold(“Percentile dark”);
run(“Convert to Mask”);
selectWindow(“-0014”);
setAutoThreshold(“Percentile dark”);
run(“Convert to Mask”);
selectWindow(“-0015”);
setAutoThreshold(“Percentile dark”);
run(“Convert to Mask”);
selectWindow(“-0016”);
setAutoThreshold(“Percentile dark”);
run(“Convert to Mask”);
selectWindow(“-0017”);
setAutoThreshold(“Percentile dark”);
run(“Convert to Mask”);
selectWindow(“-0018”);
setAutoThreshold(“Percentile dark”);
run(“Convert to Mask”);
selectWindow(“-0019”);
setAutoThreshold(“Percentile dark”);
run(“Convert to Mask”);
selectWindow(“-0020”);
setAutoThreshold(“Percentile dark”);
run(“Convert to Mask”);
selectWindow(“-0021”);
```

```
setAutoThreshold(“Percentile dark”);
run(“Convert to Mask”);
selectWindow(“-0022”);
setAutoThreshold(“Percentile dark”);
run(“Convert to Mask”);
selectWindow(“-0023”);
setAutoThreshold(“Percentile dark”);
run(“Convert to Mask”);
selectWindow(“-0024”);
setAutoThreshold(“Percentile dark”);
run(“Convert to Mask”);
selectWindow(“-0025”);
setAutoThreshold(“Percentile dark”);
run(“Convert to Mask”);
selectWindow(“-0026”);
setAutoThreshold(“Percentile dark”);
run(“Convert to Mask”);
selectWindow(“-0027”);
setAutoThreshold(“Percentile dark”);
run(“Convert to Mask”);
selectWindow(“-0028”);
setAutoThreshold(“Percentile dark”);
run(“Convert to Mask”);
selectWindow(“-0029”);
setAutoThreshold(“Percentile dark”);
run(“Convert to Mask”);
selectWindow(“-0030”);
setAutoThreshold(“Percentile dark”);
run(“Convert to Mask”);
selectWindow(“-0031”);
setAutoThreshold(“Percentile dark”);
run(“Convert to Mask”);
selectWindow(“-0032”);
setAutoThreshold(“Percentile dark”);
run(“Convert to Mask”);

run(“Images to Stack”, “name=[] title=[]”);
close();
}
```

HistogramIRM_macro.txt

```
run(“Stack to Images”);
run(“Images to Stack”, “name=Stack title=[]”);

//make sets of 4 consecutive frames at 1 frame per second
selectWindow(“Stack”);
run(“Duplicate...”, “title=Stack-1 duplicate range=1-7”);
run(“Stack to Images”);
selectWindow(“Stack-1-0002”);
close();
selectWindow(“Stack-1-0004”);
close();
selectWindow(“Stack-1-0006”);
close();
run(“Images to Stack”, “name=Stack-1 title=[] use”);

selectWindow(“Stack”);
run(“Duplicate...”, “title=Stack-2 duplicate range=9-15”);
run(“Stack to Images”);
```

```
selectWindow(“Stack-2-0002”);
close();
selectWindow(“Stack-2-0004”);
close();
selectWindow(“Stack-2-0006”);
close();
run(“Images to Stack”, “name=Stack-2 title=[] use”);

selectWindow(“Stack”);
run(“Duplicate...”, “title=Stack-3 duplicate range=17-23”);
run(“Stack to Images”);
selectWindow(“Stack-3-0002”);
close();
selectWindow(“Stack-3-0004”);
close();
selectWindow(“Stack-3-0006”);
close();
run(“Images to Stack”, “name=Stack-3 title=[] use”);

selectWindow(“Stack”);
run(“Duplicate...”, “title=Stack-4 duplicate range=25-31”);
run(“Stack to Images”);
selectWindow(“Stack-4-0002”);
close();
selectWindow(“Stack-4-0004”);
close();
selectWindow(“Stack-4-0006”);
close();
run(“Images to Stack”, “name=Stack-4 title=[] use”);

selectWindow(“Stack”);
close();

//average intensity Z-projection histogram
selectWindow(“Stack-1”);
run(“Z Project...”, “start=1 stop=4 projection=[Average Intensity]”);
run(“32-bit”);
run(“Histogram”, “bins=5 use x_min=0 x_max=255 y_max=Auto”);
selectWindow(“AVG_Stack-1”);
close();
selectWindow(“Stack-1”);
close();

selectWindow(“Stack-2”);
run(“Z Project...”, “start=1 stop=4 projection=[Average Intensity]”);
run(“32-bit”);
run(“Histogram”, “bins=5 use x_min=0 x_max=255 y_max=Auto”);
selectWindow(“AVG_Stack-2”);
close();
selectWindow(“Stack-2”);
close();

selectWindow(“Stack-3”);
run(“Z Project...”, “start=1 stop=4 projection=[Average Intensity]”);
run(“32-bit”);
run(“Histogram”, “bins=5 use x_min=0 x_max=255 y_max=Auto”);
selectWindow(“AVG_Stack-3”);
close();
selectWindow(“Stack-3”);
close();

selectWindow(“Stack-4”);
run(“Z Project...”, “start=1 stop=4 projection=[Average Intensity]”);
run(“32-bit”);
run(“Histogram”, “bins=5 use x_min=0 x_max=255 y_max=Auto”);
```

```
selectWindow(“AVG_Stack-4”);
close();
selectWindow(“Stack-4”);
close();
```

IRMProcess_NEW_NEW_2ndAnalysis.txt

The file text is truncated after analysis of the first two sets of 2 frames.

```
macro “IRM process NEW NEW 2ndAnalysis” {
//IRM processing of the stack
	run(“8-bit”);
	run(“Brightness/Contrast...”);
	run(“Enhance Contrast”, “saturated=0.35”);
	run(“Apply LUT”, “stack”);
	run(“Bandpass Filter...”, “filter_large=10 filter_small=0
suppress=None tolerance=5 autoscale saturate process”);
	run(“Median...”, “radius=2 stack”);

//Rename stack as “” (no name)
run(“Stack to Images”);
run(“Images to Stack”, “name=[] title=[]”);

//Count 4 levels difference between slices 1-3, 5-7, 9-11, 13-15, 17-19,
21-23, 25-27, 29-31
//
//Results in Summary. Important columns are “Slice” and “Total Area” or
“Area Fraction”:
//”Result of ...-3” indicates 3 level change
//”Result of ...-2” indicates 2 level change
//”Result of ...-1” indicates 1 level change
//”Result of ...” indicates no change in pixel grey level
//
//At the end, save Summary of results into excel.

//duplicate slices 1 and 3, make 4 levels, difference, count 4 levels
//1. duplicate slices
selectWindow(“”);
run(“Duplicate...”, “title=1 duplicate range=1-1”);
run(“Duplicate...”, “title=1-1”);
run(“Duplicate...”, “title=1-2”);
run(“Duplicate...”, “title=1-3”);
selectWindow(“1-3”);
setThreshold(192, 255);
run(“Convert to Mask”);
selectWindow(“1-2”);
setThreshold(128, 255);
run(“Convert to Mask”);
selectWindow(“1-1”);
setThreshold(64, 255);
run(“Convert to Mask”);
selectWindow(“1”);
setThreshold(0, 255);
run(“Convert to Mask”);
run(“Images to Stack”, “name=1 title=[]”);

selectWindow(“”);
run(“Duplicate...”, “title=3 duplicate range=3-3”);
run(“Duplicate...”, “title=3-1”);
run(“Duplicate...”, “title=3-2”);
```

```
run("Duplicate...", "title=3-3");
selectWindow("3-3");
setThreshold(192, 255);
run("Convert to Mask");
selectWindow("3-2");
setThreshold(128, 255);
run("Convert to Mask");
selectWindow("3-1");
setThreshold(64, 255);
run("Convert to Mask");
selectWindow("3");
setThreshold(0, 255);
run("Convert to Mask");
run("Images to Stack", "name=3 title=[]");

//2. make 4 levels
selectWindow("1");
run("Z Project...", "start=1 stop=4 projection=[Average Intensity]");
selectWindow("1");
close();
selectWindow("3");
run("Z Project...", "start=1 stop=4 projection=[Average Intensity]");
selectWindow("3");
close();

//3. difference
imageCalculator("Difference create", "AVG_1","AVG_3");
selectWindow("AVG_1");
close();
selectWindow("AVG_3");
close();

//4. count 4 levels
selectWindow("Result of AVG_1");
run("Duplicate...", "title=[Result of AVG_1-1]");
run("Duplicate...", "title=[Result of AVG_1-2]");
run("Duplicate...", "title=[Result of AVG_1-3]");
selectWindow("Result of AVG_1-3");
setThreshold(192, 255);
run("Convert to Mask");
run("Analyze Particles...", "size=0-Infinity circularity=0.00-1.00
show=Nothing summarize");
close();
selectWindow("Result of AVG_1-2");
setThreshold(128, 191);
run("Convert to Mask");
run("Analyze Particles...", "size=0-Infinity circularity=0.00-1.00
show=Nothing summarize");
close();
selectWindow("Result of AVG_1-1");
setThreshold(64, 127);
run("Convert to Mask");
run("Analyze Particles...", "size=0-Infinity circularity=0.00-1.00
show=Nothing summarize");
close();
selectWindow("Result of AVG_1");
setThreshold(0, 63);
run("Convert to Mask");
run("Analyze Particles...", "size=0-Infinity circularity=0.00-1.00
show=Nothing summarize");
close();

//duplicate slices 5 and 7, make 4 levels, difference, count 4 levels
//1. duplicate slices
selectWindow("");
```

```
run("Duplicate...", "title=5 duplicate range=5-5");
run("Duplicate...", "title=5-1");
run("Duplicate...", "title=5-2");
run("Duplicate...", "title=5-3");
selectWindow("5-3");
setThreshold(192, 255);
run("Convert to Mask");
selectWindow("5-2");
setThreshold(128, 255);
run("Convert to Mask");
selectWindow("5-1");
setThreshold(64, 255);
run("Convert to Mask");
selectWindow("5");
setThreshold(0, 255);
run("Convert to Mask");
run("Images to Stack", "name=5 title=[]");

selectWindow("");
run("Duplicate...", "title=7 duplicate range=7-7");
run("Duplicate...", "title=7-1");
run("Duplicate...", "title=7-2");
run("Duplicate...", "title=7-3");
selectWindow("7-3");
setThreshold(192, 255);
run("Convert to Mask");
selectWindow("7-2");
setThreshold(128, 255);
run("Convert to Mask");
selectWindow("7-1");
setThreshold(64, 255);
run("Convert to Mask");
selectWindow("7");
setThreshold(0, 255);
run("Convert to Mask");
run("Images to Stack", "name=7 title=[]");

//2. make 4 levels
selectWindow("5");
run("Z Project...", "start=1 stop=4 projection=[Average Intensity]");
selectWindow("5");
close();
selectWindow("7");
run("Z Project...", "start=1 stop=4 projection=[Average Intensity]");
selectWindow("7");
close();

//3. difference
imageCalculator("Difference create", "AVG_5","AVG_7");
selectWindow("AVG_5");
close();
selectWindow("AVG_7");
close();

//4. count 4 levels
selectWindow("Result of AVG_5");
run("Duplicate...", "title=[Result of AVG_5-1]");
run("Duplicate...", "title=[Result of AVG_5-2]");
run("Duplicate...", "title=[Result of AVG_5-3]");
selectWindow("Result of AVG_5-3");
setThreshold(192, 255);
run("Convert to Mask");
run("Analyze Particles...", "size=0-Infinity circularity=0.00-1.00
show=Nothing summarize");
close();
```

```
selectWindow(“Result of AVG_5-2”);
setThreshold(128, 191);
run(“Convert to Mask”);
run(“Analyze Particles...”, “size=0-Infinity circularity=0.00-1.00
show=Nothing summarize”);
close();
selectWindow(“Result of AVG_5-1”);
setThreshold(64, 127);
run(“Convert to Mask”);
run(“Analyze Particles...”, “size=0-Infinity circularity=0.00-1.00
show=Nothing summarize”);
close();
selectWindow(“Result of AVG_5”);
setThreshold(0, 63);
run(“Convert to Mask”);
run(“Analyze Particles...”, “size=0-Infinity circularity=0.00-1.00
show=Nothing summarize”);
close();
```

-- truncated --

IRMProcess_NEW_NEW_3rdAnalysis_NEW.txt

The file text is truncated after analysis of the first two sets of 2 frames.

```
macro “IRM process NEW NEW 3rdAnalysis_NEW” {

//IRM processing of the stack
	run(“8-bit”);
	run(“Brightness/Contrast...”);
	run(“Enhance Contrast”, “saturated=0.35”);
	run(“Apply LUT”, “stack”);
	run(“Bandpass Filter...”, “filter_large=10 filter_small=0
suppress=None tolerance=5 autoscale saturate process”);
	run(“Median...”, “radius=2 stack”);

//Rename stack as “” (no name)
run(“Stack to Images”);
run(“Images to Stack”, “name=[] title=[]”);

//Count 8 levels difference between slices 1-3, 5-7, 9-11, 13-15, 17-19,
21-23, 25-27, 29-31
//
//Results in Summary. Importante columns are “Slice” and “Total Area” or
“Area Fraction”:
//”Result of ...-7” indicates 7 level change
//”Result of ...-6” indicates 6 level change
//”Result of ...-5” indicates 5 level change
//”Result of ...-4” indicates 4 level change
//”Result of ...-3” indicates 3 level change
//”Result of ...-2” indicates 2 level change
//”Result of ...-1” indicates 1 level change
//”Result of ...” indicates no change in pixel grey level
//
//At the end, save Summary of results into excel.

//duplicate slices 1 and 3, make 8 levels, difference, count 8 levels
//1. duplicate slices
```

```
selectWindow("");
run("Duplicate...", "title=1 duplicate range=1-1");
run("Duplicate...", "title=1-1");
run("Duplicate...", "title=1-2");
run("Duplicate...", "title=1-3");
run("Duplicate...", "title=1-4");
run("Duplicate...", "title=1-5");
run("Duplicate...", "title=1-6");
run("Duplicate...", "title=1-7");
selectWindow("1-7");
setThreshold(224, 255);
run("Convert to Mask");
selectWindow("1-6");
setThreshold(192, 255);
run("Convert to Mask");
selectWindow("1-5");
setThreshold(161, 255);
run("Convert to Mask");
selectWindow("1-4");
setThreshold(128, 255);
run("Convert to Mask");
selectWindow("1-3");
setThreshold(96, 255);
run("Convert to Mask");
selectWindow("1-2");
setThreshold(64, 255);
run("Convert to Mask");
selectWindow("1-1");
setThreshold(32, 255);
run("Convert to Mask");
selectWindow("1");
setThreshold(0, 255);
run("Convert to Mask");
run("Images to Stack", "name=1 title=[]");

selectWindow("");
run("Delete Slice");

run("Duplicate...", "title=2 duplicate range=2-2");
run("Duplicate...", "title=2-1");
run("Duplicate...", "title=2-2");
run("Duplicate...", "title=2-3");
run("Duplicate...", "title=2-4");
run("Duplicate...", "title=2-5");
run("Duplicate...", "title=2-6");
run("Duplicate...", "title=2-7");
selectWindow("2-7");
setThreshold(224, 255);
run("Convert to Mask");
selectWindow("2-6");
setThreshold(192, 255);
run("Convert to Mask");
selectWindow("2-5");
setThreshold(160, 255);
run("Convert to Mask");
selectWindow("2-4");
setThreshold(128, 255);
run("Convert to Mask");
selectWindow("2-3");
setThreshold(96, 255);
run("Convert to Mask");
selectWindow("2-2");
setThreshold(64, 255);
run("Convert to Mask");
selectWindow("2-1");
```

```
setThreshold(32, 255);
run(“Convert to Mask”);
selectWindow(“2”);
setThreshold(0, 255);
run(“Convert to Mask”);
run(“Images to Stack”, “name=2 title=[]”);

//2. make 8 levels
selectWindow(“1”);
run(“Z Project...”, “start=1 stop=8 projection=[Average Intensity]”);
selectWindow(“1”);
close();
selectWindow(“2”);
run(“Z Project...”, “start=1 stop=8 projection=[Average Intensity]”);
selectWindow(“2”);
close();

//3. difference
imageCalculator(“Difference create”, “AVG_1”,”AVG_2”);
selectWindow(“AVG_1”);
close();
selectWindow(“AVG_2”);
close();

//4. count 8 levels
selectWindow(“Result of AVG_1”);
run(“Duplicate...”, “title=[Result of AVG_1-1]”);
run(“Duplicate...”, “title=[Result of AVG_1-2]”);
run(“Duplicate...”, “title=[Result of AVG_1-3]”);
run(“Duplicate...”, “title=[Result of AVG_1-4]”);
run(“Duplicate...”, “title=[Result of AVG_1-5]”);
run(“Duplicate...”, “title=[Result of AVG_1-6]”);
run(“Duplicate...”, “title=[Result of AVG_1-7]”);
selectWindow(“Result of AVG_1-7”);
setThreshold(224, 255);
run(“Convert to Mask”);
run(“Analyze Particles...”, “size=0-Infinity circularity=0.00-1.00
show=Nothing summarize”);
close();
selectWindow(“Result of AVG_1-6”);
setThreshold(192, 223);
run(“Convert to Mask”);
run(“Analyze Particles...”, “size=0-Infinity circularity=0.00-1.00
show=Nothing summarize”);
close();
selectWindow(“Result of AVG_1-5”);
setThreshold(160, 191);
run(“Convert to Mask”);
run(“Analyze Particles...”, “size=0-Infinity circularity=0.00-1.00
show=Nothing summarize”);
close();
selectWindow(“Result of AVG_1-4”);
setThreshold(128, 159);
run(“Convert to Mask”);
run(“Analyze Particles...”, “size=0-Infinity circularity=0.00-1.00
show=Nothing summarize”);
close();
selectWindow(“Result of AVG_1-3”);
setThreshold(96, 127);
run(“Convert to Mask”);
run(“Analyze Particles...”, “size=0-Infinity circularity=0.00-1.00
show=Nothing summarize”);
close();
selectWindow(“Result of AVG_1-2”);
setThreshold(64, 95);
```

```
run(“Convert to Mask”);
run(“Analyze Particles...”, “size=0-Infinity circularity=0.00-1.00
show=Nothing summarize”);
close();
selectWindow(“Result of AVG_1-1”);
setThreshold(32, 63);
run(“Convert to Mask”);
run(“Analyze Particles...”, “size=0-Infinity circularity=0.00-1.00
show=Nothing summarize”);
close();
selectWindow(“Result of AVG_1”);
setThreshold(0, 31);
run(“Convert to Mask”);
run(“Analyze Particles...”, “size=0-Infinity circularity=0.00-1.00
show=Nothing summarize”);
close();


//duplicate slices 5 and 7, make 8 levels, difference, count 8 levels
//1. duplicate slices
selectWindow(“”);
run(“Delete Slice”);
run(“Delete Slice”);
run(“Delete Slice”);

run(“Duplicate...”, “title=1 duplicate range=1-1”);
run(“Duplicate...”, “title=1-1”);
run(“Duplicate...”, “title=1-2”);
run(“Duplicate...”, “title=1-3”);
run(“Duplicate...”, “title=1-4”);
run(“Duplicate...”, “title=1-5”);
run(“Duplicate...”, “title=1-6”);
run(“Duplicate...”, “title=1-7”);
selectWindow(“1-7”);
setThreshold(224, 255);
run(“Convert to Mask”);
selectWindow(“1-6”);
setThreshold(192, 255);
run(“Convert to Mask”);
selectWindow(“1-5”);
setThreshold(161, 255);
run(“Convert to Mask”);
selectWindow(“1-4”);
setThreshold(128, 255);
run(“Convert to Mask”);
selectWindow(“1-3”);
setThreshold(96, 255);
run(“Convert to Mask”);
selectWindow(“1-2”);
setThreshold(64, 255);
run(“Convert to Mask”);
selectWindow(“1-1”);
setThreshold(32, 255);
run(“Convert to Mask”);
selectWindow(“1”);
setThreshold(0, 255);
run(“Convert to Mask”);
run(“Images to Stack”, “name=1 title=[]”);

selectWindow(“”);
run(“Delete Slice”);
run(“Duplicate...”, “title=2 duplicate range=2-2”);
run(“Duplicate...”, “title=2-1”);
run(“Duplicate...”, “title=2-2”);
run(“Duplicate...”, “title=2-3”);
```

```
run(“Duplicate...”, “title=2-4”);
run(“Duplicate...”, “title=2-5”);
run(“Duplicate...”, “title=2-6”);
run(“Duplicate...”, “title=2-7”);
selectWindow(“2-7”);
setThreshold(224, 255);
run(“Convert to Mask”);
selectWindow(“2-6”);
setThreshold(192, 255);
run(“Convert to Mask”);
selectWindow(“2-5”);
setThreshold(160, 255);
run(“Convert to Mask”);
selectWindow(“2-4”);
setThreshold(128, 255);
run(“Convert to Mask”);
selectWindow(“2-3”);
setThreshold(96, 255);
run(“Convert to Mask”);
selectWindow(“2-2”);
setThreshold(64, 255);
run(“Convert to Mask”);
selectWindow(“2-1”);
setThreshold(32, 255);
run(“Convert to Mask”);
selectWindow(“2”);
setThreshold(0, 255);
run(“Convert to Mask”);
run(“Images to Stack”, “name=2 title=[]”);

//2. make 8 levels
selectWindow(“1”);
run(“Z Project...”, “start=1 stop=8 projection=[Average Intensity]”);
selectWindow(“1”);
close();
selectWindow(“2”);
run(“Z Project...”, “start=1 stop=8 projection=[Average Intensity]”);
selectWindow(“2”);
close();

//3. difference
imageCalculator(“Difference create”, “AVG_1”,”AVG_2”);
selectWindow(“AVG_1”);
close();
selectWindow(“AVG_2”);
close();

//4. count 8 levels
selectWindow(“Result of AVG_1”);
run(“Duplicate...”, “title=[Result of AVG_1-1]”);
run(“Duplicate...”, “title=[Result of AVG_1-2]”);
run(“Duplicate...”, “title=[Result of AVG_1-3]”);
run(“Duplicate...”, “title=[Result of AVG_1-4]”);
run(“Duplicate...”, “title=[Result of AVG_1-5]”);
run(“Duplicate...”, “title=[Result of AVG_1-6]”);
run(“Duplicate...”, “title=[Result of AVG_1-7]”);
selectWindow(“Result of AVG_1-7”);
setThreshold(224, 255);
run(“Convert to Mask”);
run(“Analyze Particles...”, “size=0-Infinity circularity=0.00-1.00
show=Nothing summarize”);
close();
selectWindow(“Result of AVG_1-6”);
setThreshold(192, 223);
run(“Convert to Mask”);
```

```
run("Analyze Particles...", "size=0-Infinity circularity=0.00-1.00
show=Nothing summarize");
close();
selectWindow("Result of AVG_1-5");
setThreshold(160, 191);
run("Convert to Mask");
run("Analyze Particles...", "size=0-Infinity circularity=0.00-1.00
show=Nothing summarize");
close();
selectWindow("Result of AVG_1-4");
setThreshold(128, 159);
run("Convert to Mask");
run("Analyze Particles...", "size=0-Infinity circularity=0.00-1.00
show=Nothing summarize");
close();
selectWindow("Result of AVG_1-3");
setThreshold(96, 127);
run("Convert to Mask");
run("Analyze Particles...", "size=0-Infinity circularity=0.00-1.00
show=Nothing summarize");
close();
selectWindow("Result of AVG_1-2");
setThreshold(64, 95);
run("Convert to Mask");
run("Analyze Particles...", "size=0-Infinity circularity=0.00-1.00
show=Nothing summarize");
close();
selectWindow("Result of AVG_1-1");
setThreshold(32, 63);
run("Convert to Mask");
run("Analyze Particles...", "size=0-Infinity circularity=0.00-1.00
show=Nothing summarize");
close();
selectWindow("Result of AVG_1");
setThreshold(0, 31);
run("Convert to Mask");
run("Analyze Particles...", "size=0-Infinity circularity=0.00-1.00
show=Nothing summarize");
close();
```

-- truncated --

IRMProcess_NEW_NEW_4thAnalysis.txt

The file text is truncated after analysis of the first set of frames.

```
macro "IRM process NEW NEW 4thAnalysis" {

//IRM processing of the stack
	run("8-bit");
	run("Brightness/Contrast...");
	run("Enhance Contrast", "saturated=0.35");
	run("Apply LUT", "stack");
	run("Bandpass Filter...", "filter_large=10 filter_small=0
suppress=None tolerance=5 autoscale saturate process");
	run("Median...", "radius=2 stack");

//Rename stack as "" (no name)
```

```
run(“Stack to Images”);
run(“Images to Stack”, “name=[] title=[]”);

//Count 4 levels difference between slices 1-2, 3-4, 5-6, 7-8, 9-10, 11-12,
13-14, 15-16, 17-18, 19-20, 21-22, 23-24, 25-26, 27-28, 29-30, 31-32
//
//Results in Summary. Importante columns are “Slice” and “Total Area” or
“Area Fraction”:
//”Result of ...-3” indicates 3 level chage
//”Result of ...-2” indicates 2 level chage
//”Result of ...-1” indicates 1 level chage
//”Result of ...” indicates no change in pixel grey level
//
//At the end, save Summary of results into excel.

//duplicate slices 1 and 2, make 4 levels, difference, count 4 levels
//1. duplicate slices
selectWindow(“”);
run(“Duplicate...”, “title=1 duplicate range=1-1”);
run(“Duplicate...”, “title=1-1”);
run(“Duplicate...”, “title=1-2”);
run(“Duplicate...”, “title=1-3”);
selectWindow(“1-3”);
setThreshold(192, 255);
run(“Convert to Mask”);
selectWindow(“1-2”);
setThreshold(128, 255);
run(“Convert to Mask”);
selectWindow(“1-1”);
setThreshold(64, 255);
run(“Convert to Mask”);
selectWindow(“1”);
setThreshold(0, 255);
run(“Convert to Mask”);
run(“Images to Stack”, “name=1 title=[]”);

selectWindow(“”);
run(“Duplicate...”, “title=2 duplicate range=2-2”);
run(“Duplicate...”, “title=2-1”);
run(“Duplicate...”, “title=2-2”);
run(“Duplicate...”, “title=2-3”);
selectWindow(“2-3”);
setThreshold(192, 255);
run(“Convert to Mask”);
selectWindow(“2-2”);
setThreshold(128, 255);
run(“Convert to Mask”);
selectWindow(“2-1”);
‘’setThreshold(64, 255);
run(“Convert to Mask”);
selectWindow(“2”);
setThreshold(0, 255);
run(“Convert to Mask”);
run(“Images to Stack”, “name=2 title=[]”);

//2. make 4 levels
selectWindow(“1”);
run(“Z Project...”, “start=1 stop=4 projection=[Average Intensity]”);
selectWindow(“1”);
close();
selectWindow(“2”);
run(“Z Project...”, “start=1 stop=4 projection=[Average Intensity]”);
selectWindow(“2”);
close();
```

```
//3. difference
imageCalculator(“Difference create”, “AVG_1”,”AVG_2”);
selectWindow(“AVG_1”);
close();
selectWindow(“AVG_2”);
close();

//4. count 4 levels
selectWindow(“Result of AVG_1”);
run(“Duplicate...”, “title=[Result of AVG_1-1]”);
run(“Duplicate...”, “title=[Result of AVG_1-2]”);
run(“Duplicate...”, “title=[Result of AVG_1-3]”);
selectWindow(“Result of AVG_1-3”);
setThreshold(192, 255);
run(“Convert to Mask”);
run(“Analyze Particles...”, “size=0-Infinity circularity=0.00-1.00
show=Nothing summarize”);
close();
selectWindow(“Result of AVG_1-2”);
setThreshold(128, 191);
run(“Convert to Mask”);
run(“Analyze Particles...”, “size=0-Infinity circularity=0.00-1.00
show=Nothing summarize”);
close();
selectWindow(“Result of AVG_1-1”);
setThreshold(64, 127);
run(“Convert to Mask”);
run(“Analyze Particles...”, “size=0-Infinity circularity=0.00-1.00
show=Nothing summarize”);
close();
selectWindow(“Result of AVG_1”);
setThreshold(0, 63);
run(“Convert to Mask”);
run(“Analyze Particles...”, “size=0-Infinity circularity=0.00-1.00
show=Nothing summarize”);
close();
```

-- truncated --

IRMProcess_NEW_NEW_5thAnalysis.txt

The file text is truncated after analysis of the first set frames.

```
macro “IRM process NEW NEW 5thAnalysis” {

//IRM processing of the stack
	run(“8-bit”);
	run(“Brightness/Contrast...”);
	run(“Enhance Contrast”, “saturated=0.35”);
	run(“Apply LUT”, “stack”);
	run(“Bandpass Filter...”, “filter_large=10 filter_small=0
suppress=None tolerance=5 autoscale saturate process”);
	run(“Median...”, “radius=2 stack”);

//Rename stack as “” (no name)
run(“Stack to Images”);
run(“Images to Stack”, “name=[] title=[]”);
```

```
//Count 8 levels difference between slices 1-2, 3-4, 5-6, 7-8, 9-10, 11-12,
13-14, 15-16, 17-18, 19-20, 21-22, 23-24, 25-26, 27-28, 29-30, 31-32
//
//Results in Summary. Importante columns are “Slice” and “Total Area” or
“Area Fraction”:
//”Result of ...-7” indicates 7 level change
//”Result of ...-6” indicates 6 level change
//”Result of ...-5” indicates 5 level change
//”Result of ...-4” indicates 4 level change
//”Result of ...-3” indicates 3 level change
//”Result of ...-2” indicates 2 level change
//”Result of ...-1” indicates 1 level change
//”Result of ...” indicates no change in pixel grey level
//
//At the end, save Summary of results into excel.

//duplicate slices 1 and 2, make 8 levels, difference, count 8 levels
//1. duplicate slices
selectWindow(“”);
run(“Duplicate...”, “title=1 duplicate range=1-1”);
run(“Duplicate...”, “title=1-1”);
run(“Duplicate...”, “title=1-2”);
run(“Duplicate...”, “title=1-3”);
run(“Duplicate...”, “title=1-4”);
run(“Duplicate...”, “title=1-5”);
run(“Duplicate...”, “title=1-6”);
run(“Duplicate...”, “title=1-7”);
selectWindow(“1-7”);
setThreshold(224, 255);
run(“Convert to Mask”);
selectWindow(“1-6”);
setThreshold(192, 255);
run(“Convert to Mask”);
selectWindow(“1-5”);
setThreshold(161, 255);
run(“Convert to Mask”);
selectWindow(“1-4”);
setThreshold(128, 255);
run(“Convert to Mask”);
selectWindow(“1-3”);
setThreshold(96, 255);
run(“Convert to Mask”);
selectWindow(“1-2”);
setThreshold(64, 255);
run(“Convert to Mask”);
selectWindow(“1-1”);
setThreshold(32, 255);
run(“Convert to Mask”);
selectWindow(“1”);
setThreshold(0, 255);
run(“Convert to Mask”);
run(“Images to Stack”, “name=1 title=[]”);

selectWindow(“”);
run(“Duplicate...”, “title=2 duplicate range=2-2”);
run(“Duplicate...”, “title=2-1”);
run(“Duplicate...”, “title=2-2”);
run(“Duplicate...”, “title=2-3”);
run(“Duplicate...”, “title=2-4”);
run(“Duplicate...”, “title=2-5”);
run(“Duplicate...”, “title=2-6”);
run(“Duplicate...”, “title=2-7”);
selectWindow(“2-7”);
setThreshold(224, 255);
run(“Convert to Mask”);
```

```
selectWindow(“2-6”);
setThreshold(192, 255);
run(“Convert to Mask”);
selectWindow(“2-5”);
setThreshold(160, 255);
run(“Convert to Mask”);
selectWindow(“2-4”);
setThreshold(128, 255);
run(“Convert to Mask”);
selectWindow(“2-3”);
setThreshold(96, 255);
run(“Convert to Mask”);
selectWindow(“2-2”);
setThreshold(64, 255);
run(“Convert to Mask”);
selectWindow(“2-1”);
setThreshold(32, 255);
run(“Convert to Mask”);
selectWindow(“2”);
setThreshold(0, 255);
run(“Convert to Mask”);
run(“Images to Stack”, “name=2 title=[]”);

//2. make 8 levels
selectWindow(“1”);
run(“Z Project...”, “start=1 stop=8 projection=[Average Intensity]”);
selectWindow(“1”);
close();
selectWindow(“2”);
run(“Z Project...”, “start=1 stop=8 projection=[Average Intensity]”);
selectWindow(“2”);
close();

//3. difference
imageCalculator(“Difference create”, “AVG_1”,”AVG_2”);
selectWindow(“AVG_1”);
close();
selectWindow(“AVG_2”);
close();

//4. count 8 levels
selectWindow(“Result of AVG_1”);
run(“Duplicate...”, “title=[Result of AVG_1-1]”);
run(“Duplicate...”, “title=[Result of AVG_1-2]”);
run(“Duplicate...”, “title=[Result of AVG_1-3]”);
run(“Duplicate...”, “title=[Result of AVG_1-4]”);
run(“Duplicate...”, “title=[Result of AVG_1-5]”);
run(“Duplicate...”, “title=[Result of AVG_1-6]”);
run(“Duplicate...”, “title=[Result of AVG_1-7]”);
selectWindow(“Result of AVG_1-7”);
setThreshold(224, 255);
run(“Convert to Mask”);
run(“Analyze Particles...”, “size=0-Infinity circularity=0.00-1.00
show=Nothing summarize”);
close();
selectWindow(“Result of AVG_1-6”);
setThreshold(192, 223);
run(“Convert to Mask”);
run(“Analyze Particles...”, “size=0-Infinity circularity=0.00-1.00
show=Nothing summarize”);
close();
selectWindow(“Result of AVG_1-5”);
setThreshold(160, 191);
run(“Convert to Mask”);
run(“Analyze Particles...”, “size=0-Infinity circularity=0.00-1.00
```

```
show=Nothing summarize");
close();
selectWindow("Result of AVG_1-4");
setThreshold(128, 159);
run("Convert to Mask");
run("Analyze Particles...", "size=0-Infinity circularity=0.00-1.00
show=Nothing summarize");
close();
selectWindow("Result of AVG_1-3");
setThreshold(96, 127);
run("Convert to Mask");
run("Analyze Particles...", "size=0-Infinity circularity=0.00-1.00
show=Nothing summarize");
close();
selectWindow("Result of AVG_1-2");
setThreshold(64, 95);
run("Convert to Mask");
run("Analyze Particles...", "size=0-Infinity circularity=0.00-1.00
show=Nothing summarize");
close();
selectWindow("Result of AVG_1-1");
setThreshold(32, 63);
run("Convert to Mask");
run("Analyze Particles...", "size=0-Infinity circularity=0.00-1.00
show=Nothing summarize");
close();
selectWindow("Result of AVG_1");
setThreshold(0, 31);
run("Convert to Mask");
run("Analyze Particles...", "size=0-Infinity circularity=0.00-1.00
show=Nothing summarize");
close();
```

-- truncated --